

**REMOTE DETECTION OF LASER GENERATED  
ULTRASONICS BY FIBRE OPTIC INTERFEROMETER**

A thesis submitted

by

**Biswanath Mitra**

for the degree of

**Doctor of Philosophy**



Department of Applied Physics

Victoria University

1997



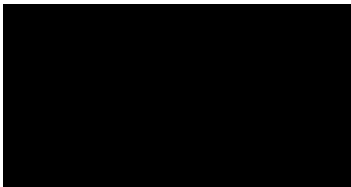
FTS THESIS  
620.11274 MIT  
30001004876035  
Mitra, Biswanath  
Remote detection of laser  
generated ultrasonics by  
fibre optic interferometer

# Declaration

I, Biswanath Mitra, declare that this thesis titled as

*“Remote detection of laser generated ultrasonics by fibre-optic interferometer”*

is my own work and has not been submitted previously, in whole or in part, in respect of any other academic award.



Biswanath Mitra

Department of Applied Physics

Victoria University of Technology

Australia

dated the 27th day of March, 1997

## Acknowledgement

I wish to express my deepest appreciation to Prof. David Booth for supervising my PhD programme. I am very fortunate in coming to know Dr. Booth. He gave me frequent advice and criticism and was the major inspiration for this project.

I would like to thank Mr Alex Shelamoff and all academic, technical and administrative staff and fellow postgraduate students in the department of Applied Physics for their help and assistance. I also wish to acknowledge my debt to Mr. Phillip Pearce for his excellent help with the preparation of the thesis.

I am grateful to the Victoria University of Technology for the financial assistance in the form of Postgraduate Research Scholarship and the Department Applied Physics for the Departmental Scholarship.

Finally let me say that the pain of converting blank pages to written manuscript was made bearable by the loving support of my wife Debi and son Biswadev.

## **Abstract**

This thesis is concerned with the development of a totally remote all-optic non-destructive testing and evaluation technique suitable for use in a range of adverse measuring environments. It differs from previous work in that the technique is made much more flexible and suitable for a greater range of measurement environments by the use of fibre optics. There is little problem in using optical fibres for delivery of high power Q-switched pulses to excite acoustic waves in target materials. However, the use of fibre optic interferometers in remote detection of these pulses presents very significant signal to noise problems. This is due to the high optical losses associated with launching a laser source into a fibre and the small amount of scattered light from a natural surface which can be re-injected into a single mode fibre to interfere with a reference beam in that fibre. This thesis describes the development of a high performance fibre optic interferometer which can be used to detect small wideband ultrasonic displacement waveforms generated in laser induced ultrasonics. The combination of laser generation and fibre interferometer detection provides a new remote optical system suitable for ultrasonic non-destructive evaluation. Experimental measurements are made to demonstrate that this new remote system performs well in detecting laser generated bulk ultrasonic waves in metallic samples using natural surfaces for reflection of the interferometer beams. This work is then extended to show that the technique can be applied to monitoring the state of cure of epoxy based thermoset resins. Measurements are made in the ablation regime throughout the entire cure phase (liquid to solid) of an epoxy target placed in a suitable plastic container with aluminium foil tape attached to provide a suitable target for optical generation and detection beams.

<b>Contents</b>	<b>Page</b>
<b>Chapter 1 Introduction</b>	
1.1 Remote optical methods for ultrasonic evaluation of materials	1.1
1.2 General objective of this work	1.3
1.3 Preview of the thesis	1.4
<b>Chapter 2 Optical Generation and Detection of ultrasonics</b>	
2.1 Introduction and general overview of the transducers for generation and detection of ultrasonics	2.1
2.2 Generation of ultrasonics using high power laser pulses	2.4
2.2.1 Physical principle	2.5
2.2.2 Mechanism for the generation of ultrasonics	2.7
2.2.3 Thermoelastic effect: thermal expansion stress	2.8
2.2.4 The ablation effect: vaporisation stress	2.13
2.2.5 Radiation pattern for laser ultrasonic sources	2.17
2.2.6 Surface modification	2.19
2.2.7 Characteristics of pulsed lasers for ultrasonic generation	2.20
2.2.8 Review of previous work on laser generation of ultrasonics	2.22
2.3 Optical detection of laser generated ultrasonics	2.39
2.3.1 Optical methods	2.39

2.3.2 Optical interferometry	2.40
2.3.3 Fibre Optic Interferometer	2.42
2.3.4 Principle of operation	2.43
2.3.4.1 Signal processing	2.47
2.3.4.2 Demodulation techniques	2.48
2.3.5 Review of the previous work on different demodulation technique	2.49
2.3.5.1 Active homodyne	2.50
2.3.5.2 Passive homodyne	2.54
2.3.5.3 Heterodyne technique	2.62
2.3.5.4 Synthetic heterodyne	2.66
2.3.5.5 Pseudo-heterodyne	2.70
2.3.5.6 Quadrature recombination heterodyne	2.72
2.3.6 Noise consideration	2.74
2.3.7 Previous work on optical methods of detection of laser generated ultrasound	2.84
2.3.8 Conclusion	2.97

## **Chapter 3 Experimental system**

3.1 Design and construction of Q-switched Nd:YAG laser	3.1
3.1.1 Characterisation of the laser	3.9
3.2 Construction and characterisation of the interferometers	3.12
3.3 Construction of the heterodyne interferometer	3.13
3.3.1 Optical layout	3.13

3.3.2 Electronics	3.16
3.3.3 Sensitivity	3.18
3.3.4 Performance	3.19
3.4 Construction of the homodyne interferometers	3.21
3.4.1 Optical layout	3.22
3.4.2 Electronics	3.24
3.4.3 Calibration	3.26
3.5 Homodyne interferometer version 2 (Ho - 2)	3.28
3.6 Homodyne interferometer version 3 (Ho - 3)	3.30
3.7 Performance	3.32
3.8 Final interferometric configuration	3.37

## **Chapter 4 Experimental results using metallic targets**

4.1 Experimental arrangement	4.2
4.2 Experimental data on remote detection of ultrasonics	4.4
4.2.1 Acoustic waveforms with different pulse energies	4.4
4.2.2 Acoustic waveforms with different incident power densities	4.9
4.2.2.1 Irradiation with the unfocused laser beam	4.9
4.2.2.2 Irradiation with the laser beam focused within the sample (varying surface power density)	4.10
4.2.2.3 Irradiation with the laser beam focused in front of the target	4.15

4.2.2.4 Irradiation with a pulse energy of 47 mJ	4.22
4.2.2.5 Irradiation with an unfocused laser beam of energy 1300 mJ	4.26
4.3 Determination of the longitudinal wave velocity in metals	4.29

## **Chapter 5 Laser generation and detection of ultrasonics for monitoring the curing of epoxy**

5.1 Detection of ultrasonics in non-metallic materials	5.1
5.2 Curing of Epoxy	5.2
5.2.1 General methods of cure monitoring	5.4
5.2.2 Optical methods of cure monitoring	5.8
5.3 Cure monitoring Results	5.12
5.3.1 Irradiation with high energy pulses (1300 mJ)	5.15
5.3.2 Acoustic waveforms with different incident power densities in a cured sample	5.25
5.3.3 Irradiation with lower pulse energies (47 mJ - 125 mJ)	5.32

## **Chapter 6 Conclusion**

# Chapter 1: Introduction

## 1.1 Remote optical methods for ultrasonic evaluation of materials

In current engineering practice, it is of major concern to be able to incorporate suitable techniques for non-destructive testing in process and quality control. In situations requiring physical measurement or inspection, the possibility of providing accurate measurement of physical parameters, without disturbing the object being investigated, is an important consideration. Measurement of displacement and characterisation of materials by ultrasonics techniques are widely used in industry. Ultrasonics has also established itself as a highly effective non-destructive testing and inspection technique for examination of engineering materials and structures. This technique is particularly suitable for testing of metals or composite materials during production or maintenance.

The demand for lightweight high-performance materials has been increasing with the escalating costs of energy and petrochemical feedstocks. As a result, in recent years there has been a significant rise in interest in composite polymer-based materials. The advantages of composite materials are of foremost importance in the transport, automotive and sporting goods industries. Particularly important applications are to be found in the aircraft and aerospace industries. In aerospace engineering, there has recently been a large increase in the use of advanced fibre reinforced composite materials, many of which have a thermoset matrix. The thermosets are polymeric materials which can be shaped only once and cannot be remoulded by heating. The high strength and stiffness of the advanced composites, relative to their weight, offsets

their high cost. The control and monitoring of the curing of these materials is essential in obtaining high performance and long life. The optimisation of cure monitoring in composites is expected to result in increase throughput, reduction in curing times, reduced costs and fewer rejections.

Laser generated ultrasonics, when combined with remote optical sensing, becomes an integrated optical system for non-destructive testing which is suitable for application in industry. This work reports the first use of an optical fibre interferometer for such an application. The optical fibre interferometer offers considerable advantages in ease of use and robustness compared to bulk optical interferometers. It uses light scattered from the rear surface of the target material (not necessarily highly reflective) and coupled back into the fibre to produce interference with a reference beam in the fibre. In such an arrangement there is no need for bulky and difficult to align mirror systems in the interferometer as is the case in a conventional bulk optic devices. However the use of a fibre interferometer offers very challenging detection problems due to the reduced signal to noise ratios which accompany the reduced light intensities in the interfering beams. The reduced intensities are due to losses in coupling into, and out of, the optical fibres both from the source and beam scattered from the target. Thus much of the work has been involved in the development of suitable optical fibre interferometers using low power laser sources which have sufficient sensitivity, wide bandwidth and low noise for this application. The work initially involved the detection of laser generated ultrasonics in metals and then went onto show that the more difficult case of monitoring such signals from curing composite materials is also possible with this technique.

## 1.2 General objective of this work

- (i) To design and construct a pulsed laser which can act as a standard optical source, suitable for generation of ultrasonics in both metals and non-metals in either thermoelastic or ablation regimes (refer chapter 2).
- (ii) To explore different demodulation techniques applicable to a two beam interferometers and to identify the most effective technique for incorporation in a fibre optic interferometer, which is appropriate for remote detection of ultrasonics.
- (iii) To design, construct and characterise fibre optic interferometers, identify the important practical limitations of these systems and attempt to improve their performance. During these investigations, special attention needs to be paid to the sensitivity attainable at the high bandwidth required for detection of laser-generated ultrasonics.
- (iv) To develop and demonstrate a practical opto-ultrasonic technique based on laser generation and remote detection by a fibre optic interferometer which is suitable for use in non-destructive material evaluation (NDE) of metals.
- (vi) To demonstrate that the new remote all-optical NDE technique can be used to monitor bulk ultrasonic waveforms throughout the entire curing phase of an epoxy-based composite material.

### **1.3 Preview of the thesis**

Chapter 2 describes the principles underlying the optical generation and detection of ultrasonics. The opening section of this chapter deals with the general overview of the different transducers for generation and detection of ultrasonics. The principles and the mechanisms involved in the generation of ultrasonics in the thermoelastic and ablation regimes using a high power laser are described in next section. This is followed by the identification of the characteristics of a laser suitable for the effective generation of ultrasonics and a review on the previous work on the different types of laser sources used for the generation of ultrasonics.

Chapter 2 also describes the principle of operation of two beam fibre optic interferometers, possible demodulation techniques and a review on different demodulation techniques which are likely to perform satisfactorily in the present application. Advantages of the optical technique used for remote detection of ultrasonic signals are identified. The primary objective of this section is to identify the most simple and practical demodulation technique which can be used with a fibre optic interferometer for remote detection of ultrasound. Since the minimum detectable signal in an interferometer is dependent on noise, a noise model is developed to analyse the contribution of the different sources of noise in an interferometer and to estimate the sensitivity attainable with higher bandwidths at different levels of optical power. The final section reviews the previous work on optical methods used in the detection of laser generated ultrasonics.

The design and construction of a high power pulsed laser and the fibre optic interferometers are outlined in chapter 3. The performance of a small pulsed Nd:YAG laser which was constructed for the generation of ultrasonic pulses in the work described in this thesis is presented. Construction and characterisation of heterodyne and active homodyne fibre optic interferometers which include an open air path for remote detection are discussed. Descriptions are given of many versions of active homodyne interferometers constructed with progressively better performance until one was produced which was capable of making the measurements required in this work. The performance of the active homodyne interferometers have been compared in terms of their ultimate measurement capability which has been expressed using a bandwidth dependent noise equivalent displacement (NED). The steps taken to optimise the performance of these interferometers are described. The optimised performance obtained with these interferometers under laboratory conditions, is found to be comparable to the most sensitive fibre optic interferometer reported to date. The final section in this chapter describes the final configuration of interferometer used in subsequent experimental work.

Chapters 4 and 5 are concerned with the experimental results obtained using laser generation and remote fibre interferometer detection of bulk ultrasonics in metallic and non-metallic targets.

The description of the complete experimental arrangement is given in chapter 4. This chapter also presents the measured acoustic waveforms in metals under thermoelastic and ablation regimes at different incident energies and power densities of the pulsed

laser. Finally, a separate section describes the application of this technique in the determination of the velocity of longitudinal acoustic waves in metals.

Chapter 5 reports the application of this technique in detection of laser generated ultrasonics in epoxy-based thermoset resins. Experimental results are reported for the first time on the remote determination of the extent of curing in epoxy. This chapter also includes a comparison of the technique with other methods previously used for similar measurements.

Chapter 6 summarises the major achievements of the work reported in this thesis together with suggestions for future extension.

## Chapter 2: Optical Generation and Detection of ultrasonics

### 2.1 Introduction and general overview of transducers for generation and detection of ultrasound

There are a number of transducers available for generation and detection of ultrasound. Most of these transducers can be used in a non-contact mode, others need to be in contact with the sample under investigation. Only laser generation and optical interferometric detection are capable of being used at substantial distances from the sample. The different techniques for generation and detection, and their possible combinations, are summarised below.

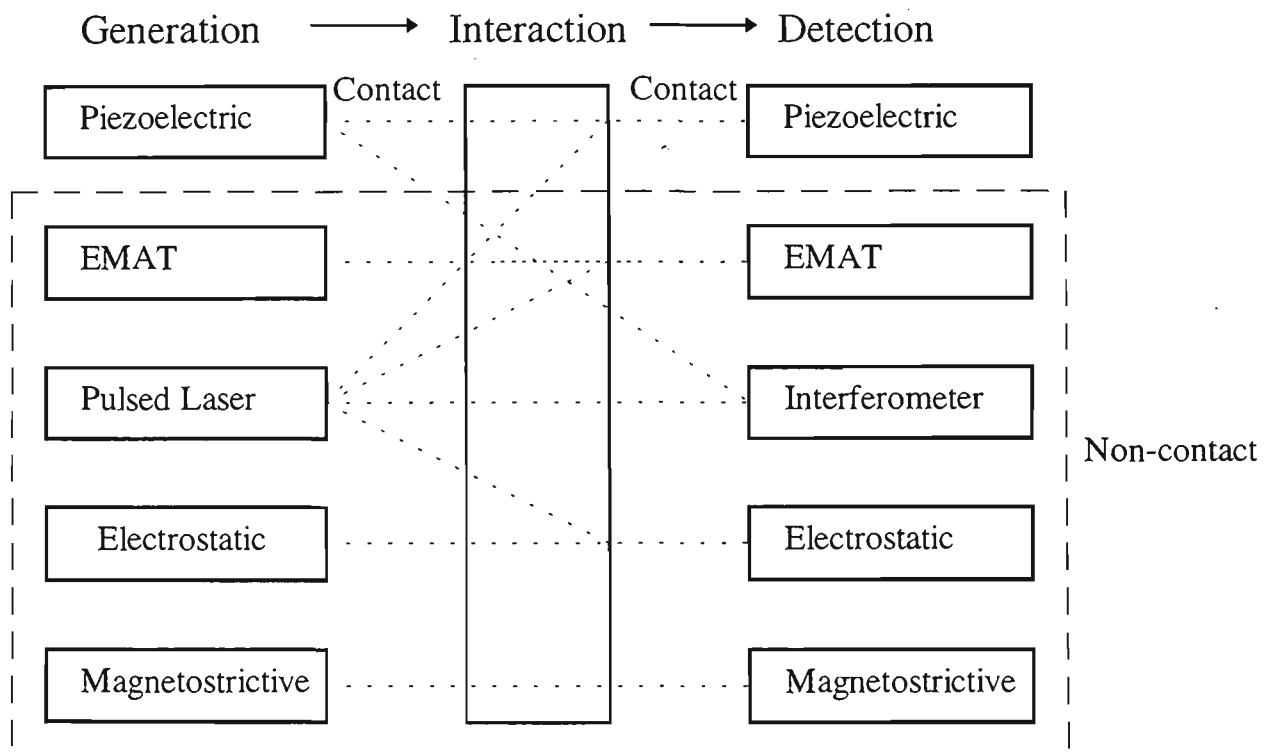


Figure 2.1.1 Different techniques for generation and detection of ultrasonics.

The conventional piezoelectric transducers (PZT) are either placed in contact with the specimen or immersed in suitable coupling fluid used to carry out ultrasonic inspection and testing of materials. These transducers are restricted to a limited temperature range because reliable fluid couplants are not available above 500°C (Scruby and Drain, 1990). It is also difficult to implement this contact technique in some cases such as hot products, moving products and samples of complex geometry and there are problems of reproducibility due to variation in bonds between transducer and sample. Also it may be noted that the PZT is a resonant transducer and that its output involves the convolution of its own frequency response with the input. Thus with pulsed inputs, there is a tendency for strong ringing in the output.

There has been a steady effort to develop non-contact transducers which are not subjected to the limitations as stated above. Accordingly, a number of non-contact techniques utilising either electromagnetic (EMAT), optical, electrostatic (capacitance), magnetostrictive or some combination of these effects can be used for generation and detection of ultrasound. However, EMATs are restricted in their use to conducting specimens or those with a conducting surface layer (Taylor *et al.*, 1990). Also, an accurate knowledge of the stand-off (distance between the test structure and EMAT), the electrical properties of the sample and the magnetic field distribution are required for its calibration (Dewhurst *et al.*, 1987). The magnetostrictive devices are only suitable for ferromagnetic materials (Scruby and Drain, 1990). The capacitance transducers require polished surfaces (Dewhurst *et al.*, 1982) and are not practical for industrial measurement (Scruby and Drain, 1990). In addition, the distance between the test structure and the EMAT cannot be more than a few tenths of a millimetre (Le Brun and Pons, 1987) and capacitance transducers need an air gap of 5-10  $\mu\text{m}$  (Tam,

1986; Dewhurst *et al.*, 1982), which in essence causes these devices to be treated as equivalent to contact ones (Green, 1987). The optical technique is free from the problems of other non-contact techniques and can be effectively used from a distance of a few metres. The unique features of the optical technique for remote generation and detection, which are very suitable for industrial applications, are the subject of this work. In this technique, a pulsed laser is used for generation of ultrasonic signals in the test sample and an interferometer is used for signal detection.

The detection of the laser generated ultrasonic pulses by non-optical methods has been demonstrated by a number of authors. PZT transducers (Von Gutfeld and Melcher, 1977a; Aindow *et al.*, 1980; Hutchins *et al.*, 1981b; Davis *et al.*, 1991), EMATs (Hutchins and Wilkins, 1985; Le Brun and Pons, 1987; Taylor *et al.*, 1990) and capacitance transducers (Scruby *et al.*, 1980; Hutchins *et al.*, 1981a; Dewhurst *et al.*, 1982) have been used for the detection of laser generated ultrasonics. A comparative study of the performances of different types of non-contact and contact transducers for detection of laser generated ultrasonic signals has been reported by Dewhurst *et al.*, (1987). The transducers investigated were: A modified bulk optic Michelson interferometer, EMATs with a stand-off of  $\sim 0.5$  mm from the target surface, capacitance with a 6 mm active area and an air gap of 10  $\mu\text{m}$  and a wide-band piezoelectric with a centre resonant frequency of 5 MHz and a bandwidth of 1 MHz. A Q-switched Nd:YAG laser with a pulse of 20 ns rise time and energy of 50 mJ, operating in the thermoelastic regime, was used as a reproducible standard acoustic source. This pulse did not produce any damage to the surface of the sample (Aluminium alloy disc of 50 mm diameter and 25.4 mm thick). It was found that the signal-to-noise ratios for identical compression waves were 16, 50, 6.6 and 90 for

interferometer, capacitance, EMAT and piezoelectric transducer respectively. Thus for this particular experiment, capacitance, interferometry and EMAT techniques are found to be 5, 15 and 23 dB less sensitive respectively than the piezoelectric transducers. Based on the data available from this experiment, the RMS noise equivalent displacements (NED) were calculated to be 8 pm, 2 pm, 15 pm and 1 pm for interferometer, capacitance, EMAT and piezoelectric respectively (Scruby and Drain, 1990). The risetimes of these transducers were not all the same but were in the range 20 ns - 80 ns. Considering the limitations of the piezoelectric and other non-contact transducers as outlined above, optical generation and detection is found to be very attractive for industrial application because the specimen may be examined remotely, rapidly and without the need for any coupling medium.

## **2.2 Generation of ultrasonics using a high power laser pulses**

The generation of ultrasonics using a pulsed laser has had a significant impact on ultrasonic testing since, in some situations, it offers a number of unique advantages over other techniques. It has the potential to replace the conventional piezoelectric transmitter with negligible loss of sensitivity in most practical non-destructive testing situations. It also offers a technique which is non contact, remote and of high resolution in space and time.

Where contact with the sample does not present any problems, most applications use piezoelectric effects to generate the ultrasonic waves. In other situations, an alternative method is to use thermoelastic excitation rather than the piezoelectric effect. The usual

method of exciting the thermoelastic stress comes from the absorption of the pulsed laser radiation. When a solid surface is illuminated by a laser light, a number of physical processes may take place, depending upon the incident power. At low incident power levels, heating, generation of thermal waves and elastic waves due to thermoelastic stress takes place. At higher incident power levels, ablation of material from the surface and formation of a plasma gives rise to vaporisation stress in the materials (Scruby and Drain, 1990).

### 2.2.1 Physical principle

The physical principles involved in the generation of ultrasonics using laser pulses are best understood by considering the processes occurring in metals. When a laser beam is incident on the surface of a metallic sample, a fraction of the energy is absorbed by the interaction of electromagnetic radiation with the conduction electrons at the surface. This process depends upon the electrical and magnetic properties of the material and the frequency of the radiation. The remaining energy of the laser beam is reflected or scattered from the surface. The absorption or reflection takes place within the layer close to the surface. The absorbed electromagnetic energy is converted to thermal energy resulting in a rapid rise in temperature, which in turn gives rise to transient thermoelastic stress and strain in a very thin surface layer as the metal tries to expand. The depth to which the beam penetrates is commonly termed the skin depth,  $\delta$ , which is given by (Silk, 1984)

$$\delta = \left( \frac{\lambda}{\pi \sigma c \mu \mu_0} \right)^{1/2}, \quad (2.2.1)$$

where  $\lambda$  is the wavelength of the incident beam,  $\sigma$  is the conductivity of the metal,  $c$  is the velocity of light,  $\mu$  is the permeability of the metal and  $\mu_0$  is the permeability of free space. As shown by Scruby *et al.* (1990), for optical frequencies up to those corresponding to visible light, the reflectivity  $\mathbf{R}$  for most of the metals is found to be approximately

$$\mathbf{R}=1-4/(\mu_0 c \delta \sigma). \quad (2.2.2)$$

Thus it can be seen that the degree of absorption of the laser beam in the metal will depend upon the irradiation wavelength, increasing at shorter wavelengths. As stated earlier, this absorbed energy mostly ends up as heat in the metal so that the laser irradiation induces a temperature rise in the surface layer. In the case of an insulator, depending upon the nature and magnitude of the absorption processes, the absorption tends to occur over a greater range of depths and the initial temperature rise is not confined to the surface layer. However, due to thermal conductivity, heat eventually becomes distributed throughout the sample in both cases (Scruby and Drain, 1990). With localised absorption, the temperature gradient induced sets up stress and strain fields by thermal expansion. These in turn generate elastic waves which propagate through the material in the form of longitudinal, shear and surface waves as shown schematically in the Figure 2.2.1. In subsequent figures, the arrival of the bulk longitudinal wave is indicated by a positive pulse (P) and/or a negative step (L). The arrival of the shear wave is seen by a sudden change of slope (S) in the waveform.

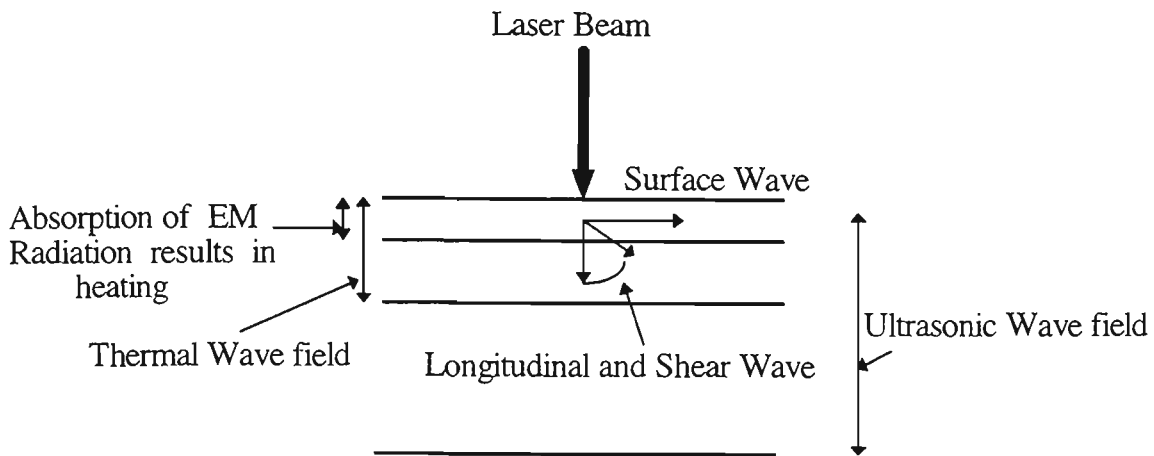


Figure 2.2.1 Physical processes involved in the generation of ultrasonics

### 2.2.2 Mechanism for the generation of ultrasonics

The mechanism for laser generated ultrasonics may be broadly divided into two categories: those that involve a change of state of the irradiated medium and those that do not. At low levels of incident power, the increase in temperature due to the laser pulse is sufficiently small to avoid any change of state in solid materials. The thermoelastic stress and strain generation are due to localised thermal expansions produced by the absorption of laser energy. At higher incident power levels above a certain threshold, a given medium may exhibit a change of state, which results in melting, vapourisation, ablation and plasma formation. A Q-switched laser pulse which can deposit enough energy in a sufficiently short time can act as both a source of thermoelastic energy and ablation energy. With a Q-switched laser pulse of moderate energy, the power density can be controlled by adjusting the irradiated area so that it can act as a non-damaging thermoelastic source of acoustic waves at low power densities and as an ablation source at higher power densities.

### 2.2.3 Thermoelastic effect: Thermal expansion stress

As discussed previously with low power densities, laser energy is absorbed strongly within a thin layer near the surface, which sets up thermoelastic stresses by thermal expansion within this zone. However the presence of the unconstrained surface implies that normal forces are small. Thus the horizontal dipolar forces are dominant and the lateral stresses act radially outward from the centre of the source. Under these conditions, the force dipole resulting from a Q-switched laser pulse has a step pulse shape and can be described using a Heaviside step function  $H(t)$  (Aussel *et al.*, 1988). The instantaneous temperature rise,  $\delta T$ , throughout the absorbing volume ( $V$ ) due to absorption of energy  $\delta E$  is given by (Scruby *et al.*, 1980)

$$\delta T = \frac{\delta E}{\rho V S} H(t), \quad (2.2.3.1)$$

where  $\rho$  is the density of the material and  $S$  is the specific thermal capacity of the material. Neglecting thermal conductivity and assuming  $\delta V$  as the thermal expansion in the volume  $V$  due to absorption of energy, the bulk strain is given by (Scruby *et al.*, 1980)

$$\frac{\delta V}{V} = 3\alpha\delta T, \quad (2.2.3.2)$$

where  $\alpha$  is the coefficient of linear expansion. Hence,

$$\delta V = \frac{3\alpha}{\rho S} \delta E H(t). \quad (2.2.3.3)$$

Thus the deposition of laser energy can be described as the elastic equivalent of the sudden insertion of an extra volume  $\delta V$  in the surface layer of the material. The factor  $3\alpha/\rho S$  is a property of the material and is known as thermoelastic coupling factor because it links absorbed energy to the elastic strain and it determines the efficiency of ultrasonic generation. It is interesting to note that raising the temperature of a sample leads to an increase in the value of this parameter and thus to increased efficiency in the generation of ultrasound (Scruby and Drain, 1990).

Neglecting the effect of the boundaries, the amplitude of the displacement ( $x$ ) caused by the ultrasonic wave field at a distance  $r$  from the strained region for most of the common metals can be shown to be (Scruby and Drain, 1990)

$$x = \frac{1}{6\pi c_{1,r}} \frac{\delta V}{\delta t} = \frac{\alpha}{2\pi\rho S c_{1,r}} \frac{\delta E}{\delta t}. \quad (2.2.3.4)$$

Where  $\delta E$  is the absorbed pulse energy which in the simplest case is assumed to be constant for the duration of the laser pulse,  $\delta t$  is the pulse length and  $c_1$  is the compression wave velocity. Thus the ultrasonic wave amplitude under thermoelastic conditions is directly proportional to the absorbed laser power. By substitution of the values of the material constants for aluminium in this equation, it can be shown that for generation of reasonable ultrasonic wave amplitudes ( typically 0.1 nm at a distance of

100 mm), an instantaneous laser power of greater than 0.1 MW is required. A pulsed laser which can deliver instantaneous optical power of this magnitude for the duration of the pulse is used in laser generation of ultrasonics.

For the convenience of calculating the effects of elastic wave propagation,  $\delta V$  can be expressed as the distribution of edge dislocation loops (Sinclair, 1979), with equal numbers in the three orthogonal directions; i.e., at large distances from the source, it is equivalent to three coincident loops,

$$b_1 A_1 = b_2 A_2 = b_3 A_3 = 1/3 \delta V \quad (2.2.3.5)$$

where  $b_i$  and  $A_i$  ( $i = 1,2,3$ ) are dislocation-loop Burger vectors and areas respectively (Scruby *et al.*, 1980). Because the irradiated volume is at the metal surface, i.e., a normal stress-free boundary, the thermoelastic stress in the  $z$  (normal) direction is zero, leaving finite  $x$  and  $y$  stress components. The above treatment is rather simplified and is given to highlight the basic physics behind the processes. A much more detailed treatment has been given in the literature which adequately described the theoretical models and all the effects observed experimentally (Knopoff, 1958; Achenbach, 1973; Sinclair, 1979; Rose, 1984; Hutchins and Tam, 1986; Doyle, 1986; Aussel *et al.*, 1988; Scruby and Drain, 1990).

Acoustic wave propagation theory has been applied in order to link the measured surface displacement waveforms to the properties of the acoustic source formed by the laser irradiation. This is covered below and the treatment mostly follows that of Scruby *et al.* (1980). This theory involved the calculation of the dynamic elastic Green's

tensor for the sample. The sample used for this study was a parallel sided disc with a diameter much greater than its thickness so that it can be approximated to an infinite plate (Scruby *et al.*, 1980). They calculated the epicentral acoustic displacement at the far side of the sample by using the Green's function for an infinite plate as given by Sinclair (1979). The normal surface displacement at the epicentre ( $U_3$ ) can be expressed in terms of Green's Function ( $G_{3i,j}$ ) and the strength of a force dipole ( $D_{ij}$ ) (Scruby *et al.*, 1980) by

$$U_3 = G_{3i,j} D_{ij}, \quad (2.2.3.6)$$

where, in this and succeeding equations, the usual summation convention is assumed. The distribution of force dipoles was related to the distribution of dislocation loops through the elastic constants,  $C_{ijkl}$ , i.e.,

$$D_{ij} = C_{ijkl} b_k A_l \quad (2.2.3.7)$$

$$U_3 = G_{3i,j} C_{ijkl} b_k A_l \quad (2.2.3.8)$$

$$U_3 = G_{3i,j} C_{ijkl} X \frac{1}{3} \delta V \quad [\text{From 2.2.3.5}] \quad (2.2.3.9)$$

$$= G_{3i,j} (\xi \delta_{ij} + 2\psi \delta_{ik} \delta_{jk}) X \frac{1}{3} \delta V, \quad (2.2.3.10)$$

since (Achenbach, 1973)

$$C_{ijkl} = \xi \delta_{ij} \delta_{kl} + \psi (\delta_{ik} \delta_{jl} + \delta_{il} \delta_{jk}), \quad (2.2.3.11)$$

where  $\xi$  and  $\psi$  are the Lamé constants and  $\delta_{ij}$  is the Kronecker  $\delta$ .

Hence,  $U_3$  can be written as,

$$U_3 = G^H_{3m,m} (\xi + 2/3 \psi) \delta V \tag{2.2.3.12}$$

$$= G^H_{3m,m} (\xi + 2/3 \psi)(3\alpha/\rho S) \delta E, \tag{2.2.3.13}$$

where  $G^H_{3m,m}$  is the appropriate Green's function for a Heaviside function source. Assuming a point source and neglecting thermal conductivity, the computed waveform generated at the epicentre of a plate is shown in the Figure 2.2.2.1. This simulated waveform predicts an overall depression of the surface at the epicentre. The primary difference between this prediction and the experimental waveform is that the theory does not predict a small positive pulse which is observed at the commencement of the waveform immediately prior to the surface depression.

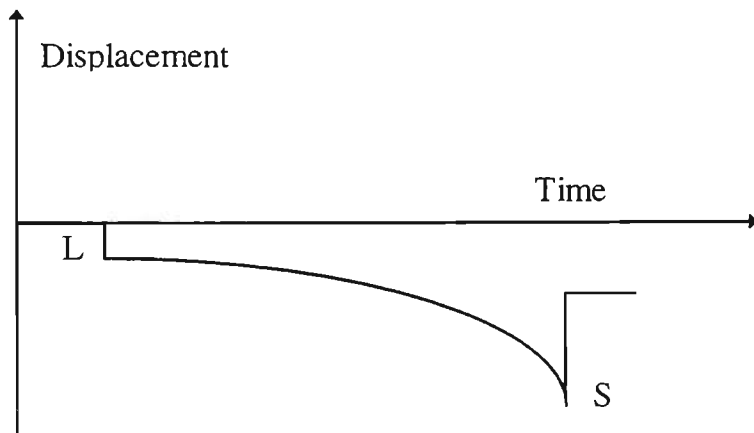


Figure 2.2.2.1 Theoretical displacement waveform calculated assuming the source to be a point expansion at the surface of an infinite plate.

Taking into consideration the fact that the acoustic source extends over a finite distance into the solid and is not confined to the surface, Doyle (1986) has addressed this problem rigorously and has confirmed that the initial spike is indeed due to the effect of thermal diffusion. The theoretical displacement waveform, after considering the effects of thermal diffusion, is shown in Figure 2.2.2.2

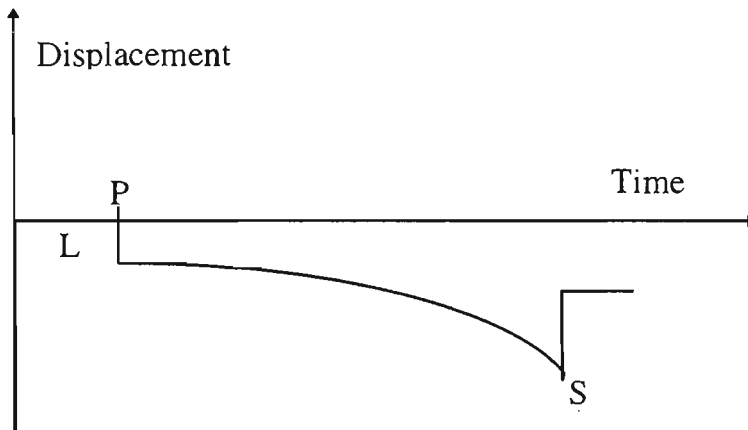


Figure 2.2.2.2 Theoretical displacement waveform calculated assuming the source to be due to a point expansion at the surface and allowing for thermal diffusion into the plate.

#### 2.2.4 The ablation effect: Vaporisation stress

With a high power density laser pulse, the increase in absorbed power gives rise to melting and then to vaporisation of a small quantity of material from the surface (Aussel *et al.*, 1988). A metal plasma is formed above the surface of the material due to the combination of ablation of surface material and high instantaneous temperature caused by absorption of the laser radiation in this ablated material (Silk, 1984). It is worthwhile noting the following physical effects which are caused by plasma generation in association with ablation (Scrubby and Drain, 1990). The vaporisation of

the material is suppressed by raising the boiling point well above its normal value, because of the high pressure exerted by the plasma. The plasma acts to shield the surface from further incoming radiation and becomes extremely hot as it absorbs light from the laser pulse and then produces an impulse reaction on the surface as it expands. Finally some of the plasma heat is radiated back to the surface, maintaining the high surface temperature for some time after the incident laser power has started to fall.

The vaporisation introduces a mechanical recoil in the surface of the material specimen and thereby provides a more direct source of elastic energy than the thermoelastic effect (Silk, 1984). Although the net production of elastic energy in the ablation regime is substantially greater than that produced by the thermoelastic effect, the net elastic energy depends on the balance of the subsequent effects caused by the plasma as outlined above (Silk, 1984). Ablation and plasma formation occur rapidly within the rise time of the incident laser pulse (typically  $\sim 10$  ns) and once established, the plasma formed by this type of laser decays away over a time of  $\sim 1$   $\mu$ s (Hutchins *et al.*, 1981a). The plasma continues to supply heat to the metal surface during this extended period and maintain it at a sufficiently high temperature for continued ablation of the material. Thus the surface initially undergoes rapid depression due to a step like force from ablation and remains depressed for several microseconds until the metal surface cools below its vaporisation temperature (Hutchins *et al.*, 1981a). The acoustic source in the ablation regime is thus expected to comprise a time varying normal force in addition to the lateral dipolar forces generated by the thermal expansion and there will be a large positive displacement of the surface in this regime which was absent in the thermoelastic regime (Dewhurst *et al.*, 1982). It may be noted that the thermal

expansion which accompanies ablation can generally be neglected at the high power densities because thermoelastic stresses are much smaller than the recoil stress generated by ablation. At higher power densities, due to the formation of plasma the acoustic source can be considered to be dominated by a normal force monopole with a time dependence that approximates to a step function (Hutchins *et al.*, 1981a).

It is difficult to calculate the amplitude of the ultrasonic wave field under ablation conditions with a laser pulse of finite duration, because under these conditions the thermal constants of the material (particularly absorption coefficient) are no longer constant as a function of temperature. Also for an irradiated area of finite size, rapid vaporisation of the molten material can cause a portion of this material to be ejected while still in liquid phase. This further increases the amplitude of normal stress due to vaporisation (Aussel *et al.*, 1988).

Ready (1973) and Krehl *et al.* (1975) analysed the temperature rise and subsequent rate of vaporisation in a material surface irradiated with a high powered laser radiation. Following these analyses, Scruby and Drain (1990) estimated the depth of heat penetration, the surface temperature (neglecting phase changes at the surface and the complexities of the plasma/light interaction), the net stress produced by the recoil momentum following the ablation of material from the surface and the net ablative force. The maximum acoustic displacement  $x_{ab}$  produced at a distance  $r$  from the source under ablation conditions is estimated to be (Scruby and Drain, 1990)

$$x_{ab} \approx \frac{F}{2\pi\rho c_l^2 r}, \quad (2.2.4.1)$$

where  $F$  is the ablative force.

At moderately high power densities, the material temperature drops rapidly to below its vaporisation temperature after the end of each laser pulse and as a result, the normal stress is pulsed. However, at very high power densities, vaporisation continues for a long time even after the end of the laser pulse. Thus in order to model the ablation regime, the force caused by the vaporisation will be assumed to act normal to the surface and to vary as either a pulse  $\delta(t)$  or as a step  $H(t)$ , depending on the power density. Scruby and Drain (1990) modelled the epicentre waveforms in the ablation regime as a point force acting normal to the irradiated surface. Using an analysis similar to that in section 2.2.3, it can be shown that the normal rear surface displacement  $U_3$ , generated at the epicentre of a parallel plate in response to a normal point force excitation  $F_3$ , is given by (Dewhurst *et al.*, 1982)

$$U_3 = G_{33} F_3, \quad (2.3.4.1)$$

where  $G_{33}$  is the appropriate Green's function. The acoustic waveform with a combination of  $\delta$  function source (normal force) and centre of expansion, used for modeling the onset of ablation is shown in Figure 2.2.4.1. The corresponding waveform obtained using a Heaviside function source appropriate to very high power ablation situations is shown in Figure 2.2.4.2.

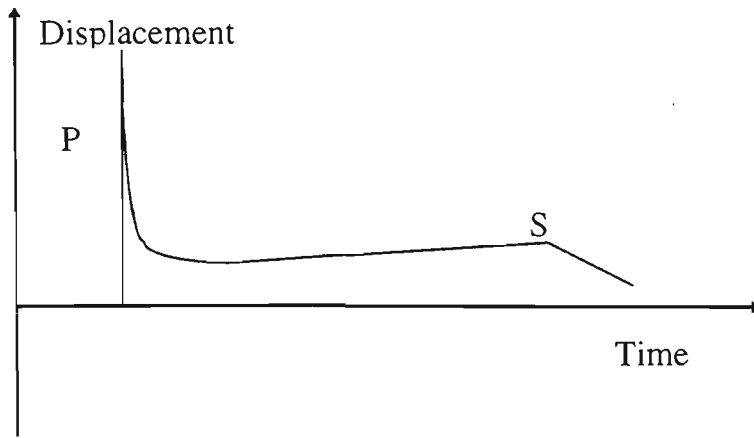


Figure 2.2.4.1 Epicentre waveforms calculated by assuming the acoustic source to be a combination of normal force and centre of expansion (low power density ablation).

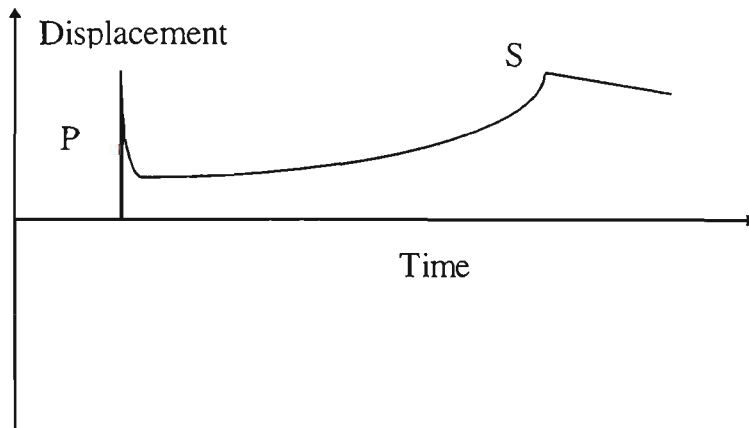


Figure 2.2.4.2 Epicentre waveform assuming the acoustic source has a Heaviside time dependence (high power density ablation).

### 2.2.5 Radiation pattern for laser ultrasonic sources

The laser generation of ultrasound takes place at or close to the surface of most solids and the effect of laser irradiation in the thermoelastic regime is equivalent to the rapid introduction of an extra volume. The source is thus a pure expansion and would give rise simply to a spherical compressional wave if situated in the bulk of the material.

However, since the source is very close to the surface, surface reflection allows mode conversion of compressional (longitudinal) waves into shear waves which are thus also radiated (Silk, 1984). The wave equation for the general case of longitudinal and shear wave propagation has been solved by Graff (1975) and following these equations, Scruby and Drain (1990) have derived an expression for the directivity pattern of acoustic waves produced by thermoelastic and ablation sources. These calculated directivity patterns were compared with the experimental patterns of Hutchins *et al.* (1981c) and excellent agreement was obtained. The angular directivity pattern of the thermoelastically-produced longitudinal wave is found to be maximum at angles in the region of  $60^\circ$  to the surface normal and the longitudinal wave amplitude is minimum in the direction normal to the specimen surface (epicentre direction) due to destructive interference between the direct wave and that reflected from the front surface (Silk, 1984). In fact, if the source were actually at the surface the longitudinal wave, amplitude would be zero at the epicentre. Since thermal diffusion gives rise to an effective source just below the surface, the cancellation of direct and reflected waves is not complete and a small positive pulse is observed as mentioned earlier. The important point to note is that if one is measuring only in the thermoelastic regime, then the epicentre is a very poor place to make observations as the longitudinal wave amplitudes are small and one primarily sees the negative step produced by having laser-induced thermal stresses in only the two lateral directions.

The amplitude of shear waves in the thermoelastic regime shows a rather narrow-lobed directivity pattern with zero amplitude in the epicentre direction and a maximum at an angle of about  $30^\circ$  to this direction.

Scruby and Drain (1990) estimated the directivity pattern of the laser ablation source by considering that it produces a simple recoil force over a small area. It was found that the longitudinal wave directivity pattern consisted of a single broad lobe with a maximum in the direction normal to the surface. The shear wave amplitude is zero in the normal (epicentre) direction and a maximum at angles greater than  $30^{\circ}$  to this direction. Thus when observing the arrival of longitudinal waves in the ablation regime, the epicentre is an excellent point at which to make observations.

### **2.2.6 Surface modifications**

As mentioned above, the effective acoustic source in the thermoelastic regime is generally in the surface region of the specimen and it is found that the surface modification affects the nature of the acoustic energy generated (Silk, 1984). These effects tend to occur either because the effective source occurs at a greater depth or by changing the nature of the reflection from the surface. Constraining the surface allows stresses to exist which are normal to the surface. The effects of a variety of liquids on metal surfaces have been studied (Von Gutfeld and Melcher, 1977a; Hutchins *et al.*, 1981b) and it has been shown that there is an increase in longitudinal wave amplitude at the epicentre and that the longitudinal wave arrival pulse becomes very similar to that produced by a plasma ablation source. It has also been shown that its directivity pattern is modified and brings it closer to that of an ablation source. Scruby and Drain (1990) have discussed four techniques for modifying the surface of the sample: Surface coating and roughness, transparent solid covering, transparent liquid covering and constrained liquid. It was found that all four techniques introduce large stresses normal to the surface, which were absent for the free surface. Thus the acoustic field

generated by a constrained surface source is similar to that of an ablation source, but at lower power densities and without any surface damage.

### **2.2.7 Characteristics of pulsed lasers for ultrasonics generation**

The main technical criteria in choosing a suitable pulsed laser for ultrasonic generation in any application depends upon certain principal characteristics of the laser, namely optical wavelength, pulse energy and beam profile, pulse width and the pulse repetition rate.

**Optical wavelength:** The optical wavelength of the laser is related to the reflectivity of the solid surface as shown in the equation 2.2.2, and hence to the efficiency with which the incident radiation energy is converted into elastic energy. Thus short wavelength laser sources are more efficient for the generation of ultrasonics. However, it may be noted that absorption also depends upon the surface condition so that a rough or blackened surface increases the efficiency at all wavelengths. The other factor which can influence the choice of laser is safety issues. The long wavelength CO<sub>2</sub> laser, although less efficient for ultrasonic excitation, is also less dangerous. This is because a higher power density is required for eye damage at this wavelength and the radiation is strongly attenuated by glass and many other materials.

**Pulse energy and beam profile:** As discussed in section 2.2.2, pulse energy (for a given spot size) is an important factor in determining the characteristics of ultrasonics generated in the thermoelastic or ablation regime. Standard optical means may be used to change the spatial profile of the laser pulse to meet the requirements of the application.

**Pulse width:** The generation mechanism and the characteristics of the ultrasonics is influenced by the duration of the laser pulse. A short pulse is necessary to deposit high instantaneous power in a small localised region for the generation of useful ultrasonic wave amplitude. The required pulse width of the laser can be estimated by assuming that the ultrasonic pulse has the same profile as the optical pulse. If the pulse is assumed to be Gaussian, then the time domain and the frequency domain representations are both Gaussian. A Gaussian pulse can be expressed in the form of  $\exp. (-t^2 / 2\sigma^2)$ , where  $\sigma$  is the standard deviation. The Fourier Transformation of this pulse is proportional to  $\exp (- 2\pi^2\sigma^2f^2)$ . This Fourier Transform falls to half of its maximum amplitude value, ie. -6 dB power, at a frequency of

$$f (-6 \text{ dB}) = 0.187/\sigma. \quad (2.2.5.1)$$

Thus if  $f (-6 \text{ dB}) = 10 \text{ MHz}$ , to ensure appreciable energy at ultrasonic frequencies, the pulse width (expressed as the standard deviation) must be approximately 20 ns (Scruby and Drain, 1990). Thus a Q-switched solid state laser, which tends to have a pulse length of about this value, is likely to be very suitable for ultrasonic generation.

**Repetition rate:** The repetition rate depends mostly on the intended application. A high repetition rate has the advantage of allowing rapid signal averaging to improve the signal-to-noise ratio, but is useless in those applications where there is ultrasonic reverberation because ultrasonic waveforms from the successive pulses may overlap. Also power dissipation considerations tend to limit the pulse energy of such lasers. However, repetition rates of 1-100 Hz are suitable for most of the ultrasonic

applications. Again, Q-switched solid state lasers tend to have pulse repetition rates in this region.

### **2.2.8 Review of previous work on laser generation of ultrasonics**

A number of authors have demonstrated and characterised the generation of ultrasonics in different metals and non metals and its application to materials characterisation. These studies were based on pulsed lasers with characteristics similar to those outlined in the previous section.

Generation of elastic waves in various materials under several transient heating conditions produced by the partial absorption of energy from a pulsed source was first demonstrated by White (1963). White used a variety of sources including electron beams, pulsed microwaves, a stroboscope and a pulsed ruby laser. The effects due to absorption of high power pulsed laser radiation at opaque surfaces were described by Ready (1965). In describing the generation of elastic waves, White and Ready assumed that the heat flow is one dimensional, that the dimensions of the laser beam are large compared to the depth of penetration of heat during the pulse, and that the laser power density on the target surface is constant over the illuminated area. However, recent work has treated the generation of elastic wave fields by a laser source in three dimensions since for use as an ultrasonic source, the laser pulse diameter is likely to be much smaller than the ultrasonic propagation paths (Scruby and Drain, 1990) and thus the effects are better approximated by considering a point source.

A preliminary investigation on the optical excitation and detection of nanosecond acoustic pulses for non-destructive testing was described by Bonderenko *et al.* (1976).

They reported the use of a Q-switched ruby laser with pulse widths of 30-50 ns and power up to 50 MW as an excitation source for short acoustic signals. The laser pulse was focussed onto the surface of a stainless steel plate of 1 cm thick and the acoustic signal was detected on the opposite surface by a bulk optic dual-beam interferometer with a sensitivity of 1 nm and a bandwidth of 5 kHz to 150 MHz. The device was reported to be useful for practical application in thickness gauging, high-resolution flaw detection and determination of the velocity of sound and elastic modulus for the target material.

Von Gotfeld and Melcher (1977a and 1977b), reported the generation of acoustic waves from pulsed thermoelastic expansion of constrained surfaces with sufficiently large elastic amplitudes in the megahertz frequency range for applications in non-destructive testing. The constrained surface condition was achieved by bonding a piece of transparent polished quartz plate onto the optically absorbing surface of an aluminium or Ge block. A nitrogen laser of 337.1 nm wavelength and pulse width of 10 ns and a nitrogen-laser-pumped rhodamine 6G laser with wavelength of 580 nm and pulse width of 5 ns were used as the excitation sources. The laser pulses were focussed onto a variety of constrained and free metal surfaces. The acoustic waves at the opposite surface were detected by a piezoelectric transducer. An increase of up to 46 dB in elastic wave amplitude was recorded in a constrained surface when compared to that of a free surface. With this large amplitude enhancement technique, they demonstrated the detection of acoustic waves in a structure designed to simulate a laminate. The target structure in this experiment was an aluminium cylinder with polished ends of diameter 1.6 cm and length 1 cm. The target surface was one of the ends on which a 4 mil thick microscope cover slide was acoustically bonded.

Budenkov and Kaunov (1979) presented both predicted and experimental data on the dependencies of displacement amplitudes and elastic wave stresses as a function of the relevant parameters of the exciting laser pulse. The excitation source was a ruby laser of wavelength 694.3 nm, pulse energy of 0.4 J and pulse width of 30 ns. The experimental data obtained by using EMAT and PZT transducers was compared with theoretical data based on one dimensional analysis. They also described an experimental arrangement for obtaining the relationship between the amplitude of elastic displacements and temperature at the epicentre of a hot metallic plate.

Aindow *et al.* (1980) discussed the characteristics of a laser-generated acoustic source in metals based on measurements carried out using a Q-switched Nd:YAG laser of 17 ns pulse duration with output energies up to 60 mJ and a piezoelectric ceramic transducer. The generation of longitudinal, shear and surface waves in aluminium and steel, without prior modification to the surface, were demonstrated at low laser pulse energies. The variation of generation efficiency with laser energy and power density were also described. It was observed that in the non-plasma regime, the amplitude of the longitudinal and shear pulses were proportional to the laser energy. In the plasma regime, ablation of the material away from the surface of the metal and expansion of the plasma caused a momentum pulse to be transmitted to the solid which enhanced the longitudinal pulse normally generated by thermal effects. The shear pulse amplitude was observed to be a maximum at a given laser power density within the plasma regime and at higher power densities, the generation efficiency of the shear pulse amplitude was found to decrease. Aindow *at al.* attributed this behaviour to a decoupling of laser energy to lateral thermal gradients within the solid due to the presence of the plasma. They postulated a decrease in the lateral and normal

temperature gradients in the acoustic source due to plasma shielding. For the case of a longitudinal pulse, this effect was masked by momentum transfer. Using three different laser sources (Nd:YAG, CO<sub>2</sub> and KrF lasers of wavelength 1064 nm, 10.6 μm and 249 nm respectively), they confirmed that in the thermoelastic regime, the amplitude of the measured signals varies inversely with the laser wavelength. No decrease in longitudinal pulse amplitude at very high laser power densities was observed.

A study on the acoustic waveforms generated by a pulsed laser in a 25 mm thick aluminium alloy disc and a quantitative comparison with theory was reported by Scruby *et al.*, (1980). The experimental measurements involved a study of the thermoelastic generation of elastic waves by an unfocused multimode Q-switched Nd:YAG laser of pulse width 24 ns and pulse energy  $\leq 60$  mJ at 1064 nm. The acoustic waveforms were recorded by a wideband calibrated capacitance transducer. It was observed that the thermoelastic source generated both longitudinal and shear waves and at the epicentre, the normal displacement amplitude of the shear wave is about four times that of the longitudinal wave. Both types of wave amplitudes were found to be proportional to the incident energy in the laser pulse. The longitudinal displacement was approximately 1 pm with an incident energy of 1 mJ. The detected waveforms were highly reproducible and to a first approximation were independent of small changes in the spatial profile and area of the laser pulse at constant energy. A theoretical model was developed from these measurements by considering the thermoelastic source as the instantaneous expansion of a point volume of metal at the surface. Most of the features of the measured waveforms can be predicted by this model except the detailed time dependence of longitudinal and shear arrivals, because

it neglects thermal diffusion and the finite dimension of the source. It was estimated from the acoustic measurements that about 9% of the incident radiant energy was absorbed and converted into elastic waves. This figure was in good agreement with that obtained from independent reflectivity data.

Hutchins *et al.* (1981a, 1981b and 1981c) investigated a laser generated acoustic sources in metals and modified metal surfaces using a Q-switched Nd:YAG laser of 24 - 27 ns pulse width and energy of up to 40 mJ. Using capacitance transducers, they reported the detection of acoustic displacement waveforms generated in aluminium and mild steel discs of thickness 25 mm and 18.4 mm respectively and also compared the generation at modified and free surfaces at different optical power densities. The metal surface was modified by using constraining layers and coatings. The changes in the generation efficiency and directivity pattern of the acoustic waveforms on different surfaces were also demonstrated. The underlying generation mechanisms responsible for three different types of acoustic source were discussed. These sources were characterised by a horizontal force dipole and a normal force monopole, each with step-function time dependence and a normal force monopole with  $\delta$ -function time dependence. Their results have shown that it is possible to produce three types of standard acoustic source behaviour using laser generation.

Dewhurst *et al.* (1982) extended the quantitative investigation of Scruby *et al.* (1980) to study acoustic generation in metallic samples over a wide range of laser power densities which included those high enough to form a plasma on the target surface. The effect of modifying the metal surface (by bonding a glass slide on the surface) was also examined. A Q-switched Nd:YAG laser with a pulsed energy of 40 mJ and a pulse

duration of 27 ns was used to generate the ultrasonic waves. The laser power was incident on a 25 mm thick aluminium disc and the power density was varied by movement of a 10 cm focal length plano-convex in front of the target surface. Using a capacitance transducer for detection, they reported quantitative measurements of the bulk acoustic waves in the sample. It was observed that in the ablation regime, the amplitude of longitudinal pulses increased and that of the shear pulses decreased with increasing power density. As the power density was increased further so that a plasma spark was clearly visible, the amplitude of the longitudinal pulse went through a maximum and subsequently decreased. The step normally observed at the time of arrival of the shear wave virtually disappeared to become simply a change in slope. Another series of experiments were conducted to examine the effect of varying optical energy at a constant power density. Under these conditions the amplitude of each waveform was a linear function of the incident laser energy. A theoretical model was developed to link the measured surface displacement waveforms with the properties of the laser-generated acoustic sources by the application of acoustic wave propagation theory and the appropriate Green's function. The observations were restricted to the arrival of acoustic waves at the epicentre. The measured experimental data closely followed the waveforms produced by the theoretical model using thermoelastic and normal force sources. It was also found that the normal force component varies temporally with power density and becomes more asymmetric with increases in power density. At sufficiently high laser power densities, the time dependence of the force approached a step-like function. The effects of the modification of the incident metal surface with a transparent liquid or solid layer were also studied. It was demonstrated that the modifications significantly enhanced the longitudinal wave at the epicentre.

This was interpreted in terms of generation of an acoustic source where forces normal to the surface predominated.

A number of experiments which combined laser generation and interferometric detection of ultrasonic pulses in metals have been described by Hutchins and Nadeau (1983). Single pulses from a Q-switched Nd:YAG laser operating at 1064 nm with a pulse width of 15 ns and energy of 0.86 J were incident upon a 10 mm thick aluminium plate. The acoustic waveforms were detected at the epicentre with a bulk optic Michelson type interferometer incorporating a 5 mW laser by polishing the detection surface. The sensitivity of the interferometer was reported to be 0.02 nm in a bandwidth of 40 MHz. The detected waveforms obtained in the thermoelastic and ablation regimes and also at modified surfaces were in good agreement with the prediction of wave propagation theory. These authors were the first to demonstrate that all-optical remote generation and detection of ultrasonics was possible in a single system.

Tam (1984) reported the generation and detection of the ultra-short acoustic pulses from a stainless steel film of thickness ranging from 12 to 260  $\mu\text{m}$ . A 337 nm Nitrogen laser having a pulse width of 0.5 ns and energy of 1 mJ was used as an excitation source in this experiment. The acoustic pulses were detected by a transducer which consists of approximately 5  $\mu\text{m}$  thick ZnO film placed between 100 nm thick gold electrodes which was coupled to the sample via a single crystal sapphire rod. It was demonstrated that thickness measurement with an accuracy of 1% for the 12  $\mu\text{m}$ -thick stainless steel film is possible once the ultrasonic velocity in stainless steel is known. In another experiment, Tam and Leung (1984) have reported the measurement of the

small elastic anisotropy in commercial bars of an aluminium alloy of 4.76 mm or 9.6 mm thickness using laser-induced ultrasonic pulses. A nitrogen laser with a pulse duration of 8 ns and energy  $<1$  mJ was used as the excitation source and a polyvinylidene difluoride (PVF<sub>2</sub>) piezoelectric transducer as a receiving transducer. It was demonstrated that a single laser-induced acoustic pulse propagation measurement over a path length of 47 mm provided a longitudinal ultrasonic velocity measurement with an accuracy of 0.02%. The longitudinal velocities at  $\pm 45^\circ$  from the extruding direction Z were found to be 2% larger than the velocity along Z, indicating that most of the aluminium crystallites were oriented with a principal axis parallel to Z.

The development of a non-contact technique for ultrasonic inspection and testing of a conducting sample, based on laser generation and EMAT detection, was described by Hutchins and Wilkins, (1985). In this work, a 347 nm Q-switched frequency-doubled ruby laser with a pulse width of 30 ns and energy of  $\leq 225$  mJ was used to excite acoustic waves in 25 mm or 50 mm thick parallel-sided metallic plates of aluminium or steel.

Low energy optical generation and detection of acoustic pulses in metals and non-metals (composite) for a potential portable NDE system was described by Bourkoff and Palmer (1985). They used the focused beam of a 595 nm tunable dye laser of pulse width 6 ns and energy varying from 20-210  $\mu$ J for generation together with a calibrated laser interferometer for detection (sensitivity of about 50 pm over a 10 MHz bandwidth). A thin glass slide bonded with India ink to the top surface of the 63.5 mm thick Aluminium target plate was used to increase the longitudinal wave signal at the epicentre by allowing normal surface forces and by increasing the absorption of laser

energy. The arrival of longitudinal waves were also detected without any surface modification in a 6.33 mm thick polyamide-glass fibre composite and a graphite epoxy composite of same thickness. These measurements were made with a laser energy of 66  $\mu\text{J}$  and a rather high power density of 3.5.GW/cm<sup>2</sup>. These authors also showed data could be usefully recorded with a receiver bandwidth of 1 MHz.

Vogel and Bruinsma (1987) used a Q-switched Nd:YAG laser with a pulse width of 15 ns to generate acoustic waves in aluminium targets and a PZT transducer to detect these waves. The study concentrated on the directivity pattern of the laser generated longitudinal and shear waves in the thermoelastic regime. The maximum amplitude of the longitudinal waves at the detector occurred at an angle of around 60° to the epicentre direction. The corresponding maximum for the shear waves occurred at an angle of 30°. Results are also presented on the control of beamwidth and the directivity pattern of the laser generated ultrasonic beam by using a fibre optic phased array to deliver the pulsed laser beam on the target surface.

An experimental set-up used for comparing the performance of an interferometer with other ultrasonic transducers for the detection of laser generated ultrasonics in thermoelastic regime has been described by Dewhurst *et al.*, (1987). A Q-switched Nd:YAG laser with a rise time of 20 ns and pulse energy of 50 mJ was used to irradiate an aluminium alloy disc (50 mm diameter and 25.4 mm thick) in this arrangement. The results of this experiment have been discussed in section 2.1.

Generation of a train of acoustic pulses with a high repetition rate by repetitively Q-switching a Nd:YAG laser during a single flash lamp pulse was reported by Wagner *et*

*al.* (1988). This system used 10 Q-switched pulses, of energy 5 - 15 mJ, spaced at an interval of 18.7  $\mu\text{s}$  to generate repetitive acoustic pulses in the ablation regime. The spectrum of the multiple excitation source is dominated by a narrow peak at the pulse repetition frequency. This increased the amplitude of the acoustic signal at this frequency and also permitted narrow bandwidth detection. This multiple Q-switching method of excitation is similar in principle to the PZT toneburst technique and the overall result is significantly enhanced sensitivity in situations where high temporal resolution is not required (the overall source pulse length is  $\sim 200 \mu\text{s}$ ).

A treatment of various theoretical models describing the acoustic displacements generated by a point laser impact in different excitation regimes was described by Aussel *et al.*, (1988). These models were then validated by measurements of the ultrasonic displacements generated under both ablation and thermoelastic conditions. A Michelson type laser interferometer was used to measure the displacement waveforms. A Q-switched Nd:YAG laser operating with a pulse duration of 10 or 20 ns and a maximum energy of 330 mJ was used as an excitation source. The incident energy density was adjusted by using a set of lenses and calibrated optical attenuator to vary the incident power densities from 8  $\text{MW}/\text{cm}^2$  to 1870  $\text{MW}/\text{cm}^2$ . The investigations were carried out on steel and aluminium plates and half cylinders of different dimensions. Under ablation conditions, they demonstrated that the acoustic displacement was a maximum at the epicentre while under thermoelastic condition, the maximum occurred well away from this direction. The shape of the waveforms under thermoelastic conditions did not change significantly with varying energy but under ablation conditions, the waveform shapes were found to vary considerably with the power density of the incident laser pulse.

A Q-switched Nd:YAG laser (Laser Dynamics Limited NL - 100) with a pulsewidth of 25 ns and a variable pulse energy of 5 - 80 mJ was used by Scala and Doyle (1989) to generate surface acoustic waves in the thermoelastic regime. A wideband PZT sensor was used for the detection of the surface waves to establish a quantitative basis for the application of laser ultrasonics in the non destructive evaluation of material surfaces. This ultrasonic system was used by the authors (Doyle and Scala, 1993) for the determination of the elastic constants for a boron-epoxy plate and also to calculate complex interface wave velocities for the case of this plate bonded to various metallic substrates.

A precision method of ultrasonic velocity measurement and elastic constant determination in PZT ceramic, metal-ceramic composites and single crystal germanium has been described by Aussel and Monchalin (1989). A pulsed Nd:YAG laser that provides 10 ns pulses of 0.75 J maximum energy was used for ultrasonic generation in the thermoelastic and slight ablation regime and a laser interferometer was used for the detection of the acoustic displacement. The ultrasonic velocities were measured by crosscorrelation of consecutive echoes and it was reported that with this technique, reliable and reproducible results were obtained even with the poor signal-to noise ratios.

Using a single pulse up to 8 mJ in 30 ps from a mode-locked Nd:YAG laser Dewhurst and Al'Rubai (1989) demonstrated the generation of ultrasound in a 250  $\mu\text{m}$  thick aluminium sheet. Ultrasound detection was achieved by using either a PVDF transducer or by a laser interferometer. Much shorter ultrasonic pulses generated by

this type of laser pulses may be used to study structural effects in new materials (Scruby and Drain, 1990).

Edwards *et al.*(1989) reported the use of a high powered TEA-CO<sub>2</sub> laser of 10.6 μm wavelength, rise time of 50 ns and energy of 1 J to generate ultrasonic transients in metal using an air breakdown method. In this method, the laser beam is focused to a point in air just above the surface of the metal and as a result, the air breaks down to form a plasma. A detonation wave is generated in the air which strikes the surface of the specimen and causes a normal force which in turn acts as a source of ultrasonic waves in the solid. The force exerted on the surface is an impulse and thus the acoustic source resembles that generated by ablation of material from the surface. There is no damage to the surface of the specimen which makes the technique suitable for NDE. The air break down method is particularly useful with this type of laser because the high reflectivity of metals at this wavelength means that there is essentially no surface absorption.

Using the same technique, Taylor *et al.* (1990) reported the generation of ultrasonics in non-metals by using an industrial TEA-CO<sub>2</sub> laser operating at 10.6 μm with energy of about 1 J and a pulse rise time of 50 ns. Interferometer and EMAT detectors were used for acoustic wave detection at different incident power densities. This paper described three types of generation mechanism: thermoelastic, ablation and plasma breakdown just above the metal surface and presented theoretically calculated acoustic waveforms to match those recorded experimentally.

Davis *et al.* (1991) reported the generation and detection of ultrasonic waves for the purpose of ultrasonic velocity determination using an optical fibre for delivery of the laser pulse. A 600  $\mu\text{m}$  core fibre was used to deliver light pulses from a Q-switched Nd:YAG laser (details not available) to the top surfaces of a metallic plate, an epoxy plate and a curing epoxy specimen. The acoustic detection system was a fibre optic Michelson interferometer, the sensing arm of which was embedded in the curing epoxy specimen.

Using a Q-switched Nd:YAG laser operated at 1.06  $\mu\text{m}$  with nominal pulse energy of 85 mJ and duration of 10 ns, Hrovatin and Mozina (1993) used optical and acoustic detection to demonstrate evidence of plasma shielding by focusing the laser pulse at varying depths within and above the specimen. They also presented data on how the air breakdown and plasma absorption may affect optoacoustic measurements at high beam intensities. The same authors (Mozina and Hrovatin, 1996) reported the detection of low intensity XeCl excimer laser-induced ultrasonic displacement amplitudes of about 10 pm using a bulk optic Michelson interferometer. Sub-picometre displacements could be measured using a PZT transducer. Details of the excimer laser were not available.

A summary of previous work on the generation of ultrasonics using different types of laser is shown in Table 2.2.6.1

Type of Laser	Wavelength	Pulse Energy	Pulse width	Target
Ruby (Bondarenko <i>et al.</i> 1976)	694.3 nm	Not quoted	30-50 ns	Stainless steel plate (1 cm thick)
Ruby (Budenkov and Kaunov, 1979)	694.3 nm	400 mJ	30 ns	Quartz specimen with a silver plated detection surface
Nitrogen and nitrogen pumped rhodamine 6G (Von Gutfeld and Melcher, 1977)	337.1 and 580 nm	Not quoted	10 and 5 ns	Mo or W evaporated onto a thin polished slab of Quartz.
Nd:YAG CO <sub>2</sub> KrF (Aindow <i>et al.</i> , 1980)	1064 nm 10.6 μm 249 nm	Up to 60 mJ Not quoted Not quoted	17 ns Not quoted Not quoted	2.5 cm thick machined finish aluminium sample.
Nd:YAG (Scruby <i>et al.</i> , 1980)	1060 nm	Up to 60 mJ	24 ns	25 mm thick Aluminium disc

Type of Laser	Wavelength	Pulse Energy	Pulse width	Target
Nd:YAG (Hutchins <i>et al.</i> 1981a, 1981b, 1981c)	1060 nm	Up to 40 mJ	24 ns	Unmodified and modified Aluminium alloy (22 mm thick)
Nd:YAG (Dewhurst <i>et al.</i> , 1982)	1060 nm	40 mJ	27 ns	25 mm thick Aluminium disc
Nd:YAG (Hutchins and Nadeau, 1983).	1060 nm	860 mJ	15 ns	10.1 mm thick Aluminium plate
Pulsed nitrogen (Tam and Leung, 1984)	337 nm	1 mJ	8 ns	Aluminium alloy 4.76 mm thick
Pulsed nitrogen (Tam, 1984)	337 nm	1.5 mJ	0.5 ns	Stainless steel film of thickness ranging from 12 to 260 $\mu\text{m}$
Frequency doubled Ruby (Hutchins and Wilkins, 1985)	347 nm	Up to 225 mJ	30 ns	Aluminium and Steel plate (25.4 or 50.8 mm Thick)

Type of Laser	Wavelength	Pulse Energy	Pulse width	Target
Nd:YAG (Vogel and Bruinsma, 1987)	1060	Not quoted	15 ns	Hemispherical aluminium sample
Nd:YAG (Dewhurst <i>et al.</i> , 1987)	1060 nm	50 mJ	20 ns	25.4 mm thick Aluminium disc
Nd:YAG (Wagner <i>et al.</i> , 1988)	1060 nm	5 - 15 mJ		Metallic sample
Nd:YAG (Aussel <i>et al.</i> , 1988)	1060 nm	330 mJ	10 or 20 ns	Steel (5 and 10 mm thick), Aluminium (20 and 25 mm thick)
Nd:YAG (Scala and Doyle, 1989)	1060 nm	5 - 80 mJ	25 ns	Composite materials

Type of Laser	Wavelength	Pulse Energy	Pulse width	Target
Mode-locked Nd:YAG (Dewhurst and Al'Rubai, 1989)	1060 nm	Up to 8 mJ  (Single pulse)	30 ps	Aluminium sheet  250 $\mu\text{m}$  Duraluminium  plate (250 $\mu\text{m}$ -  3 mm thick)
TEA-CO <sub>2</sub> (Edwards <i>et al.</i> , 1989)	10.06 $\mu\text{m}$	1 J	50 ns (rise time)	Stainless steel (10 mm thick)
TEA-CO <sub>2</sub> Taylor <i>et al.</i> , 1990	10.6 $\mu\text{m}$	1 J	50 ns (rise time)	Perspex and glass (12 mm thick)
Nd:YAG (Hrovatin and Mozina, 1993)	1060 nm	85 mJ	10 ns	5 mm thick  Aluminium and  4.5 mm thick  stainless steel  sample.
XeCl excimer (Mozina and Hrovatin, 1996)	351 nm	Not quoted	Not quoted	Metallic sample

Table 2.2.6.1 Summary of the different types of laser sources used for generation of ultrasonics.

From the above summary it is clear that different types of pulsed lasers at wavelengths ranging from 337 nm to 10.6  $\mu\text{m}$  with pulse widths from 30 ps to about 100 ns and energies from less than 1 mJ to 1 J have been used to generate ultrasonics in materials of different thickness (12 $\mu\text{m}$  - 50.8 mm). However most of the work in recent times has been dominated by the use of pulsed Nd:YAG lasers with 1.06  $\mu\text{m}$  wavelength. This laser has proved itself to be a versatile excitation source which is suitable for use with a range of materials. Its pulse length and available range of pulse energies are close to ideal for ultrasonics studies (Scruby and Drain, 1990). Considering the requirements of this work and the characteristics of the laser as discussed above, a Q-switched Nd:YAG laser was designed and constructed for the experimental studies.

## **2.3 Optical detection of laser generated ultrasonics**

### **2.3.1 Optical methods**

Optical techniques for ultrasonic wave detection using lasers have been widely used and have proved to be very flexible in operation and have excellent performance. These techniques can be classified into two categories: non-interferometric and interferometric. Non-interferometric methods for acoustic detection in solids which are based on the use of knife edges, surface-gratings, reflectivity variations and light filters have limited application compared to interferometric methods ( Monchalin, 1986). As such most of the work on the detection of laser generated ultrasonics has been based on interferometric detection and the discussion in this thesis will concentrate only on the interferometric sensors. The advantages of using a laser interferometer for the detection of ultrasonics are as follows (Scruby and Drain, 1990):

- 1) It does not adversely affect the dynamics of the system (by loading the surface).
- 2) It is remote and is particularly useful when the attachment or close proximity of a transducer to the specimen is not practical due to heat, distance or hostile environment.
- 3) It has exceptionally high resolution, both spatial and temporal. A diffraction limited spot of a few microns diameter can be used to probe a surface with a time resolution in the order of nanoseconds.
- 4) It can provide absolute calibration in terms of the wavelength of light (Kline *et al.*, 1978).

However, it may be noted that the optical methods are less sensitive on rough or poorly reflecting surfaces when compared with conventional transducers. Other potential drawbacks are its relatively high cost, complexity and bulk and the need for safety precautions.

### **2.3.2 Optical interferometry**

An optical sensor is a device in which an optical signal is modulated in response to a measurand field. It can be shown that a range of physical measurands can be transduced to phase or polarisation modulation. The phase modulation of an optical carrier is detected by interfering the modulated wave with a reference (unmodulated) wave. The resulting interference pattern can allow very high resolution detection since phase shifts corresponding to a small fraction of a fringe can be measured. One of the most common interferometric arrangements is the Michelson interferometer which is illustrated schematically in Figure 2.3.2.

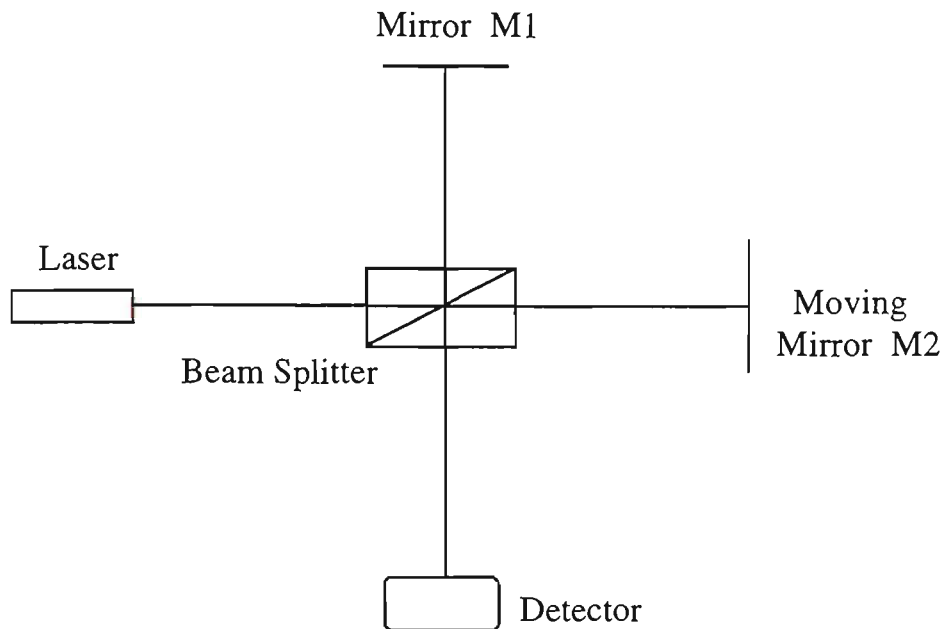


Figure 2.3.2 The basic Michelson interferometer.

Light from a laser is divided into two beams by the beam splitter; one beam following the reference path to the detector via mirror M1 and the other following a similar path via M2 in which the modulation occurs (eg. by movement of M2). The relative phase of the beams at the detector depends on the difference between the optical paths. Thus, the ability to detect an extremely small change in the phase of the combined beams translates into the ability to detect a similarly small change in the movement of the reflecting surface M2.

A second very common interferometer arrangement is the Mach-Zehnder interferometer (Figure 2.3.4.1) which is slightly more complex than the Michelson type as it requires an extra beam splitter and mirror. However, it offers two significant advantages over the Michelson interferometer:

(1) Minimisation of optical feedback to the laser source since there is no output directed back towards the source as exists in the case of the Michelson interferometer.

This is a significant advantage as optical feedback can ( particularly with a laser source) give rise to instability and increased noise from the source. This is a serious problem which requires an isolator for elimination.

(2) There are two antiphase outputs from the interferometer which are equal in magnitude only at the quadrature point and can be used as a differential input for a servo to maintain the interferometer at maximum sensitivity ( Jackson, 1987). This approach also tends to reduce the effect of intensity noise in the laser output (Dandridge *et al.*, 1980).

### **2.3.3 Fibre Optic Interferometer**

The classical bulk optic technique of interferometry demands the use of precision optical components mounted with high stability and is thus generally difficult to implement outside the laboratory (Jones, 1992). The use of optical fibre in the optical sensor has greatly extended the range of the application of interferometry in situations where the environment is not ideal. Optical fibres are small and flexible and since the interfering light is fully contained within the fibre (except possibly in the sensing region), extremely simple interferometer arrangements are possible. In fibre interferometers, the beam splitters used in the bulk optic interferometers are replaced by fibre couplers and the two arms are formed by guiding the injected beam through the single mode fibres.

Many different types of interferometers have been exploited for sensor application but the two beam interferometer which is simple and compact, and also allows the measurement of extremely small phase shifts will be used to analyse the principle of operation.

### 2.3.4 Principle of operation

The optical phase delay  $\phi$  (in radian) of light passing through a fibre is given by (Dandridge, 1991)

$$\phi = n\kappa L, \quad (2.3.4.1)$$

where  $n$  is the refractive index of the fibre core,  $\kappa$  the optical wave number in vacuum ( $2\pi/\lambda$  where  $\lambda$  is the wavelength in vacuum) and  $L$  is the physical length of the fibre. Neglecting the effect of polarisation, small variations in the phase delay are found by differentiation of the above equation (Dandridge, 1991):

$$\frac{d\phi}{\phi} = \frac{dL}{L} + \frac{dn}{n} + \frac{d\kappa}{\kappa}. \quad (2.3.4.2)$$

The first two terms are related to the physical changes in the fibre caused by the perturbation to be measured. Thus they describe the transduction mechanism by which fibres can act as sensors. The last term takes into account any wavelength (or frequency) variation associated with the laser source.

A typical all-fibre Mach-Zehnder interferometer which is based on the mixing of two optical beams is shown in Figure 2.3.4.1

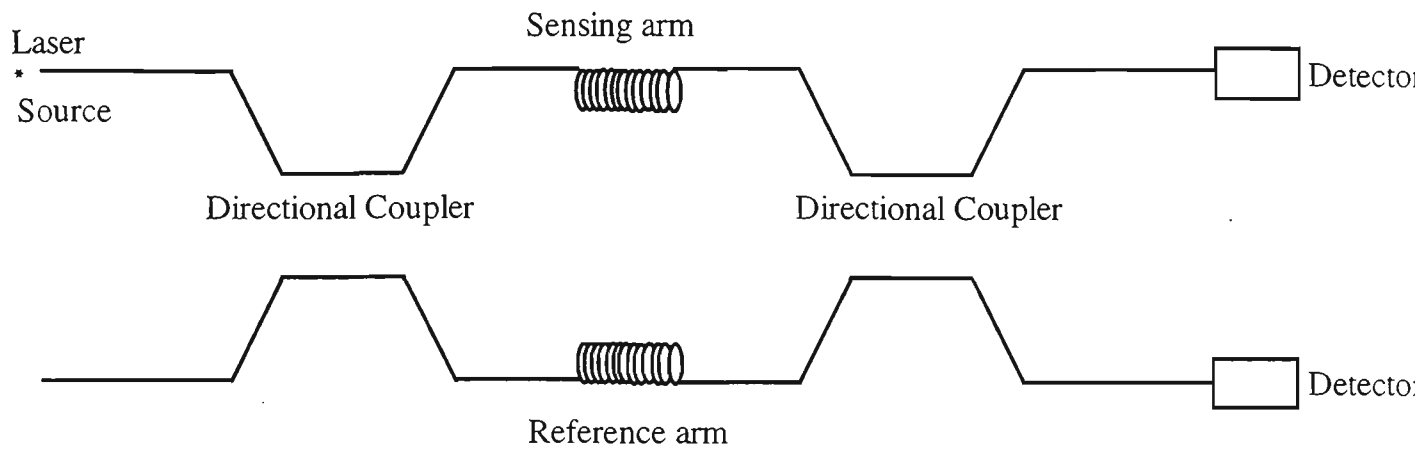


Figure 2.3.4.1 Fibre version of the Mach-Zehnder interferometer.

The light launched from a coherent single mode laser source is split into two beams of nominal equal intensity by a directional coupler, part being sent through the sensing fibre arm, the remainder through the reference arm. These two beams are recombined by the second directional coupler, giving two optical outputs at the detectors.

Following the approach of Dandridge (1991), the optical fields at one output of the interferometer originating from the signal ( $E_S$ ) and reference ( $E_R$ ) arms can be expressed as

$$E_R = E_0 (\alpha_r k_1 k_2)^{1/2} \cos(\omega_0 t + \phi_r) \quad (2.3.4.3)$$

and

$$E_S = E_0 \{ \alpha_s (1 - k_1)(1 - k_2) \}^{1/2} \cos(\omega_0 t + \phi_{sg}), \quad (2.3.4.4)$$

where  $E_0$  is the optical source field with angular frequency  $\omega_0$ ,  $k_1$  and  $k_2$  are the power coupling coefficient of the two couplers,  $\alpha_r$  and  $\alpha_s$  are the optical loss factor associated with the reference and sensing arm respectively and  $\phi_r$  and  $\phi_{sg}$  are the phase delay in the reference and sensing arms.

Assuming perfect coherence and ignoring the effect of polarisation, the output intensity of the interferometer at one of the detectors ( $I_a$ ) can be written as

$$I_a = \langle E_r^2 \rangle + \langle E_s^2 \rangle + 2 \langle E_r E_s \rangle, \quad (2.3.4.5)$$

where  $\langle \rangle$  denotes the time average over a period much longer than  $2\pi/\omega_0$ . Thus the output intensity can be written as

$$I_a = I_0 [ \alpha_r k_1 k_2 + \alpha_s (1 - k_1)(1 - k_2) + 2 \{ \alpha_r \alpha_s k_1 k_2 (1 - k_1)(1 - k_2) \}^{1/2} \cos(\phi_r - \phi_{sg}) ], \quad (2.3.4.6)$$

where  $I_0$  is the optical source intensity. The complementary output of the interferometer ( $I_b$ ) can be denoted as

$$I_b = I_0 [ \alpha_r k_1 (1 - k_2) + \alpha_s (1 - k_1) k_2 + 2 \{ \alpha_r \alpha_s k_1 k_2 (1 - k_1)(1 - k_2) \} \cos(\phi_{sg} - \phi_r) ]. \quad (2.3.4.7)$$

It can be seen from these equations that the interferometer does not measure the absolute phase delays of the two arms separately, but can only determine the difference between the phases. Assuming  $\alpha_r = \alpha_s = \alpha$ ,  $G = k_1 k_2 + (1 - k_1)(1 - k_2)$ ,  $H = 2 \{ k_1 k_2 (1 - k_1)(1 - k_2) \}^{1/2}$ ,  $J = k_1 (1 - k_2) + (1 - k_1) k_2$  and  $\Delta\phi = (\phi_r - \phi_{sg})$ , the above equations can be rewritten as

$$I_a = I_0 \alpha ( G + H \cos \Delta\phi ) \quad (2.3.4.8)$$

and

$$I_b = I_0 \alpha (J - H \cos \Delta\phi). \quad (2.3.4.9)$$

If  $k_1 = k_2 = 0.5$ , the above equations can be simplified to

$$I_a = \frac{I_0 \alpha}{2} (1 + \cos \Delta\phi) \quad (2.3.4.10)$$

and

$$I_b = \frac{I_0 \alpha}{2} (1 - \cos \Delta\phi). \quad (2.3.4.11)$$

The differential phase shift  $\Delta\phi$  in the interferometer may be separated into a signal term of amplitude  $\phi_s$  with angular frequency  $\omega$  and a slowly varying phase shift  $\phi_d$ . Thus the above equations may be further expressed as

$$I_a = \frac{I_0 \alpha}{2} [1 + \cos (\phi_d + \phi_s \sin \omega t)] \quad (2.3.4.12)$$

and

$$I_b = \frac{I_0 \alpha}{2} [1 - \cos (\phi_d + \phi_s \sin \omega t)]. \quad (2.3.4.13)$$

From the above equations, it may be noted that the transfer function (output plotted as a function of phase change) is periodic in nature. But interferometric sensors are usually measuring small changes and are operated in such a way that the output is linearly related to the induced optical change. The linearisation of the transfer function of the

interferometer has been achieved by a number of demodulation techniques used for signal processing.

### 2.3.4.1 Signal processing

The purpose of signal processing is to transform the optical output of the interferometer into an electrical signal proportional to the amplitude of the relative phase. The optical intensity outputs are converted to electric current by photodetectors. Differential combinations of these photocurrents produce an output

$$i = \epsilon I_0 \alpha \cos (\phi_D + \phi_S \sin \omega t), \quad (2.3.4.14)$$

where  $\epsilon$  is the responsivity of the photodetectors. The general signal processing problem is to recover the part of the phase difference which arises in the presence of slowly varying phase shift  $\phi_D$ . The frequency spectrum of the signal can be found from an expansion in terms of Bessel functions since,

$$\begin{aligned} \cos (\phi_D + \phi_S \sin \omega t) &= \cos \phi_D \{ J_0 (\phi_S) \\ &+ 2 \sum_{i=1}^{\infty} J_{2i} (\phi_S) \cos (2i \omega t) \} \\ &- \sin \phi_D \{ 2 \sum_{i=0}^{\infty} J_{2i+1} (\phi_S) \sin [(2i+1) \omega t] \}, \end{aligned} \quad (2.3.4.15)$$

where  $J_i(\phi_S)$  is the Bessel function of order  $i$  and argument  $\phi_S$ . For  $\phi_S \ll 1$  i.e., for small argument  $J_0 = 1$  and  $J_1(\phi_S) = \phi_S / 2$ , and considering only the time varying portion, the above equation can be simplified to

$$i \sim \epsilon I_0 \alpha \phi_s \sin \omega t \sin \phi_d. \quad (2.3.4.16)$$

From the above equation, it can be seen that the amplitude of the signal  $\phi_s \sin \omega t$  depends on the value of  $\sin \phi_d$  and the small-signal sensitivity ( $di/d\phi$ ) of the interferometer is also dependent on  $\sin \phi_d$ . Thus when  $\phi_d = 0$  (modulo  $\pi$ ), the signal fades completely. Ideally in order to get maximum sensitivity, the interferometer should be operated with  $\phi_d = \pi/2$  (modulo  $\pi$ ) and this is called the quadrature condition. Under this condition, the primary objective of any demodulation scheme, to produce a small signal output of constant sensitivity (which is linear with respect to the measurand), is achieved.

#### 2.3.4.2 Demodulation techniques

Signal processing schemes can be classified into two categories, homodyne or heterodyne, depending on whether the optical frequencies of the interfering beams are the same or different. Further, homodyne processing can be accomplished by two demodulation techniques; active homodyne and passive homodyne. Both techniques require the combination of two signals which are  $90^\circ$  out of phase (quadrature signals). In the active homodyne case this is achieved by active feedback to some element in the interferometer which can produce a controlled relative phase shift between the beams so that  $\phi_d$  is maintained at  $90^\circ$ . In the passive homodyne case, multiple outputs from the interferometer are electronically processed to obtain two quadrature signals and there is no need to control  $\phi_d$ . The essential requirement of having two quadrature signals ensures that the two signals do not fade simultaneously and there is always a non-zero sensitivity.

Heterodyne processing provides an alternative class of technique for recovering phase information from interferometer. The essential difference from homodyne processing is that rather than translating the optical frequency component of the signal phase directly to a dc level, a beat frequency is generated by shifting the frequency of the optical carrier wave travelling in one arm of the interferometer. This beat frequency is phase modulated by the measurand and the signal phase can be recovered by techniques akin to those used in FM radio communication such as the use of an FM discriminator or a phase locked loop (PLL) (Handerek, 1995). The FM discriminator technique is appropriate when the signal shifts the beat frequency appreciably and PLL processing is more suitable when smaller deviation of signal phase is expected.

A measure of the minimum detectable change in the measurand determines the resolution or the performance of the sensor. This is limited by the noise floor in the system. The principle sources of noise are environmental, receiver and source. Environmental noise arises from acoustic vibration, air currents and fluctuations in temperature, which cause phase changes indistinguishable from that produced by the measurand at those frequencies. Receiver noise is contributed by the photodetector and the processing electronics. Source noise which is introduced by the laser source is of two types; intensity noise and frequency noise. It is obvious that the minimisation of these sources of noise plays an important part in the design of the system.

### **2.3.5 Review of previous work on different demodulation techniques**

The following sections contain a brief review of the various homodyne and heterodyne signal processing techniques which have been used and the performance which can be obtained with them. Later in this chapter this is followed by a detailed noise analysis

and finally a review of previous work in using interferometers for detecting laser generated (wideband) ultrasonics.

### 2.3.5.1 Active homodyne

Measurement of small phase shifts using a single-mode all-fibre Mach-Zehnder interferometer was demonstrated for the first time by Jackson *et al.* (1980a). The mirror / beam splitter combinations of a bulk optic interferometer were replaced by two optical fibre couplers. The couplers are linked by two single mode optical fibres with the same numerical aperture as that of coupler. The optical length of one of the arms of the interferometer was modulated by stretching the fibre. The plastic coating of a small section of one of the fibres joining the couplers was removed and the fibre glued to the outside of a piezoelectric cylinder such that the axis of the fibre was parallel to the cylinder axis. The cylinder was driven at frequencies between 40 Hz and 10 kHz in order to induce periodic phase changes of amplitude about  $10^{-6}$  radian. The output was detected with a PIN photo diode at either output of the second fibre coupler (combiner). In order to minimise environmental noise, the complete interferometer (with the exception of the laser source) was mounted inside an evacuated chamber, which was then mounted on a conventional optical vibration table to further reduce low-frequency coupling into the interferometer. It was found that the change in length of the fibre was close to that of the piezoelectric cylinder alone. The minimum detectable induced phase shift (signal to noise ratio = 1) was found to be of the order of one  $\mu$ radian at frequencies above 300 Hz, which was equivalent to the minimum detectable displacement of  $10^{-13}$  m. The bandwidth of the detection scheme was not reported, but it was probably quite small as there is no need for a broad bandwidth receiver with this type of measurement. The performance of the interferometer was

promising but in absence of any method to lock it at the quadrature point to eliminate fading, it was not suitable to make any measurements outside the evacuated chamber.

In order to eliminate the fading or drift problem in a homodyne interferometer as described above, Jackson *et al.* (1980b) introduced the idea of active phase control using a servo-driven piezoelectricity stretched coiled fibre in the reference arm. A hundred turns of single-mode fibre were wrapped in a single layer onto the cylinder. Two of these cylinders were incorporated into the interferometer, one in the signal arm, the other in the reference arm. In this configuration, information and drift simulation signals were applied to the piezoelectric cylinder in the signal arm and the correction and modulation signal (if required) were applied to the cylinder in the reference arm. The two outputs of the beam combining coupler, which are  $180^\circ$  out of phase, were converted to electrical signals by a pair of photodiodes. These two signals were then combined in a difference amplifier to produce a signal proportional to the cosine of phase difference and which was suitable to act as an error signal. This error signal was integrated with an operational amplifier integrator and was then applied to the piezoelectric cylinder as the correction signal. The detected phase shift was found to be of the order of  $10^{-5}$  radian and the corresponding minimum detectable displacement was 0.001 nm at a frequency of about 1 kHz in a bandwidth of 30 Hz. It was found that the detector noise increased markedly at low frequency due to random environmental noise modulating the phase of the interferometer. Due to simple configuration of the optics and electronics in this system, this approach has found widespread use in high performance laboratory grade sensors and they have extremely good noise performance (Dandridge, 1991). However, in order to compensate large amounts of environmental drift, this technique requires the use of a large piezoelectric phase modulator or an

increase in drive voltage to the piezoelectric phase modulator as well as fast reset circuitry to recover from episodes where the drift excursion exceeds the capability of the feedback and the interferometer has lost lock. Also the use of an electrically active element in the feedback loop may make it unsuitable in some environments.

Liu *et al.* (1990) reported the detection of acoustic emission within composite materials with a fibre optic Michelson interferometer by using active homodyne demodulation techniques. The output arms of the interferometer was embedded in the composite material. The same technique was used for the detection of acoustic emissions (Measures, 1990, 1992) and ultrasonics (Davis *et al.*, 1991; Ohn *et al.*, 1992).

A similar technique but without the use of an electrically active component in the interferometer has been demonstrated by Dandridge and Tveten (1982). In this system the phase bias is maintained in the quadrature condition in an unbalanced interferometer by current-induced frequency tuning of the solid state laser source. In a diode laser, a change in drive current leads to a change in its emission frequency (wavelength). If the arms of the interferometer are of unequal length (unbalanced) this optical frequency change produces a relative phase shift at the output. The optical phase delay of light  $\phi$  passing through a fibre in terms of the optical frequency  $\nu$  and velocity of light  $c$  is given by

$$\phi = \frac{2\pi n L \nu}{c}. \quad (2.3.5.1)$$

The optical phase delay can be varied by changing the emission frequency of light by  $dv$ . The differential phase shift ( $\Delta\phi$ ) between the two arms of the interferometer is proportional to the optical path difference  $n\Delta L$  and is given by

$$\Delta\phi = \frac{2\pi n\Delta L dv}{c} \quad (2.3.5.2)$$

This scheme operates in the same way as that of the piezoelectric stretcher except that the correction term is generated by a correction current applied to the laser by the mechanism described above. It may be noted that in an unbalanced interferometer powered by a diode laser, the primary noise source becomes the phase noise due to fluctuations of the emission frequency of the laser. Thus a tradeoff situation arises as the tracking range and phase noise are both proportional to the path difference in the interferometer. Careful choice of the laser source is necessary to maximise the ratio of  $dv_f / dv_n$  (where  $dv_f$  is the frequency range over which the laser may be driven in a single longitudinal mode and  $dv_n$  is the RMS frequency instability of the laser source) (Dandridge *et al.*, 1982), and also to provide good response of modulation index  $dv/di$  at high frequencies, where in this case  $i$  is the drive current. In this scheme, a minimum detectable phase shift in the order of  $10^{-5}$  radian is possible but with a low tracking range.

Andersson *et al.* (1985) reported the construction of a fibre optic interferometer using integrated optics in which fibre directional couplers had been replaced by channel waveguides in LiNbO<sub>3</sub>. The light source was a 1300 nm single-mode laser diode. The 1300 nm laser source was chosen to minimise the photorefractive effect in the LiNbO<sub>3</sub>

waveguides. The light was coupled with standard microscopic lenses into a polarisation-preserving single mode fibre leading to the LiNbO<sub>3</sub> chip. Light launched into the fibre was observed at the other end by a vidicon camera and the fibres were then mechanically rotated until their bow-tie structures were seen to be aligned to the optical axis of the LiNbO<sub>3</sub> chip and then they were secured with epoxy. The length of the two fibres constituting the interferometer arms were kept equal to within at least 1 mm. The phase sensitivity was found to be 6 μrad / √Hz in a bandwidth of 30 kHz, which corresponds to the displacement of about 0.2 nm. The main drawback of the detection scheme was that it was difficult to maintain the quadrature condition due to any variation of intensities in the interferometer arms. The variations depended on altered coupling efficiency from the laser to the fibre and from the fibre to the LiNbO<sub>3</sub> devices due to temperature variations in the translator used. The insertion loss in this system was 33 dB.

### 2.3.5.2 Passive homodyne

The disadvantages of limiting tracking range and the requirement of active phase element in the interferometer have led to the development of an alternative demodulation scheme. A number of configurations have been developed to allow passive demodulation (without feedback) and an all-optical interrogation of the optical fibre interferometric sensors. The approach of this technique is to generate two signals ( $I_C$  and  $I_D$ ) that are shifted in optical phase by  $\pi/2$ , so that the outputs are in the form of

$$I_C = \frac{\epsilon I_0 \alpha}{2} (1 + \cos \Delta\phi) \quad (2.3.5.3)$$

and

$$I_D = \frac{\epsilon I_0 \alpha}{2} (1 + \sin \Delta\phi), \quad (2.3.5.4)$$

and their response to a small phase shift  $d\phi$  is given by

$$dI_C = \frac{\epsilon I_0 \alpha}{2} d\phi \sin \Delta\phi \quad (2.3.5.5)$$

and

$$dI_D = \frac{\epsilon I_0 \alpha}{2} d\phi \cos \Delta\phi. \quad (2.3.5.6)$$

It can be seen from the above that even though the magnitude of the signal may vary with time, there is no possibility of the two signals to vanish simultaneously from the outputs. There are a number of techniques to generate these quadrature outputs and subsequent processing of these outputs to extract the signal which is linear in phase.

Sheem *et al.* (1982) presented experimental verification of three optical techniques used to solve the signal fading problems by yielding both the sine and cosine terms of differential optical phases. The first approach was to switch the laser wavelength periodically between two values (current modulation) which yielded the required phase bias. The second approach utilised two polarisation states of a single mode fibre so that the birefringence between the two eigenmodes produced the required  $90^\circ$  phase difference. The third approach used a 3x3 directional coupler to combine the signal and reference beams so that three outputs are available with  $120^\circ$  phase difference between them.

The signal processing in the first scheme was based on adding the absolute values of  $dI_C$  and  $dI_D$  and then normalising this signal by the sum of the two outputs. The normalised signal is always equal to the absolute value of  $d\phi$  regardless of the instantaneous value of  $\phi$  which fluctuates randomly. Another approach was to use electronics to square  $dI_C$  and  $dI_D$ , add, and then take the square root, so that

$$d_i = (dI_C^2 + dI_D^2)^{1/2} = \frac{\epsilon I_o \alpha}{2} d\phi. \quad (2.3.5.7)$$

Although these approaches prevent signal fading, they break down when  $d\phi > 0.1$  radian, and this leads to non linearity and distortion of the recovered signal. The electronic manipulation of addition, squaring and square rooting as stated above may introduce extra noise and more importantly the accuracy of each step imposes the ultimate limit on the minimum detectable signal level. The work described showed only the feasibility of the demodulation methods and did not evaluate the performance which can be achieved using the various techniques or the preferred electronic processing for each technique.

Dandridge *et al.* (1982) described and experimentally demonstrated the method of passive homodyne demodulation in which the quadrature signals were generated by a technique called phase generated carrier. In this technique, a large amplitude phase shift was introduced at a frequency outside of the signal band. These large amplitude signals carry, as sidebands, the signals of interest. These large amplitude modulation signals were added to the interferometer by either using a piezoelectric fibre stretcher or modulating the emission frequency of the laser diode (modulating the laser drive

current) in an unbalanced interferometer. The piezoelectric method has the advantage that a zero optical path difference may be used in the interferometer. The second method has the advantage of eliminating the piezoelectric cylinder, as well as allowing the interferometer part of the fibre system to be removed from electrical components. If the phase carrier modulation has an amplitude  $\phi_C$  and angular frequency  $\omega_C$ , the output of the interferometer can be written as (Dandridge, 1991),

$$\begin{aligned}
 i &= \epsilon I_0 \alpha \cos \Delta\phi \\
 &= \epsilon I_0 \alpha \cos (\phi_D + \phi_S \sin \omega t + \phi_C \cos \omega_C t). \quad (2.3.5.8)
 \end{aligned}$$

Expanding in terms of Bessel functions, it can be shown (Dandridge *et al.*, 1982) that the signal  $\phi_S \sin \omega t$  appears as a sideband to either the even or odd multiples of the carrier terms ( $\omega_C$ ). When  $\phi_D = 0$ , even (odd) multiples of  $\omega$  are present in the output centred about the even (odd) multiples of  $\omega_C$ . When  $\phi_D = \pi/2$ , even (odd) multiples of  $\omega$  are present about the odd (even) multiples of  $\omega_C$ . The signal is recovered by mixing the total output signal with the proper multiple of  $\omega_C$  and low pass filtering to remove the terms above the highest frequency of interest (Dandridge, 1991). The amplitudes of the carrier components for  $0$ ,  $\omega_C$ ,  $2\omega_C$  and  $3\omega_C$  after mixing and filtering contain sine and cosine terms of  $\phi_D + \phi_S \sin \omega t$ . The amplitudes of the phase carriers are then adjusted to obtain a pair of equal quadrature components (i.e.,  $0$  and  $\omega_C$ ,  $\omega_C$  and  $2\omega_C$ , etc ), containing the sine and cosine terms (assuming the amplitude of the mixing signals are equal). This output is of the form required for passive homodyne demodulation. The time derivatives of the sine and cosine terms are cross multiplied

with the cosine and sine terms respectively, to yield the sine and cosine squared terms. These two signals were then combined in a differential amplifier and finally integrated to obtain the desired signal.

The experimental configuration employed to demonstrate this scheme was that of a bulk optic Michelson interferometer, which was reported to be capable of high sensitivity ( $10^{-6}$  radian detectability at 1 kHz) when a piezoelectric stretcher was employed to produce the phase carrier. When current induced frequency modulation was used to produce the phase carrier, a 2 cm path difference was necessary and the sensitivity was limited to 9  $\mu$ radian at 1 kHz. Although there was no reset problem, this scheme is electronically more complex than the active homodyne schemes described above. This phase generated approach also has the following problems (Brown *et al.*, 1991):

- (a) A requirement for an expensive stable source having long coherence length.
- (b) High set up complexity requiring FFT calibration of the phase generated spectral component to ensure the Bessel Function balance and orthogonality.
- (c) Additional laser noise is induced due to unbalanced path.
- (d) Fluctuations in sensor output due to scale factor instability ( scale factor quantifies circuit conversion of optical phase in radians to electrical output in volts).
- (e) The signal appears as the sidebands of the carrier frequency and its harmonics.
- (f) Noisy operation due to mode hopping often induced from the superimposed current modulation.

Bush and Sherman (1992) described a phase reading digital approach for the demodulation of passive signals and applied it to a fibre interferometer. In this

approach, standard analogue modulation and mixing techniques are used to obtain the two quadrature signals and then these signals are subsequently digitally processed rather than processed in the conventional way using analogue FM discrimination circuitry. In this approach, measurement of phase can be made directly through an inverse trigonometric operation. The performance of this digital approach was reported to be better than that of the analogue approach. Advantages included DC sensing capabilities and insensitivity to common mode gain variations due to variations in laser power and link attenuations.

Kersey *et al.* (1982) reported the details of an infinite range passive compensation scheme by generating the orthogonal polarisation states at the output of a polarisation selective Mach-Zehnder interferometer. In this configuration, linearly polarised light in the reference arm is converted into circularly polarised light by a quarter-wave plate, oriented with the fast axis in the reference plane. The two output beams, produced by recombining the light in the signal and the reference arm with a beam splitter, pass through linear polarisers oriented with their transmission axis parallel and perpendicular to the reference direction respectively. These signals, which AC components which are  $90^\circ$  out of phase, are then high pass filtered and combined electronically to produce the desired signal which does not suffer from fading. A minimum detectable phase shift of the order of a  $\mu$ radian was achieved at frequencies  $> 1$  kHz, using bulk optic components. Although the scheme was demonstrated using a bulk optic interferometer, it is capable of implementation in a fibre optic system using single mode birefringent fibre. However fibre couplers are a problem with polarisation preserving systems.

A demodulation scheme suitable for use with a fibre interferometric sensor and based on switching the frequency of the laser source by adjusting the drive current at a high rate between two optical frequencies such that the effective phase change of  $\pi/2$  is induced in an unbalanced interferometer was described by Kersey *et al.* (1983). A bulk optic Mach Zehnder interferometer was employed to demonstrate the feasibility of this demodulation scheme. Switching of the laser frequency was achieved by the addition of current square wave to the DC bias current of the laser. Analogue gates were used for sampling the signal at the switched rate. The sampled signals were processed electronically by the use of a bandpass filter, phase shifter, summing network and finally by direct phase comparison with the laser modulation or by using a phase locked loop. The minimum detectable phase shift was of the order of  $10^{-5}$  radian in a bandwidth of 1 Hz. The sensitivity was limited by the free running phase noise of the diode laser.

Maggi (1993) reported the feasibility of a passive demodulation technique for a free running Mach-Zehnder interferometric sensor having a 2x2 coupler used as the recombining coupler. The outputs of a 2 x 2 coupler with a phase dependent loss are capable of being combined in a way which yields signals which are quadrature components of the phase difference between the inputs. However, investigations into the relative phase variations of the output coupler have shown that the relative phase of the outputs are sensitive to variations in the state of polarisation. Thus polarisation control is necessary in a practical implementation of the scheme.

A passive scheme using a 3x3 fibre directional coupler and a suitable signal processing unit was successfully demonstrated by Koo *et al.* (1982). In this configuration, the

conventional 2x2 directional coupler combiner was replaced by a 3x3 coupler. The optical outputs  $I_1$ ,  $I_2$  and  $I_3$  of the 3x3 coupler containing  $\cos \Delta\phi$  and  $\sin \Delta\phi$  terms can be represented by

$$I_1 = -2A_2 ( 1+ \cos \Delta\phi ), \quad (2.3.5.9)$$

$$I_2 = A_1 + A_2 \cos \Delta\phi + A_3 \sin \Delta\phi, \quad ( 2.3.5.10)$$

$$I_3 = A_1 + A_2 \cos \Delta\phi - A_3 \sin \Delta\phi, \quad ( 2.3.5.11)$$

where  $A_1$ ,  $A_2$  and  $A_3$  are constants determined by the coupling coefficient between the fibres within the coupling region (Dandridge, 1991). Two outputs with the required  $\pi/2$  relative phase shift were obtained by processing  $I_2$  and  $I_3$  in a way which included taking their sum and differences. After gain adjustment and offset subtraction, these signals were analysed by the differentiate and cross-multiply technique discussed earlier. A minimum detectable phase shift in the  $\mu$ radian range at 1 kHz and 1 Hz bandwidth has been reported. However the stability of the system was dependent on the properties of a 3x3 directional coupler which was polarisation sensitive. To obtain optimum performance, a polarisation insensitive directional coupler or a fibre interferometer using polarisation preserving fibres is needed (Koo *et al.*, 1983).

A method for demodulation of a fibre optic sensor using all three phase modulated outputs of a 3x3 coupler has been described by Brown *et al.* (1991). These outputs are used in a symmetric manner to recreate the stimulus inducing the original optical phase

modulated signal. In order to verify the performance of this scheme for large amplitude modulation ( $5\pi$  radian), the phase modulated signals were generated by wrapping each arm of the interferometer around a separate piezoelectric cylinder and driving the cylinders  $180^\circ$  out of phase to double the modulation achieved. A complex electronic processing unit was used to recover the modulation signal. This unit incorporated a number of functions including summation, multiplication, subtraction and integration as well as an AGC. The minimum detectable phase shift was reported to be  $220 \mu$  radian  $\sqrt{\text{Hz}}$  and the dynamic range was 116 dB.

Niemeier *et al.* (1986) demonstrated that quadrature outputs can be obtained for use in the interferometer by using a four fold self-imaging stripe wave guide as a 4x4 coupler. Mortimore (1990) has reported the theory, fabrication and performance of monolithic 4x4 single-mode fused coupler, which exhibited excellent coupling uniformity and low excess loss. In spite of these developments and a new structure for the 4 x 4 coupler homodyne receiver proposed by Xiaopin *et al.* (1988), no high performance interferometer based on 4 x 4 couplers has yet been demonstrated. It may be noted that the detector electronics in these configurations is complicated and has limited bandwidth. This restricts the range of applications of the interferometer.

### **2.3.5.3 Heterodyne Techniques**

In heterodyne signal processing, detection is performed by shifting the optical frequency in one of the arms of the interferometer with respect to the other. Coherent light from a laser is divided into two parts and then propagates through the signal and reference arms. Light in the signal arm undergoes a phase change induced by the signal. Using a frequency shifter (eg. Bragg cell) in the reference arm, the output signal (i)

from the detector includes a carrier at the shifting frequency and sidebands and is found to vary as:

$$i \propto \cos(\omega_B t + \phi_D + \phi_S \sin \omega t), \quad (2.3.5.12)$$

where  $\omega_B$  is the offset frequency. This signal represents a carrier at frequency  $\omega_B$  which is phase modulated by  $\phi_D + \phi_S \sin \omega t$ . Demodulation of this signal is accomplished by the standard electronic techniques of frequency discrimination or phase locked loop.

A number of sensors based on a bulk optic Michelson heterodyne interferometer have been described in the literature and differ in their optical configuration or electronic processing techniques. Generally they use a Bragg cell to shift the optical frequency. A bulk optic laser Doppler vibration sensor, based on the principle of optical heterodyne detection of the Doppler shift of light scattered from a small area of the surface on the object and incorporating a Bragg cell has been reported by Buchave (1975). This system had a bandwidth of 100 kHz and a measurable displacement of less than 0.1 nm. Dandliker and Willemin (1981) have described a system in which two acousto-optic modulators were used (one in each arm) to generate the necessary frequency offset for the heterodyne detection. The phase modulated signal was processed by using a commercial spectrum analyser. This system used a 2 mW He-Ne laser source and was capable of measuring both in-plane and out-of plane vibrations with amplitudes down to 1 nm and spatial resolution of 35  $\mu\text{m}$  in a bandwidth of 5 kHz to 5 MHz.

A compact heterodyne interferometer using a combination of a collinear beam Bragg cell (70 MHz) and a polarising beam splitter has been described by Royer *et al.*, (1985).

The output signal was processed electronically by a coherent detection scheme. This system, which uses a 2.2 mW HeNe laser, achieved a sensitivity of  $10^{-5}$  nm/ $\sqrt{\text{Hz}}$  which is very close to the quantum noise limit. Monchalin (1985a) and Monchalin *et al.* (1986), also described a bulk optic heterodyne interferometer using a Bragg cell as frequency shifter. This system was quantum noise limited and was capable of measuring continuous displacements with amplitudes of less than 0.1 nm from rough surfaces. Monchalin (1986) reviewed different types of electronics used for the detection of ultrasound by bulk optic heterodyne interferometers. Yang *et al.* (1987) demonstrated measurements of the thickness of thin films using a modified heterodyne interferometer incorporating a Bragg cell and 20 mW He-Ne laser. In this system a lens was placed between the target and the Bragg cell so that the reference beam was reflected from the film and the frequency-shifted beam was reflected from the substrate. The minimum thickness which could be measured was 2.5 nm.

All of the above systems were constructed using bulk optics and hence the laser powers were quite large and quantum noise limited operation is possible. Nokes *et al.* (1978) described an optical heterodyne interferometer for vibration measurement utilising a fibre optic target probe and a digital phase tracking system. This system includes bulk optics for all sections except the target probe. Thus it suffers the losses associated with injecting the laser in only one of the interferometer arms. Hence, in terms of optical signal levels in the interferometer, it is somewhere between a bulk optic device and an all fibre one. A Bragg cell was used as a frequency shifter (40 MHz) in the bulk optic arm in this interferometer configuration. The heterodyne signal was processed using an all electronic homodyne process. In this process signal detection is ultimately performed by multiplying two signals of the same frequency. The 40 MHz reference

signal was translated into a 100 kHz reference signal (by mixing with 39.9 MHz) to allow high gain amplifiers to be used in the tracking feedback. An AGC unit maintains the 100 kHz phase modulated carrier at a constant amplitude. This carrier signal is then mixed with a 100kHz local oscillator which has an electrically controlled phase. The feedback electronics produces a low frequency output which varies with the phase difference between local oscillator and heterodyne signal. This feedback adjusts the phase of the local oscillator so that it tracks the phase modulated carrier signal with a constant  $90^\circ$  phase difference. For small phase changes, the feedback signal is directly proportional to the phase variations of the carrier (to within the phase tracking accuracy of the electronic phase control circuit which is about  $3^\circ$ ). This scheme has a drawback in practical design because a switched bank of resistors are used to change the phase in the digital phase shifting electronics and the resistance at each step needs to be individually adjusted to maintain uniformity of phase change. This is difficult with a large number of steps. The maximum sensitivity of this heterodyne interferometer system for a simulated biological target in aqueous medium was found to be  $5 \times 10^{-12} \text{ m}/\sqrt{\text{Hz}}$  for a signal to noise ratio of unity.

Jackson (1984) described a bulk optic differential heterodyne Mach-Zehnder interferometer using a digital phase tracking scheme which is in principle very similar to the system described by Noakes. This system used two Bragg cells with a frequency difference of 100 kHz in the two interferometer arms to obtain the 100 kHz phase modulated carrier signal. A more elaborate phase tracking system was used which avoided some of the problems associated with the circuit used by Noakes. This device can track phase drift of up to  $200 \pi \text{ rad s}^{-1}$  whilst simultaneously presenting the phase

shift information in a digital format. A phase resolution of  $10^{-5}$  radian is possible with the use of available 18 bit electronics in the digital phase control.

The Bragg cell is an electrically active discrete bulk optic component and is not very compatible with monomode optical fibre as the light has to be reinserted into the fibre after passing through it. Also extra noise is generated in the circuit due to the problem associated with phase stability of the oscillator generating the offset frequency. Thus its use is mostly restricted to bulk optic interferometers.

Risk, *et al.*, (1984,1986) reported the development of fibre optic based frequency shifter using acousto optic modal coupling in birefringent monomode fibre, but the reported efficiency was low (about 5%) and as such could not be incorporated in the system. Considerable effort has been directed to the development of alternative methods of producing a phase modulated carrier. These new methods can be classified as synthetic heterodyne, pseudo heterodyne and quadrature recombination heterodyne or passive heterodyne. These methods were reviewed by Jackson (1987).

#### **2.3.5.4 Synthetic Heterodyne**

This technique is similar to the phase generated carrier homodyne technique discussed earlier in which the fibre optic interferometer is phase modulated at a frequency  $\omega_m$  which is much higher than the maximum frequency of the signal of interest by using either a PZT phase modulator or by sinusoidally sweeping the frequency of the laser source. A phase modulated carrier can be produced if the output signal is conditioned by multiplying it by a phase related harmonics of carrier frequency  $\omega_m$  (Jackson 1987). The output of the interferometer (i) is found to be proportional to

$$i \propto \cos(\phi_m \sin \omega_m t + \phi_d + \phi_s \sin \omega t), \quad (2.3.5.13)$$

where  $\phi_m$  is the amplitude phase modulating signal. Cole *et al.* (1982) described a synthetic heterodyne interferometric demodulation technique in which the output can be expanded in terms of Bessel function and can be shown proportional to:

$$J_0(\phi_m) - J_1(\phi_m) \sin \omega_m t \sin(\phi_d + \phi_s \sin \omega t) + J_2(\phi_m) \cos 2\omega_m t \cos(\phi_d + \phi_s \sin \omega t) + \dots \quad (2.3.5.14)$$

Filtering the carrier components at  $\omega_m$  and  $2\omega_m$ , the outputs are found to be proportional to

$$J_1(\phi_m) \sin \omega_m t \sin(\phi_d + \phi_s \sin \omega t) \quad (2.3.5.15)$$

and to

$$J_2(\phi_m) \cos 2\omega_m t \cos(\phi_d + \phi_s \sin \omega t). \quad (2.3.5.16)$$

Thus it can be seen that the desired signal is always present as a side band to either of the carrier components  $\omega_m$  or  $2\omega_m$  since both carrier components cannot fade to zero simultaneously. The synthetic heterodyne technique processes each carrier and combines them to form a non-fading carrier. It is accomplished by multiplying the  $\omega_m$  channel with a local oscillator at  $2\omega_m$  while the  $2\omega_m$  channel is multiplied with a local oscillator at  $\omega_m$ , resulting in the signal as shown in the following equation being proportional to

$$J_1(\phi_m) \sin \omega_m t \sin (\phi_d + \phi_s \sin \omega_t) \cos (2\omega_m t + \theta) \quad (2.3.5.17)$$

and

$$J_2(\phi_m) \cos 2\omega_m t \cos(\phi_d + \phi_s \sin \omega_t) \cos (\omega_m t + \theta), \quad (2.3.5.18) .$$

where  $\theta$  is the static phase term representing the phase difference between local oscillators and the incoming phase modulated signal. The two local oscillators are synthesised in phase by dividing down a 1 MHz clock frequency and appropriately filtering the output. The signals are bandpass filtered at  $3\omega_m$  providing the outputs which are proportional to

$$J_1(\phi_m) \sin (3\omega_m t + \theta) \sin (\phi_d + \phi_s \sin \omega_t) \quad (2.3.5.19)$$

and

$$J_2(\phi_m) \cos (3\omega_m t + \theta) \cos (\phi_d + \phi_s \sin \omega_t). \quad (2.3.5.20)$$

By adjusting the amplitude of the modulator or by employing a relative gain difference between channels, these two signals can be made to have equal amplitudes. After taking the difference between the two signals, the output can be represented as being proportional to

$$J_1(\phi_m) \cos (3\omega_m t + \theta + \phi_d + \phi_s \sin \omega_t), \quad (2.3.5.21)$$

which is in the same form as true heterodyne and can be processed by using standard FM or PM techniques. A phase locked loop FM discriminator and a low pass filter were used by Cole *et al.* (1982) to recover the signal. It was found that this technique is

immuned to signal fading from amplitude (optical intensity) fluctuation and the minimum detectable phase shift was  $10^{-3}$  radian which was 3 orders of magnitude higher than that was demonstrated by the active homodyne technique. In addition to the common problems associated with the phase generated carrier (Brown *et al.*, 1991), another disadvantage of this approach is that the phase drifts and the amplitude mismatches will give rise to an output signal that is not a pure heterodyne signal and hence will corrupt the output of the FM discriminator and limit the minimum detectable signal.

Kersey *et al.* (1984) demonstrated an electronically simpler approach for generating the carrier, in which sinusoidal phase modulation is applied directly to a piezo electric fibre stretcher. The output of the interferometer signal is of the form as shown in Equation 2.3.5.14 and is proportional to

$$J_0(\phi_m) - J_1(\phi_m) \sin \omega_m t \sin (\phi_d + \phi_s \sin \omega t) + J_2(\phi_m) \cos 2\omega_m t \cos (\phi_d + \phi_s \sin \omega t) + \dots$$

This signal is gated by a square wave  $G(t)$  with an equal mark and space ratio derived from the oscillator driving the phase modulator. The gated square wave can be represented as

$$G(t) = \frac{1}{2} + \frac{2}{\pi} (\cos \omega_m t - \frac{1}{3} \cos 3\omega_m t + \dots). \quad (2.3.5.22)$$

The resultant signal after multiplication is band pass filtered at  $2\omega_m$ . It will be composed of two sets of terms which are dependent on

$$\cos(\phi_d + \phi_s \sin \omega t) \cos 2\omega_m t \quad (2.3.5.23)$$

and

$$\sin(\phi_d + \phi_s \sin \omega t) \sin 2\omega_m t. \quad (2.3.5.24)$$

The complete resultant signal at the carrier frequency of  $2\omega_m$  after some manipulation is found to be a phase modulated carrier and is proportional to

$$\cos[2\omega_m t \pm (\phi_d + \phi_s \sin \omega t)]. \quad (2.3.5.25)$$

A suitable phase tracking technique was used to recover the signal of interest (details not reported). The primary purpose of this experiment was to test the signal processing technique. As such, no great care was taken to optimise the detection sensitivity of the system which was found to be of the order of mrad.

### 2.3.5.5 Pseudo-heterodyne.

As discussed earlier, it is possible to change the relative optical phase difference between the two arms of an unbalanced interferometer by varying the absolute frequency of the injected laser light. Utilising this fact, the pseudo-heterodyne demodulation generates a heterodyne type output by creating a moving fringe pattern at the optical output of an unbalanced interferometer by ramping the emission frequency of the laser source. During the linearly rising part of the ramp, a constant rate of change of phase is produced, which is equivalent to a frequency shift (Jackson *et al.*, 1982).

$$\frac{d\phi}{dt} = \frac{2\pi n\Delta L}{c} \frac{dv}{di} \frac{di}{dt}, \quad (2.3.5.26)$$

where  $n\Delta L$  is the optical path imbalance in the interferometer. During the flyback, the phase returns to its original value and the process repeats. But because of this flyback, the frequency shift is impure, i.e. it is not a true single sideband frequency shift in the sense that the flyback corresponds to a frequency shift of opposite sign. The resultant spectrum of the photo detector current is complex and contains components at the harmonics of the ramp repetition frequency  $f_r$ . The distribution of power in each of these components depends on the total phase excursion during the ramp period. It is possible to concentrate most of the power in the  $m^{\text{th}}$  harmonics when the interferometer output is driven over any integer number ( $m$ ) complete fringes during the period  $\mathbf{T}$ , so that

$$\frac{d\phi}{dt} \mathbf{T} = 2m\pi . \quad (2.3.5.27)$$

Band pass filtering at  $f_r$  produces a distortion free carrier at  $f_r$ , with a phase modulation identical to that of the interferometer, i.e. the output is identical to that produced by conventional heterodyne modulation (Jackson *et al.*, 1982). They have demonstrated that the dynamic range of the pseudo-heterodyne processing is of the order of 90 dBV with a minimum detectable phase sensitivity of about  $10^{-4}$  rad. A serious drawback of this approach is the limited frequency range in which this scheme can be operated using conventional diode lasers. It is found that the modulation response characteristics of this type of laser falls off appreciably above  $\sim 100$  kHz. Also due to strong harmonic

structure of a ramp wave form, the modulation applied to the injection current is not faithfully transformed into frequency modulation if the repetition rate exceeds ~10 kHz. Therefore, this scheme is mostly viable only for low carrier frequencies.

In order to produce a strong carrier signal free from distortion caused by flyback, serrodyne frequency modulation (infinitesimally small ramp flyback time) technique may be used. It can be shown that under the condition set by equation 2.3.5.27, band pass filtering at the frequency  $m\omega_T$  the signal is proportional to

$$\cos(m\omega_T t + \phi_D + \phi_S \sin \omega t). \quad (2.3.5.28)$$

The phase of this carrier is equivalent to that between the two arms of the interferometer. This signal can be further processed by standard technique using an FM discriminator or phase tracking. Assuming perfect linearity of each portion of the sawtooth and an ideal slope, the spurious sideband power levels approach zero as the fly-back time approaches zero. To maintain greater than 40 dB sideband suppression, the fly-back time must be less than 1% of the period. Therefore, the range of serrodyne frequency translation is typically limited by the bandwidth of the phase modulation technique and the drive electronics.

### 2.3.5.6 Quadrature recombination heterodyne

Jackson *et al.* (1984) demonstrated that it is possible to generate an electronic heterodyne carrier by developing the passive homodyne technique without using an optical frequency shifting element. The quadrature signals are obtained from the passive homodyne technique by utilising highly birefringent fibres and polarisation

mode selection. The signals are translated in frequency by multiplying them with quadrature components of a high frequency local oscillator. If  $\omega_c$  is the angular frequency of the oscillator the resultant signals can be written as proportional to

$$\cos\omega_c t \sin(\phi_d + \phi_s \sin \omega t) \quad (2.3.5.29)$$

and

$$\sin\omega_c t \cos(\phi_d + \phi_s \sin \omega t). \quad (2.3.5.30)$$

Linear combination of these signals produces a phase modulated heterodyne carrier which is proportional to

$$\sin(\omega_c t + \phi_d + \phi_s \sin \omega t). \quad (2.3.5.31)$$

This heterodyne type signal was recovered by demodulation of the above output using the simple phase tracking technique. This detection technique was developed for the use in a fibre gyroscope.

The advantage of the heterodyne detection system is that there is no requirement for feedback to the interferometer. However, the technique is rather difficult to apply in the case of fibre interferometers due to the losses associated with the incorporation of Bragg cells into fibre systems. In addition, the alternatives to genuine heterodyne which involve a means of producing heterodyne-like signals are fairly complicated and do not have sensitivities which are comparable to the active homodyne interferometer.

### 2.3.6 Noise considerations

The ultimate limitation on performance of the interferometer is set by the noise floor of the system and as such, a study of the noise sources and their minimisation is an important consideration in the design. The limiting noise performance of an interferometer sensor is determined by a range of noise producing effects which are associated with the optical and electronic components of the interferometer as well as its interaction with the environment through vibrations, temperature variations and air currents. The discussion which follows considers and quantifies each of the major noise sources in turn. In a subsequent chapter, where the performance of experimental systems is being considered, the treatment of this section is applied to calculate the noise equivalent displacement of the system. A knowledge of the individual noise components is then used to identify the major limitations to improved performance and then modifications were made to reduce these particular noise sources. The principal optical and electronic noise sources are discussed below:

#### *Detector noise*

There are three main sources of detector noise.

*Thermal noise:* This noise is caused by the random thermally excited motion of the charge carriers in a conductor. The motion of these charges causes random currents which add to the signal current in the detector load and shunt (internal) resistor. The mean value of this current is zero but the RMS value ( $I_{RSH}$ ) is not. This noise is broadband “white” noise and is expressed as noise power per unit bandwidth. The expression of thermal noise of the detector shunt resistance is (Palais, 1992)

$$I_{\text{RSH}} = \sqrt{4kT/R_{\text{SH}}} \text{ A}/\sqrt{\text{Hz}}, \quad (2.3.6.1)$$

where  $k$  is Boltzman's constant,  $T$  is the absolute temperature in degree Kelvin and  $R_{\text{SH}}$  is the shunt resistance of the photodiode junction in ohms. At a very low signal power levels, the dominant noise contribution comes from thermal noise.

*Shot noise:* Shot noise ( $I_{\text{SH}}$ ) is the statistical noise associated with the photocurrent and dark current. The shot noise in the signal current is caused by the statistical fluctuation in the arrival rate of photons, even at constant average power. This noise source increases with optical power and is broadband and hence can be expressed as noise per unit bandwidth. The expression for shot noise is (Palais, 1992):

$$I_{\text{SH}} = \sqrt{2e(I + I_{\text{DK}})} \text{ A}/\sqrt{\text{Hz}}, \quad (2.3.6.2)$$

where  $e$  is the charge carried by an electron,  $I$  is the photocurrent and  $I_{\text{DK}}$  is the dark current.

*1/f noise:* The mechanism for 1/f noise is not particularly well understood but the major causes of it in semiconductor devices is traceable to properties of the surface of the material. The generation and recombination of carriers in surface energy states and the density of surface states are the important factors (Motchenbacher, 1993). The characteristics are often empirically determined for individual families of photodetectors. The 1/f noise is governed by the following characteristics (Melles Griot, Application note) :

$$I_{1/f}(s) = I_i \left( \frac{I}{s} \right)^\beta A/\sqrt{\text{Hz}}, \quad (2.3.6.3)$$

where  $I_i$  is typically an inverse function of the active area,  $\beta$  is an empirically derived constant that will vary from 0.25 to 1.0 depending upon the specific construction of the detector and  $s$  is Laplace operator ( $j\omega$ ). It may be noted that 1/f noise is especially troublesome at low audio frequencies (Motchenbacher, 1993) and for higher frequency applications, detector performance is limited by other noise sources.

### *Source noise*

The laser source introduces two types of excess noise into the system; intensity noise and frequency noise. The intensity noise is due to power fluctuations of the source and can result from: (1) intrinsic fluctuations of intensity in the laser source, (2) mechanical jitter in the laser to fibre coupling mount and (3) microbend losses in the fibre and mechanical vibration in the fibre to detector mounts. In typical systems, mechanisms (1) and (2) usually dominate (Bucholtz *et al.*, 1988). Intensity noise can be compensated by choice of a suitable signal processing scheme. In an active homodyne scheme in which complementary outputs are accessible (eg Mach-Zehnder), the quadrature reference level is zero, provided the two output signals are subtracted after the adjustment of the gains so that the two channels have equal amplitude. Under these conditions, the system is rendered relatively insensitive to common mode source intensity fluctuations. Frequency noise is created by frequency jitter in the output of the laser due to mode instability and gain fluctuations. Also it can be seen from equation 2.3.5.2, the effect of frequency noise in an interferometer with an optical path imbalance will cause phase changes in the output which are indistinguishable from

those produced by the measurand. Thus it is evident that the effect of frequency noise can be reduced by minimising the imbalance in optical path, and for a perfectly balanced interferometer, frequency noise has no effect.

### ***Environmental noise***

Ambient noise, such as table vibration or air turbulence, is normally only significant in the low frequency region and can be disregarded when detecting high frequency measurands using a technique which permits frequency discrimination. Perturbations due to vibration and changes in temperature gives rise to environmental noise which, acting on the sensing element, causes phase changes indistinguishable from those produced by the measurand. Vibration noise can be minimised by proper packaging, vibration isolation and use of an electronic feedback circuit (Dandridge *et al.*, 1980). The effects produced by temperature changes are very low frequency in nature and can readily be removed, mostly by using feedback circuits and filtering.

### ***Noise associated with the electronics***

Noise at the output of the electronics arises from a number of different sources. In addition to the thermal, shot and  $1/f$  noise in the detector itself, there is also dark current noise in the detector, thermal noise in the load resistor and noise added by each of the amplifier stages.

### ***Noise in practical electronics circuits:***

***Dark current noise:*** In a photodetector dark current noise is caused by thermal generation of free charge carriers in the detector. Because of its thermal origin, it will increase with temperature and ranges from a fraction of nanoampere to more than

several hundred nanoamperes depending on the type of detector used. In general, for common visible and near infrared materials, silicon photodetectors have the lowest dark current.

*Thermal noise from the load resistor:* The choice of optimum load resistor in practice is critical because a large load resistor is needed to obtain a high signal voltage and also to reduce thermal noise current, but a small load resistor is needed to obtain a large bandwidth and wide dynamic range.

*Noise generated in the amplifiers:* It is difficult to analyse an amplifier from an individual component noise standpoint as it contains many components. However by referring all noise to the input port and considering the amplifier to be noise-free, a noise model can be developed which is helpful to simplify noise analysis. The amplifier noise can be adequately represented by a zero impedance voltage generator  $V_A$  in series with the input port and an infinite impedance current generator  $I_A$  in parallel with the input port. An amplifier is commonly designed by using either a field effect transistor or a bipolar junction transistor. Noise in the field effect transistor is contributed by the thermal noise generated by the drain-source channel conductance and biasing resistors, shot noise arising from the leakage current between the gate and the source and  $1/f$  mechanisms. In a bipolar transistor, the major sources of noise are thermal noise generated by the biasing resistors and base spreading resistor (ohmic resistance of the lightly doped base region between external base contact and active base region),  $1/f$  noise due to the flow of base current through base-emitter depletion region and shot noise due to the flow of base current and collector current at their respective junctions (Motchenbacher, 1993). The noise power generated in the field

effect transistor is found to be proportional to the cube of the bandwidth and in bipolar transistors it is proportional to the square of the bandwidth (Palais, 1992).

The main objective of the design of a signal processing unit is to obtain useable signals at its output with maximum signal to noise ratio. A signal processing unit mainly consists of a photodetector and an associated amplifier together with the necessary signal recovery circuits. The function of the photodetector is to detect the incident light signal and convert it to an electric current and the amplifier converts this current into a useable voltage while introducing the minimum amount of additional noise to corrupt the signal. The choice of configuration depends upon dynamic range and noise considerations. Since most of the noise is generated in the front end (the photodetector and the first amplifier), its design is the principal factor in determining the performance of the signal processing unit (Smith and Personic, 1972 ). The equivalent circuit of the front end consists of a photodetector and a voltage amplifier (Gower 1984) as shown in Figure 2.3.6.1.

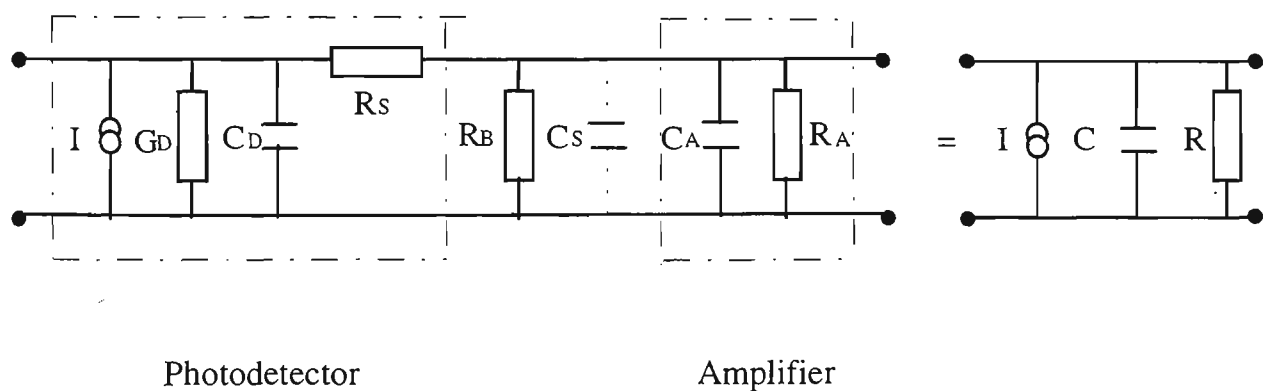


Figure 2.3.6.1 Equivalent circuit for the front end of the signal processing unit.

In this figure,  $I$  is the photogenerated current,  $G_D$  is the shunt conductance which represents the slope of the reverse bias current-voltage characteristics of the photodiode,  $C_D$  is junction capacitance,  $R_S$  is the bulk semiconductor and contact resistance,  $R_B$  is the bias resistance,  $C_S$  is the additional distributed stray capacitance and  $R_A$  is the input impedance of the amplifier which is shunted by a capacitance  $C_A$ . Assuming  $R_S \ll R_A$  and since usually  $1/R_B$  and  $G_D$  are much smaller than  $1/R_A$ , we can write

$$\frac{1}{R_A} + \frac{1}{R_B} + G_D = \frac{1}{R}$$

and

$$C = C_D + C_S + C_A.$$

A configuration with transimpedance feedback amplifier at the front end is a preferred design because of its low noise as well as wide dynamic range. As shown in the Figure 2.3.6.2, the equivalent noise circuit can be modelled as (Gower, 1984):

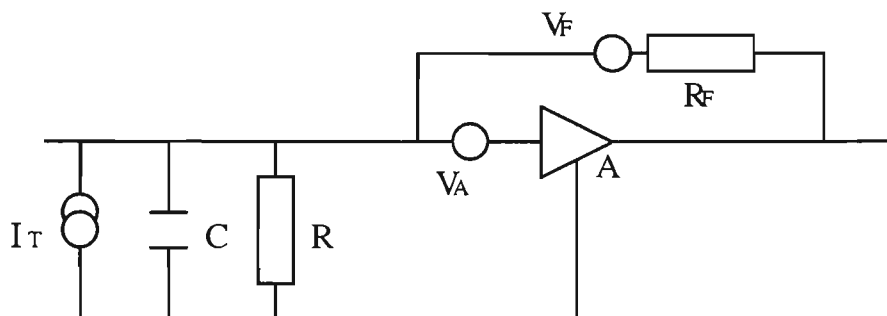


Figure 2.3.6.2 Equivalent noise circuit for the transimpedance amplifier.

In this figure,  $V_A$  is equivalent voltage noise in the amplifier and  $V_F$  is voltage noise generated in the feedback resistor  $R_F$ .  $I_T$  represents the total noise current which includes shot noise, thermal noise of the biasing and amplifier input resistances as well as the amplifier current noise and is given by (Gower, 1984)

$$(I_T)^2 = (I_{SH})^2 + (I_{TH})^2 + (I_A)^2 \quad (2.3.6.3)$$

In this equation,  $I_{SH}^2 = (2 e I \Delta f)$  is the shot noise originating in the photodetector in a bandwidth  $\Delta f$  and  $I_{TH}^2 = (4kT\Delta f / R)$  is the noise originating in the resistive element in the same bandwidth.

Assuming each of these noise sources is independent of and uncorrelated with the others, the total noise can be represented by the sum of the mean square value of each of the individual sources. The RMS signal to noise ratio at the receiver front end is found to be (Gower, 1984)

$$\frac{V}{V_N} = \frac{I}{[V_A^2 \left\{ \left( \frac{1}{R} + \frac{1}{R_F} \right)^2 + \frac{4\pi^2}{3} C^2 (\Delta f)^2 \right\} + 2eI + 4kT \left( \frac{1}{R} + \frac{1}{R_F} \right) + I_A^2]^{1/2} \Delta f^{1/2}}, \quad (2.3.6.4)$$

(a)                      (b)                      (c)                      (d)                      (e)

where  $V$  is signal voltage and  $V_N$  is total RMS noise voltage. The five noise terms in the denominator (a-e) may be separately identified for general design of the system and evaluating its expected performance. It can be seen that (a), (b) and (e) are the amplifier noise terms, (c) is the shot noise term and (d) is the thermal noise term. The value of

the front-end resistors may be increased in order to reduce the terms (a) and (d), but high gain and high input impedance may make the circuit prone to high frequency oscillations as a result of positive feedback via parasitic capacitance. These high frequency oscillations may be avoided by careful layout and effective screening of the sensitive components. At higher frequencies, the total input capacitance must be minimised in order to reduce the effect of the term (b). The shot noise term (c) is dependent on the level of the received signal and dominates all other terms at high optical input levels.

When two complementary outputs are available, a differential amplifier stage is normally used (to reduce the common mode noise) following the transimpedance amplifiers of the signal processing unit. In order to find the noise contribution of this stage, it is necessary to analyse the noise performance of an operational amplifier which is configured with differential input. Following the approach of Motchenbacher (1993), a differential amplifier with all noise sources in place can be represented as shown in Figure 2.3.6.3 below.

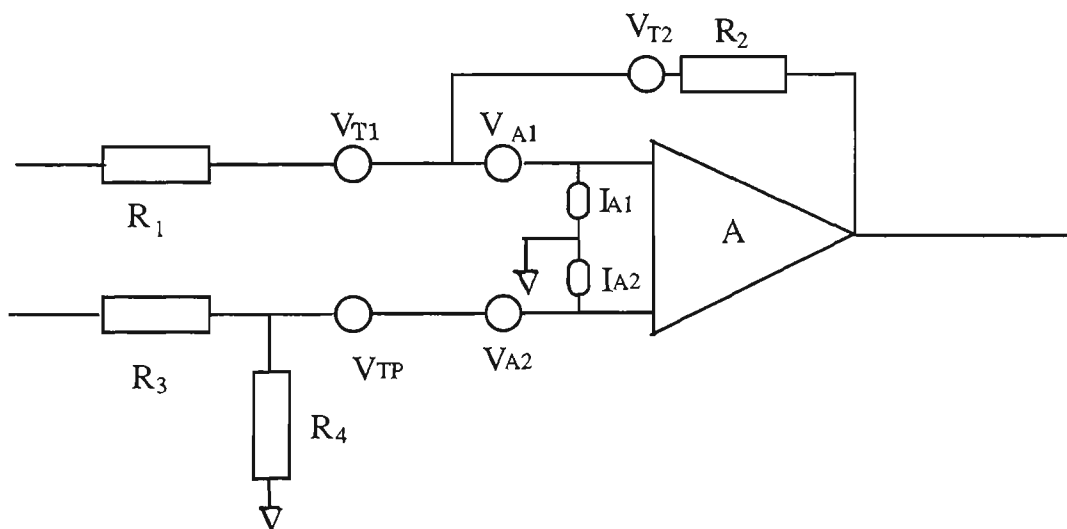


Figure 2.3.6.3 Noise equivalent circuit of the differential amplifier.

Assuming  $R_2/R_1 = R_4/R_3$  for an ideal differential amplifier and putting  $R_p$  equivalent to the parallel combination of  $R_3$  and  $R_4$ , equivalent input noise of the differential amplifier ( $V_{eq}$ ) can be expressed as

$$V_{eq}^2 = \left(1 + \frac{R_1}{R_2}\right)^2 \left(V_{A1}^2 + V_{A2}^2 + V_{TP}^2\right) + V_{T1}^2 + \frac{R_1^2}{R_2^2} V_{T2}^2 + I_{A1}^2 R_1^2 + I_{A2}^2 R_p^2 \left(1 + \frac{R_1}{R_2}\right)^2, \quad (2.3.6.5)$$

where  $R_1$ ,  $R_3$  and  $R_4$  are input resistances,  $R_2$  is feedback resistance,  $V_{A1}$  and  $I_{A1}$  are noise voltage and current contribution from the amplifier reflected into the inverting input of the operational amplifier,  $V_{A2}$  and  $I_{A2}$  are noise voltage and current contribution from the amplifier reflected into the non-inverting input of the operational amplifier and  $V_{T1}$ ,  $V_{T2}$  and  $V_{TP}$  are thermal noise voltage sources due to the resistances  $R_1$ ,  $R_2$  and  $R_p$ .

Figures for the various noise voltages and currents of the various components which are included in the discussions above are available in the manufacturer's data sheets. By working progressively through the circuit, calculating the input noise due to the various uncorrelated sources (from equation 2.3.6.4 and 2.3.6.5) and then multiplying by the gain to get the noise at the output of each stage, the noise at the final output can be obtained. When a number of amplifier stages are connected in series, the input noise and the noise from the early stages dominates at the final output as it is this noise which is multiplied by the largest gain.

### 2.3.7 Previous work on optical methods of detection of laser generated ultrasound

A number of authors have reported the detection of laser generated ultrasound in bulk materials using interferometers to detect the acoustic waves on the rear surface of the material. Similar systems have been used in optical detection of surface acoustic waves. Although this thesis is not concerned with surface acoustic waves, some references to this work have been included in order to give a more comprehensive discussion of optical detection methods suitable for use with bulk waves. The discussion which follows concentrates on the details of optical detection systems for ultrasonic waves. Since laser generated ultrasound requires very high bandwidth for detection (higher than with some other generation techniques), the discussion principally involves work where optical generation as well as optical detection is used. The papers discussed below have mostly already been referred to in a previous section where the optical generation aspects of the work have been discussed.

The detection of laser generated ultrasound by an optical method was first reported by Bonderenko *et al.* (1976). A series of experiments was conducted to measure the longitudinal wave velocity and hence deduce the elastic modulus of a steel cylinder. A bulk optic dual beam homodyne interferometer with a sensitivity of 1 nm in a bandwidth of 5 kHz to 150 MHz was used. This interferometer was capable of measuring amplitudes in the range 1 - 100 nm. A feedback system was used to compensate for low frequency mechanical vibrations. The reflectivity of the rear surface was not mentioned.

Hutchins and Nadeau (1983) used a bulk optic Michelson interferometer to detect ultrasonic waveforms at the epicentre of an aluminium plate. The optical power of the

He-Ne laser used in this interferometer was 5 mW. The interferometer was stabilised against low frequency vibration and had a sensitivity of the order of 0.02 nm with a bandwidth of 40 MHz. Noise on the detected signal was reduced by polishing the rear surface of the sample and by using an interference filter to allow the entry of only 632.8 nm He-Ne light to the detector. The ultrasonic waveforms detected in the thermoelastic, ablation and with modified surfaces (a thin oil layer and adhesive tape were used on the target surface ) agreed well with prediction.

The detection of acoustic pulses generated by a low energy pulsed laser at the epicentre in metallic and non-metallic targets was reported by Bourkoff and Palmer (1985). A sensitive bulk optic laser interferometer (Palmer, 1984) was used in this experimental arrangement. An electronic control system was included to improve fringe stability so that the entire system can be operated in the vicinity of low frequency noise sources. The high frequency intensity noise of the laser source was eliminated by subtraction of two complementary (orthogonally polarised) interferometer outputs. The sensitivity of the interferometer was about 50 pm over a bandwidth of 10 MHz. The detection surface of the metallic plate was polished and for non-metallic samples (cured composites), a tiny mirror was bonded to the rear surface to enhance specular reflection.

A bulk optic confocal Fabry Perot interferometer for the detection of laser generated ultrasonics by measuring the Doppler shift in a laser beam reflected from the rear surface of a machined steel plate was reported by Monchalin (1985b). The target surface for ultrasonic generation was modified by covering with a water film. The experimental setup used a 5 mW He-Ne laser and a confocal Fabry-Perot of 3.75 cm

thickness and electronic bandwidth of approximately 1 MHz - 13 MHz, giving an etendue of  $\approx 10^{-3} \text{ mm}^2 \text{ sr}^2$ . Such an etendue enabled the reception of light at 1.5 m from a 1 mm diameter spot through a 5 cm diameter lens aperture. The detection was reported to be limited by quantum noise. Monchalin *et al.* (1989) discussed broadband optical detection of ultrasound using an interesting variation of a heterodyne receiver. A reference signal was obtained from the signal beam by using a confocal Fabry-Perot interferometer which was tuned to the laser line to strip the modulation sidebands. Two arrangements for overlapping the signal and reference beam were compared. No results were reported for optimised performance of this novel system but the authors did conclude that its performance was superior to a velocity interferometry (time delay interferometry) scheme at frequencies above 6 MHz. This latter approach uses frequency demodulation by the slope of an optical filter (interferometer) (Monchalin, 1986).

Scruby *et al.* (1986) reported the measurement of frequency-dependent ultrasonic attenuation in steels with different microstructure by using laser generation and a stabilised bulk optic laser interferometer. The interferometer was used to measure the surface displacement at the epicentre of steel samples under the ablation regime. A small amount of volatile liquid was applied on the generating surface to enhance the amplitude of ultrasonic pulses. The interferometer used was highly developed and was similar to that described by Moss (1984). The reference beam of the interferometer was frequency shifted electro-optically by using a Pockel cell device to avoid the problem of directional ambiguity. This interferometer used a 5 mW He-Ne laser and was stabilised against low frequency vibration by a phase-locking system. It had a working bandwidth of  $\sim 100$  MHz and was limited by noise to the detection of

displacements greater than  $\sim 0.1$  nm from a polished steel surface without signal averaging. The data was recorded by averaging 10 signal pulses to reduce electronic noise to less than 0.2% of the full scale signal. The target surface was modified with a very thin layer of light oil or solvent to generate acoustic pulses with increased amplitudes.

Dewhurst *et al.* (1987) detected laser generated acoustic waveforms in an aluminium alloy of 50 mm diameter and 25.4 mm thickness by using a modified bulk optic Michelson interferometer. The interferometer used a 5 mW polarised He-Ne and was stabilised against low frequency vibration by feedback to an electro-mechanical vibrator controlling the position of the reference mirror. Intensity fluctuation of the He-Ne laser was minimised by electronic subtraction of two orthogonally polarised outputs. The sensitivity of the interferometer was  $20 \text{ mV nm}^{-1}$  and the bandwidth was 700 Hz - 130 MHz. Detection of 25 pm displacement was reported to be possible from a polished surface under the experimental conditions described in this paper. This is a relatively straightforward interferometer and the performance achieved is very good.

A Michelson type laser displacement interferometer, having a bandwidth of 10 kHz - 50 MHz was used for the detection of laser generated ultrasonics in different metallic samples by Aussel *et al.* (1988). The interferometer has been described by Drain *et al.* (1977) and is similar to that of Moss (1984). Acoustic displacements of longitudinal, shear and surface waves generated under thermoelastic and ablation regimes were recorded. A bulk optic heterodyne Michelson interferometer was used by Aussel and Monchalin, (1989) to detect laser generated acoustic waveforms at the epicentre of PZT ceramic and metal-ceramic composite materials to measure the acoustic velocities and

the elastic constants of these materials. The interferometer has been described in detail by Monchalin (1985a) and was reported to be quantum noise limited with a sensitivity of  $10^{-14}$  m for a bandwidth of 1 Hz. In order to obtain greater sensitivity from the polished surface of the materials, a 1 W single mode cw Argon laser was used to increase the optical power level in the detector. The bandwidth of the interferometer was 250 kHz to 35 MHz.

A commercial type of bulk optic heterodyne interferometer (ULTRAOPTEC OP-35-i/o) using a 5 mW He Ne laser was used by Moreau *et al.* (1990) for detection of laser generated surface waves in a thin film. The interferometer had a bandwidth of 0.5-35 MHz and a sensitivity 1 nm (limited by the wideband electronic noise level) and was used for the determination of ultrasonic velocity in thin films.

Davis *et al.* (1991) have reported the use of a fibre optic Michelson interferometer incorporating an active homodyne demodulation technique for detection of ultrasonics by placing the sensing arm in contact with the rear surface of the metal or by embedding it in epoxy based material. Similar work from the same group using the same type of interferometer to detect ultrasonics and acoustic emission was described by Ohn *et al.* (1992), Liu *et al.* (1990) and Measures (1990, 1992). Signal fading due to the random orientation of the state of polarisation (SOP) of the optical beam in the fibre was minimised in these experiments by adjusting the input SOP and securing the lead fibres against vibration and air currents. The output signal was recovered through a high pass filter with a cut off frequency of 70 kHz. The work of this group represents the only previous work in which fibre optic interferometric detection of acoustic waves

is used to monitor the curing of epoxy-based composites. The authors had to embed the sensing fibre in the composite and no remote measurements were reported.

Hrovatin and Mozina (1993) demonstrated the detection of laser generated acoustic waves at the epicentre of a metallic sample using a stabilised bulk optic Michelson interferometer. The interferometer used a He-Ne laser source and its sensitivity in the linear range was reported to be  $59.5 \text{ mVnm}^{-1}$  with a bandwidth 150 kHz to 60 MHz. The same type of interferometer was used by the authors (Mozina and Hrovatin, 1996) for detection of laser-induced ultrasonic amplitudes of about 10 pm in a metallic sample.

A laser based ultrasonic system which is suitable for a wide range of applications, including crack sizing, bond assessment in aircraft components and also for improved characterisation of conventional transducers, was described by Bowles and Scala (1993). A commercial heterodyne Mach-Zehnder interferometer with a bandwidth of 10 kHz to 35 MHz and a 5 mW He-Ne laser source, was used for detection of the surface acoustic waves generated by a pulsed laser. The interferometer was also used to measure the displacement across the front face of a 10 MHz ultrasonic probe. It was demonstrated that displacements as small as 0.02 nm could be mapped across the polished transducer surface.

Shan *et al.* (1996) reported the detection of laser generated ultrasonics by using a confocal Fabry-Perot interferometer to analyse the light reflected from the rear surface of the target. This scheme makes use of both the reflected and transmitted beams from the interferometer. By recording the difference between reflected and transmitted

signals, a significant sensitivity improvement (between 2 and 17) is made compared to either of the individual signals and also there is some reduction of common mode noise. A 30 mW argon-ion laser operating on a single longitudinal mode was used with this interferometer to demonstrate the sensitivity improvement in detection of laser generated ultrasound at the epicentre of a 1.5 mm thick aluminium sample.

An interesting variation of a fibre optic Michelson interferometer has been described by the group at Virginia Polytechnic (Murphy *et al.*, 1991; Claus *et al.*, 1992). This system used a fibre coupler which had been cleaved and polished just beyond the coupling region as the sensing element. One of the fibre cores was coated with aluminium to provide a reference beam and the other was reflected from the surface of a material placed very close to the sensor. The sensor was able to detect surface acoustic waves of minimum amplitude 0.18 nm with unspecified bandwidth. The disadvantage of this sensor was that it had to be placed very close to the surface being measured and a separation of only 30  $\mu\text{m}$  resulted in a 3 dB drop in return signal level. It is not possible to provide feedback control of drift in this sensor arrangement. This sensor was compared to a standard fibre Michelson interferometer (without any thermal drift control) and found to have superior thermal stability. Claus *et al.* (1992) also demonstrated that surface acoustic waves could be detected using a fibre optic Fabry-Perot interferometer placed in contact with the surface.

Bruinsma (1987), Vogel and Bruinsma (1987) and Bowers (1982) have used variations of the fibre optic time delay interferometer to measure ultrasonics or surface acoustic waves. These interferometers use the scattering from the surface and a long path difference interferometer to obtain a signal which, for surface displacements much less

than an optical wavelength, is proportional to the velocity of the surface vibration. The principle of operation is easiest seen by observing that the scattered light is interfering with a delayed version of itself and the phase of the interference (and hence the magnitude of the signal) is dependent on the displacement of the surface during the delay time of the interferometer (and hence the surface velocity). The reason for the long path difference in the interferometer (of the order of a metre) is that one needs to delay the light by a substantial fraction of the acoustic period in order to obtain a significant phase difference (movement of the surface). This type of interferometer has a basic sensitivity similar to that of an interferometer using a normal reference beam. However, there are a number of other considerations to be taken into account. The sensitivity of the interferometer is dependent on acoustic frequency and for maximum response the path difference between the arms of the interferometer needs to be adjusted so that the phase difference is  $90^\circ$ . In addition, the interferometer is subject to intensity fluctuations produced by speckle and it is common to incorporate a low frequency modulator in the interferometer to effectively provide continuous calibration. With this type of interferometer, Bruinsma (1987) obtained an amplitude detection limit of 0.02 nm in a 10 MHz bandwidth with the fibre placed very close to the surface (distance not specified). Bowers (1982) used this type of interferometer with a low coherence source and an optical modulator which averaged the output signal over several cycles to obtain an output which depends on the amplitude of the acoustic wave. With a fibre-to-surface distance of 10  $\mu\text{m}$ , this system can detect surface acoustic waves over a 110 dB dynamic range with a minimum amplitude sensitivity of 0.003 nm when using a lock-in integration time of 0.1 s. When used in this way the system is, of course, not capable of recording acoustic waveforms.

Lewin *et al.* (1985) used a mixed fibre optic and bulk optic interferometer arrangement which was operated in both active homodyne and pseudo-heterodyne modes to detect surface vibrations in an open air path. This system launched a He-Ne laser into one arm of a directional coupler and so the interferometer operated with reduced light levels due to fibre injection loss. The mixing of the reference beam from the fibre and the light from the other fibre arm of the directional coupler (after being scattered from the target surface) was done using a lens and beamsplitter arrangement and so the interferometer avoided the extra losses associated with injecting the scattered beam back into an optical fibre. The interferometer performance was measured using an uncoated microscope slide mounted on a PZT transducer as the target surface. The source fibre-to-target distance was greater than 2 metres. With active homodyne detection, using the reference arm fibre wrapped around a PZT cylinder, the NED varied from 0.02 nm (at 10 Hz) to 0.001 (at 10 kHz). The bandwidth is not given. With pseudoheterodyne detection, the NED was 0.01 nm at 100 Hz in a bandwidth of 500 Hz.

Philp and Booth (1994) used a type of fibre optic active homodyne Mach-Zehnder interferometer to measure small transverse mechanical vibrations in structures excited thermoelastically using modulated laser diodes. They used lenses to increase the fibre to surface distances to between 15 cm to 100 cm and natural aluminium targets. The signal could also be detected at distances upto one metre through an intervening glass window. The interferometer operated at a wavelength of 1523 nm and had a sensitivity of 0.3 nm and a 30 kHz bandwidth. While this system is not suitable for ultrasonics it does indicate that if the bandwidth and sensitivity can be improved, then large fibre-to-target operating distances should be possible with all-fibre systems.

Lin *et al.* (1994) reported the development of a high precision hybrid bulk/fibre optic Mach-Zehnder type interferometer for displacement measurement. A 1mW frequency stabilised He-Ne laser was used as a light source. The system for coupling light from the laser into the fibre of the interferometer incorporated an optical isolator and a polariser/quarter wave plate combination (circular polarised light) before a beam splitter for separation of signal and reference beams. A micrometer translation stage was used to create the displacement for measurement. A phase-locked synthetic heterodyne techniques were used in signal processing. The system resolution was greatly improved by utilising a frequency division method involving high frequency sampling to give good phase resolution. A minimum detectable amplitude of displacement of 0.063nm was obtained.

A fibre optic Michelson interferometer used for the in-process measurement of Acoustic Emission (AE) generated by a cutting tool has been described by Carolan *et al.* (1996). The interferometer signal arm was terminated in a rugged optical probe containing a lens to focus the light onto the target surface at a distance of 25mm. A fraction of the light scattered by the target surface was collected by the probe lens and recoupled into the fibre, which simultaneously supported the outgoing and return light signals. Light in the reference arm was guided to a fibre loop reflector, which acted as a controllable mirror for matching the reference beam to the optical state of the signal beam. An active homodyne phase control system was implemented in which piezoelectric cylinders were used as fibre stretchers in the reference arm as part of a servo loop to maintain the interferometer at phase quadrature. The desired high frequency AE signal was recovered via a 100kHz - 1 MHz bandpass filter. The NED of

the interferometer was reported to be 0.1nm over the full 0.1 - 1 MHz bandwidth (~0.1 pm/ $\sqrt{\text{Hz}}$ ).

A summary of the previous work on different types of interferometer actually been used for the detection of laser generated ultrasound in bulk materials is given below.

Interferometer	Laser Used	Bandwidth	Sensitivity	Target Surface
Bulk optic dual beam homodyne (Bondarenko <i>et al.</i> 1976)	He-Ne	5 kHz - 150 MHz	1 nm	45% reflectivity
Bulk optic Homodyne Michelson (Hutchins and Nadeau, 1983)	5 mW He-Ne	40 MHz	0.02 nm	Polished
Bulk optic Michelson (Bourkoff and Palmer, 1985)	He-Ne	10 MHz	0.05 nm	Mirror bonded to non-metallic sample, metallic sample polished.
Bulk optic confocal Fabry-Perot (Monchalin, 1985b)	He-Ne 5 mW	13 MHz	Not quoted	Machined but not polished steel plate

Interferometer	Laser Used	Bandwidth	Sensitivity	Target Surface
Bulk optic Homodyne (Scruby <i>et al.</i> , 1986)	He-Ne 5 mW	100 MHz	0.1 nm	Polished Surface
Bulk optic Homodyne Michelson (Dewhurst <i>et al.</i> , 1987)	He-Ne 5 mW	130 MHz	0.025 nm	Polished
Bulk optic Michelson (Aussel <i>et al.</i> , 1988)	Not quoted	10 kHz - 50 MHz	Not quoted	Polished
Bulk optic heterodyne Aussel and Monchalin (1989)	1W Argon-ion	250 kHz - 35 MHz	Not quoted	Polished

Interferometer	Laser Used	Bandwidth	Sensitivity	Target Surface
Fibre optic, Active homodyne Michelson (Davis <i>et al.</i> , 1991)	Not quoted	Not quoted	Not quoted	Optical fibre adhered to Aluminium plate. Optical fibre embedded in the epoxy plate.
Bulk optic Michelson (Hrovatin and Mozina, 1993)	He-Ne	150 kHz - 60 MHz	59.5 mVnm <sup>-1</sup>	Not quoted
Bulk optic confocal Fabry- Perot (Shan <i>et al.</i> , 1996)	Argon-ion, 30 mW	Not quoted	Not quoted	Unpolished

Table 2.3.8 Summary of the previous work on the detection of laser generated ultrasonics by interferometers.

### 2.3.8 Conclusion

The interest in this thesis is in attempting to develop a system which is capable of making remote measurements of ultrasonic signals from curing epoxy samples. For maximum usefulness in practical situations this system should be based on optical fibres so that the interferometer can be located away from the measurement environment and less than ideal measurement situations may be more easily accommodated. The work described in this chapter has shown that remote measurements using optical generation and optical detection are certainly possible with bulk optic interferometers and with optical fibres embedded in the target. While the sensitivity and NED of a fibre interferometer is worse than that of a similar bulk optic device, it does appear possible that fibre interferometers may be useful provided it is carefully constructed and the acoustic displacements are large enough.

The magnitude of the acoustic displacements at the rear surface of a target when a Q-switched laser pulse is incident on the front surface can be estimated from analysis of the results of measurements contained in the various papers referred to earlier in this chapter. It can also be estimated from calculations involving the relevant system parameters. Such a calculation has been reported by Scruby and Drain (1990).

Scruby and Drain (1990) estimated the magnitude of the ultrasonic field generated by a Q-switched Nd:YAG laser of pulse energy 100 mJ. The maximum displacement with a 100 mm thick target from 6 mJ absorbed energy in an aluminium sample (assuming reflectivity of 94%) was found to be  $\sim 0.9$  nm in the thermoelastic regime. Any pulse broadening due to source aperture, losses in the material or receiver response was not taken into consideration in the estimated figure. The peak compression-wave

displacements in the ablation regime was found to be in the range of 0.3 - 3 nm with the ablative forces in the range of 5 - 50N (generated by focusing the 100 mJ pulsed laser). These figures are a little higher than the typical displacements obtained in the experimental systems discussed earlier (after allowing for the approximate  $1/r$  dependence on thickness). For example, for measurements at the epicentre, Aussel *et al.* (1988) reported displacements in aluminium and steel ranging from less than 0.05 nm (onset of ablation) to greater than 20 nm (strong ablation) for targets of thickness 10 mm - 25 mm. In the thermoelastic regime, the initial steps are quite small and often hard to read from figures but the total displacement by the time of arrival of the S wave can be up to 10 - 20 nm. These figures will vary substantially with the type of material and the angle of observation of the acoustic waves. However, it is clear that if one is aiming at non-contact optical generation and detection of bulk acoustic waves in a target material using a fibre interferometer for detection, then for reasonable performance the fibre interferometer needs to have a NED of less than about 1 nm with a bandwidth of at least 10 MHz. In addition, the fibre interferometer needs to be able to operate with fibre-to-target distances of at least 10 cm for reasonable flexibility in practical measurement situations. Such a performance has not yet been realised with all-fibre interferometers but it does appear possible.

The next chapter describes the details of construction of a Q-switched Nd:YAG laser suitable for generation of ultrasonics in metallic and non-metallic samples. Details are also given of the development of a number of fibre optic interferometers. The performance of the best of these interferometers exceeds the minimum performance figures specified above.

As a starting point of this work, it was decided to fabricate and characterise similar types of interferometers using heterodyne and homodyne demodulation techniques to carry out investigation on the sensitivity achievable at higher bandwidths. Construction details and characterisation of the interferometers are described in the next chapter.

## Chapter 3: Experimental systems

In this chapter, the design and construction of a Q-switched Nd:YAG laser for generation of ultrasonics is presented and construction and characterisation of heterodyne and active homodyne interferometers are described. Four different models of active homodyne fibre optic interferometers incorporating open air paths were built and tested. Each model displayed progressively better performance with the final one being suitable for the detection of ultrasonics. This final interferometer was used in the measurements reported in later chapters.

### 3.1 Design and construction of the Q-switched Nd:YAG laser

The Nd:YAG laser constructed for use in this work used a small flat/flat Nd:YAG rod pumped by a single linear flashtube in a diffusively reflecting cavity. The laser used a polariser and Pockels cell inside the cavity to provide Q-switched pulses of approximately 20 ns duration and energy up to about 60 mJ. The laser is shown schematically in Figure 3.1 and the various elements of this system are briefly described below.

*Pump Cavity:* The mechanical design of the diffuse reflecting pump cavity of 12 cm length and 7.8 cm diameter is shown in Figure 3.2. It consists of two concentric cylindrical tubes. The lamp and the laser rod were placed close coupled near the axis of the inner tube which was made up of glass. The outer tube was made up of perspex. The annular region between the two concentric tubes was filled with barium sulphate

powder to provide a reasonably efficient diffuse reflecting cavity in which the only significant optical absorber was the YAG rod. The inner tube was filled with water to provide cooling for the laser rod. Viton O-rings were used for sealing polished aluminium end plates to the cavity and also for sealing the laser rod and flashtube into the end plates.

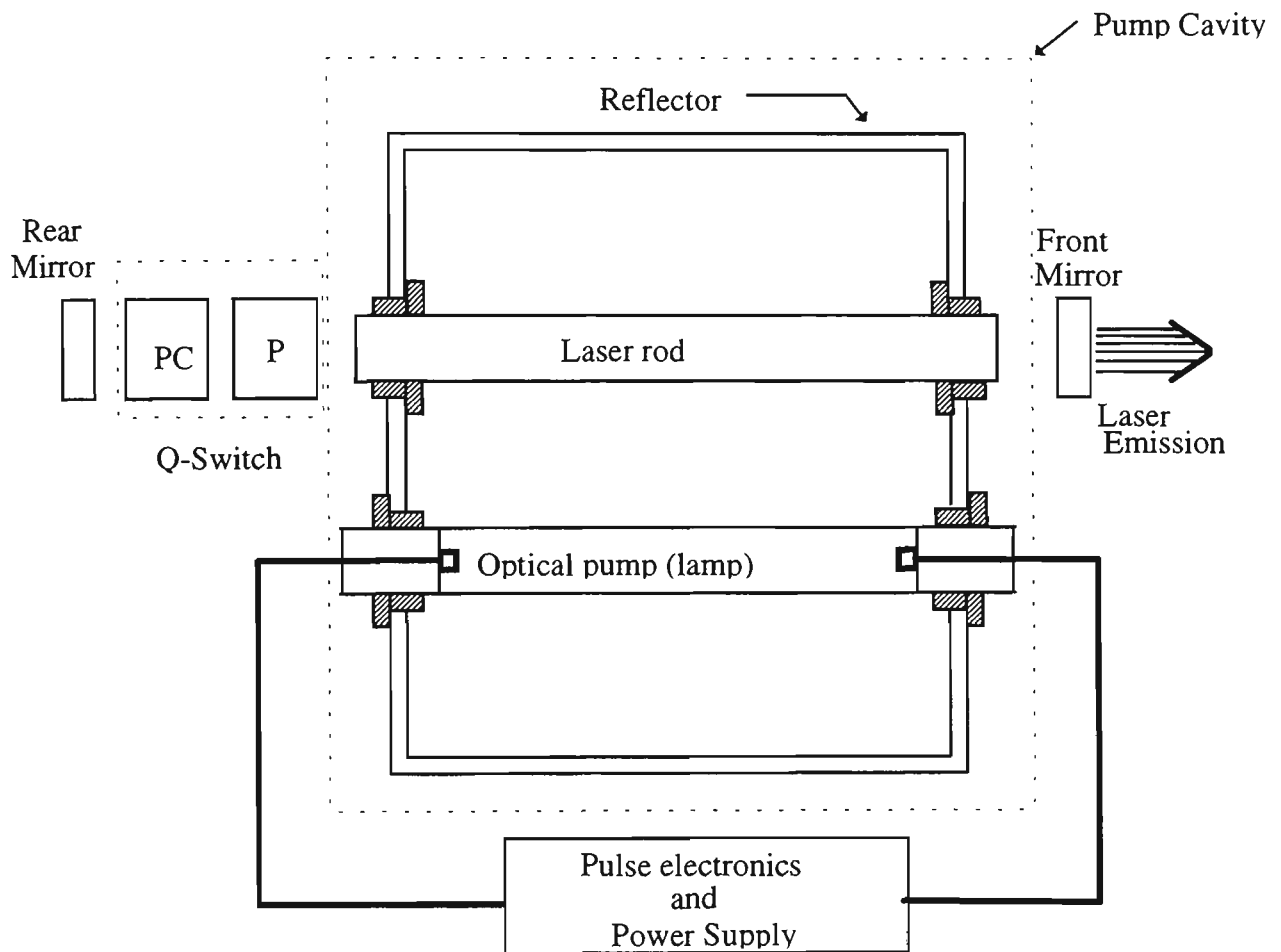


Figure 3.1 Optically pumped laser configuration.

*Coolant:* The coolant is necessary to remove heat generated in the laser rod and flashtube. Water is used as the coolant as it is by far the most convenient fluid to use and also because of its high specific heat, good thermal conductivity, low viscosity and chemical stability under the influence of strong UV radiation from the flashtube. The

cavity used a small pump to circulate distilled and de-ionised water through the laser cavity and then into a reservoir of about 70 litre capacity which also acted as a heat exchanger. Since the anode operates at a higher temperature than the cathode, the water flow was directed from anode to cathode and a flow of 6 to 10 litres/minute was maintained during operation.

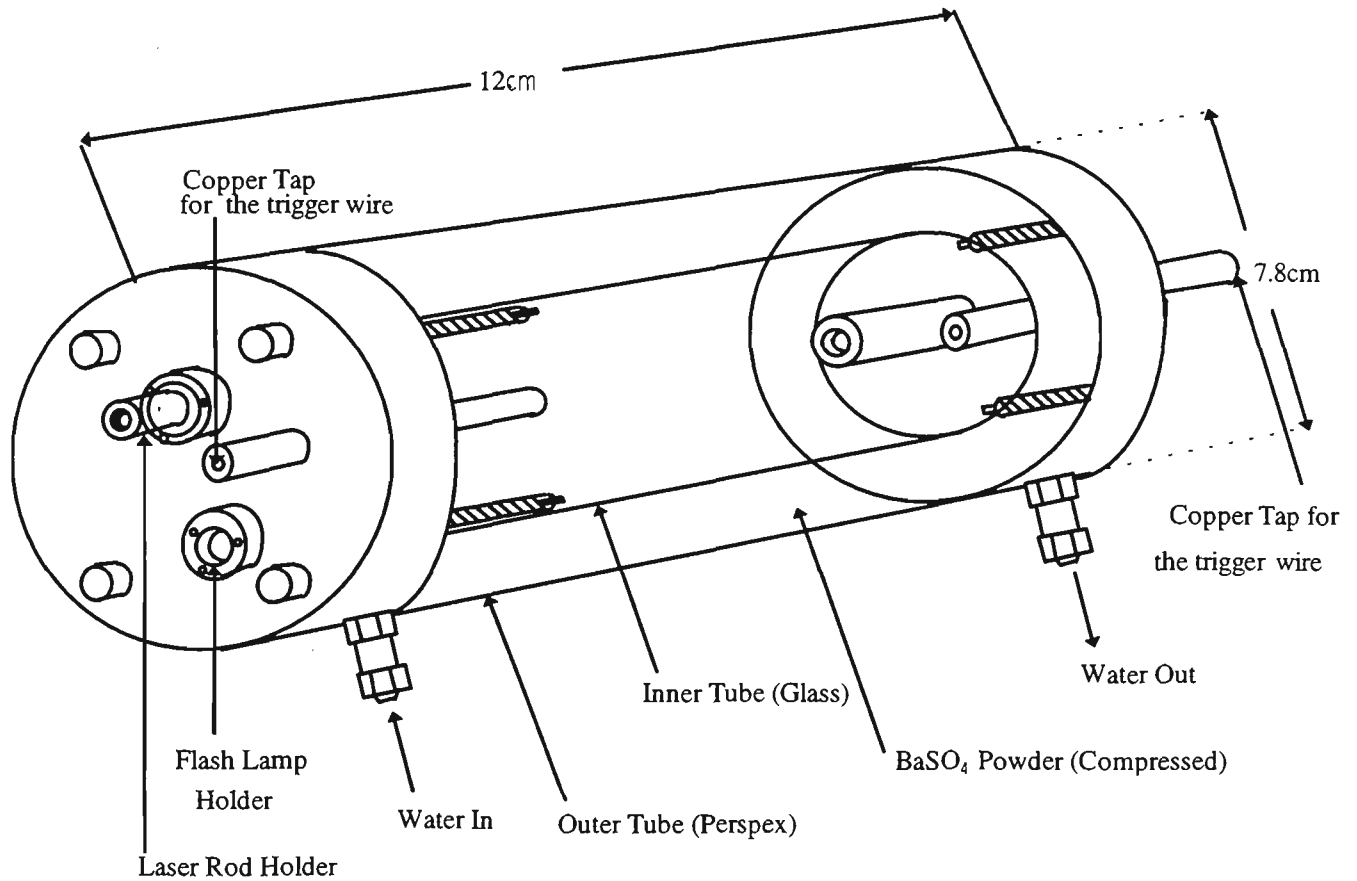


Figure 3.2 Laser pump cavity.

*Optical components within the pump and optical cavities:* The laser used a single Heraeus Xenon flashtube (4X76XFP) of 4 mm bore and length 76.2 mm. The YAG rod used had flat uncoated end faces, length 76.6 mm and diameter 6.3 mm. The optical cavity used two flat dielectric mirrors of reflectivity 99.5% and 90%. Q-switching was achieved using a Glan prism polariser and KD\*P Pockels cell within the optical cavity.

*Power Supply:* The major components of a power supply employed in the laser are a high voltage capacitor charging unit, a pulse forming network and a flashlamp trigger circuit. The high voltage power supply uses variable transformer in the primary of a step-up transformer and high voltage rectifier to provide a variable voltage supply for the capacitor storage bank. The energy is released by discharging the capacitor into the flash lamp through a suitable inductor by using a single LC pulse forming network. The values of inductance and capacitance were determined from the equations describing the networks (Markiewicz *et al.*, 1966):

$$E_0 = C \frac{V_0^2}{2} \quad (3.1.1)$$

$$\tau = \sqrt{LC} \quad (3.1.2)$$

$$T = 3\tau \quad (3.1.3)$$

$$C^3 = \frac{2E_0\eta^4\tau^2}{k_0^4} \quad (3.1.4)$$

where  $E_0$  is the energy stored in capacitor,  $C$  is the capacitance,  $v_0$  is the initial voltage across capacitor,  $\tau$  is the time constant of the circuit,  $L$  is the inductance,  $T$  is the pulse length at 1/3 peak height, during which time approximately 97% of the energy is developed,  $\eta$  is the damping parameter and  $k_0$  is the impedance constant of the lamp which depends on its physical dimension and the type and pressure of gas fill.

It can be shown that for the value of  $\eta = 0.8$  there is no reversal of current through the lamp and in this condition the circuit is critically damped. Under critically damped condition the pulse length is defined by equation 3.1.3. It can also be shown that for a given pulse lamp with specified pulse energy and pulse width, there is only one value each for C, L, and  $v_0$  that will result in critical damping, a requirement for maximum efficiency and lamp life. In this experiment the circuit was designed with values for C, L and  $v_0$  of 70  $\mu\text{F}$ , 90  $\mu\text{H}$  and 925V respectively. These values correspond to a flashtube pulse length ( $T$ ) of 230  $\mu\text{s}$  and discharge energy of 30 J into the flashtube. A single layer inductor coil was fabricated by using the following design formula of Dobbie *et al.* (1934)

$$L_s = \frac{0.10028 a^2 N^2 K}{l} \quad (3.1.5)$$

where  $L_s$  is the cylindrical current sheet inductance in  $\mu\text{H}$ ,  $a$  is the radius of the coil in inches,  $N$  is the total number of turns,  $l$  is the length of the solenoid in inches and  $K$  is a function of  $a/l$  (Nagaoka constant). This formula worked quite well and the measured value of inductance was found to be within 1% of the value of  $L_s$  calculated using equation 3.1.5.

The flash lamp was triggered externally using a trigger wire wound around the flashtube. This trigger wire was connected to the secondary of a high voltage trigger transformer which caused ionisation of the Xenon gas when a trigger pulse was applied. The circuit diagram of the trigger circuit is shown in Figure 3.3. The capacitor C3 is charged by a voltage doubler circuit which is connected to the output of the

transformer T1 (A&R 2064). The high voltage was generated by discharging the capacitor through the primary of the EG&G transformer (T2: type TR1700 ). A silicon controlled rectifier (SCR1 C122E ) is used as a switching element. It is triggered at its input by a pulse from the Q timer circuit ( Figure 3.4). The resistance R5 is used as a current limiter in the charging circuit.

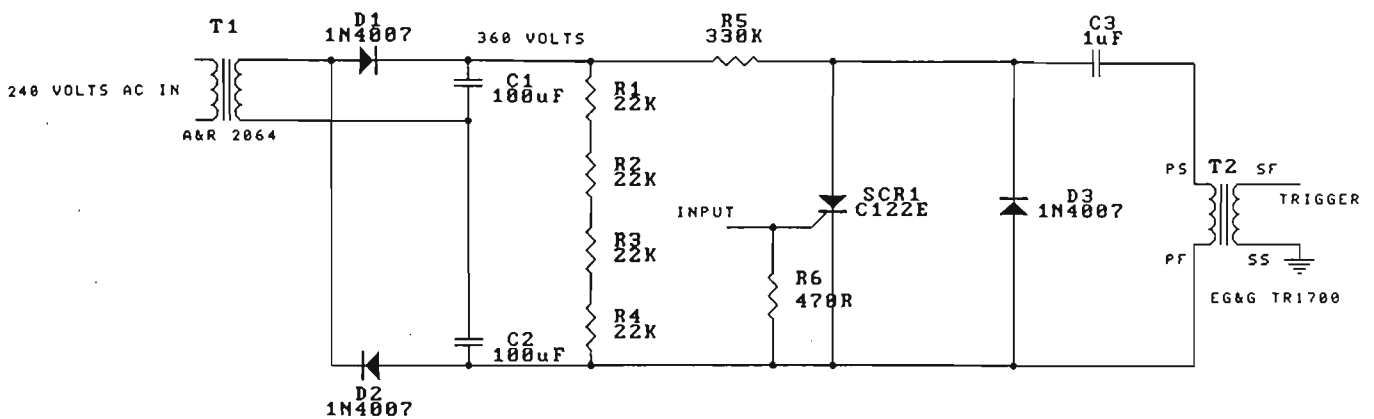


Figure 3.3 Flash lamp trigger circuit.

*Q-switching*: This is the technique by which high power short duration pulses are produced from the laser. The technique involves inserting a high optical loss within the laser resonator (low Q) to prevent lasing and facilitate energy storage during the major part of the flashtube pumping time. This loss is then switched out (high Q) during the latter part of the flashtube pumping pulse, allowing a rapid build up of optical power within the cavity and the emission of a single short laser pulse provided there is insufficient pumping energy remaining in the flashtube to again reach threshold. As shown in Figure 3.1, a Pockel cell and a polariser (Q-switching elements) are placed in the resonator cavity. During the flash lamp pulse, a voltage is

applied to the Pockel cell such that the linearly polarised light passing through the polariser becomes circularly polarised. After reflection from the rear mirror, this light undergoes another quarter wavelength retardation on the second pass through the Pockels cell, thus becoming linearly polarised at  $90^{\circ}$  to its original polarisation direction. Optical feedback is then prevented due to the ejection of this radiation from the laser cavity by the polariser. When the voltage is effectively removed from the Pockels cell, it becomes essentially transparent, allowing optical feedback and the rapid build up of polarised radiation within the cavity and the emission of a giant laser pulse.

A Newport Glan polariser (10GLO 8AR.33) in conjunction with Cleveland KD\*P crystal Pockels cell (QX 1020 QR ) was used for Q-switching in this laser. A high voltage DC power supply (Stanford Research PS 350) was used to bias the Pockel cell at 3.2 kV and this bias was rapidly removed using a fast semiconductor switch (Quanta Ray high speed driver Model HSD2). The Q-switch circuit is shown schematically in Figure 3.4. The design of the avalanche switching circuit (not shown) is based on high voltage avalanche transistors. The Q switch timer circuit which controls the timing of the flash lamp trigger and the avalanche module was designed using NE555 timers. The time delay between the flash trigger and avalanche module is controlled by potentiometer VR2 and the adjustment for pulse repetition rate by potentiometer VR3.

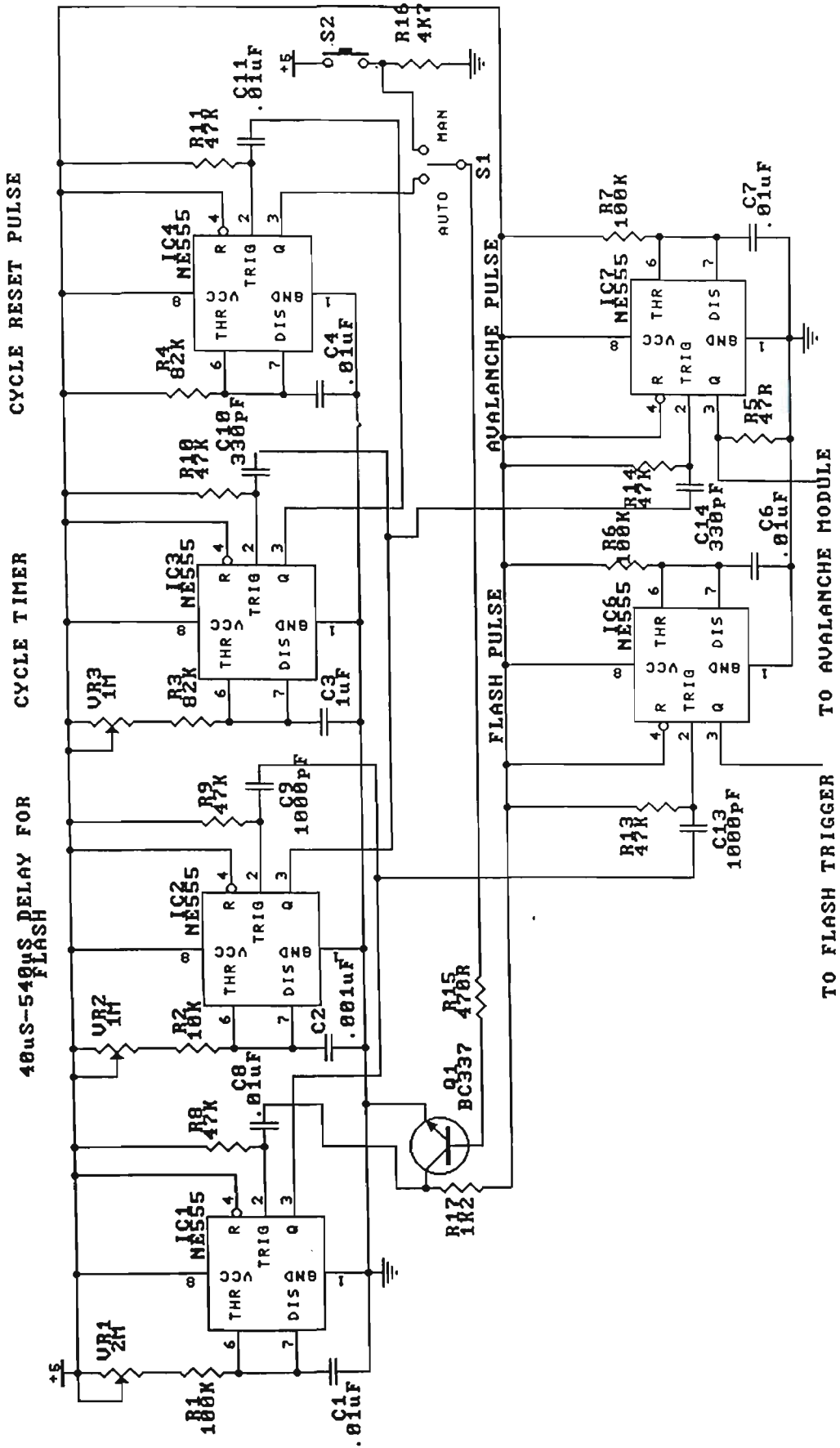


Figure 3.4 Q-switch Timer circuit.

### 3.1.1 Characterisation of the laser

The laser pulse energy in normal and Q-switched mode was measured by a commercial EG&G Radiometer with the indicator unit ( Model 581-15) and the detector unit (Model 581-28). An oscilloscope (Tektronix 602A) was connected to record the respective waveforms. The typical output traces of the laser pulse under normal mode and under Q-switched mode are shown in Figures 3.5 and 3.6 respectively. It may be noted that the input signal from the detector head in this instrument is negative. The pulse width of the Q-switched pulse was found to be about 20 ns.

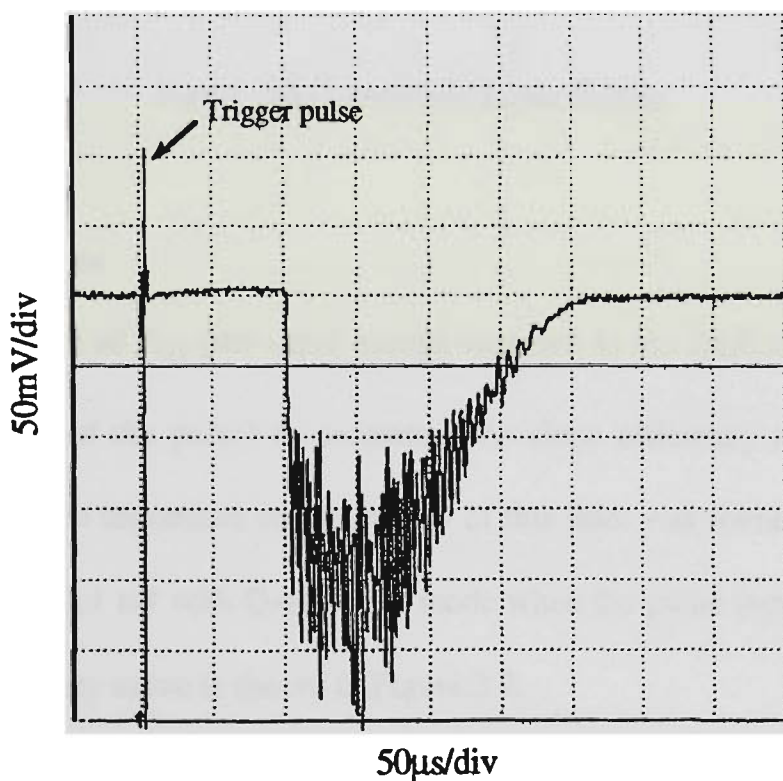


Figure 3.5 Laser pulse in normal mode.

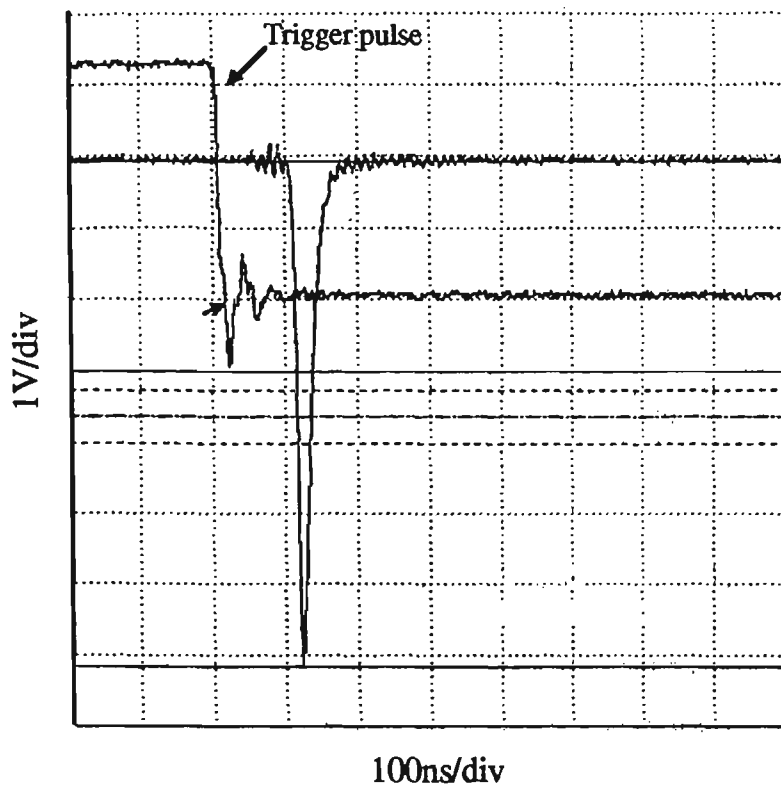


Figure 3.6 Q-switched Laser Pulses.

*Slope efficiency curve*

A graph was plotted of  $E_{in}$  (the input energy supplied to the flash tube) versus  $E_{out}$  (the output energy of the pulse) to determine the slope efficiency and the threshold pumping energy. The maximum output energy of this laser was found to be 105 mJ in normal mode and 63.1 mJ with Q-switched mode when the pump input energy was 50 J. The slope efficiency curve is shown in Figure 3.7.

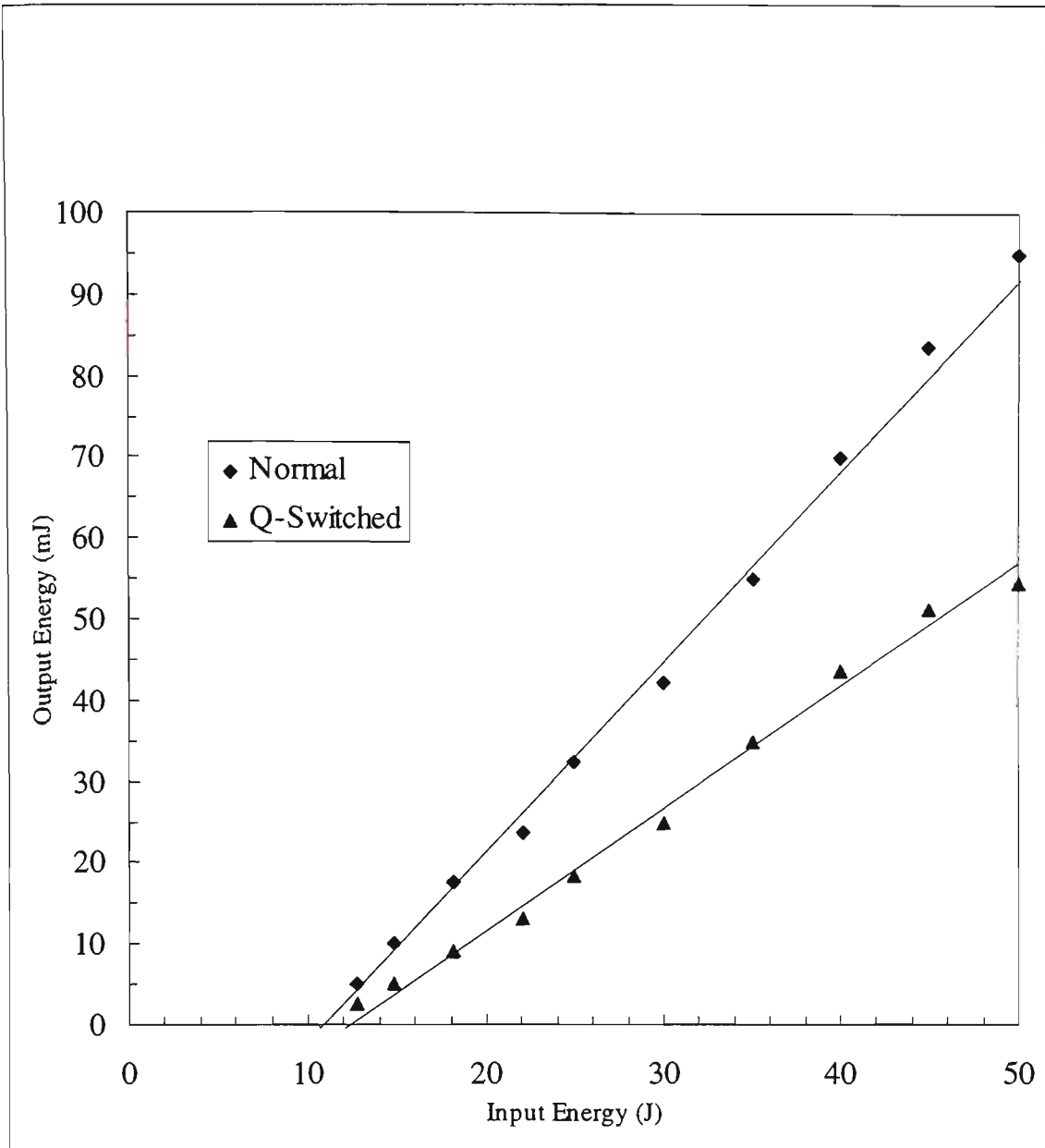


Figure 3.7 Slope Efficiency curve.

The threshold input energy level for Q-switched laser was found to be 12.25 J, which is slightly higher than that of the normal mode because of the insertion losses of Q-switched components in the optical resonator.

### 3.2 Construction and characterisation of the interferometers

An optical fibre interferometer suitable for the remote detection of ultrasonics in materials needs to satisfy some very stringent performance requirements. Surface vibration amplitudes produced by acoustic waves can be significantly less than 1 nm in the thermoelastic regime and possibly up to about 10 nm for ablation-generated waves (Scruby and Drain, 1990). Acoustic velocities of  $\sim 5,000 \text{ ms}^{-1}$  and propagation distances of  $\sim 1 \text{ cm}$  imply acoustic wave transit times of  $\sim 2 \text{ }\mu\text{s}$  across a sample. Accurate recording of such times to reveal meaningful changes in acoustic velocity requires an interferometer with a bandwidth of at least 10 MHz. In addition to the above sensitivity and bandwidth, the interferometer needs to be able to measure signals from poorly reflecting or scattering surfaces located at significant distances from the optical fibre tip (at least 10 cm). The interferometer must also have a large dynamic measurement range, good mechanical stability and be easily calibrated, preferably in situ.

These are demanding requirements, particularly for an optical fibre interferometer which must necessarily work at lower light levels than its bulk optic equivalent due to losses in coupling the light into and out of the fibre. The sections below describe the development of an optical fibre interferometer suitable for detection of ultrasonics and its ultimate performance. A number of versions of this interferometer were constructed with progressively improved optics and electronics. Initially a heterodyne approach was attempted. This was followed by superior designs which used active phase tracking homodyne techniques to compensate for thermal drift and lock the interferometer to the

quadrature point. A critical issue in the development of these systems involved the design and construction of wide bandwidth, low noise amplifiers and electronics for signal processing. The noise level of the overall system determines the minimum detectable vibration amplitude which can be sensed by the interferometer. This chapter includes a noise model which was developed to identify limiting noise sources and optimise the performance of the homodyne interferometer systems. The ultimate limitation to performance for a given optical signal level with the thermal noise limited detectors in these low power interferometer systems is due to a combination of environmental noise and noise in the receiver electronics.

### **3.3 Construction of the heterodyne interferometer**

#### **3.3.1 Optical Layout**

A schematic diagram of the interferometer arrangement using active heterodyne processing technique is shown in Figure 3.3.1.1. The light source was a He-Ne laser (Spectra-Physics 117A) emitting approximately 2.5 mW of light at a wavelength of 632.8 nm. Light was launched into one arm of a 633 nm single mode directional coupler (DC1) by means of a x10 microscope objective lens mounted in a Newport MF-915T positioner, which in turn was mounted directly in front of the laser. The coupler divided the light into reference and signal paths. A second x10 microscope objective lens mounted in another Newport MF-915T positioner collimated light from one of the outputs of DC1 to the vibrating surface, the second output of DC1 constituted the reference arm. In this work, the separation between the fibre and the vibrating surface (open air path) was 30 cm.

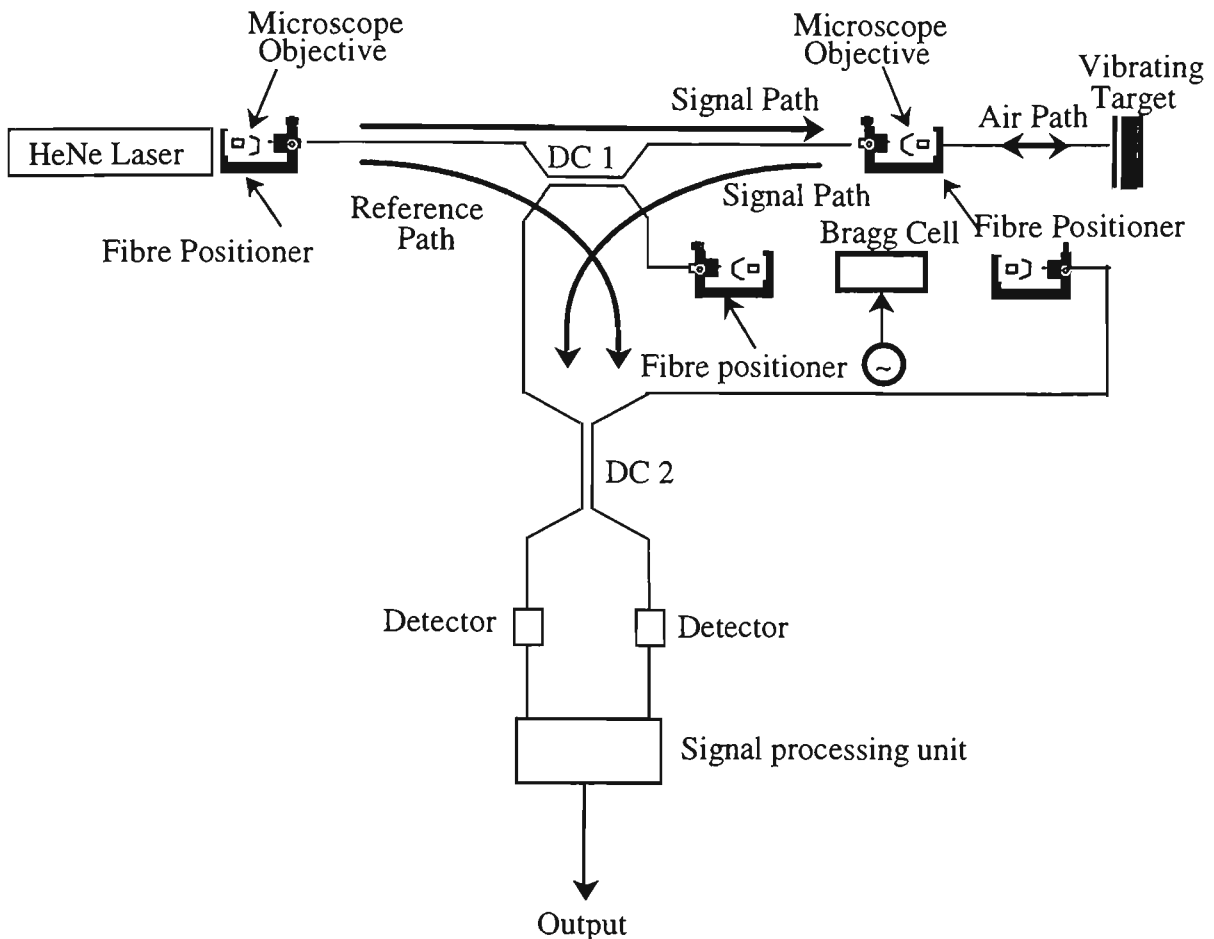


Figure 3.3.1.1 Optical layout of heterodyne interferometer.

An acousto optic modulator (Bragg cell) was inserted in the reference path to produce a frequency offset of 40 MHz between the two arms of the interferometer. This cell causes a small change in the laser propagation direction and a frequency shift due to collisions between the laser photons and the phonons generated by the piezoelectric modulator. The drive power to the Bragg cell (AOM 40) and necessary drive frequency was provided by an RF oscillator (IntraAction ME-40).

The light in the reference path is collimated by the combination of microscope objective (x10) and fibre positioner and allowed to pass through the Bragg cell at the

appropriate angle. The resultant frequency shifted beam was then launched into one arm of a second 633 nm single mode directional coupler (DC2) by another microscope objective (x10) and fibre positioner. The signal and reference beams were combined in DC2, the outputs of which were coupled into two silicon photodetectors to produce signals at beat frequency of 40 MHz.

In this interferometer, it is important that spurious interference effects are minimised by making sure that unwanted reflections are kept to a minimum. Joins between the various fibres were fusion spliced using a fully automatic fusion splicer which achieved a splice loss of less than 0.05 dB. The exception to this use of fusion splicing was that the outputs of the DC2 were terminated in FC-connectorised 50µm core multimode pigtailed which were mechanically spliced to the coupler fibre. There is little loss at these splices (about 0.2 dB) because light is travelling from a 4µm core fibre to a relatively large 50µm core fibre.

With this interferometer, the detector signal is phase modulated by the frequency of the vibrating surface and this vibration signal appears as sidebands of the beat (carrier) frequency. Small vibration amplitudes are readily found from the ratio of the power at the carrier frequency to that of the first sideband (Dandliker and Willemin, 1984). If  $x$  is the displacement of the vibrating surface, it can be shown that the amplitude of the first sideband is  $2\pi x/\lambda$  times that of the carrier frequency (Monchalin, 1985a). In this way, an absolute measurement of the displacement amplitude is readily obtained by comparing the amplitude of the sideband to that at the carrier frequency using a spectrum analyser. The sensitivity of the interferometer is essentially limited by the signal to noise ratio of the first side band signal (Dandliker and Willemin, 1984).

### 3.3.2 Electronics

The circuit diagram of the detector electronics is shown in the Figure 3.3.2.1. This first stage consists of Si photodetectors (OPF 480) and an NE 5212 transimpedance amplifier. This is followed by an LM733 wideband amplifier to provide further gain in the signal and then the output is taken from an emitter follower. This output was used as the input to an RF spectrum analyser (Tektronix 2711).

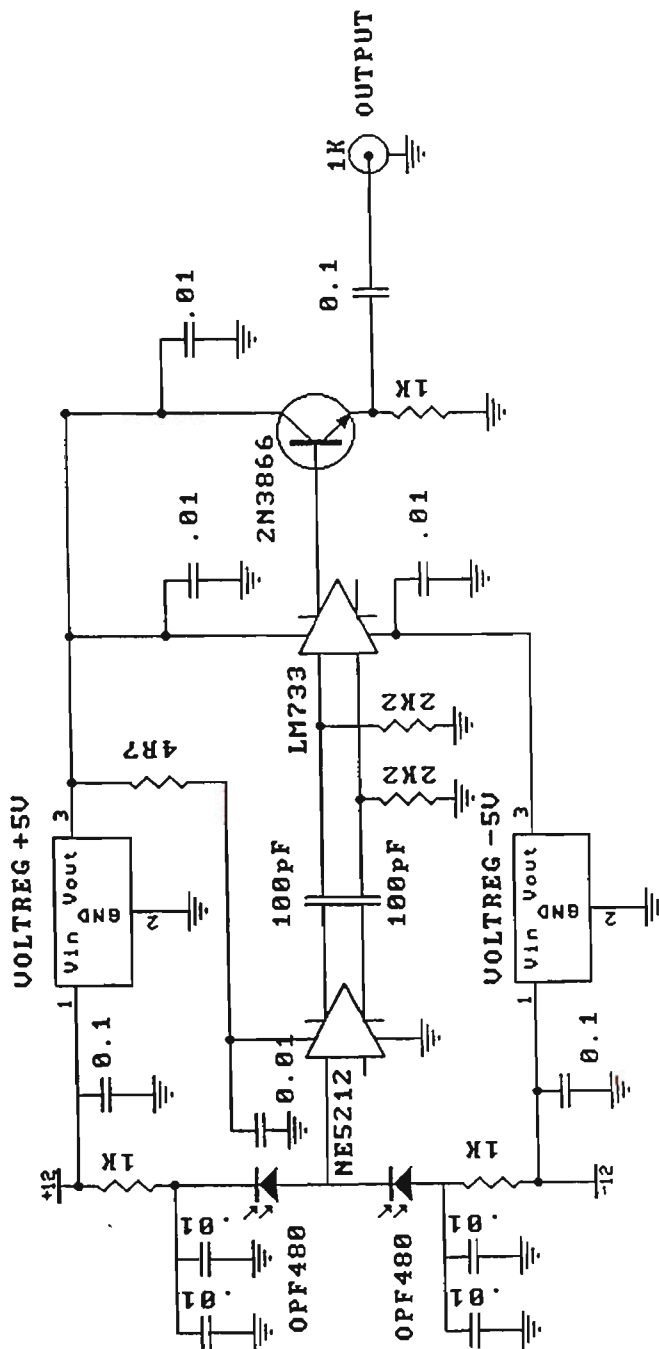


Figure 3.3.2.1 Schematic diagram of the detector electronics of the heterodyne interferometer.

Using the arrangement described above, the noise equivalent displacement (NED) obtained using the RF spectrum analyser was measured to be 3 nm when using a 3 kHz resolution bandwidth. This is nowhere near good enough performance for the remote detection of ultrasonics. Even without the necessary increase in bandwidth (which will increase the NED), the sensitivity is insufficient.

It is impractical to dedicate a commercial RF spectrum for use in the interferometer electronics. Hence, it was decided to build a dedicated demodulation circuit and see if better performance could be obtained with a more simple arrangement. This circuit is shown in Figure 3.3.2.2. In this circuit, the output from the emitter follower of the detector circuit (Figure 3.3.2.1) was processed using an integrated AM radio receiver chip (TDA 1572) which can be used for RF signals of frequency up to 50 MHz and amplitude up to 500 mV. The IF frequency was adjusted to 1 MHz and the bandpass of the single tuned circuit in the IF stage was approximately 40 kHz (thus the bandwidth after demodulation was 20 kHz). The signal was detected as full AM, with bandwidth of the final output determined by an RC filter using a 12 k $\Omega$  resistor and a 3.3 nF capacitor (approximately 4 kHz). The performance of the heterodyne interferometer when using this combination of detector and demodulation electronics is described in the following sections.



frequency displacement of up to about 300 nm peak to peak. For a sinusoidal displacement ( $x \cos 2\pi ft$ ) of the surface and normal incidence and reflection, the output of the interferometer  $V$  has the form (Scruby and Drain, 1990)

$$V = \bar{V} + V_0 \cos\left(2\pi f_s t + \frac{4\pi x}{\lambda} \cos 2\pi ft\right), \quad (3.3.3.1)$$

where  $\bar{V}$  is a dc bias,  $V_0$  is the amplitude of the beat signal and  $f_s$  is the frequency of the beat signal. For small amplitude displacements,  $x \ll \lambda/2$ , only the first sidebands are significant and their amplitude reduces to (Scruby and Drain, 1990)

$$V_{\pm 1} = V_0 (2\pi x / \lambda). \quad (3.3.3.2)$$

One of these sidebands was selected by the demodulation electronics to obtain an output proportional to the mirror displacement. The smallest measurable displacement is determined by the output noise level and this is most easily characterised by the noise equivalent displacement which is the displacement which gives rise to a signal equal in amplitude to the RMS noise level. In this interferometer, the NED is measured to be 0.75 nm in a bandwidth of 4 kHz.

### 3.3.4 Performance

The performance of this arrangement is considerably better than obtained when using the Tektronix RF spectrum analyser. However, it is still far from that required for a system which is to be used for remote detection of ultrasonics. There are some obvious ways in which the electronics described above could be improved. However it was

considered unlikely that the signal to noise could be increased sufficiently to allow the interferometer to be used in a flexible way for ultrasonic detection. The noise could be reduced but the basic problem lies in the fact that the heterodyne arrangement using a Bragg cell has too low an optical signal level at the detector for very high sensitivity. In round figures, the insertion of the Bragg cell and associated optical components results in a reduction of reference arm power at the detector from about 20  $\mu\text{W}$  down to 0.3 - 0.4  $\mu\text{W}$ . This signal reduction is considered to be too great for compensation to be possible by improvements in electronics design which result in lower noise in the signal output. Hence it was decided to abandon the heterodyne interferometer and concentrate on homodyne systems which do not have such high losses in the reference arm. These homodyne systems are described in subsequent sections.

Before describing the homodyne systems, it is worth making some further comments on the detection and demodulation electronics described in Figures 3.3.2.1 and 3.3.2.2. In Figure 3.3.2.1, a very simple differential input stage was used for the two photodetectors. This involved generating opposite polarity signals in the two detectors using opposite polarity supplies. For this to work adequately, the two photodiodes have to be chosen to have similar responsivities. If this is not the case then the offset current at the input can result in saturation of the transimpedance amplifier. It is probably better to design the system with two completely separate photodiodes and transimpedance amplifiers followed by a difference amplifier. The reason for the choice of the simple system used was to decrease the number of amplifiers in the hope of reducing the noise levels.

The first stage of the radio receiver chip is in fact a differential amplifier. Hence it would be possible to remove the rather noisy LM733 and the emitter follower in Figure 3.3.2.1 and use the output of the NE5212 transimpedance amplifier directly into the radio chip. There would need to be some changes in gains in other stages but this should result in reduced noise. The IF stage could also be improved by using several tuned circuits to flatten the frequency response and increase the roll-off of the bandwidth-determining elements. This is common in most radios and would improve the operation of the AGC (less influence from frequencies outside the bandpass). To achieve a large bandwidth (about 10 MHz) for the signal using this circuit, the local oscillator which is used to demodulate the 40 MHz input signal would need to be replaced with an external signal derived from the Bragg cell modulator so that the whole circuit operates as a synchronous demodulator. As stated above, none of these changes were judged likely to make sufficient improvements to overcome the relatively poor sensitivity of the system and hence they were not implemented.

### **3.4 Construction of the homodyne interferometers**

Four different versions of homodyne interferometers were fabricated and characterised with progressively better performance. The first version of the interferometer was fabricated by using a stabilised 1523 nm laser source, the second version utilised the same source but with modified detector electronics using lower noise electronic components. The third version was constructed using a laser source of wavelength 633 nm and low noise silicon detectors. This confirmed the improvements in sensitivity at lower wavelengths. Based on the performance of the third version and the noise model

developed in section 2.3.8, the fabrication and the characterisation of the final version of the interferometer was undertaken. This final version was also based on a 633 nm source and silicon detectors but had improved electronics.

### 3.4.1 Optical layout

The optical layout of the first version of the homodyne interferometer (Ho-1), which is identical to that of heterodyne system as described in section 3.3.1 but without using any frequency shifter in the reference path, is shown in Figure 3.4.1.

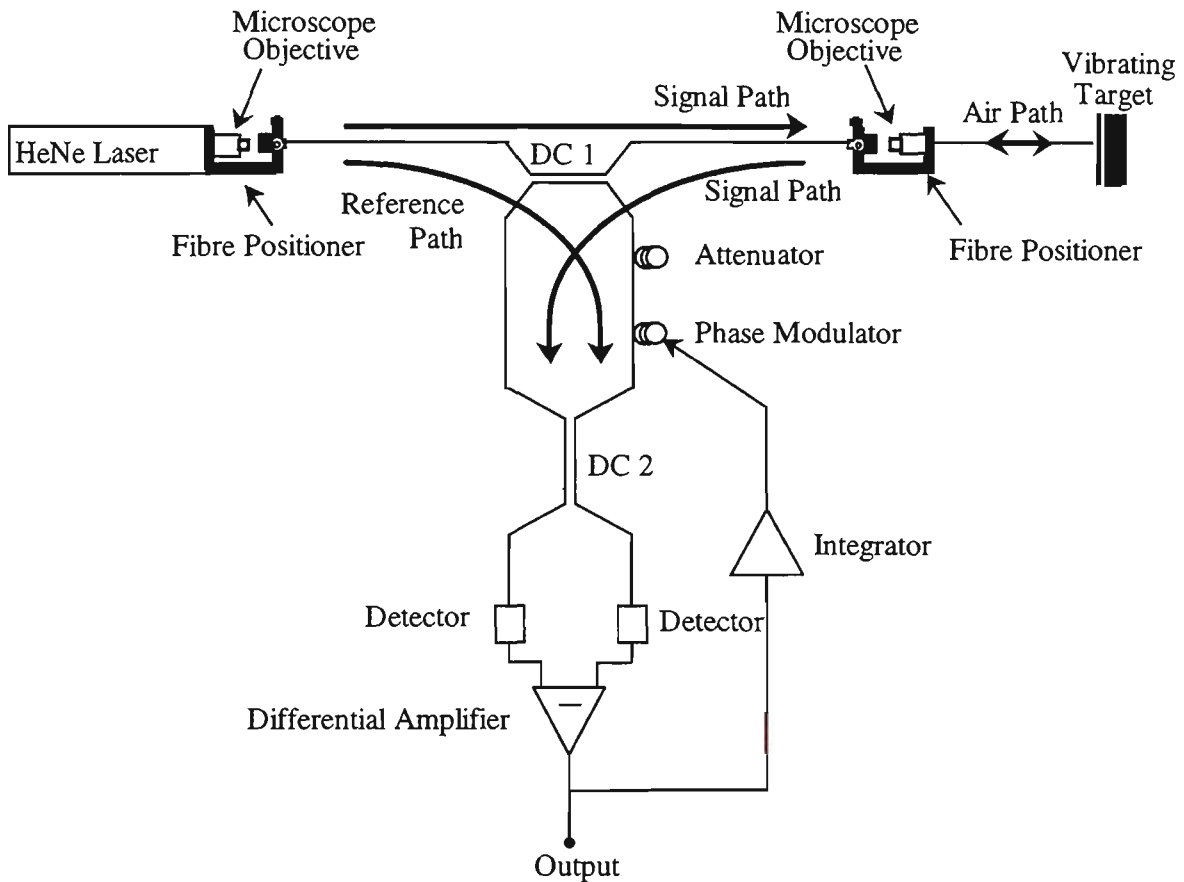


Figure 3.4.1 Optical layout of homodyne interferometer.

The light source was a He-Ne laser (Melles Griot OS SIP 871), emitting approximately 1.2 mW of light at a wavelength of 633 nm. The directional couplers DC1 and DC2

were standard 1550 nm communications devices. In order to obtain high fringe visibility, the optical power in the signal arm was approximately matched to the optical power in the reference arm by using an optical attenuator which was formed by winding a number of small radius turns of fibre in the reference arm. This attenuation is considerably smaller than that introduced by the Bragg cell in the heterodyne arrangement. Where possible, the two optical fibres (reference and signal arms) were paired closely together and therefore were largely subjected to the same non-signal perturbations and hence the same perturbation-induced phase changes. This tended to minimise thermal drift. The optical path lengths of the each arm was 700 cm (input DC1 to input DC2).

In order to hold the interferometer at the quadrature position, a phase modulator was incorporated in the reference arm of the interferometer. This phase modulator was constructed by winding 30 turns of single mode fibre (Corning Flexcor 633) around a piezo-electric cylinder (Tokin XOZ-138) of outside diameter 38 mm, inside diameter 36 mm and height 30 mm. This phase modulator was similar to that described by a number of other workers (Martini, 1987; Jackson *et al.*, 1980; Kingsley, 1978) and involved phase change being induced into the reference fibre by a voltage-induced radial change in the dimensions of the PZT which applied a longitudinal strain to the wound fibre. The induced phase shift in these devices is given by (Digonnet and Kim, 1988)

$$\delta\phi = \frac{2\pi}{\lambda}(L\Delta n+n\Delta L), \quad (3.4.1)$$

where  $\Delta n$  and  $\Delta L$  are variations of the refractive index and the fibre length respectively. Martini (1987) gives a detailed analysis of the phase modulation efficiency (m radian  $V^{-1}\text{turn}^{-1}$ ) which can be obtained with PZT-type modulators. Kingsley (1978) and Jackson *et al.* (1980), operating at frequencies well below the first mechanical resonance, obtained values 70 volt-turn and 100 volt-turn respectively for a  $2\pi$  radian phase shift at 633 nm using Vernitron PZT-5H ceramic piezoelectric transducers. These values are in general agreement with what would be expected from the calculations of Martini. In the arrangement described above using a Tokin PZT cylinder, the number of volt-turns for a  $2\pi$  radian phase shift was not measured but it was found that a 15 - 18 volt supply provided ample drift compensation range for the interferometer (much more than  $2\pi$  radian phase shift).

To avoid thermal effects, the directional couplers, attenuator and piezoelectric cylinder were housed in a box made by cutting appropriately-shaped compartments in a solid block of styrofoam. The channels in which the fibre was routed were made so as to avoid small radius bends thus reducing unwanted signal losses.

### **3.4.2 Electronics.**

The two output signals of the interferometer are in antiphase; subtraction of these signals in a differential amplifier not only reduces the common mode noise but also increases the signal-to-noise ratio. The circuit diagram for the detector electronics and signal processing unit using off the shelf components for the homodyne interferometer (Ho-1) is shown in Figure 3.4.2.1. Two InGaAs Photo detectors (LYTEL 0981) with optimised spectral response in 1150 - 1600 nm region followed by NE 5532

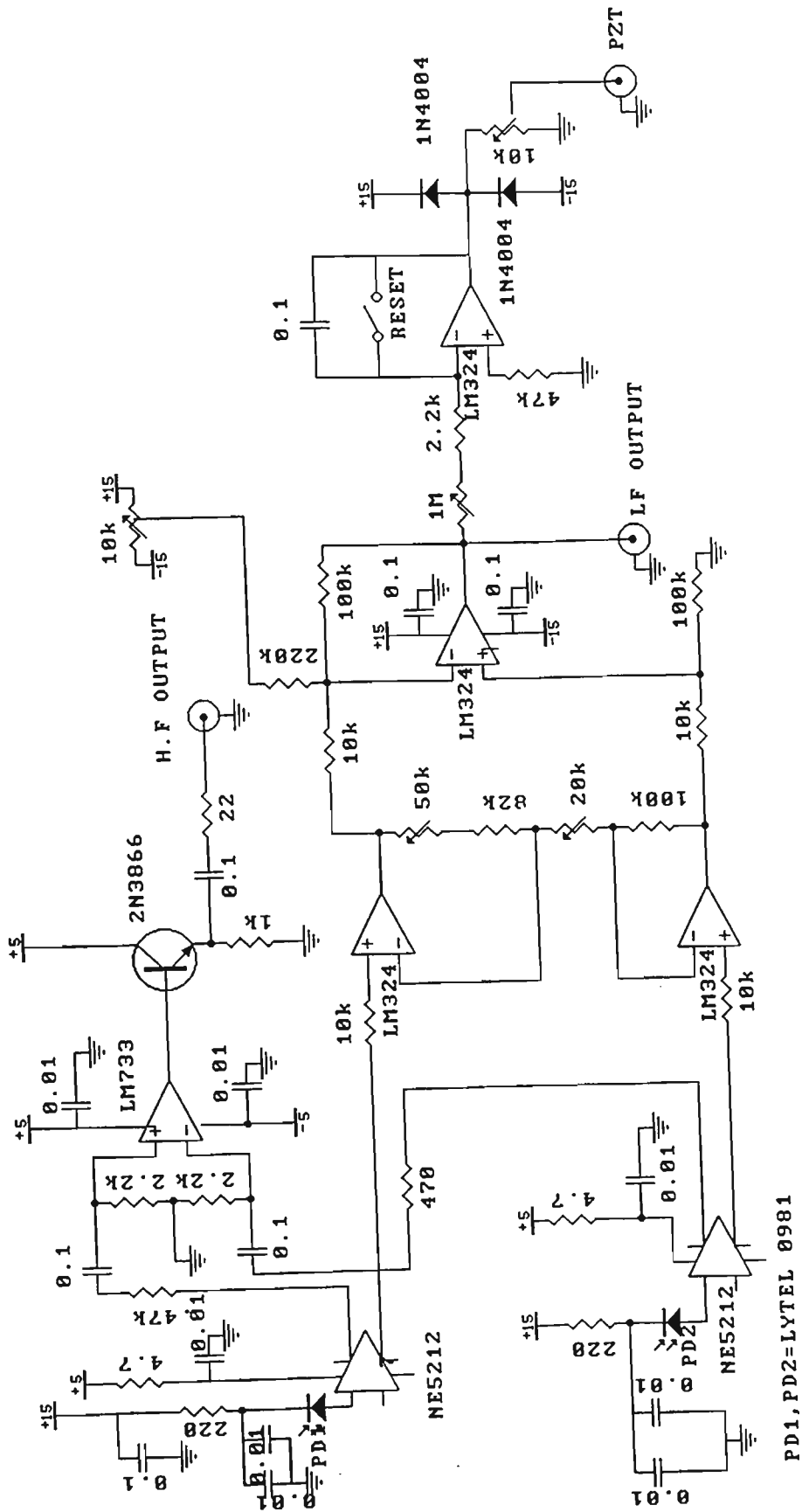


Figure 3.4.2.1 Schematic diagram of the detector electronics and signal processing unit of the first homodyne interferometer (Ho-1).

transimpedance amplifiers constituted the front end of the circuit. The four differential outputs of the two NE5532 were combined to form two output channels (low frequency and high frequency). The low frequency channel was used to drive the piezoelectric cylinder which was used in a negative feedback loop to compensate for low frequency drift (temperature fluctuations, air current etc.). Three operational amplifiers of an LM324 quad operational amplifier were used in an instrumentation amplifier configuration to provide further gain while ensuring the signals from each detector were of the same amplitude. The measured bandwidth was found to be from DC to 200 kHz, and was used for measuring low frequency vibrations such as those obtained during calibration. The remaining operational amplifier of the LM324 was used as an integrator which was required to generate the correction signal to the piezoelectric cylinder in the feedback loop to maintain the interferometer bias at the quadrature point. The output from the high-pass channel was used to measure the sensor response to high frequency signals. The high frequency signal from the NE5212 amplifiers was further amplified in a wideband LM733 differential amplifier and connected to an emitter follower. The bandwidth of this high frequency channel was found to be from about 10 kHz to 75 MHz.

### 3.4.3 Calibration

The low frequency channel of the interferometer was tested and calibrated by using the PZMS which was biased at +250V and was modulated by an ac voltage at a frequency of 410 Hz. The detector output,  $V$ , is related to the displacement,  $x$ , by the relation (Scruby and Drain, 1990)

$$V = \bar{V} + V_0 \sin(4\pi x / \lambda), \quad (3.4.3.1)$$

where  $\lambda$  is the wavelength,  $V_0$  is the amplitude of the interference or beat signal and  $\bar{V}$  is the DC bias. The proportionality constant between the output of the interferometer and displacement depends on the optical signal levels and amplifier gains and calibration under operating conditions is necessary for absolute measurement of displacement. This was accomplished by switching off the PZT feedback and using sufficient vibration amplitude on the PZMS to take the interferometer output through a number of fringes. The peak interferometer signal voltage is then the parameter  $V_0$  in equation 3.4.3.1. When the feedback is restored and the vibration amplitude of the PZMS is restricted so that the amplitude of the AC component of the interferometer output is less than  $V_0$ , it can be shown ( Scruby and Drain 1990) that the displacement  $x$  is related to the output  $V$  by

$$x = \frac{\lambda}{4\pi} \sin^{-1} \frac{V}{V_0}$$

$$\approx \frac{\lambda}{4\pi} \frac{V}{V_0} \quad \text{if } V \ll V_0 . \quad (3.4.3.2)$$

The noise equivalent displacement,  $x_N$ , which is the displacement corresponding to the RMS noise level, is given by (Scruby and Drain, 1990)

$$x_N = \frac{\lambda}{4\pi} \frac{\langle V_N^2 \rangle^{\frac{1}{2}}}{V_0} \quad (3.4.3.3)$$

where  $\langle V_N^2 \rangle$  is the mean square noise at the output of the detector. The NED was found to be 0.36 nm in the low frequency channel with a bandwidth of 200 kHz.

The high frequency channel was calibrated in a similar way by detecting signal from a piezoelectric ultrasonic transducer (RS 307-351) driven at a frequency of 40 kHz. The NED of the high frequency channel was found to be 8 nm in the bandwidth of 75 MHz.

### **3.5 Homodyne interferometer version 2 (Ho-2)**

In order to improve the sensitivity of this type of interferometer, the signal processing electronics was modified as shown in the Figure 3.5.1. The aim of the changes was to see if the NED could be usefully improved by the use of lower noise components and better circuit design. Hence, for this version of the interferometer, only the low frequency channel was constructed. The intention was to add a similarly-modified high frequency channel later if the improvements were thought to be significant enough.

The InGaAs photodetectors were now used in zero bias photoconductive mode. The NE5212 transimpedance amplifiers were replaced by NE5532 low noise operational amplifiers used in a transimpedance amplifier configuration. In addition, the LM324 used in the previous circuit was replaced by an LF347 low noise operational amplifier and metal film resistors were used instead of the carbon film resistors in the front end part of the circuit.



The measured bandwidth of this circuit was 100 kHz and the NED was found to be 0.16 nm in this bandwidth. This represents a small improvement on the previous circuit of about a factor of 1.6 after allowance is made for the reduced bandwidth. This was not considered significant enough and so rather than proceed with modifications to the high frequency channel, a much more fundamental change in the design was made.

### **3.6 Homodyne interferometer version 3 (Ho-3)**

Since the sensitivity of the interferometer is directly proportional to wavelength as shown in equation 3.4.3.2 and also because silicon detectors have reduced noise levels compared to InGaAs, a third version of the interferometer (Ho-3) was constructed using a 632.8 nm stabilised laser source (Spectra-Physics 117A) with an output power of approximately 2.5 mW. The optical layout using single mode 633 nm fibre (Corning Flexcor 633) and 633 nm directional couplers was the same as described in section 3.3.2. However the number of turns on the piezoelectric cylinder was reduced from 30 to 20 and the optical path lengths in each of the arms was 443 mm. The distance between the tip of the output fibre and the target was 57 cm. The electronics used in this version of the interferometer was broadly similar in design. The InGaAs detectors used in the Ho-2 circuit were replaced by silicon photodetectors (OPF480). An LM741 operational amplifier was used to invert the output of the integrator and also to double the voltage swing to the phase modulator to increase its tracking range is shown in Figure 3.6.1. Again, with this version of the interferometer, only a low frequency channel was constructed in order to evaluate the magnitude of the improvement in performance which could be obtained.

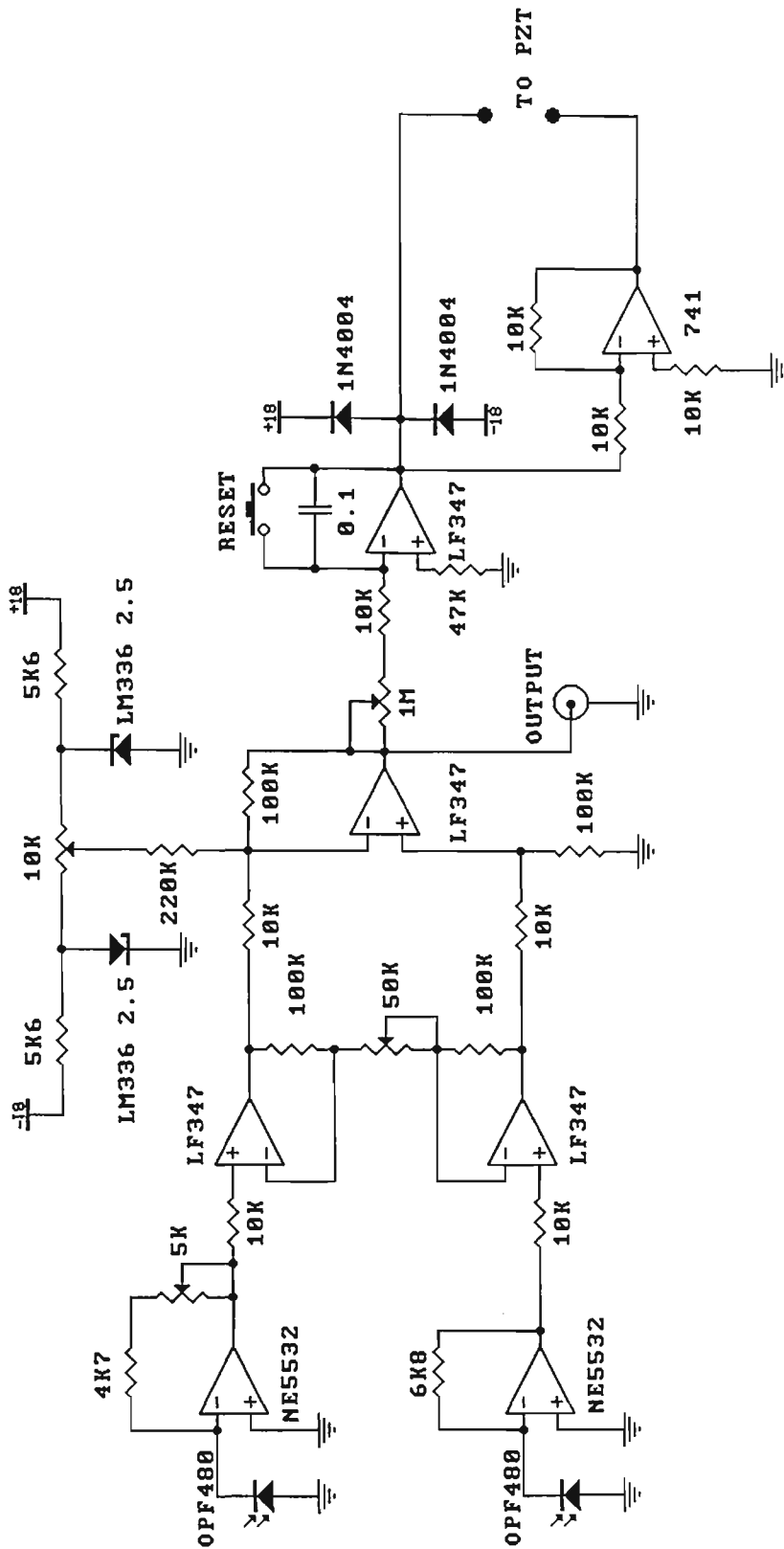


Figure 3.6.1 Schematic diagram of the detector electronics and signal processing unit of the third homodyne interferometer (Ho-3).

The interferometer was calibrated with the PZMS and the NED was found to be 0.04 nm in a bandwidth of 200 kHz. This is quite a substantial improvement. If the optical signal is removed by blocking the output of the laser, the contribution of the electronic noise produced in the detector and receiver circuits can be estimated. This gave a noise level equivalent to a NED of 0.03 nm which is only marginally smaller than the total figure of 0.04 nm obtained from the interferometer. Clearly, without increasing the optical power from the He-Ne laser, the only way to make improvements in the interferometer is to concentrate further on the electronics. Before doing so, the performance of the various homodyne interferometers constructed so far is compared in the next section.

### **3.7 Performance**

The characteristics and the comparative performance of these three types of active homodyne interferometer are presented in table 3.7.1. This table lists figures for the low frequency channel only since only the first version was constructed with a high frequency channel. From the table below, it is clear that each modification has improved the performance of the interferometer. The figure of merit which is most useful in making this comparison is the NED divided by the square root of the bandwidth. This figure of merit has improved at each change and has decreased by a factor of about 10 between first and third versions. It should be noted, however, all the measurements made so far and summarised in Table 3.7.1 have been made using the PZMS with a fully reflecting mirror mounted in the mirror shaker. This gives a high  $V_o$  for a given laser power and hence a low NED for a given noise level. If natural

Characteristics	Ho-1	Ho-2	Ho-3
Wavelength(nm)	1523	1523	633
Detector	LYTEL 0981 (InGaAs)	LYTEL 0981 (InGaAs)	OPF 480 (Si)
Laser	Melles Griot 05 SIP 871 (1.5 mW)	Melles Griot 05 SIP 871 (1.5 mW)	Spectra Physics 117A (2.5 mW)
Total optical path length(cm)	700	700	443
Air path length (cm)	100	100	57
Bandwidth (kHz)	200	100	200
RMS Noise(mv)	12	5.7	3.45
Total NED (nm)	0.36	0.16	0.04
NED/ $\sqrt{\text{Hz}}$ ( $\times 10^{-13}$ m/ $\sqrt{\text{Hz}}$ )	8.05	5.06	0.89
RMS Electronic noise (mv)	4	2.5	2.5
NED (nm) due to Electronic noise	0.12	0.07	0.03

Table 3.7.1 Performance of the different versions of the active homodyne interferometer.

reflecting surfaces are used, much lower values of  $V_0$  are obtained and hence the NED figures are considerably worse. Scruby and Drain (1990) found about a hundred-fold

difference in sensitivity between reflecting and rough surfaces. When a natural aluminium surface is used as a reflector in the PZMS, the NED for the third version of the interferometer changes from 0.04 nm to 0.5 nm.

Another point which should be noted with regard to the figures quoted in Table 3.7.1 is that in order to make meaningful comparisons, all figures were measured under quiet laboratory conditions. Since there is an open air path in the interferometer, noise at lower frequencies is affected by the presence of air currents induced by the air conditioning system. Also acoustic noise from motors and other electrical equipment in the room affects the PZMS mirror and can increase the signal noise at particular frequencies. The figures quoted in the table above were measured with the air conditioning turned off and equipment containing motors and fans turned off.

Before constructing a final version of the interferometer electronics (including a suitable high frequency channel) for use in detecting ultrasonic signals from natural surfaces, it is useful to apply the noise model of chapter 2 to the third version of the interferometer. This facilitates a better appreciation of the origin of the limitations in that system.

Combining the noise contributions of the transimpedance amplifier and detector as given by equation 2.3.6.4 (multiplied by the appropriate impedance) as well the noise of the differential amplifier as given by equation 2.3.6.5 and assuming that all the noise sources are uncorrelated, the total electronic noise was calculated for the interferometer Ho-3 using the 633 nm laser source. The calculated noise, assuming an input optical

signal of magnitude  $10 \mu\text{W}$  and using manufacturer's typical data for the chips and gains of the various stages as calculated from the nominal resistances, was  $2.8 \text{ mV}$ . The measured value was  $2.5 \text{ mV}$ . This is quite reasonable agreement.

In approximate terms, the noise at the output is due to roughly equal contributions due to the first transimpedance amplifier and all subsequent stages. The major contributions to the noise from the transimpedance stage are equivalent input current noise of the NE5532 and the thermal noise in the detector load (mostly feedback resistor). The shot noise at an input optical power of  $10 \mu\text{W}$  is about half the thermal noise. The noise model calculations were extended to bandwidths of  $10 \text{ MHz}$ ,  $50 \text{ MHz}$ ,  $75 \text{ MHz}$  and  $100 \text{ MHz}$  with different levels of optical signal at the detectors. The results of these calculations are shown in Figure 3.7.1. These calculations show that provided one can get  $10 \mu\text{W}$  of optical signal, it should be possible to have a NED of less than  $1 \text{ nm}$  for frequencies up to  $100 \text{ MHz}$ . The problem is getting the  $10 \mu\text{W}$  with poorly reflecting or highly scattering surfaces. Provided the surface is reasonably reflective, it should be possible to achieve a NED of less than  $1 \text{ nm}$  at bandwidths of  $10 - 15 \text{ MHz}$  with the types of circuit that have been used and laser powers of  $2.5 \text{ mW}$ .

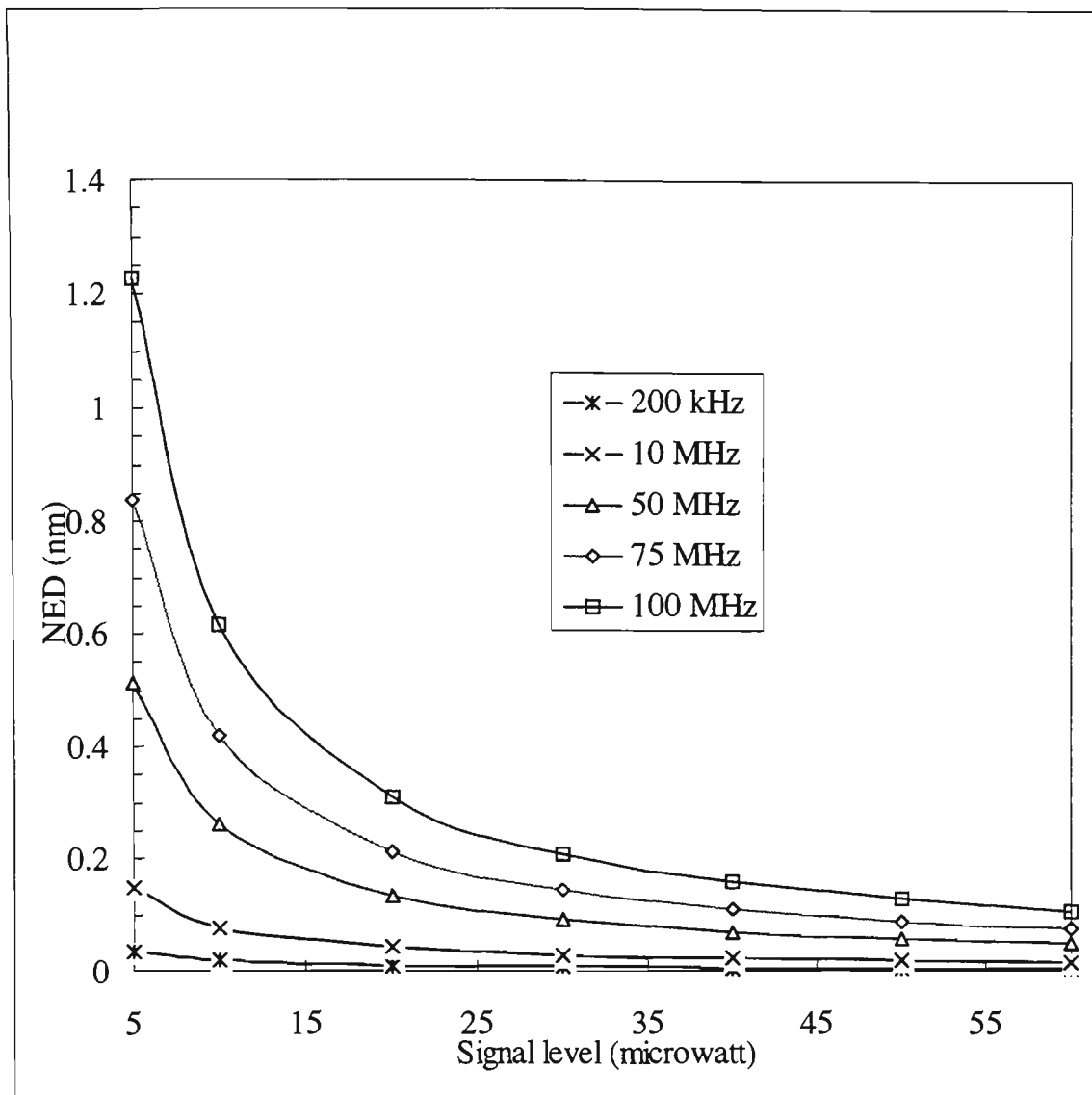


Figure 3.7.1 Noise model calculations showing the variation of electronic NED with the level of detector optical signal at various bandwidths.

In choosing a bandwidth for the detection system it is important to realise that there is a trade-off between detection sensitivity (which is improved by the greater signal to noise ratio achievable at lower bandwidths) and improved arrival time determination and detected acoustic signal power (which is improved by using higher bandwidths) (Wagner *et al.*, 1990). Ideally one should set the bandwidth so that the passband includes most of the frequency spectrum of the acoustic pulse generated by the laser. For an acoustic pulse of duration 50 ns, most of the spectral energy is contained within

frequencies below that corresponding to the reciprocal of the acoustic pulse width (20 MHz). Scruby and Moss (1993) found a 20 MHz bandwidth a reasonable compromise for data recording with improved sensitivity when measuring acoustic displacements with a bulk optic Michelson homodyne interferometer which had a bandwidth capability of 100 MHz (this system used a single mode argon laser of output power 250 mW in the interferometer and natural machined surfaces as targets). In view of the above, it seems that a high frequency channel of bandwidth 15 - 20 MHz may be a reasonable choice in the present application. Because the optical powers available in a fibre optic interferometer are so much less than those available in bulk optic systems, a bandwidth of 15 MHz was chosen.

### **3.8 Final interferometric configuration**

The optical layout of the final version of the active homodyne interferometer is same as described in section 3.4.1. However, the optical path length was reduced to 300 cm and the interferometer was made more compact. The interferometer was also shielded using a cardboard box to reduce the effect of air currents and was placed on a vibration isolation table. These latter changes were probably not very significant but were made to ensure the best possible operating conditions. The detector circuit was modified to have a bandwidth of 15 MHz and the circuit diagram is shown in Figure 3.8.

In this circuit, the subtraction of the currents in the photodiodes (OPF480) is done before amplification to minimise the common mode noise (this arrangement is similar to that described in the heterodyne interferometer electronics). An NE5212

transimpedance amplifier with a bandwidth of 140 MHz was used as preamplifier for the detector signal. This choice was made to maximise to bandwidth capability and allow some gain to be incorporated and still achieve the desired overall bandwidth of 15 MHz. Two channels were derived from the output of the preamplifier. The first was used to recover the desired signal (high frequency channel) and the second was used to give a low frequency output (70 kHz, labeled "TEST" in the diagram). The low frequency output was integrated using an LF347 amplifier before being used to stabilise the interferometer from low frequency drift. A bipolar signal is used to extend the locking range of the PZT modulator. In the high frequency channel, the transimpedance output was high pass filtered and then amplified to provide further gain using another NE5212 as a voltage amplifier. The desired signal can be recovered from either of the differential outputs of this second amplifier. In order to isolate the circuit from the mains supply and from noise and electrical pick up in supply leads, the circuit was powered by batteries mounted inside the shielded detector box which gave a supply voltage of  $\pm 18$  Volts. The bandwidth of the high frequency channel of the interferometer was measured to be 30kHz-15MHz. The interferometer was calibrated using the unpolished surface of an ultrasonic transducer at 140 kHz. The NED is found to be 0.4 nm in this bandwidth. The optical power at the detectors was not measured but the NED obtained appears to be in fairly good agreement with the value one would expect from the noise model for a detected optical power of around  $10 \mu\text{W}$ .



## Chapter 4: Experimental results using metallic targets

In this chapter, experiments will be described on the application of the laser-ultrasonic technique, which combines laser generation and fibre optic interferometer for remote detection of acoustic waveforms in metals. The experiments were conducted on metals in the thermoelastic as well as the ablation regime by varying the energy and the power density of the laser pulses incident on the surface of the sample. One series of experiments was conducted with an incident energy of 47 mJ to study the suitability of the Q-switched Nd:YAG laser designed and constructed for this work. The main problem encountered when using low pulsed laser energies with the fibre optic interferometer is poor signal to noise ratio. With low laser excitation energies and power densities, the amplitude of the acoustic pulses generated in the sample is small. This, together with the low optical power of the 633 nm He-Ne laser used in the interferometer, gives rise to a low signal to noise ratio for the recorded signals. It was found that useful signal to noise ratios could be obtained with low excitation energy only by using a lens to partially focus the excitation pulse and thus increase the power density on the sample. Significantly greater improvement can be obtained in the signal to noise ratio if much higher excitation energies are used. A second series of experiments were performed using Q-switched Nd:YAG laser excitation energies up to 1300 mJ (available temporarily from the laser used to pump a Spectra Physics MOPO which was operating in the same laboratory). With this laser it was possible to excite the sample much further into the ablation regime and produce longitudinal ultrasonic pulses with amplitudes of the same order of magnitude as conventional ultrasonic transducers (Aussel and Monchalin, 1989).

Excitation in the low ablation regime, achievable even with low energy focused lasers, produces signals which are suitable for reasonably accurate measurements of longitudinal acoustic wave velocity. A series of measurements of this velocity in a number of different metals are also reported in this chapter. The accuracy of these measurements is limited by the rise time of the recording electronics and the resolution of the digital recording system. While no attempt was made to make very accurate measurements during this work as exact compositions of materials were not known, velocities with uncertainties in the range 0.5% to 2% are readily achieved, even without optimisation of the system for this purpose.

## 4.1 Experimental Arrangement

The experimental arrangement for this work is shown schematically in Figure 4.1. For lower power excitation, the laser described in chapter 3 was used to produce acoustic pulses in the targets. For high power excitation, the laser used was a Q-switched Nd:YAG laser operating at a wavelength of  $1.06\ \mu\text{m}$  with a pulse width of about 10 ns with a maximum energy of 1300 mJ. This laser was directed on the metallic targets and was placed at a distance of 15 m. No special preparation was given to the target surfaces which were used in either the natural (oxidised) state or after normal machining. Two types of samples were commonly used. These were either metallic plates with different thicknesses or a semi-cylindrical block with a radius of 12.5 mm. In all cases the unimportant dimensions were chosen to minimise the confusion generated in the measured signals by spurious reflections. A semi cylindrical block of aluminium was chosen for the first part of the experiment to allow the possibility of



increased the reflected intensity and thus improved the signal-to-noise ratio of the measurements, it was found in this experiment that a useful signal could easily be detected when using machined or natural surfaces. A small fraction of each Nd:YAG laser pulse scattered from the front surface of the sample was detected by a photodetector (OPF 480), the rising edge of which then triggers the oscilloscope and thereby provides a temporal reference point (T) from which the propagation time of the ultrasonic pulses could be measured. The output of the interferometer was recorded using a digital storage oscilloscope (Tektronix DSA 602) and this stored signal was subsequently read and processed using a personal computer. The incident laser beam was modified to vary the optical power density on the surface of the sample by focusing the beam through a lens placed at different positions between the laser beam and the target surface. The energy of the incident laser beam was able to be adjusted over a wide range using known optical attenuators.

## **4.2 Experimental data on remote detection of ultrasonics**

### **4.2.1 Acoustic waveforms with different pulse energies**

Using the experimental procedure as outlined in section 4.1, a first series of experiments were conducted with a high pulse energy of 1300 mJ to test the performance of the experimental set up. The pulse energy was gradually reduced to study the variation of acoustic waveforms with excitation energy. Typical acoustic waveforms obtained using different laser excitation energies are displayed in Figures 4.2.1 - 4.2.5. In Figure 4.2.1, the acoustic waveform was produced with a laser pulse energy of 1300 mJ and a beam diameter of 8 mm. As expected, due to the high energy

of laser pulse, the waveform is characterised by two major features; one corresponded to the arrival of the direct longitudinal wave (P-arrival) and the other corresponded to the arrival of the shear wave (S-arrival). This waveform is similar to that reported by many other workers using bulk optic interferometers and some other transducers and is formed by a combination of dipolar stresses due to thermoelastic expansion together with a  $\delta$ -like normal component of force resulting from ablation of surface material induced by the laser (Dewhurst *et al.*, 1988). It should be pointed out that Figure 4.2.1 is a waveform resulting from a single laser pulse. This, as with all other such waveforms in this work, is highly reproducible and shot-to-shot variations are negligible.

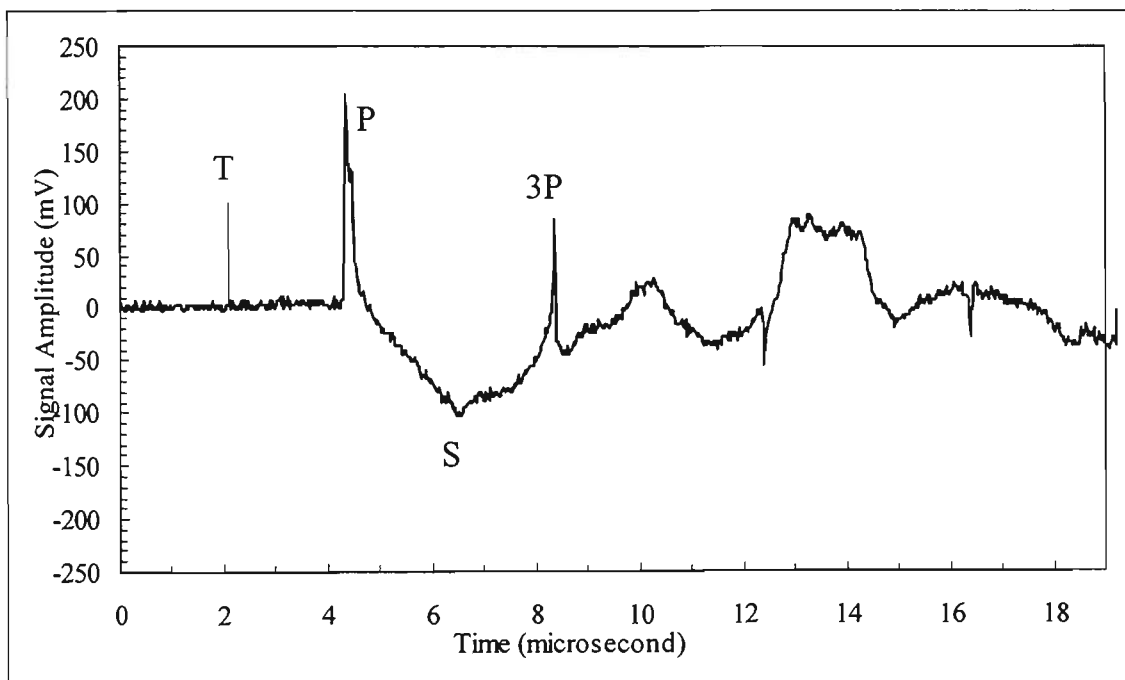


Figure 4.2.1 Acoustic displacement waveform measured at the epicentre of a semi cylindrical aluminium block of 12.5 mm radius with a single unfocused laser pulse of energy 1300 mJ and diameter 8 mm. Note: 3P is used in this figure to denote the twice-reflected P wave which has traversed the sample three times.

Figure 4.2.2 shows a broadly similar behaviour when the pulse energy is reduced to 600 mJ. However, the amplitude of the P-arrival is considerably lower than the one shown in Figure 4.2.1, whereas the S-arrival amplitude is increased. This is consistent with the decrease in laser energy resulting in an acoustic excitation which is dominated by the thermoelastic stresses in the plane of the surface with a step-like time dependence (Scruby *et al.*, 1980).

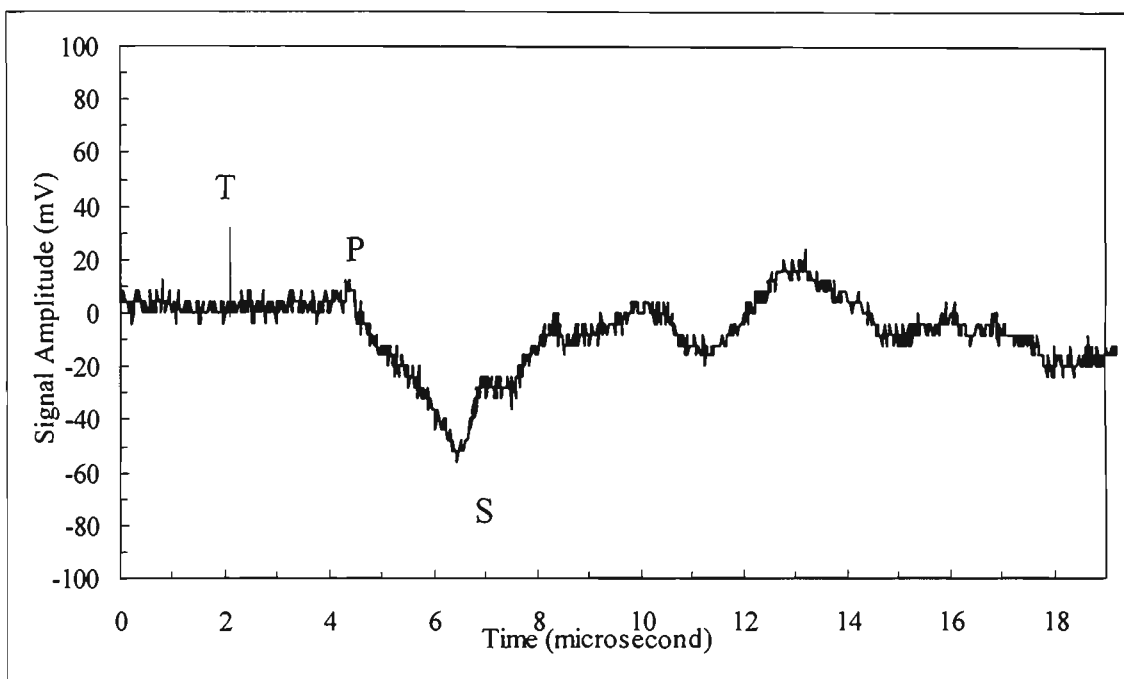


Figure 4.2.2 Acoustic displacement waveform measured at the epicentre of a semi cylindrical aluminium block of 12.5 mm radius with a single unfocused laser pulse of energy 600mJ and diameter 8 mm.

The shape of the measured acoustic waveforms shown in Figure 4.2.3 - 4.2.5 were produced with the same unfocused diameter of 8 mm and laser energies of 115, 50 and 28 mJ respectively. The waveforms clearly show situations in which the laser power causes only thermoelastic expansion of the irradiated region of the sample surface. The

observed waveforms are consistent with those already published in previous works (Scruby *et al.*, 1980; Hutchins *et al.*, 1981a; Aussel *et al.*, 1988). The signal to noise clearly decreases with excitation energy. It should be noted that the acoustic waveform with a pulse energy of 28 mJ (Figure 4.2.5) was obtained by averaging 125 waveforms (other figures are records of a single waveform).

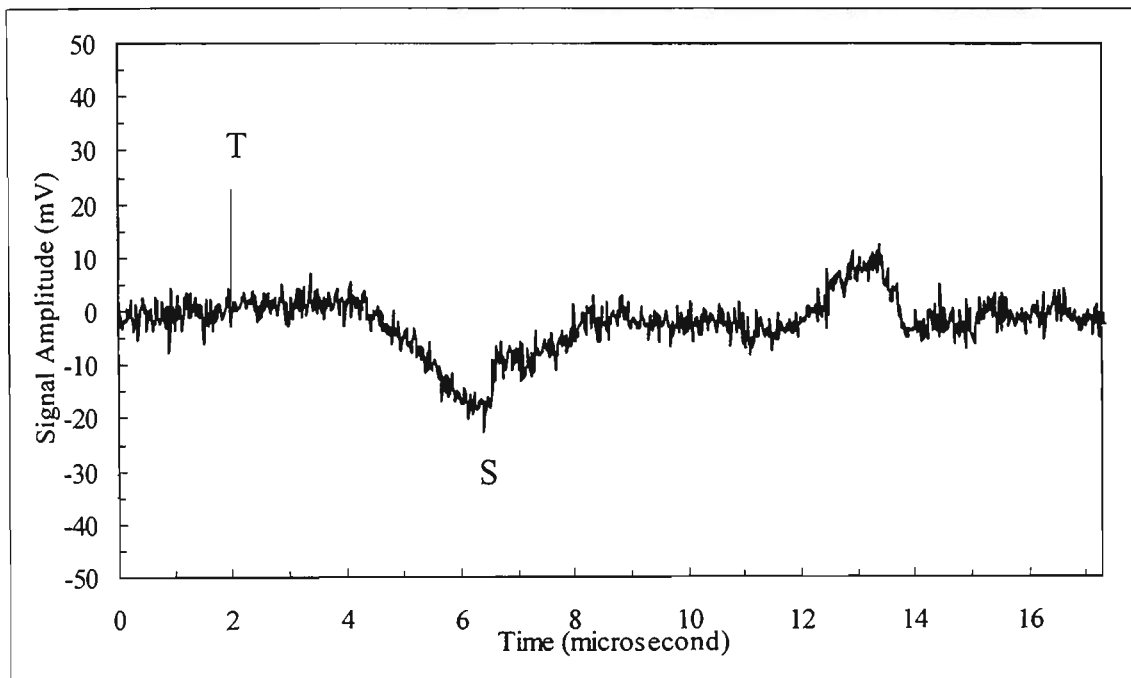


Figure 4.2.3 Acoustic displacement waveform measured at the epicentre of a semi cylindrical aluminium block of 12.5 mm radius with a single unfocused laser pulse of energy 150 mJ and diameter 8 mm.

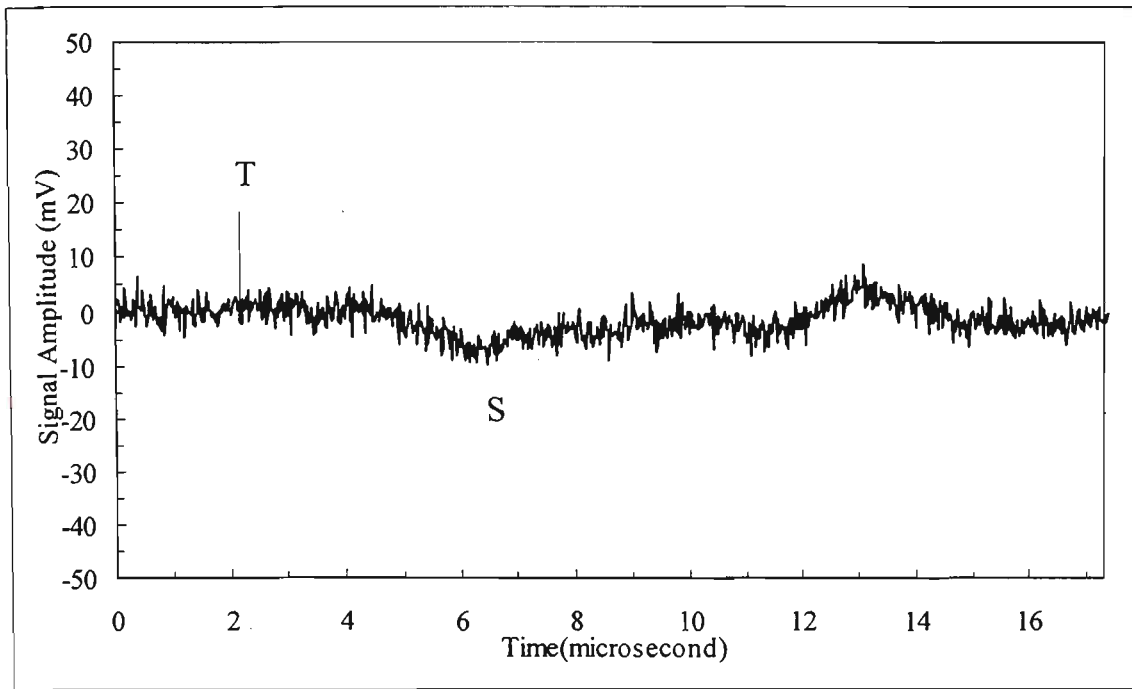


Figure 4.2.4 Acoustic displacement waveform measured at the epicentre of a semi cylindrical aluminium block of 12.5 mm radius with a single unfocused laser pulse of energy 50mJ and diameter 8 mm.

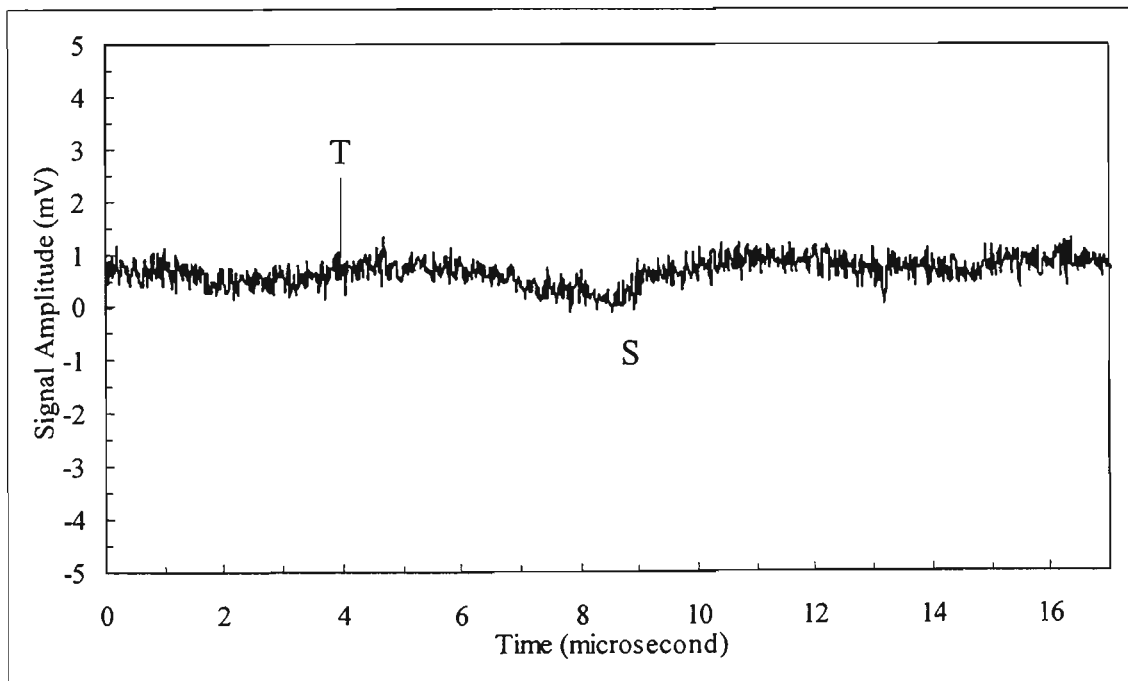


Figure 4.2.5 Acoustic displacement waveform measured at the epicentre of a semi cylindrical aluminium block of 12.5 mm radius with an unfocused laser pulse of energy 28mJ and diameter 8 mm (average of 125 waveforms).

## 4.2.2 Acoustic waveforms with different incident power densities

Typical acoustic waveforms, measured with a constant laser pulse energy of 113 mJ and under different focusing conditions, are described below. The excitation conditions are varied by changing the surface power density when focusing within the sample and also the position of the focal point with respect to the surface when focusing in front of the sample.

### 4.2.2.1 Irradiation with the unfocused laser beam

The incident power density of the unfocused laser beam was found to be  $\approx 19 \text{ MW/cm}^2$  and the observed waveform is shown in figure 4.2.6. The quoted power density is an average for the central region of the irradiated area and is obtained by assuming that the 1064 nm beam is Gaussian and that 85% of the measured energy of the pulse is contained within the stated diameter and that the pulse width is 10 ns. The figure is given as approximate since the absolute uncertainties are not likely to be less than about 20% - 30% despite the fact that the incident beam is well controlled and appears to be a nice single mode (no equipment to measure the beam profile of a high power short pulse laser is available in the laboratories). The waveform clearly shows that the excitation for this pulse is well within the thermoelastic regime. Labels have been used to indicate a number of the principal features evident in the waveform. With reference to the trigger point T, the longitudinal wave arrival has been denoted by a negative step L, indicating a negative displacement corresponding to a depression at the rear surface of the sample which is due to the stress field at the unconstrained irradiated surface being approximated by equal orthogonal force dipoles lying in the surface as discussed in Chapter 2 (Scruby *et al.*, 1980; Dewhurst *et al.*, 1982). This depression of the surface continued after the L arrival, until the arrival of the shear wave which is detected as a

positive step S. The position of initial small positive pulse P (which is due to thermal diffusion and the finite size of the acoustic source and detector area) is not visible on this particular waveform due to it being within the noise limit.

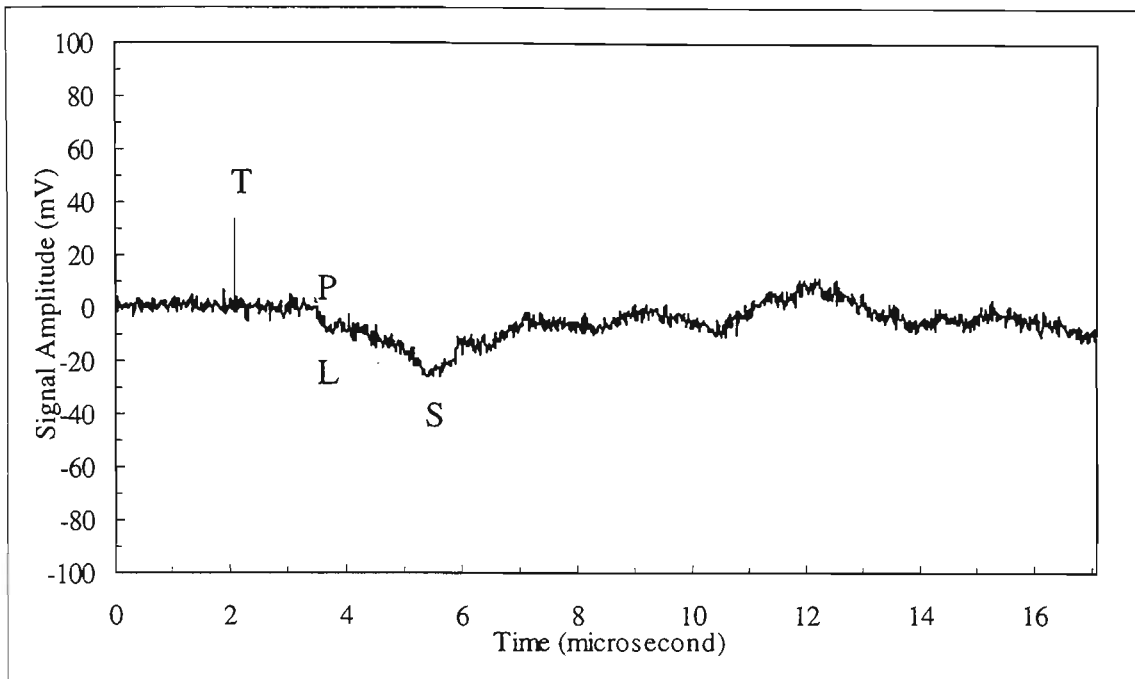


Figure 4.2.6 Acoustic waveform measured at the epicentre with an unfocused laser pulse of energy 113 mJ (incident power density of  $\approx 19 \text{ MW/cm}^2$ ).

#### 4.2.2.2 Irradiation with the laser beam focused within the sample (varying surface power density)

The incident power density of the laser pulse in this experiment was modified by focusing the beam through a plano-convex lens of 500 mm focal length (Newport KPX118) which was placed in front of the target surface. The measured interferometer waveforms obtained with the plano-convex lens placed at a distance of 250 mm from the target surface is shown in the figure 4.2.7. The irradiation area has been reduced by this focusing action and the incident power density is now  $\approx 76 \text{ MW/cm}^2$ . When

using the focusing lens, the beam size and average power density in the central region was estimated by simulating the experimental arrangement using the ZEEMAX optical design software (includes diffraction) and the known properties of the lens. The observed acoustic waveform is very similar to Figure 4.2.6 and clearly shows that the excitation is still in the thermoelastic regime. A small positive pulse (P) is now evident at the time of arrival of the longitudinal wave pulse and this is consistent with the increased excitation power density (Scruby *et al.*, 1980).

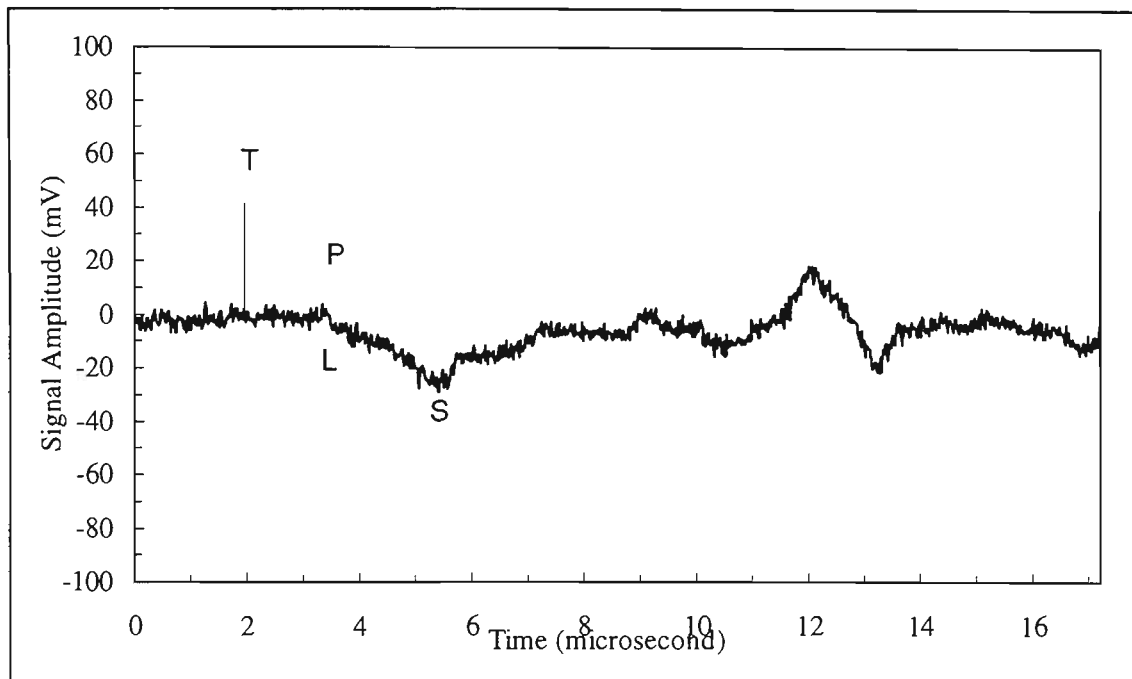


Figure 4.2.7 Acoustic waveform measured at the epicentre with an incident power density of  $\approx 76 \text{ MW/cm}^2$  obtained by placing a plano-convex lens at a distance of 250 mm from the target surface.

The estimated power density is increased to  $\approx 200 \text{ MW/cm}^2$  when the plano-convex lens is moved to a distance of 350 mm from the target surface. The observed acoustic waveform for this case is shown in Figure 4.2.8 and has the same characteristics as that shown in Figure 4.2.1 which was obtained at a similar power density. In this situation,

the acoustic source is formed by a combination of thermoelastic stresses together with a normal component due to the force resulting from ablation of surface material. This normal component of the force increases with increasing laser power density, so that normal forces become dominant as the power density is increased (Figures 4.2.9 - 4.2.11).

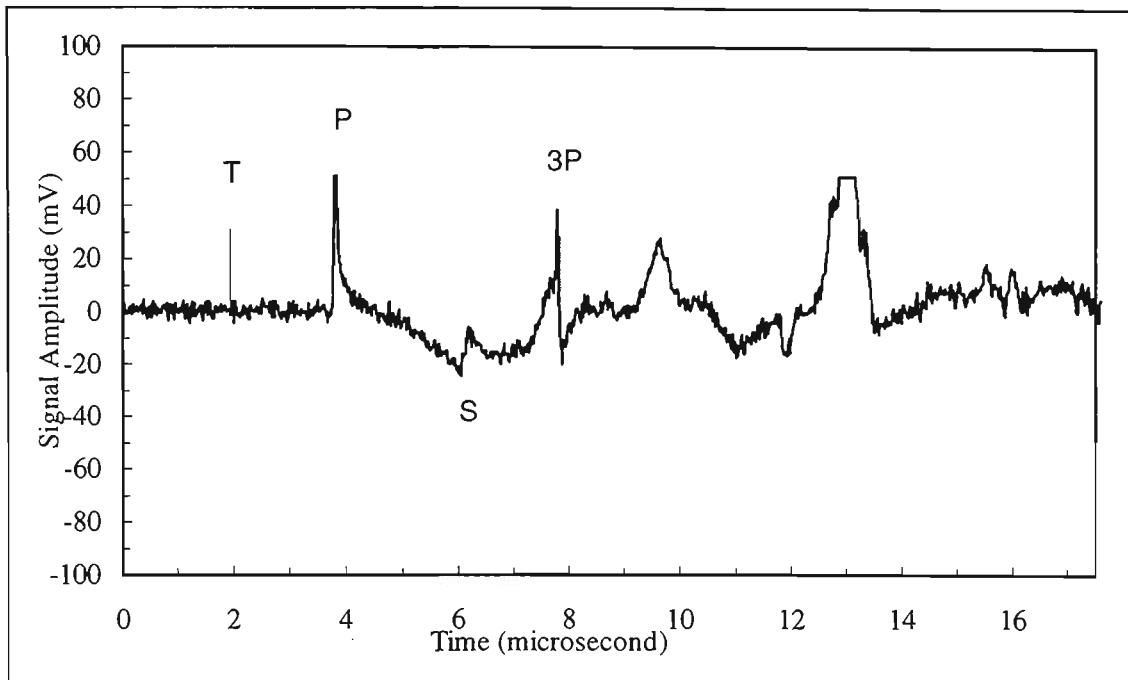


Figure 4.2.8 Acoustic waveform with an incident power density of  $\approx 200 \text{ MW/cm}^2$  obtained by placing a plano-convex lens at a distance of 350 mm from the target surface.

In this regime, ablating material carries momentum away from the surface, which causes the sample to experience an impulse normal to the irradiated surface (Dewhurst *et al.* 1982). With increases in power density, the normal force dominates over the lateral dipolar stress. This is evident from the marked changes in both shape and amplitude of the waveforms at higher power densities. It may also be noted that the P

wave amplitudes have increased with increase in power density and the shear wave step has disappeared to become a change in slope.

The effects of further increase in the incident power density were investigated by placing the lens at a distance of 400, 450 and 475 mm from the target surface which corresponds to the estimated incident power densities of  $\approx 440 \text{ MW/cm}^2$ ,  $\approx 1.5 \text{ GW/cm}^2$  and  $\approx 4.8 \text{ GW/cm}^2$  respectively. A typical acoustic waveform with the lens placed at a distance of 400 mm from the target surface is shown in the Figure 4.2.9.

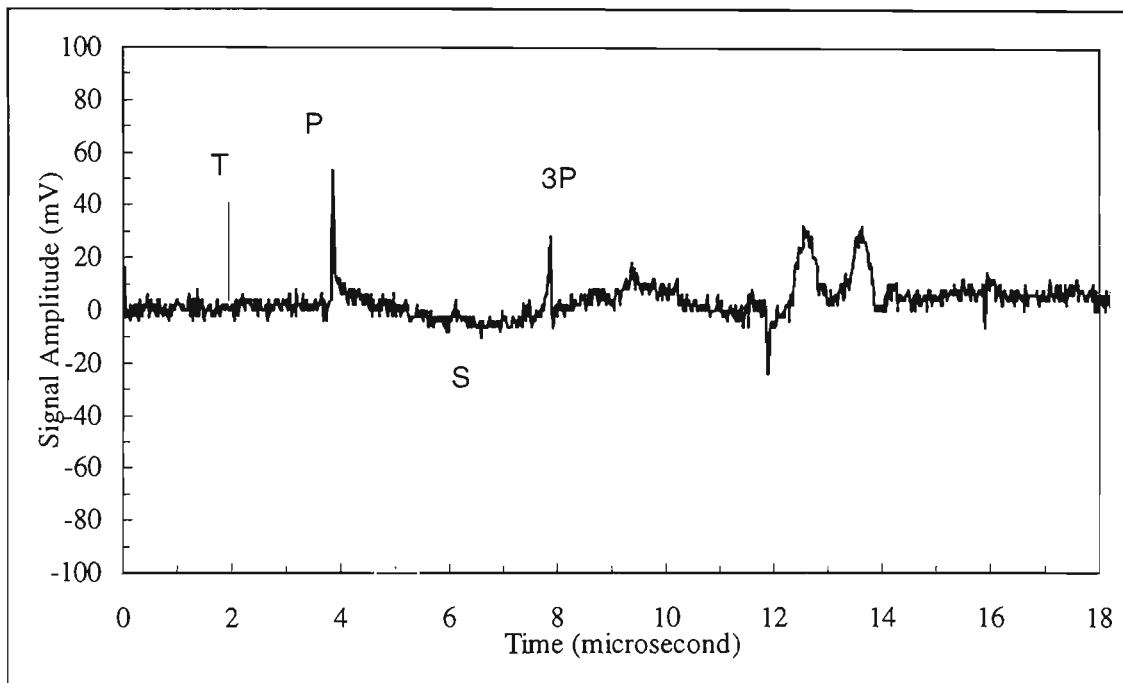


Figure 4.2.9 Acoustic waveform with an incident power density of  $\approx 440 \text{ MW/cm}^2$  obtained by placing a plano-convex lens at a distance of 400 mm from the target surface.

The amplitude of the first longitudinal pulse (P) is similar to that of Figure 4.2.8, but the amplitude of shear pulse is found to reduced considerably. At very high power densities, the observed waveforms are shown in Figures 4.2.10 and 4.2.11. It is

observed that the longitudinal P wave pulse is maximised at about  $1.5 \text{ GW/cm}^2$  and with further increase in power density there is a reduction in the amplitude of the longitudinal displacement resulting from the arrival of the P wave. This is consistent with observations reported by others using different detection systems, where the decrease in amplitude of the longitudinal arrival amplitude at higher optical power density is reported to be due to plasma formation near the surface of material and the consequent shielding of the surface from part of the incident radiation (Dewhurst *et al.*, 1982).

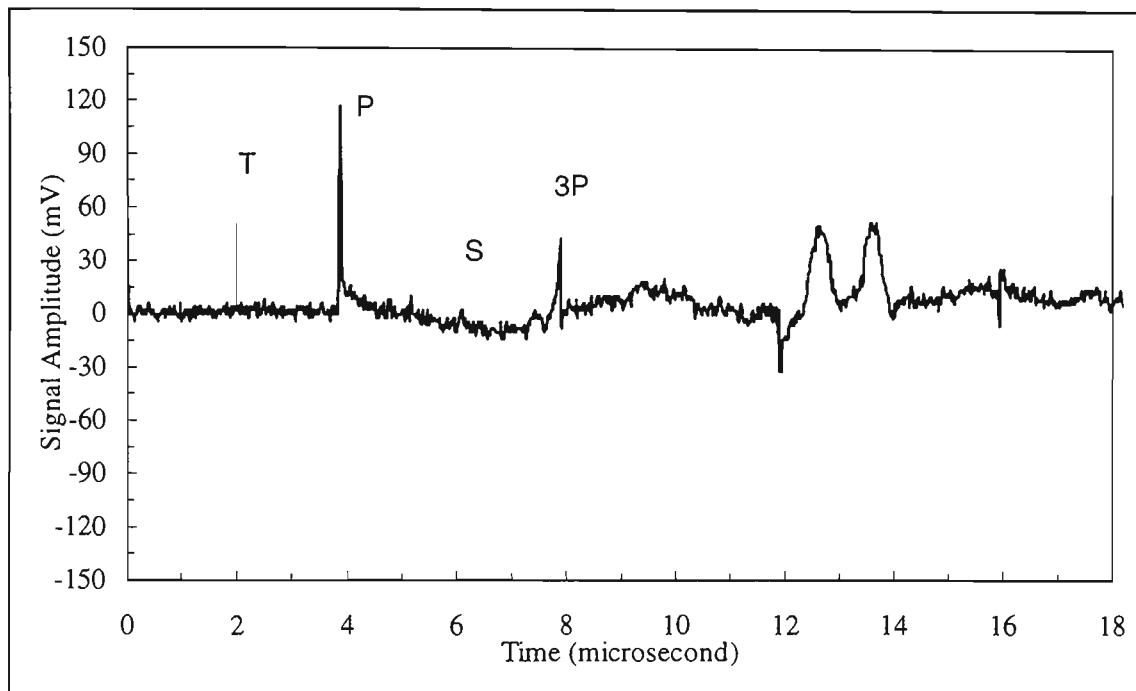


Figure 4.2.10 Acoustic waveform with an incident power density of  $\approx 1.5 \text{ GW/cm}^2$  obtained by placing a plano-convex lens at a distance of 450 mm from the target surface.

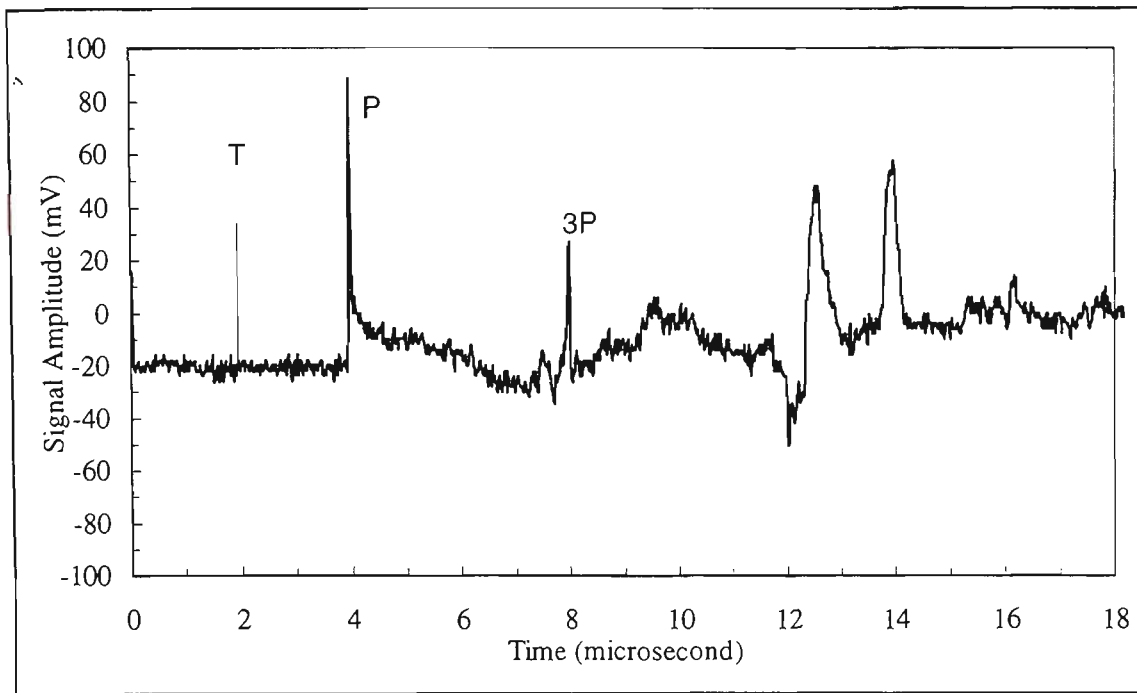


Figure 4.2.11 Acoustic waveform with an incident power density of  $\approx 4.8 \text{ GW/cm}^2$  obtained by placing a plano-convex lens at a distance of 475 mm from the target surface.

#### 4.2.2.3 Irradiation with laser beam focused in front of the target

The laser beam was focused in front of the target, and the examples of typical acoustic displacement waveforms obtained by placing the lens at a distance of 525 mm and 550 mm are shown in Figures 4.2.12 and 4.2.13 respectively. An examination of these waveforms shows that the arrival of the acoustic waves now resembles a step shape rather than a sharp pulse. These waveforms are characteristic of a normal force with Heaviside time dependence due to relatively long lifetime of the expanding plasma formed above the target surface (Hutchins *et al.*, 1981a). When the laser beam is focused in the air above the surface, the power density at the focal point (estimated to be about  $65 \text{ GW/cm}^2$ ) is sufficient to cause air breakdown. The shock wave propagating to the sample surface from the air breakdown provides a source of ultrasound (Edwards *et al.*, 1989). When the lens is placed at a distance of 525 mm

from the surface, the incident power density on the target surface in the absence of attenuation effects from the air breakdown is estimated to be about  $13.9 \text{ GW/cm}^2$ . This is well above the level necessary to cause ablation and plasma formation on the surface. Thus the surface can come under the influence of the combined effects of plasma formation due to air breakdown and plasma formation with material ablation due to high surface power density. Since the plasma is produced in front of the sample at a distance of 25 mm, only the beginning of the laser pulse reaches the sample unattenuated. The rest of the pulse suffers some absorption or defocusing by the plasma, effectively shielding the surface from the incoming light (Hrovatin and Mozina, 1993). The long lifetime of the air plasma and its interaction with the target surface generates an acoustic source with an approximately Heaviside time dependence (Edwards *et al.*, 1989; Taylor *et al.*, 1990). Evaporated material from the sample surface also lowers the plasma formation threshold, thus increasing shielding and reducing the optical energy delivered to the sample. This leads to a decrease in the ultrasonic wave amplitude in the material which is strongly dependent on the incident power density (Hrovatin and Mozina, 1993). The effect of high incident surface power density which causes ablation and plasma formation in ablated material is also known to result in a Heaviside-like step function excitation. This is regularly observed when very high power densities are focused on the surface (Aussel, *et al.*, 1989; Scruby, and Drain, 1990). Thus for the situation described above, there are two mechanisms for exciting the acoustic wave which each give rise to a Heaviside-like excitation function.

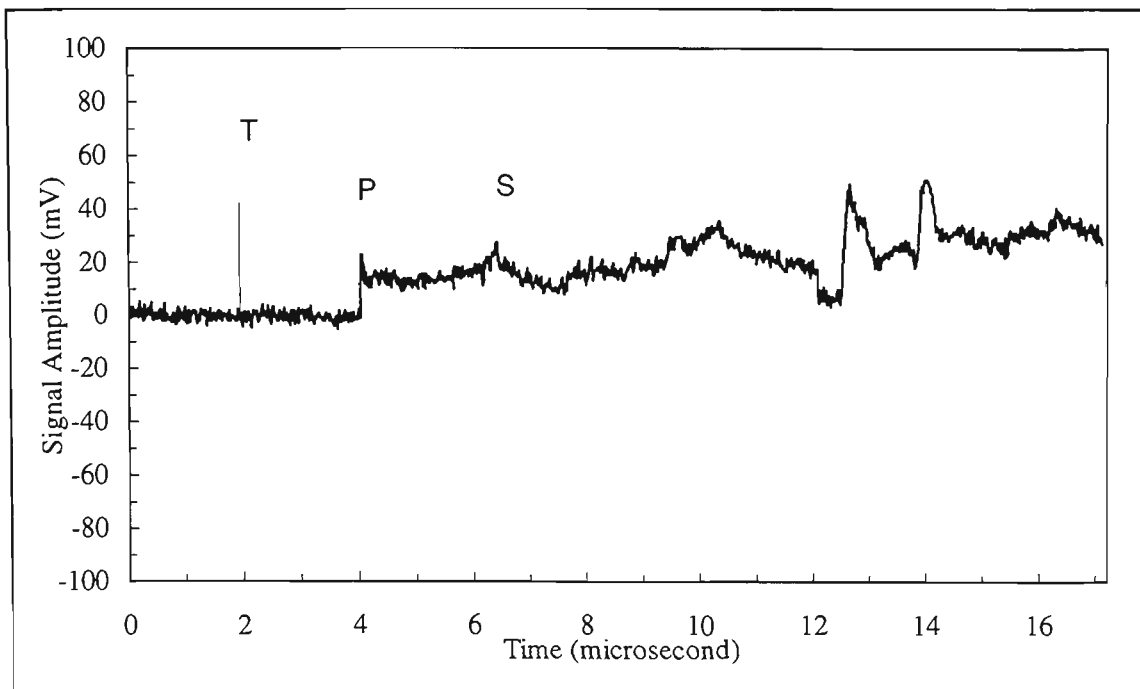


Figure 4.2.12 Acoustic waveform with the estimated unattenuated incident surface power density of  $\approx 13.9 \text{ GW/cm}^2$ , obtained by placing the lens ( $f = 500 \text{ mm}$ ), at a distance of 525 mm from the target.

The reduction of the P arrival amplitude in Figure 4.2.12 compared to Figure 4.2.11 may be explained as a consequence of plasma shielding. This is so for the case of Figure 4.2.12, even though the focal point is 25 mm above the target surface since the laser power density is high. Figure 4.2.13 shows a similar behaviour when the laser is focused 50 mm above the surface except that there is an increase in the amplitude of P wave and the appearance of a pulse due to the arrival of the twice-reflected longitudinal wave (3P). Clearly focusing at larger distances from the surface in this case results in more efficient excitation of acoustic waves in the sample. The increase in P amplitude in Figure 4.2.13 compared to Figure 4.2.12 may be explained as arising from a reduction in plasma shielding of the surface. The incident power density on the target surface in the absence of attenuation effects from the plasma is reduced to about  $2.6 \text{ GW/cm}^2$  for the case of Figure 4.2.13 (from  $13.9 \text{ GW/cm}^2$  in Figure 4.2.12). The

interesting result is that the excitation for the case of Figure 4.2.13 is still a Heaviside function. This must be arising due to ionisation and plasma formation above the surface as this behaviour was not observed for similar high surface power densities when the focal point was inside the target material. For example, Figure 4.2.11 shows a very different waveform with focusing inside the target at a surface power density of  $4.8 \text{ GW/cm}^2$ . One possible interpretation of these results is that the air plasma is effective in exciting acoustic waves in the sample with a step-like excitation even at distances as large as 50 mm from the sample surface. This is considerably larger than distances previously reported for metals by Hrovatin and Mozina (1993) using 85 mJ of 1064 nm radiation (not much effect beyond 10 mm from the surface) and Edwards *et al.* (1989) using 1 J of  $10.6 \text{ }\mu\text{m}$   $\text{CO}_2$  laser radiation (maximum effect when the focal point is 15 mm from the surface). These are the only reported results for this type of measurement with metallic targets. The results with  $10.6 \text{ }\mu\text{m}$   $\text{CO}_2$  laser radiation are qualitatively different than those using 1064 nm as the long wavelength radiation is almost totally reflected by the metal sample and ablation is not present. Hence at this wavelength all effects are due to the air plasma alone. At 1064 nm, plasmas can be produced in the air or in the ablated material.

The results of Figure 4.2.13 appear at first sight to be rather different from those of Hrovatin and Mozina (1993). However, they used lower energy excitation (85 mJ compared to 113 mJ) and the behaviour in this region is likely to be highly non-linear. More importantly, they used a 75 mm focal length lens to focus the radiation and the data of Figure 4.2.13 was measured using a 500 mm focal length lens. This longer focal length lens would give rise to a much slower variation of power density with distance from focus than was the case in the experiments of Hrovatin and Mozina.

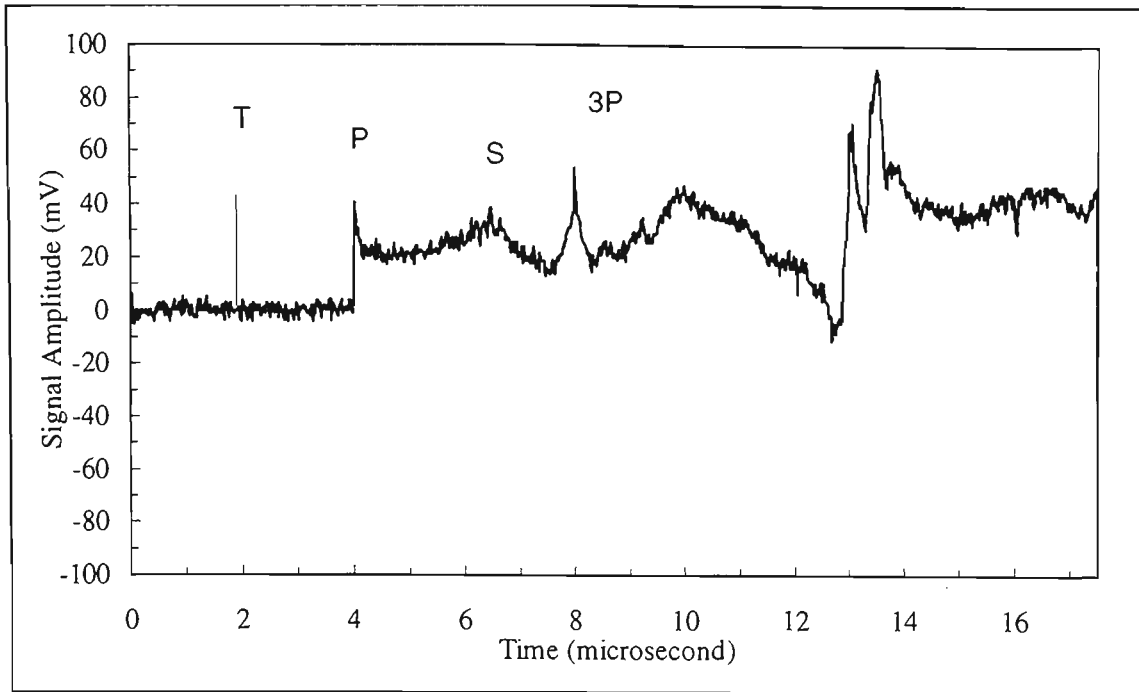


Figure 4.2.13 Acoustic waveform with the estimated unshielded incident surface power density of  $\approx 2.6 \text{ GW/cm}^2$ , obtained by placing the lens ( $f = 500 \text{ mm}$ ), at a distance of 550 mm from the target.

The variation of the longitudinal wave arrival amplitude with different positions of the plano-convex lens was investigated further and the results are shown in Figure 4.2.14. It may be noted that the P wave amplitude does not change significantly when the lens is positioned close to the target, which is expected for a source entirely within the thermoelastic regime. The P wave increases in amplitude due to the increase in power density with focusing distances up to 450 mm as ablation takes place. Focusing close to the surface results in decreased P wave amplitude as the very strong plasma which results gives rise to strong shielding of the surface from the incident energy. No measurement was made with the laser energy focused exactly on the target surface but one would expect minimum acoustic generation at this point (Hrovatin and Mozina,

1993; Edwards *et al.*, 1989). For this reason no dotting is used in Figure 4.2.14 in the region near a lens-to-target distance of 500 mm. With focusing in front of the target surface, the P wave amplitude is dependent on the incident surface power density (which determines the amount of ablation) as well as the strength and position of the plasma formed in the air and ablated material (which determines the effect of the plasma on the surface and the extent of shielding of the incoming radiation). The amplitude of the P wave can be seen to increase with distance of the focal point above the surface, reaching a maximum at about 100 mm and decreasing to very small levels at about 200 mm.

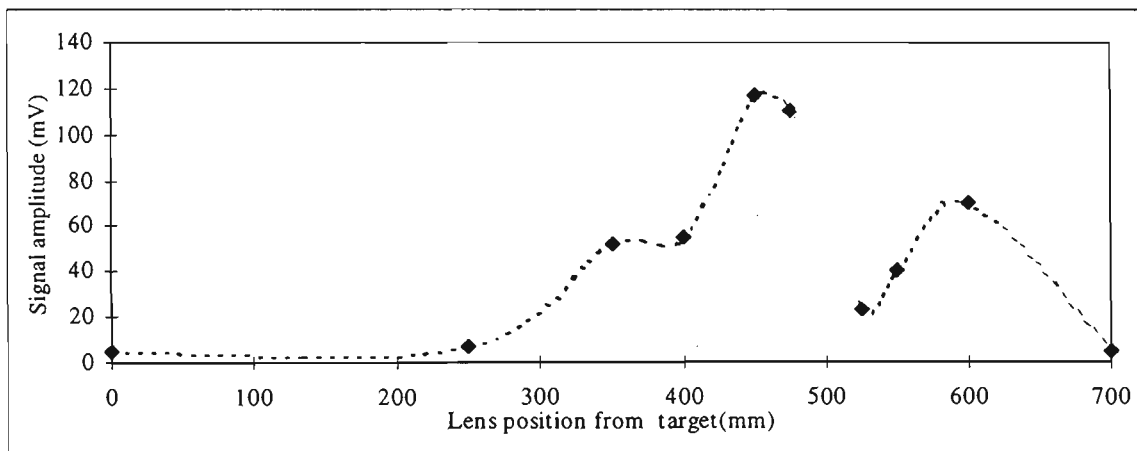


Figure 4.2.14 Variation of the amplitude of the first arrival of longitudinal waves with the position of plano-convex lens (focal length = 500 mm) in front of the target at a constant pulse energy of 113 mJ.

For laser excitation with the incident pulse focused within the target material, the amplitude of the longitudinal P wave at the epicentre is shown as a function of incident

surface power density in Figure 4.2.15. For these measurements the incident laser energy is again maintained at 113 mJ. It may be noted that P wave amplitude does not

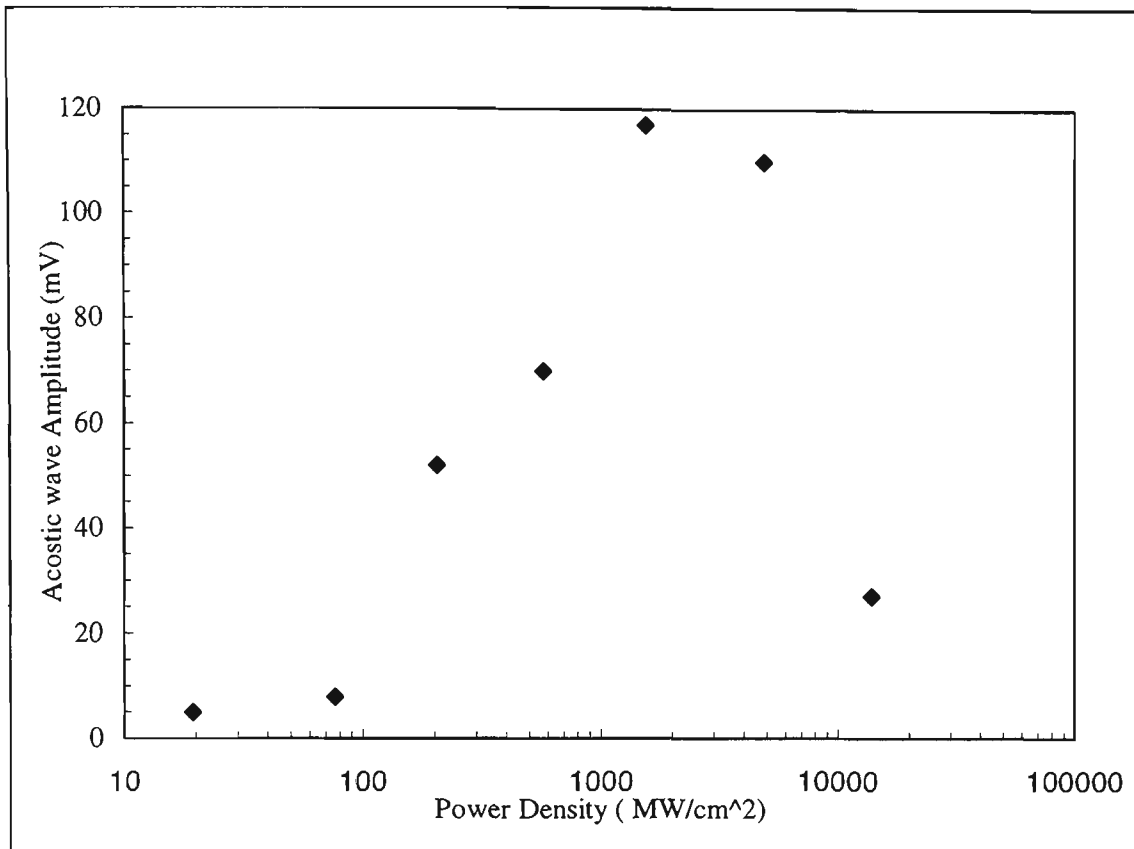


Figure 4.2.15 Variation of longitudinal P wave arrival amplitude as a function of laser power density at a constant laser pulse energy of 113 mJ.

change significantly within the thermoelastic regime (up to  $76 \text{ MW/cm}^2$ ). As ablation sets in, there is a steep increase in the amplitude of longitudinal wave which was found to be maximised at a surface power density of about  $1.5 \text{ GW/cm}^2$ . Above this level the P wave amplitude decreases. This trend is in agreement with the published results of Dewhurst *et al.* (1982) which were obtained at an incident energy of 33 mJ. However, Dewhurst *et al.* obtained a maximum P wave amplitude at a surface power density of about  $0.3 \text{ GW/cm}^2$ . This is considerably lower than the figure of  $1.5 \text{ GW/cm}^2$  obtained above. It should be noted, however, that the surface power density

for maximum P wave amplitude varies with material used and also total incident energy. Bourkoff and Palmer (1985) point out in commenting on the results of Dewhurst *et al.* (1982) that application of Gaussian optics to their situation would give about  $100 \text{ GW/cm}^2$  for their 27 ns pulse. Aussel *et al.* (1988) also observed a similar trend and obtained a figure of about  $1.05 \text{ GW/cm}^2$  in a steel sample using a laser pulse of energy 330 mJ.

#### **4.2.2.4 Irradiation with a pulse energy of 47 mJ**

Similar experiments to those reported above were carried out with a pulse energy of 47 mJ and the same hemispherical aluminium target to confirm suitability of low energy pulsed laser designed and constructed for this work and to see how the results varied with total laser energy. The acoustic waveform obtained from the interferometer with an unfocussed laser beam and an incident surface power density of  $\approx 8 \text{ MW/cm}^2$  is shown in Figure 4.2.16. This waveform broadly shows the characteristics of a thermoelastic source. However at this low incident power density, the signal to noise ratio is too low for any useful measurements. The resulting acoustic waveforms obtained when the laser beam is gradually focused by including a lens, are shown in Figures 4.2.17 - 4.2.19. The P wave amplitude increases with increasing power density of the incident beam. However, the signal to noise ratio at similar power densities is considerably worse than was obtained previously with 113 mJ as the amplitude of the P wave is considerably reduced since this amplitude is also dependent on total incident energy. The detected waveforms are highly reproducible and clearly demonstrate that remote detection of low amplitude laser generated acoustic waves is possible with the combination of low energy pulsed laser and the fibre optic interferometer.

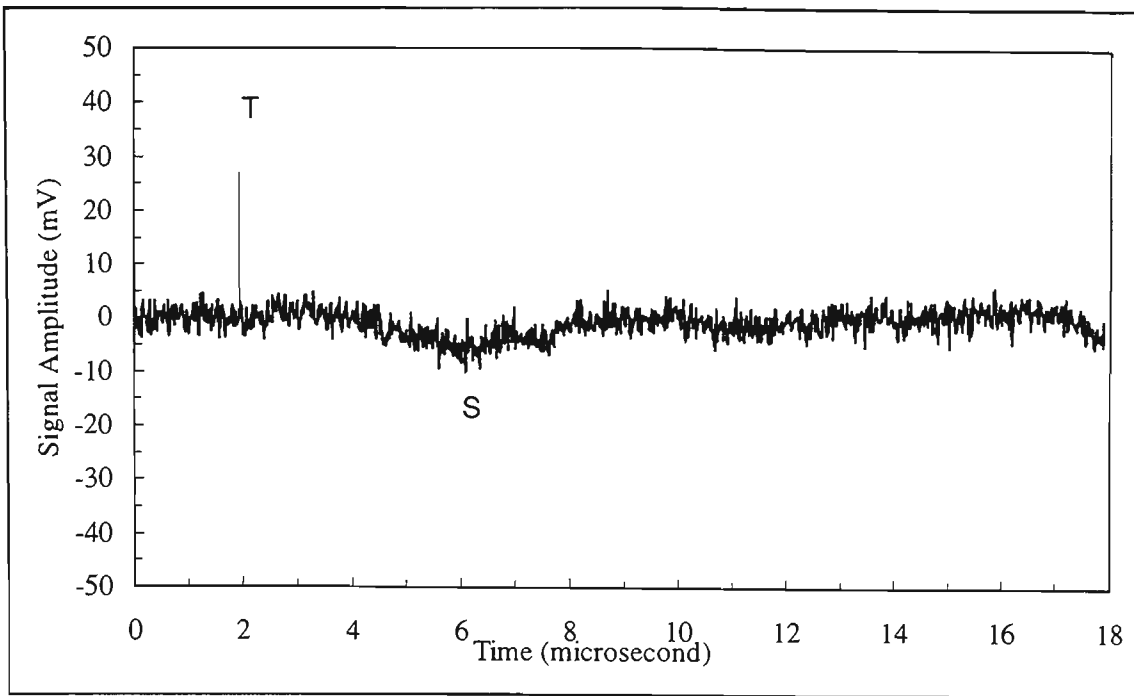


Figure 4.2.16 Acoustic displacement waveform measured at epicentre with an unfocussed laser beam with an estimated incident surface power density of  $\approx 8$  MW/cm<sup>2</sup> (laser energy = 47 mJ).

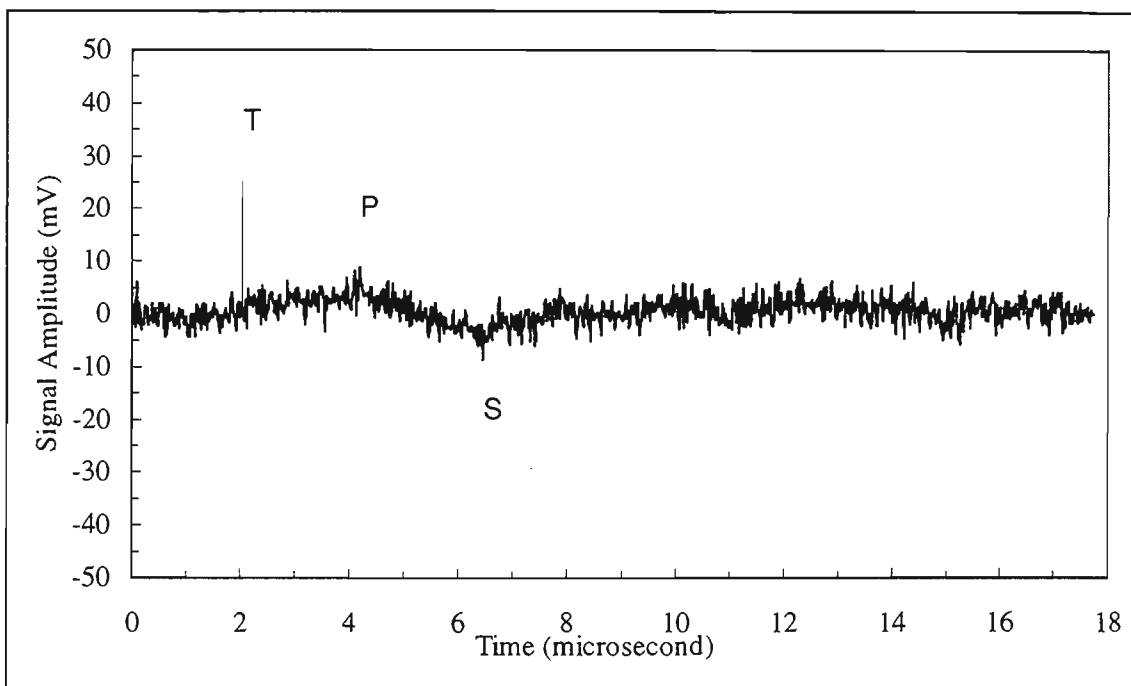


Figure 4.2.17 Acoustic waveform measured at the epicentre with an estimated incident surface power density of  $\approx 30$  MW/cm<sup>2</sup>, obtained by placing the lens ( $f=500$  mm) at a distance of 250 mm from the target (laser energy = 47 mJ).

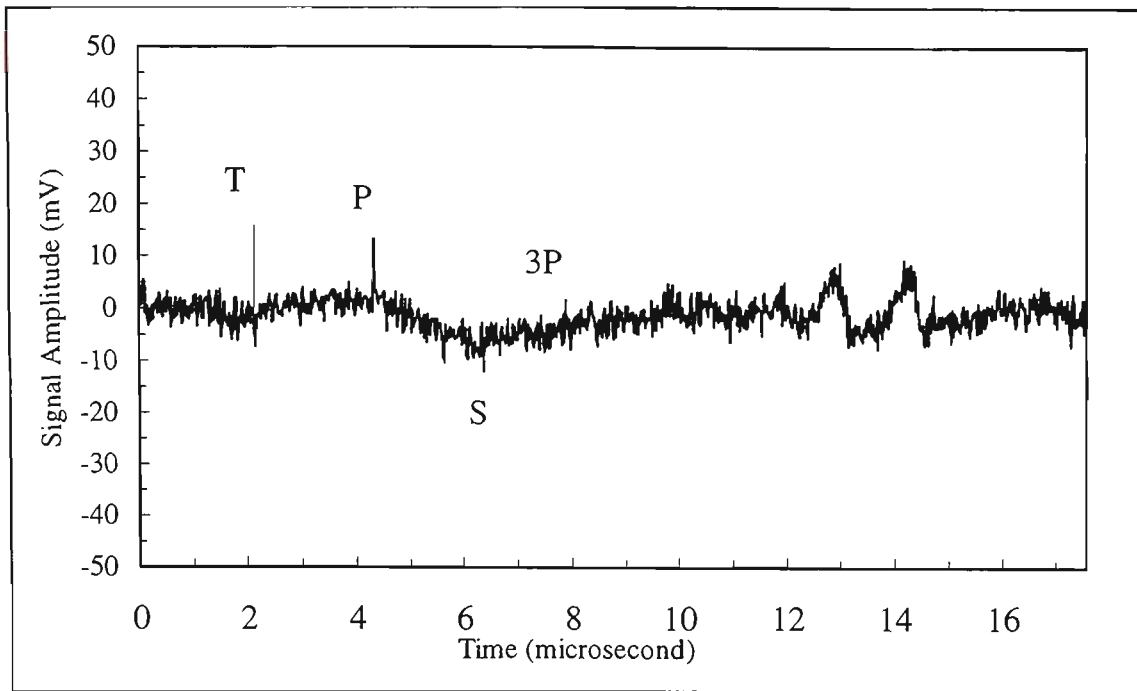


Figure 4.2.18 Acoustic waveform measured at the epicentre with an estimated incident surface power density of  $\approx 640 \text{ MW/cm}^2$ , obtained by placing the lens ( $f=500 \text{ mm}$ ) at a distance of  $450 \text{ mm}$  from the target (laser energy =  $47 \text{ mJ}$ ).

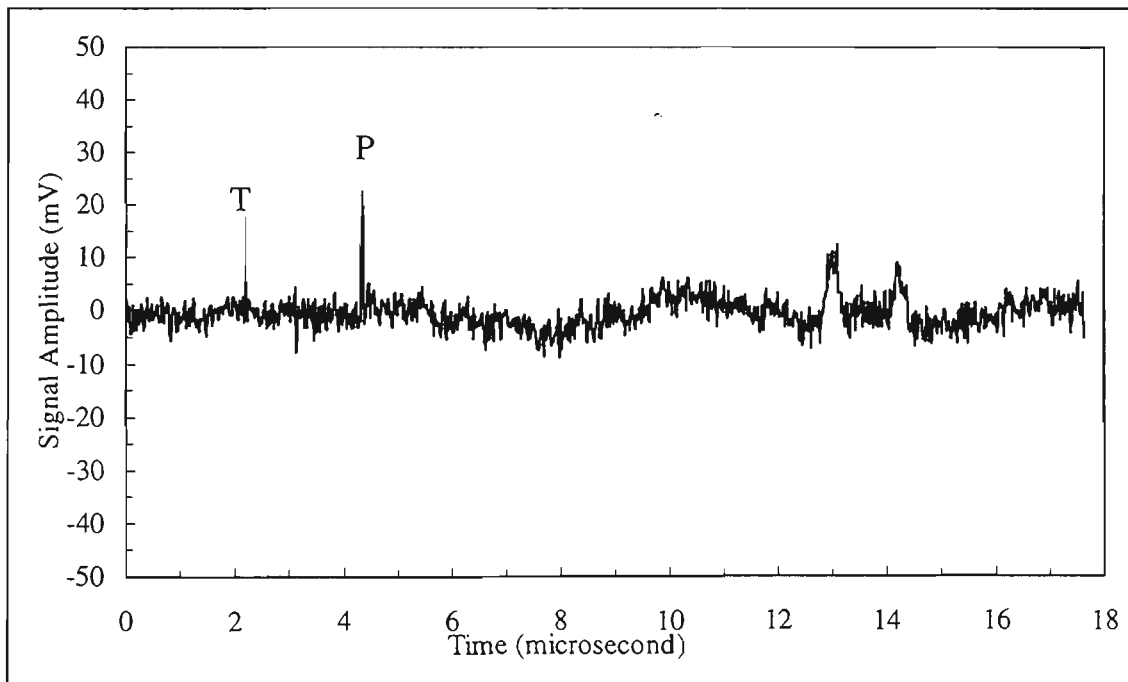


Figure 4.2.19 Acoustic waveform measured at the epicentre with an estimated incident surface power density of  $\approx 2.3 \text{ GW/cm}^2$ , obtained by placing the lens ( $f=500 \text{ mm}$ ) at a distance of  $475 \text{ mm}$  from the target (laser energy =  $47 \text{ mJ}$ ).

The variation of the amplitude of the P wave with position of the plano-convex lens at a constant laser pulse energy of 47 mJ is summarised in figure 4.2.20. When the laser is focused at reasonable distance within the target, the wave amplitude is found to increase with the increase in incident power density as previously mentioned. The reduction in amplitude at the focal point (500 mm) is expected and, as explained earlier, is due to plasma shielding of the surface. The peaks in wave amplitude on either side of the focus are similar to those observed earlier. When the laser is focused in front of the target at this lower energy, the peak amplitude of the P wave occurs at much smaller target-to-focal point distance than was observed earlier with 113 mJ incident energy. This behaviour is consistent with the results reported by Hrovatin and Mozina (1993).

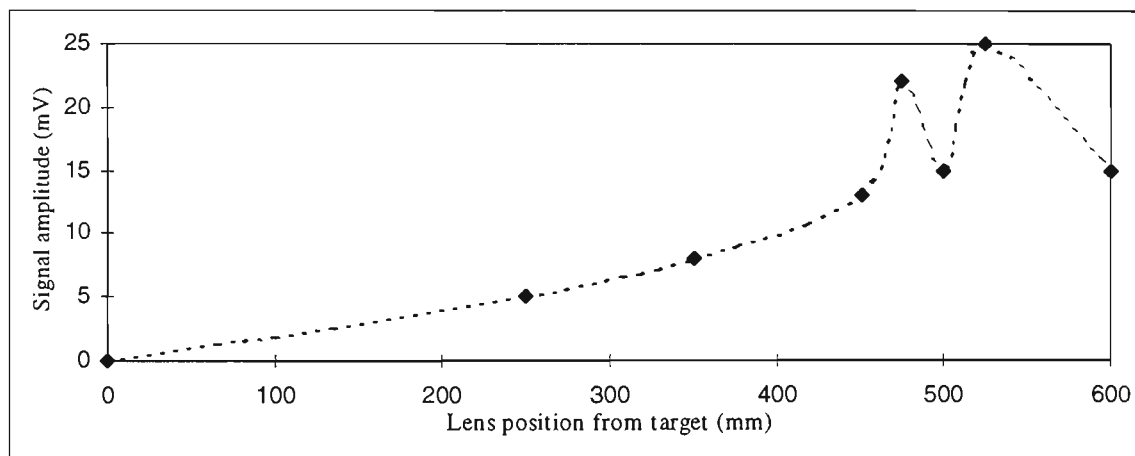


Figure 4.2.20 Variation of the amplitude of the P wave with the position of the plano-convex lens (focal length = 500 mm) in front of the target at a constant pulse energy of 47 mJ.

#### 4.2.2.5 Irradiation with an unfocused laser beam of energy 1300 mJ

Further improvement in signal to noise ratio was obtained with an unfocused laser energy of 1300 mJ. The acoustic waveform detected at the epicentre of a 12.5 cm x 9 cm machined (unpolished) aluminium plate of thickness 3.95 cm is shown in Figure 4.2.21. The thickness of the plate was chosen to be smaller than the other dimensions, so that the reflections from other walls arrive too late at the detector to interfere with measurement of the direct longitudinal and shear arrival. The acoustic wave arrivals are labelled according to the number of longitudinal (P) wave passes through the specimen. At these high power levels, the time of arrival of the S waves cannot easily be detected as changes in slope are small.

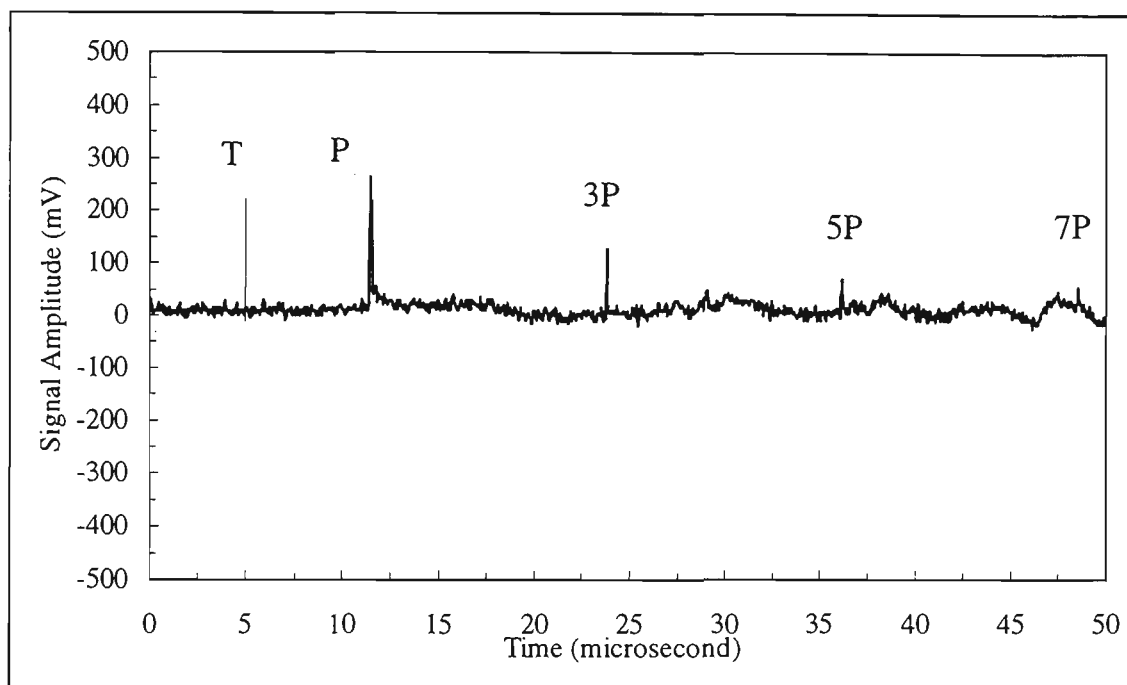


Figure 4.2.21 Acoustic waveform measured at the epicentre for an aluminium plate of thickness 39.5 mm irradiated with an unfocused laser pulse of energy 1300 mJ.

Similar waveforms were measured when the aluminium sample was replaced with different metals. The P wave exhibited the expected characteristic velocities and the relative heights of the various peaks in the waveforms were changed as the wave propagation characteristics are also material dependent as discussed in Chapter 2. Typical oscilloscope records of the acoustic waveforms obtained from brass (15 cm x 3.2 cm x 0.95 cm ), mild steel (12 cm x 5 cm x 0.93 cm ) and stainless steel (15 cm x 2.5 cm x 0.78 cm ) are shown in Figures 4.2.22, 4.2.23, 4.2.24 respectively. It may be noted that the width of the various peaks are now obvious due to the change in time scale of the horizontal axis.

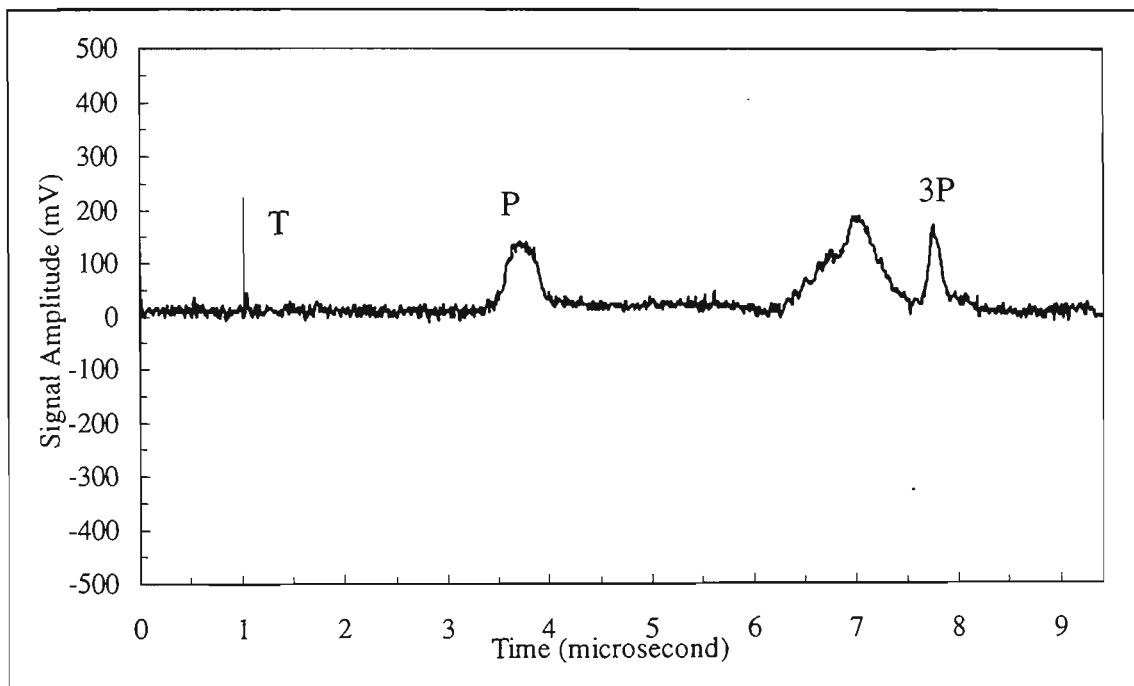


Figure 4.2.22 Acoustic waveform measured at the epicentre for a 9.5 mm thick brass plate irradiated with an unfocused laser pulse of energy 1300 mJ.

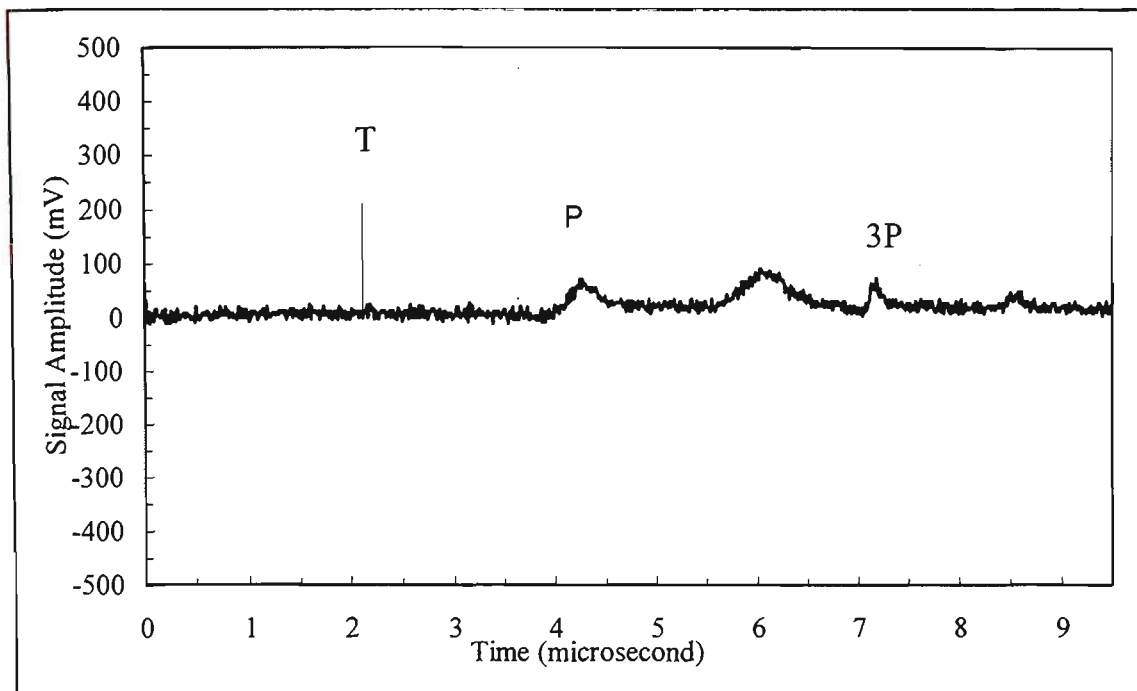


Figure 4.2.23 Acoustic waveform at the epicentre for a 9.3 mm thick mild steel plate irradiated with an unfocused laser pulse of energy 1300 mJ.

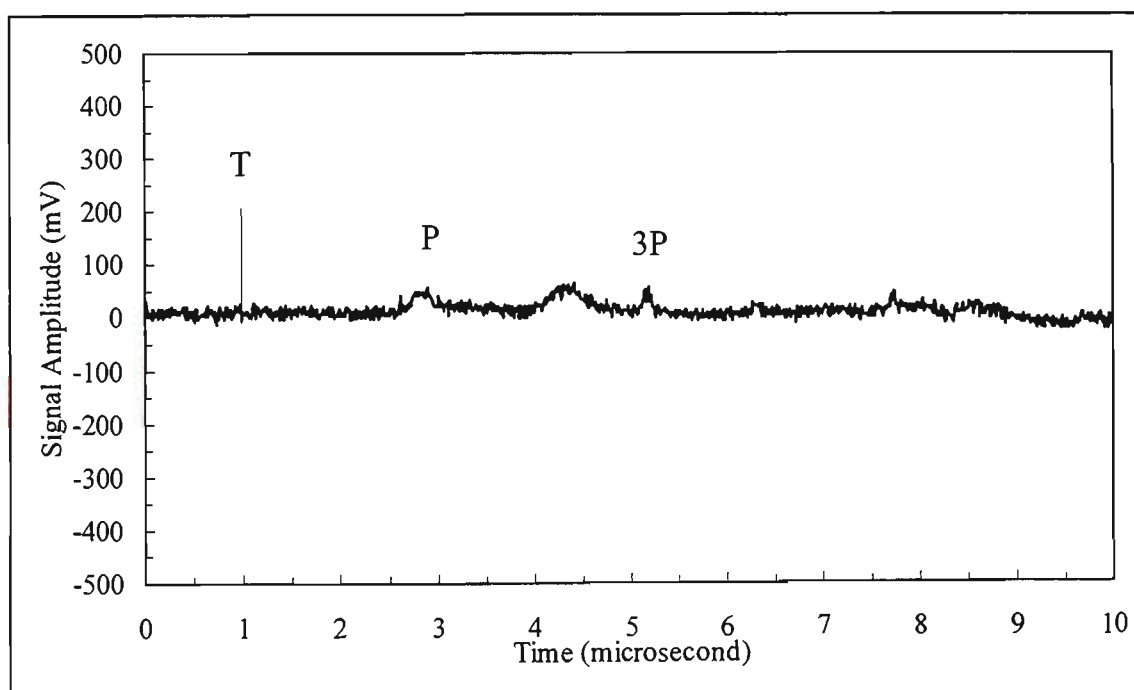


Figure 4.2.24 Acoustic waveform at the epicentre for a 7.8 mm thick stainless steel plate irradiated with an unfocused laser pulse of energy 1300 mJ.

### 4.3 Determination of the longitudinal wave velocity in metals

Longitudinal velocity measurements of ultrasonic waves have been widely used in many areas of material characterisation such as the measurement of principal elastic moduli and in non-destructive evaluation. The velocity of longitudinal and shear waves can be calculated from the fibre optic sensor signal by measuring appropriate time intervals and knowing the thickness of the sample. One can either measure the time of arrival of the first longitudinal wave which has propagated once across the sample or the time interval between two successive wave arrivals which involves propagation over a distance of twice the sample thickness. The best choice depends on the experimental conditions and the amplitudes of the various peaks in the waveform. For the data of the previous section, it makes little difference which method is used as the calculated uncertainties are very similar.

Table 4.3.1 below summarises the calculated values of the longitudinal wave velocity in the various materials as well as representative values for those materials obtained from the literature (McMaster, 1959). It should be noted that none of these are pure materials and the velocity depends on the exact composition which was not known for the laboratory samples used here.

It is clear from these measurements that, if one arranges the experimental conditions to get good quality waveforms, quite accurate measurements of longitudinal velocity are possible. In the present case the velocities have uncertainties of about 2% or less. These measurements could be improved by some focusing of the incident laser energy

to increase the amplitude of the peaks and also by improving the bandwidth of the interferometer detector electronics.

<b>Material</b>	<b>Longitudinal Velocity (Experimental) in m/s</b>	<b>Longitudinal Velocity (Documented) in m/s</b>
<b>Aluminium</b>	6320 ± 33	6250-6350
<b>Brass</b>	4470 ± 77	4430
<b>Stainless steel</b>	6117 ± 139	5660-7390
<b>Mild steel</b>	5757 ± 102	5850

Table 4.3.1 Longitudinal wave velocity in different materials.

# Chapter 5: Laser generation and detection of ultrasonics for monitoring the curing of composites

## 5.1 Detection of ultrasonics in non-metallic materials

A cured sample of epoxy in a plastic container (1.45 cm thickness) was used for initial measurements designed to assess the suitability of the laser/fibre interferometric technique for non-contact generation and detection of acoustic waves in non-metallic materials. The technique was found to work quite satisfactorily and an example of a typical acoustic waveform at the epicentre of the sample, obtained using a single laser pulse, is shown in Figure 5.1.1.

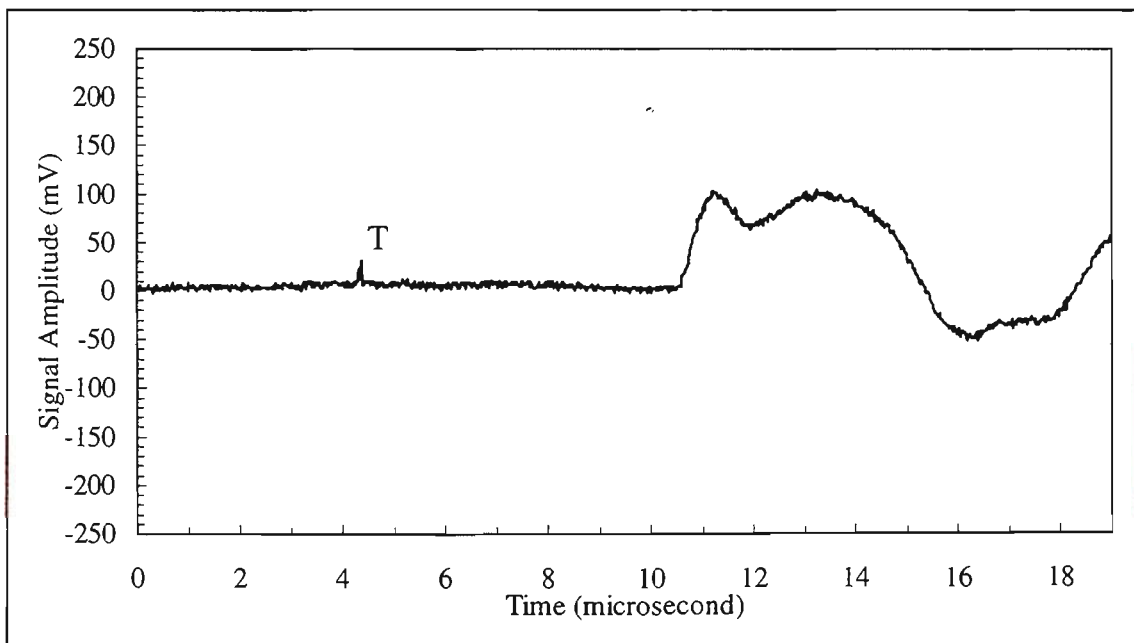


Figure 5.1.1 Acoustic waveform at the epicentre of a cured epoxy sample (14.5 mm thick) obtained with a pulse energy of 1300 mJ.

For these measurements, the unfocused laser beam with a pulse energy of 1300 mJ was used for the generation of acoustic pulses. Aluminium cooking foil was used on the front surface of the sample to provide an ablative target and the rear surface of the sample was painted to improve the signal to noise ratio of the interferometer. As discussed in section 4.3.1, the longitudinal velocity of the acoustic wave in epoxy was calculated by measuring the time of arrival of the first longitudinal pulse and the thickness of the plate. The longitudinal wave velocity was found to be  $2727 \pm 80$  m/s, which is well within the reported range of typical values for epoxy materials of 2400-2900 m/s (Krautkramer and Krautkramer, 1990).

## **5.2 Curing of Epoxy**

Resins are used as a matrix material for fibre reinforced composite (FRC) structures. Of all the resins used in the manufacture of FRC, epoxy resins have, by far, gained the widest acceptance. Characteristically, the epoxy resin shrinks less during cure than most other thermoset resins, and no volatile byproducts are generated during the cure. Epoxies also provide excellent electrical insulating characteristics, outstanding chemical and solvent resistance and above all, they can be used as excellent adhesives (May, 1985). Curing is a process during which a thermoset polymer resin changes its physical character from a viscous liquid to viscoelastic rubber, and finally to a hardened solid. During this process, the polymer molecules grow into longer chains with branches and cross linking also occurring on the microscopic level. The knowledge of property changes during cure is essential to the establishment of an ideal process cycle of these resins for commercial applications such as resin matrix

composites. This knowledge is also essential for prevention of over and under cure. Since the viscosity of the epoxy depends on the extent of the cure, monitoring the degree of cure can provide information which can be used to control applied pressure and other parameters so as to optimise the moulding operation. The rate at which the cross-linking reaction progresses depends on many variable such as resin chemical composition and temperature. Since typically these variables are not absolutely controllable, a monitor of the extent of chemical reaction or degree of cure provides important information which is useful for controlling the cure process (Winfree and Parker, 1984).

In the manufacture of FRC materials with thermosetting resins, the first stage is the production of prepeg, which is a tape or sheet of fibres impregnated with resin. Prior to further processing, the cold prepeg is warmed up to the ambient conditions, placed in a proper mould and then cured under appropriate temperature and pressure conditions. For optimal mechanical properties, pressure is applied at a predetermined temperature to squeeze the excess resinous material and to improve the fibre/matrix wetting and adhesion prior to complete moulding and cross-linking. It was found that, in most cases pressure should be applied when the viscosity of the polymerizable resin is at a minimum level.

There are many techniques available for cure monitoring which are based on the changes of properties of one type or another. Some of the properties frequently used are electrical resistance, dielectric loss measurement, wave absorbency, heat generation and measurement of elastic modulus or properties dependent on it. A summary of the

most common methods for monitoring cure, with particular emphasis on optical methods, is given below.

### **5.2.1 General methods of monitoring cure**

Warfield (1965) has described a contact method involving the application of electrical resistivity measurements in the determination of rate and extent of the polymerisation of bulk polymer to study the hardening of thermosetting polymer. In the initial stages of cure, the slopes of the log resistivity vs. temperature plots are approximately constant over the range of temperature examined. At a higher degree of polymerisation, the resistivity tends to level off to a constant value. When the log resistivity vs. time plot exhibits a zero slope, the reaction is complete at the particular temperature at which the polymerisation was conducted. The limitation of this measurement is that the exact relationship between observed resistivity and the structural parameters of the polymer that determine the magnitude of the resistivity is not known and also the measurement requires contact between the electrodes and the epoxy.

An ultrasonic technique using PZT transducers has been examined as means for monitoring reaction extent and the development of solid phase moduli in a curing epoxy by Lindrose (1978). The epoxy system studied was DER 332/Jeffamine T403 mixed 100/36 parts by weight and was cast immediately after mixing and evacuated (de-gassed) in a 12 cm diameter aluminium disc. This experiment was performed on the propagation of 1 MHz acoustic waves using a pulse echo technique and involved contact between the sample and both the acoustic source and monitoring detector. Signal attenuation and wave speed data were recorded as a function of cure time for the 1 MHz longitudinal and shear waves. The behaviour observed was interpreted in terms

of the linear-viscoelastic wave propagation theory and then from the wave speed, apparent elastic moduli were calculated as a function of cure time. It was demonstrated that the changes in acoustic wave propagation characteristics can be used to monitor the reaction extent of curing epoxies, and these changes are indicators of underlying effects occurring in instantaneous moduli, equilibrium moduli and relaxation spectra. Thus the equilibrium modulus criteria commonly used to assess the state of cure can be correlated with the data provided by the ultrasonic technique

Monitoring the degree of epoxy cure using ultrasonic velocity measurements was also reported by Winfree and Parker, (1984). A parallel plate glass cell with a 20 MHz broadband damped transducer bonded to one of the faces was used to contain the epoxy. The mixture of curing agent and resin was placed inside the cell and an acoustic wave was propagated through the glass into the resin layer and the resulting echoes from the rear surface of the resin layer were monitored. During the curing process, the longitudinal velocity was found to increase monotonically as the moduli of the epoxy increases. Measurements of the velocity during the epoxy cure were made at various temperatures and with various reactant concentrations. The rate of change in the longitudinal velocity with respect to the cure time was shown to vary as predicted by the reaction kinetics, and this demonstrated that the longitudinal velocity was a good measure of the degree of cure.

Hahn (1984) has described an ultrasonic characterisation of cure using PZT transducers to propagate longitudinal waves. Two epoxy systems (Epon 828/Z and Epon 815/V140) were used in this investigation. The wave speed and attenuation were measured at three different cure temperatures by using an ultrasonic flaw detector at a

frequency of 10 MHz and also by a 10 MHz transducer in the pulse-echo mode. It was observed that the wave speed increased monotonically as the epoxy hardened. The relative attenuation also increased but after reaching a peak, it dropped down to a value lower than the initial value in the liquid state. He also developed a simple constitutive model to optimise the cure cycle.

Cure cycle monitoring by dielectric loss measurements were carried out by Ungarish *et al.* (1990) to establish optimal cure condition for the various prepreg polymer composites with respect to heating rates, curing temperature and timing for pressure application. For dielectric measurements, two plies of prepreg for each composites were isolated by alternating layers of Tedlar and glass fabric from two metallic plates measuring 20 x 30 mm. This arrangement served as the capacitor for the dielectric measurements. To reduce external interference, the whole capacitor was wrapped in aluminium foil. It was then connected to a LCR meter (HP 4262A) for measuring the dielectric loss factor and capacitance during cure monitoring. As the resin is subjected to heating at a defined rate, the curve of loss factor vs. time exhibits two peaks; the first of which is attributed to solid/liquid transition in the material, which softens and begins to flow. The second peak appears when the cross linking reaction becomes more dominant, overtaking the tendency of the losses to increase as the temperature rises. Thus, the chemical changes resulting in cross linking bring about a decrease in the loss factor. Consequently, from the loss factor curves it is possible to detect the stage of resin flow and hence to determine when to apply pressure to improve final composite quality. This is a contact method for cure monitoring of composites which is difficult to apply in practical situations.

The use of ultrasonics to monitor the process state of an epoxy resin was investigated and compared to a standard thermal cure characterisation technique involving differential scanning calorimetry (DSC) by White and Mather (1991). In the ultrasonic cure monitor technique, an ultrasonic transducer was used to generate an acoustic wave in the material. The wave was monitored in either through-transmission mode or pulse-echo mode. In the through-transmission mode, the wave passes once through the material and is monitored by a second transducer. In the pulse-echo mode this wave travels through the material, is reflected at the back surface, and then monitored by the excitation transducer. The time for the acoustic waves to traverse through the material (wave speed), and the energy absorbed by the material (attenuation) are the two basic parameters which are related to the mechanical response of the material. By monitoring the changes in wave speed and attenuation during cure, an assessment of the cure state of the material can be made.

In DSC, a sample is heated at a constant rate (dynamic scanning) or maintained at a particular temperature (isothermal scanning) and the heat flow to or from the material is monitored. Since the cross linking reaction in a thermosetting polymer is exothermic, DSC can monitor this exothermic flow of heat and a characterisation of the cure state of material can be made. The modulus extent (obtained from a knowledge of the experimental effective bulk modulus as well as the bulk moduli of the individual components), a process characterisation parameter for use in the ultrasonic cure monitor technique was developed and a comparison was made to the degree of cure as measured by the DSC. Results showed that the degree of cure does not accurately reflect the mechanical property development during cure. Significant changes in the

modulus extent occur during the latter stages of cure when the degree of cure is fully developed.

Nuclear magnetic resonance (NMR) imaging was utilised to monitor the curing process in a small scale sample made from a continuous carbon-fibre reinforced epoxy resin by Jackson (1992). Using suitable techniques, it was possible to obtain internal images and hence measure local internal viscosity non-invasively during the curing process. However, it is not feasible to use NMR technique under autoclave conditions and its practical and economic benefits are also questionable (Spooner, 1992).

### **5.2.2 Optical methods of monitoring cure**

Afromowitz (1988) reported a technique in which a small cylindrical section of the optical fibre, which was made from a fully cured sample of the epoxy resin undergoing the curing process, was used as a sensor element. Conventional step index or graded index fibre of convenient diameter was used to guide light to and from the sensor element. In this system, the uncured resin acts as a waveguide cladding. As the epoxy resin cures, the index of refraction increases and the light guiding properties of the sensing region decreases. The light transmission approaches almost zero as the epoxy resin reaches its cured state. This optical fibre cure monitoring technique thus employed dedicated sensors that are used solely for evaluating the state of the cure. Utilising the technique proposed by Afromowitz, Zimmermann *et al.* (1990) showed that a maximum resin fibre length exists, beyond which sensitivity is sacrificed during the later stages of cure. The main disadvantages of this technique is that it is difficult to couple the silica fibre to the cured sample of the epoxy resin fibre.

Real time in situ monitoring of the chemical states of epoxy resins during cure in an autoclave using Infrared evanescent spectroscopy has been reported by Druy *et al.*(1989). In this work a sapphire fibre was used as the sensor cell portion of the probe embedded between the plies of a prepeg sample. Heavy metal fluoride glass optical fibre cables were designed for connecting a Fourier Transform Infrared (FTIR) spectrometer to the sensor fibre within the autoclave. They used a multiple internal reflectance technique with the embedded optical fibres coupled to a FTIR spectrometer to monitor the progress of cure in an epoxy resin system. The feasibility of using an embedded optical fibre in autoclave curing of composites as a means of monitoring curing chemistry was demonstrated. The main disadvantages of this technique are the need for an expensive FTIR spectrometer to be dedicated to this experimental set up and the need for fragile fluoride fibre to transmit the infrared signals.

George *et al.* (1991) reported real time monitoring of the cure reaction of an epoxy resin (MY 720 and MY721) using fibre optic FTIR spectroscopy. By operating in the near-IR part of the spectrum, direct measurement of the consumption of epoxide and primary amine and growth in hydroxyl groups was possible. They demonstrated that it was possible to track the rate of cure of this type of material with the near-infrared spectra using a microcapillary cell connected to an FTIR spectrometer via a single optical fibre. This work demonstrated that the amine-based resin system can be effectively monitored in the near-IR part of the spectrum.

The development of an intrinsic silica fibre optic sensor based on evanescent-wave FTIR spectroscopy has been reported by Tapanes *et al.* (1992). This sensor has demonstrated the capability to detect and monitor absorption bands of particular

molecules in liquids and during the cure of a polymeric material. However the sensitivity of the sensor for monitoring absorption bands during the cure of epoxies was reported to be poor. This was attributed to the epoxy having a higher refractive index than the silica optical fibre used.

The feasibility of using hypersonic spontaneous Brillouin scattering, photon correlation spectroscopy and ultrasonic measurements to study structural changes during the curing reaction a type of epoxy resin was investigated by Alig *et al.* (1992). The epoxy resin system was diglycidal ether of bisphenol A with butane-1,4-diol. They found that the primary relaxation time could be measured by BS at earlier stages of curing and by ultrasonic experiments at longer curing times. This is an indirect method for monitoring the cure and involved correlating the ultrasonic absorption and velocity to the rate of gelation.

A preliminary experiment to test the feasibility of employing an opto-ultrasonic technique for the cure monitoring of a room temperature cured epoxy specimen was discussed by Davis *et al.* (1991). Hysel TE6175 epoxy and Hysel HD3561 hardner were the epoxy system used in this experiment. The thoroughly mixed epoxy and hardner were poured into a teflon mould. A 600  $\mu\text{m}$  core fibre was used to deliver light pulses from Q-switched Nd:YAG laser to the top surface of the curing epoxy specimen. A fibre optic Michelson interferometer was used for detection of the arrival of ultrasonic signal. The sensing arm of this Michelson interferometer was embedded in the curing epoxy specimen. The experiment was designed to measure the variation of time delay between the laser excitation and the arrival of ultrasonic signal as a function of curing time. In epoxy cure monitoring, it was observed that time delay between the

laser excitation and the arrival of the ultrasonic pulse decreased as the cure progresses. This trend was in agreement with the increase in the velocity of ultrasonic waves as an epoxy cures. This experiment clearly demonstrated that optical generation could be combined with fibre optic detection to give a viable method of monitoring cure. However, the interferometer had to have one arm buried in the epoxy to detect the arrival of acoustic waves and so the technique could not be considered as a remote one.

Ohn *et al.*(1992) reported an ultrasonic scheme for cure monitoring in room temperature cured epoxy (Hysel EPK 907) and composites (Hercules AS4/1919) using a similar technique to that reported by Davis *et al.* (1991) (this is the same group at the University of Toronto). They employed a pulsed PZT transducer as a source of ultrasound. An embedded interferometric fibre optic sensor with an active homodyne demodulation technique was used for the detection of the propagating ultrasonic pulses in epoxies and composites. The sum of the transit times of the longitudinal wave from the source (transducer) to the embedded sensor and the intrinsic electronic system delay, defined as the  $\tau$  parameter, was measured as a function of the cure time. The  $\tau$  parameter was found to decrease monotonically as the cure progresses and exhibited the same trend as the change of viscosity during the cure of epoxy and epoxy-based composite. This technique provides a satisfactory means of cure monitoring during fabrication. Again, it is not a remote measurement as the transducer needs to be placed in contact with the sample and the fibre sensor needs to be embedded in the sample.

Most of the work reported so far on cure monitoring employed contact or hybrid methods for generation and detection of ultrasound and there is a growing interest in the use of laser ultrasonics for the characterisation of non-metallic materials by making

measurements of velocity and attenuation (Scruby and Drain, 1990). The ultrasonic cure monitor is a non-destructive technique which can be adapted to on-line process monitoring and control. It needs to be on-line to provide the needed real time feedback of the cure state for practical materials manufacturing applications.

The remainder of this chapter reports fully remote optical measurements of cure monitoring using the same type of system as described in Chapter 4.

### **5.3 Cure Monitoring Results**

The following sections contain the results of measurements of the variation of the ultrasonic longitudinal wave velocity in a curing epoxy sample using the same non-contact optical excitation and detection method as was used for metals in Chapter 4. The longitudinal wave velocity was chosen as a measure of the extent of cure since Hahn (1984) had previously demonstrated a monotonic increase in this velocity as the cure progresses. The change in longitudinal velocity is related to the extent of cure because the elastic moduli are dependent on the cross-link density in the epoxy and this density increases with cure time (Winfrey and Parker, 1984). Measurements of the longitudinal acoustic wave velocity are particularly suitable for cure monitoring since, as shown in chapter 4, under the right conditions this can be measured quite accurately. Also, again under the right conditions, the longitudinal wave velocity can be measured at all stages of the curing process and is not limited to just identifying a discontinuity at some point in the cure cycle.

Epoxy and other similar materials exhibit much higher attenuation and dispersion than metals such as aluminium (Davis *et al.*, 1991). For this reason, the interferometer waveforms are rather simpler and the principal features have significantly longer rise times than for metals, particularly in the early stages of cure when the material is essentially in a liquid state. Nevertheless, satisfactory measurements of acoustic wave velocity are possible throughout the cure process and the accuracy achievable towards the end of the cure process approaches that obtainable in metals.

The data of this chapter is presented in terms of propagation time and relative wave speed rather than absolute longitudinal wave velocity. This is similar to the approach of Davis *et al.* (1991) and Ohn *et al.* (1992) who used a fibre optic Michelson interferometer with one arm embedded in the epoxy slab for acoustic wave detection. For the case of the work reported in these two papers, this approach was necessary when using a single excitation point as it was difficult to define the thickness of the sample and the use of relative propagation times also avoided some effects of the detector electronics. With the use of the remote interferometer as described in this thesis, there is no such problem defining the thickness of the epoxy but the use of relative times and relative speeds is simpler and it does avoid allowing for the effects produced within the container needed to hold the epoxy while its viscosity is low.

The emphasis in the experiments is on following the curing process from the moment of casting to the fully cured state by monitoring the propagation of the acoustic waves through the material. In the early stages of curing, the signal to noise ratios of the interferometer waveforms are rather poor and this means that fairly high powers and power densities are required for the measurements - significantly higher than those

required if one only wished to measure the propagation time or wave speed towards the end of the curing process. This high power creates difficulties for the container used to hold the sample with surface damage, holes and epoxy leakage possible in a small number of shots at the highest energies available. To avoid this, a number of different types of container arrangements were used. The first used a thin piece of brass shim (thickness 0.05 mm) in contact with the epoxy as the target and a second used the walls of a simple plastic container which had aluminium cooking foil placed on the inner surface (between container and epoxy). With this second arrangement, the target was translated transverse to the laser propagation axis during the measurements to avoid severe container damage. While this arrangement did produce measurable interferometer waveforms, the signal to noise ratios are not good and the system is usable only with large laser energies. With lower energies one needed to focus the laser to obtain sufficient power density for usable measurements and at this power density, the damage to both the plastic container and aluminium cooking foil was too great for the repetitive measurements needed for continuous monitoring. In fact the cooking foil was too fragile to withstand the power density needed for useful acoustic measurements. A third arrangement was also tried in which a rather thicker aluminium foil tape (thickness 0.12 mm) was used as the target for the laser irradiation (Scotch No. 425 pressure sensitive aluminium foil tape). This tape worked very well, but because of the higher reflectivity of the aluminium compared to brass at the wavelength used for this series of measurement, it required slightly higher laser powers than brass for comparable results. Results are presented below for measurements with the various types of container arrangement and in which the interferometer was detecting acoustic waves at the epicentre.

Since the purpose of the work described in this chapter is to demonstrate the feasibility of making remote optical measurements of wave speed with curing epoxies, rather than conduct studies in real composite materials, a fast-curing epoxy was chosen for the sample. The epoxy chosen was of a type that cured in about an hour at room temperature as this reduced the time required to collect data (Rapid cure epoxy, ATL composite).

### **5.3.1 Irradiation with high energy pulses (1300 mJ)**

For the first series of measurements, the experimental cell was a thin-walled (about 0.5 mm) cylindrical plastic container of thickness 1.3 cm and diameter 6.0 cm. Two holes were drilled through its centre to form two windows for transmission of acoustic pulses. The walls of the container were lined with brass shim to avoid leakage of epoxy. The brass shim acts as a suitable target for high power pulses, reduces the heating of the epoxy by the laser and provides a reasonable reflecting surface to improve the signal to noise of the interferometer. The unfocused laser pulse (energy 1300 mJ, diameter 8 mm and pulse width 10 ns) was directed onto one surface of the experimental cell. The laser generated acoustic displacement propagates in the sample and is detected on the opposite face of the experimental cell (at the epicentre) with the interferometer. The epoxy was mixed with its curing agent, degassed and was then poured into the cell at room temperature. The experiment essentially consists of measuring the propagation time (the time difference between trigger pulse and arrival of acoustic pulse) for the arrival of longitudinal acoustic signals as a function of time while the sample is curing. The data was collected using single pulses to record waveforms and a number of samples were used with very similar results. It should be noted that this data is recorded in the ablation regime as this gives the best signal to

noise ratio. In this regime, signal averaging does not give the expected improvement in signal to noise ratio and hence single pulses were used to record waveforms. The lack of effectiveness of signal averaging in the ablation regime has also been observed by Aussel and Monchalin (1989) who ascribe this to lack of pointing stability (variation between excitation and sensing spots) in the pulsed laser used for excitation.

Records of the interferometer waveforms as the cure progresses are shown for a typical sample in the Figures 5.3.1 and 5.3.2. Measurements were initially made at 5-minute intervals. As the cure progresses, the rate of change of the acoustic properties slows, allowing the interval between the measurements to increase to 10 minutes. The slow rise, broad peaks and relatively low amplitude signals evident in the early stages of cure is due to the high dispersion and loss for acoustic waves propagating in the liquid state of the epoxy system. As the cure progresses, changes in attenuation can be rather complex due to phase changes and changes in viscosity (Hahn, 1984). However, solidification generally results in reduced attenuation of the acoustic wave amplitude and also a reduction in the rise time of the peaks due to reduced dispersion.

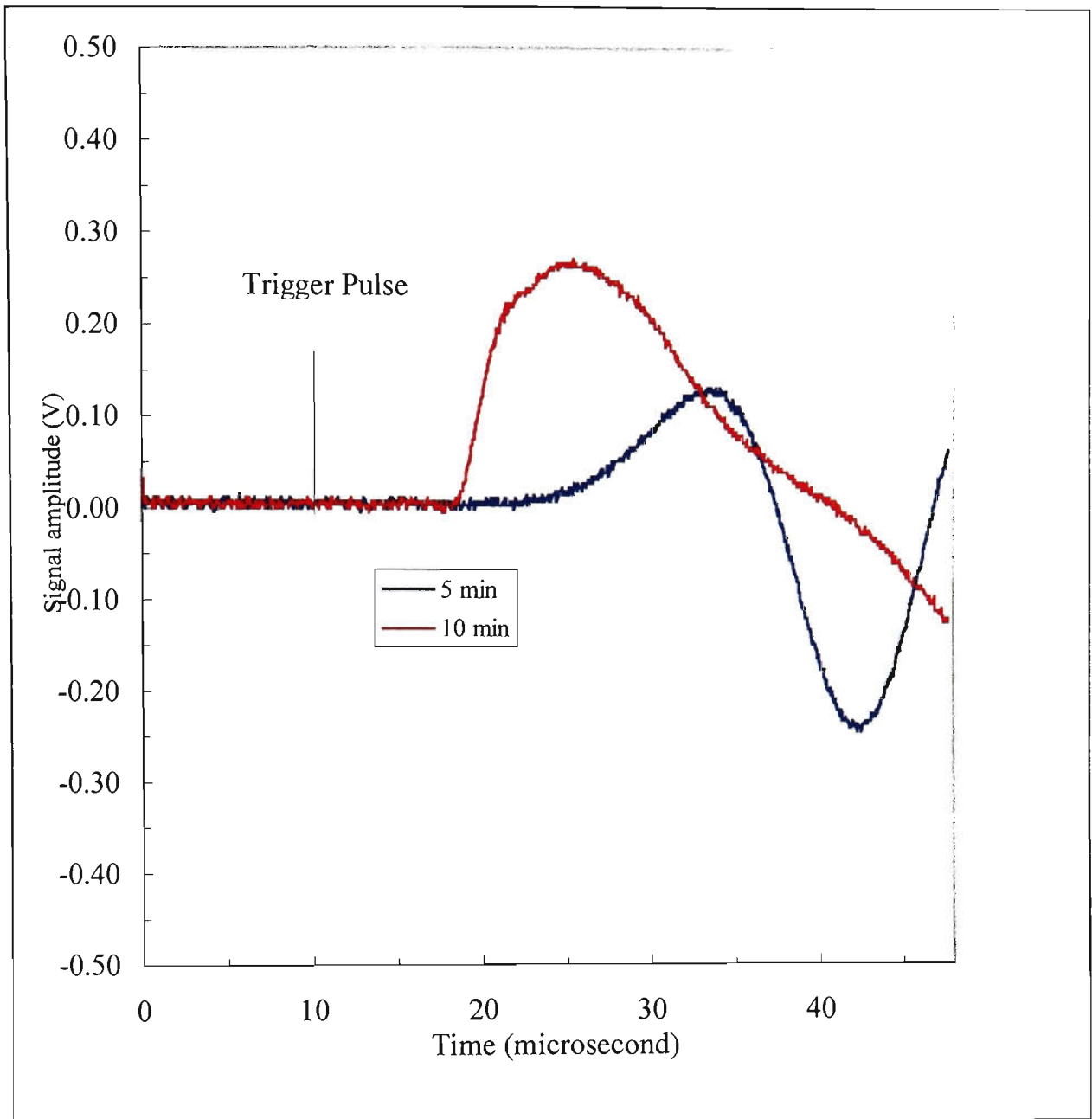


Figure. 5.3.1 Interferometer waveforms for the arrival of acoustic waves during the early stages of cure in a rapid cure room temperature epoxy. Sample excited using a brass shim in contact with epoxy and a single laser pulse of energy 1300 mJ.

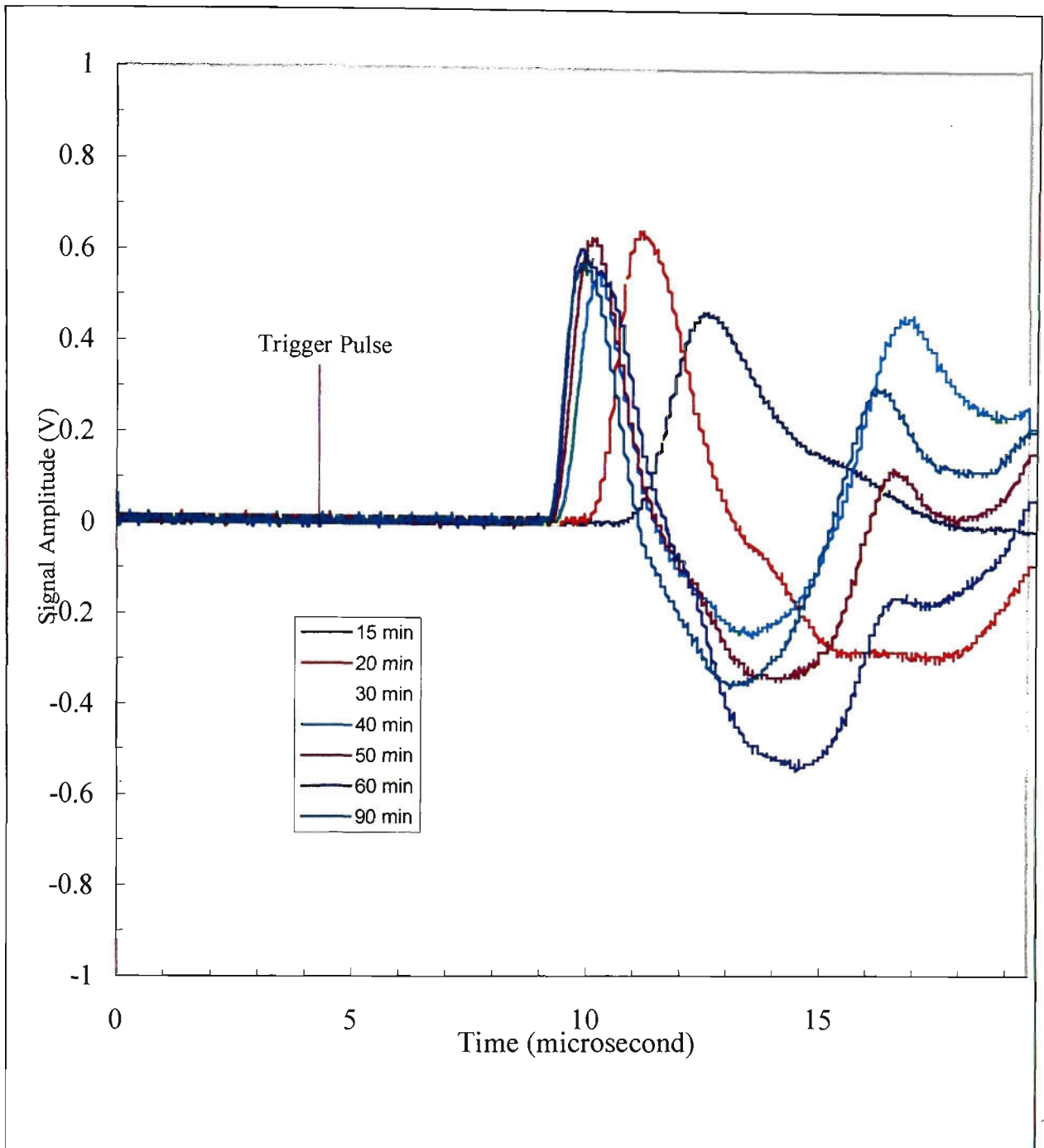


Figure 5.3.2 Interferometer waveforms for the arrival of acoustic waves after the early stages of cure in a rapid cure room temperature epoxy. Sample excited using a brass shim in contact with epoxy and a single laser pulse of energy 1300 mJ.

The variation of propagation time for acoustic pulses through the epoxy decreases as the cure progresses, as shown in Figure 5.3.3. These times were measured from the trigger pulse to the onset of rise of the acoustic pulse in the interferometer waveform. The uncertainty in determining the latter time is the major source of uncertainty in the results.

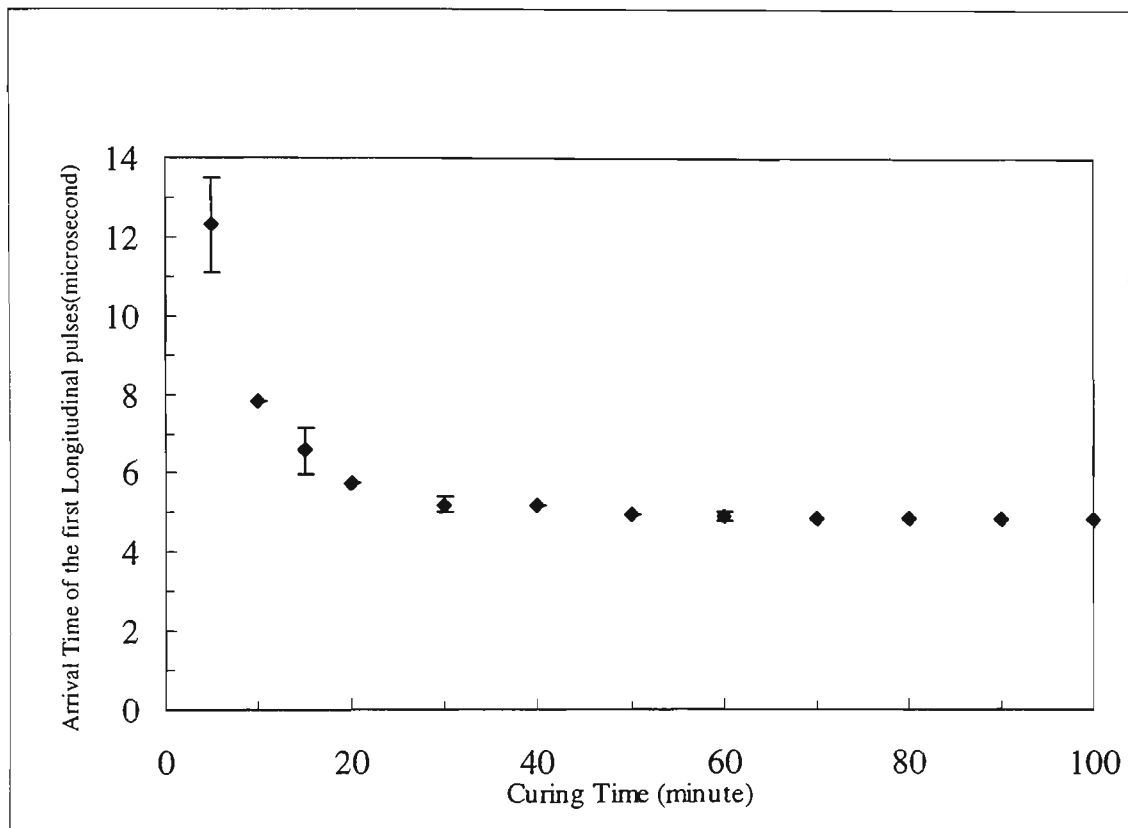


Figure 5.3.3 Variation of arrival time of the first longitudinal pulses with epoxy curing time. Some error bars have been included. Near the end of cure, the error bars are too small to be adequately represented on this figure.

The wave speed can be determined from a measurement of the thickness of the specimen and arrival time of the first longitudinal pulse (if the propagation time through the container walls and any shrinkage during cure are neglected). The wave

speed, calculated in this way and normalised with respect to the final wave speed is shown in Figure 5.3.4. The speed can be seen to increase monotonically with cure time in agreement with the results of Hahn (1984) who used a quite different type of epoxy.

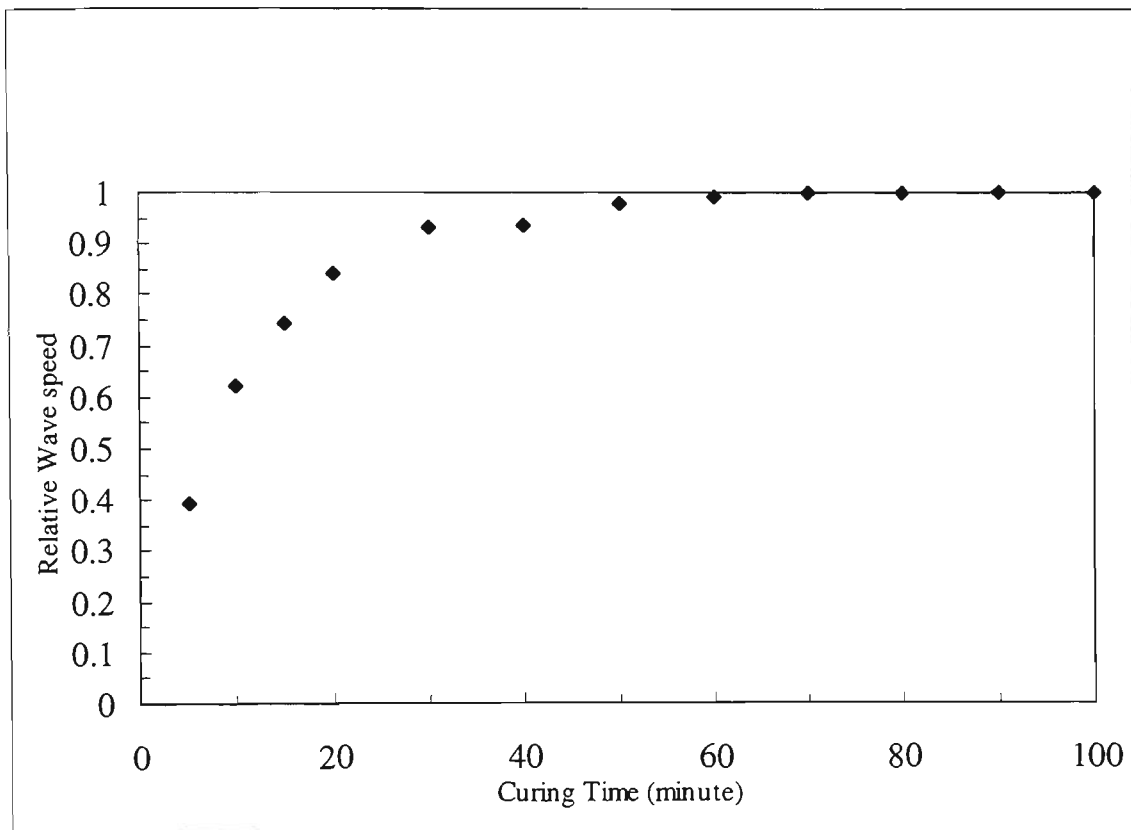


Figure 5.3.4 Relative wave speed as a function of epoxy curing time.

The relative attenuation (RA), which gives an indication of the attenuation coefficient of the acoustic pulses, was also measured during the process of curing. Expressed in dB, RA can be defined by Hahn (1984) as

$$RA = 20 \log \frac{A_L}{A} \quad , \quad (5.3.1)$$

where  $A_L$  is the initial amplitude of the acoustic pulse and  $A$  is the amplitude during curing. The measured variation in RA with curing time is shown in Figure 5.3.5. It can

be seen that the attenuation drops by a little less than an order of magnitude as the cure progresses.

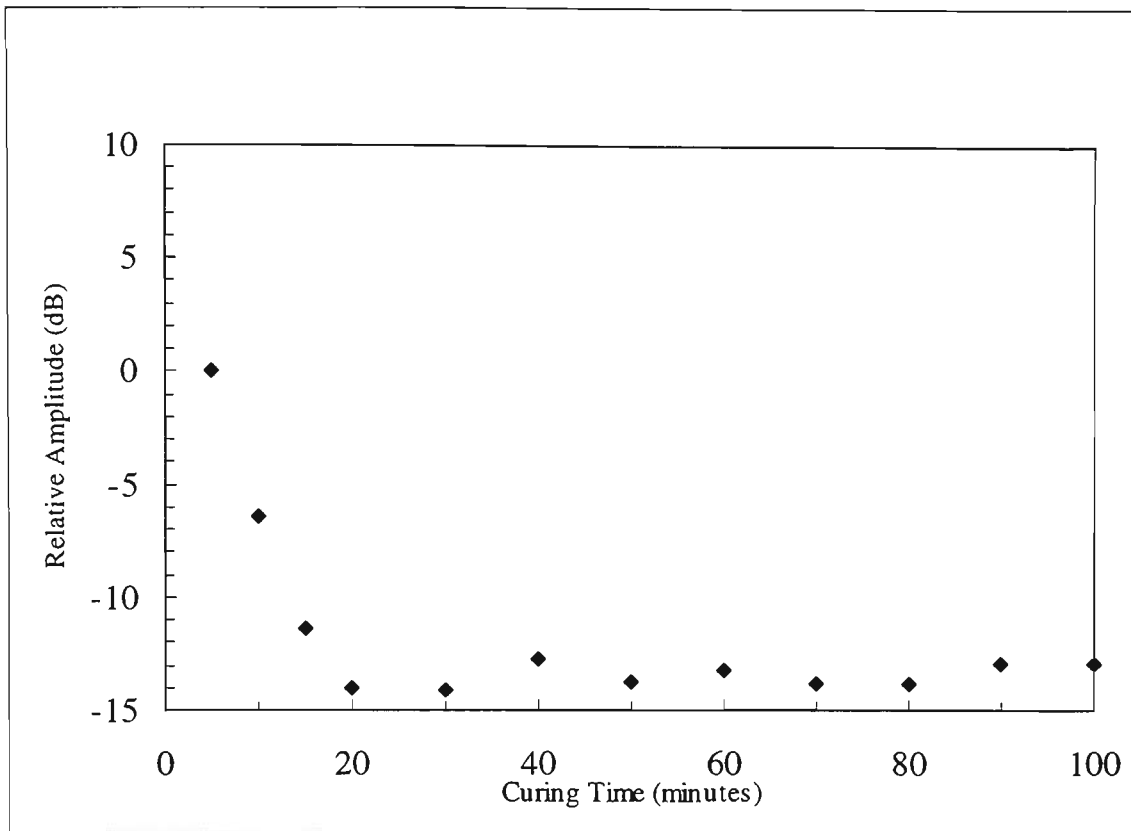


Figure 5.3.5 Relative attenuation as a function of curing time of epoxy.

The trend observed in the cure monitoring data provided by the measurements (Figure 5.3.3-5.3.5) is consistent with the previous work (Ohn *et al.*, 1992; Davis *et al.*, 1991; Hahn, 1984; Lindrose, 1978). The results above clearly indicate that this remote optical technique can be used to monitor the degree of cure by measuring the relative wave speed and attenuation of the acoustic pulses. However the system needed an opaque target for the incoming laser radiation (brass shim) as direct irradiation of the epoxy produced sample damage through heating and ablation.

In order to assess the usefulness of the technique with a far less ideal remote measurement arrangement, the experimental cell with the brass shim as described above was replaced with an small plastic confectionery container of dimensions 59 x 35 x 14.5 mm. A coat of paint was applied on the rear surface of the container to improve the poor signal-to-noise ratio of the interferometer when the clear plastic container alone was used. This paint made the rear surface opaque and provided a reasonable scattering (rather than reflecting) surface. Also, to overcome damage on the plastic container and epoxy due to the high energy of laser pulse (1300 mJ), a small amount of normal kitchen grade aluminium foil was used to line the inside of the front face of the container. The container was slightly laterally moved to ensure a reasonable interferometer reflection before measurements were made. The monitoring of the interferometer signal was done by lightly tapping the plastic box and observing the signal produced at the output of the low frequency channel of the interferometer electronics. The interferometer waveforms for the arrival of the first longitudinal acoustic pulses in the epoxy sample and their variation with time after cure commences is shown in Figures 5.3.6 and 5.3.7. The trend is similar to that observed in the previous experiments except that the amplitude of the signal is lower compared to that of Figures 5.3.1 and 5.3.2 by a factor of about 8. However, the signals are still quite measurable over the whole of the curing cycle.

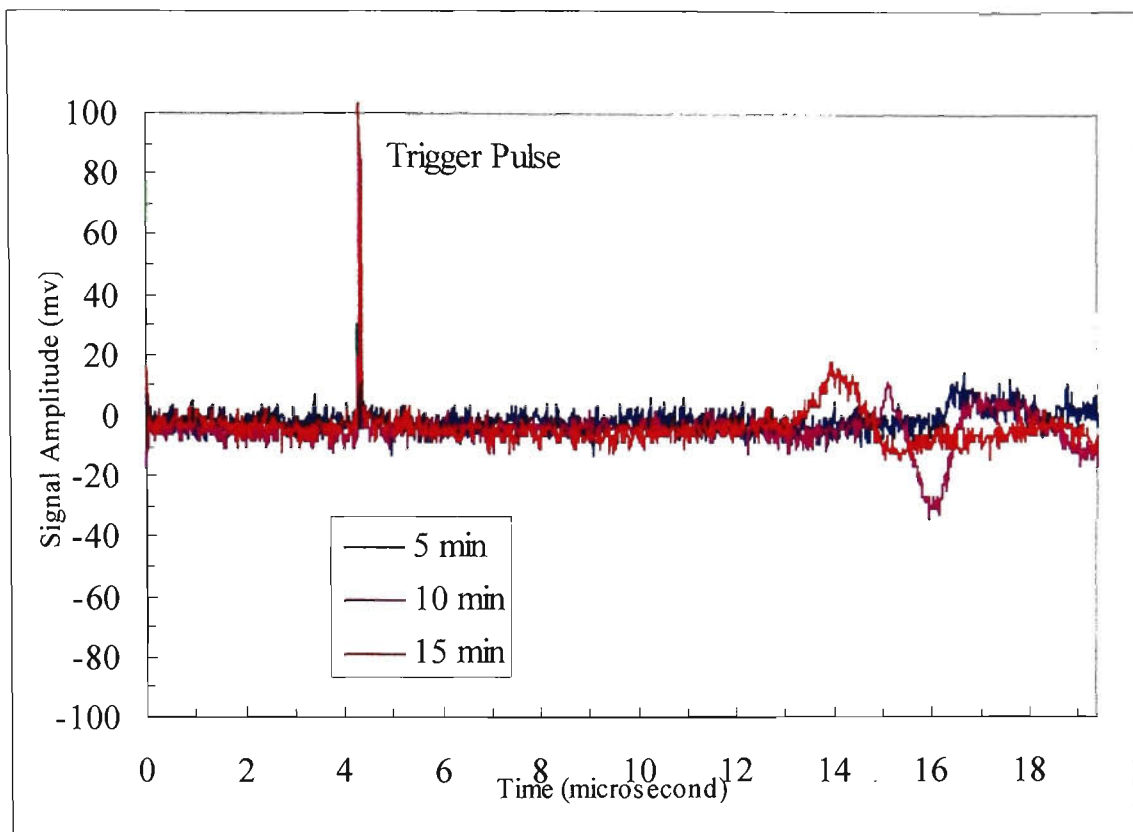


Figure 5.3.6 Interferometer waveforms for the arrival of acoustic waves during the early stages of cure in a rapid cure room temperature epoxy. Sample contained in a small plastic box with aluminium cooking foil on the inside of the front surface and paint on the exterior of the rear surface. Records obtained using a single laser pulse of energy 1300 mJ.

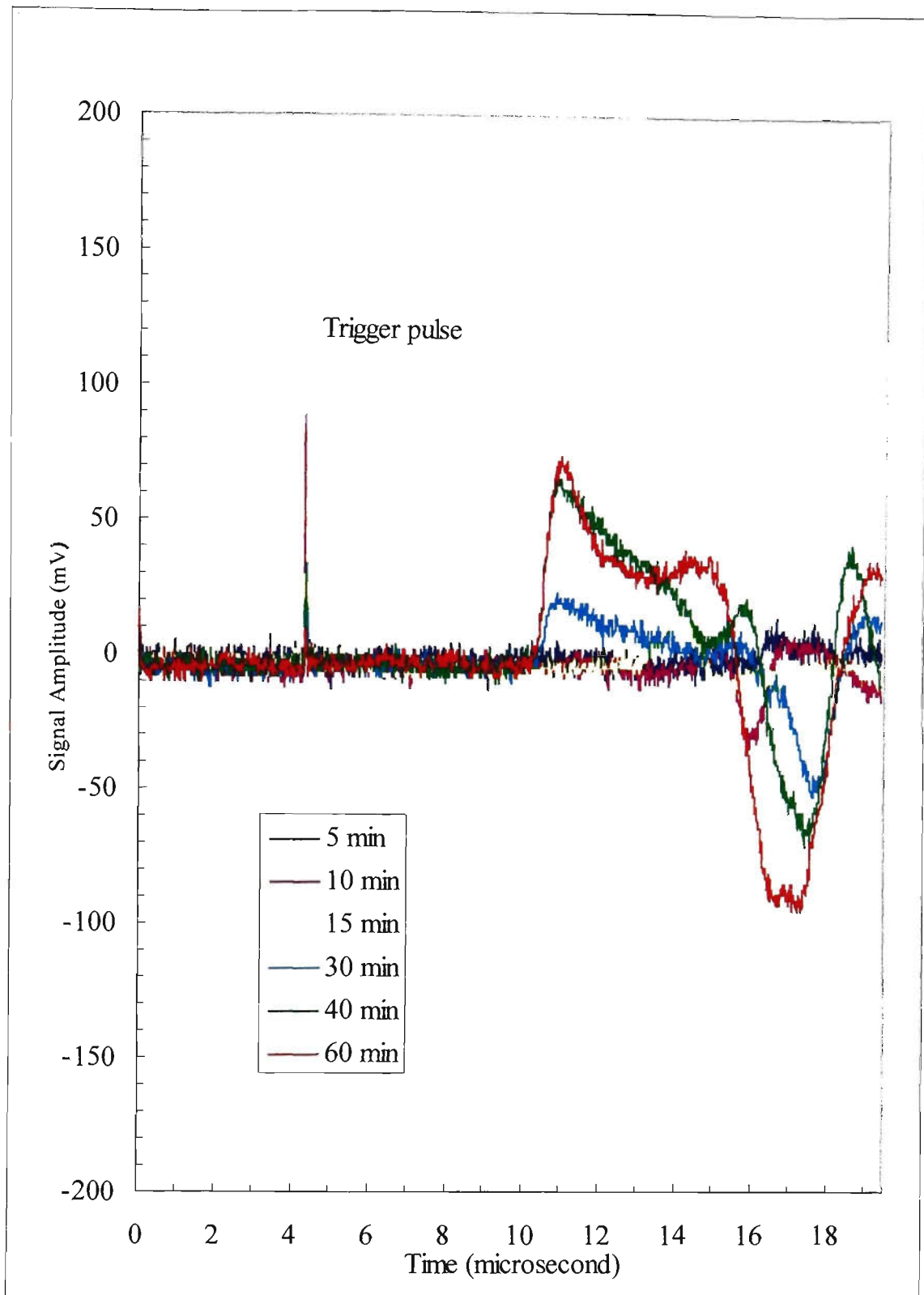


Figure 5.3.7 Interferometer waveforms for the arrival of acoustic waves during the curing period in a rapid cure room temperature epoxy. Sample contained in a small plastic box with aluminium cooking foil on the inside of the front surface and paint on the exterior of the rear surface. Records obtained using a single laser pulse of energy 1300 mJ.

This later experimental arrangement clearly shows that at 1300 mJ, cure monitoring is possible using this technique without the need for inclusion of brass shim as a target for the laser excitation and also for reflecting the interferometer sensing beam. However, at this energy the technique was limited by damage produced in the outer plastic container used to hold the target samples. This damage resulted in a decrease in excitation efficiency and interferometer signal amplitude with repetitive pulses. In order to try to overcome this problem, it was decided to investigate the use of lower laser excitation energies and results for such measurements are included in subsequent sections. Inevitably, the use of lower laser energy requires some focusing to increase the power density to obtain satisfactory interferometer signals (ablation regime necessary). Thus before lower power measurements were attempted, a short investigation was carried out to assess the effect of power density.

### **5.3.2 Acoustic waveforms with different incident power densities in a cured sample**

The simplest way of assessing the effect of variation of power density for a given laser energy was to partially focus the laser onto the target surface and record the interferometer waveforms as the lens position was varied. For these measurements a cured sample with brass shim on both sides was used (first sample arrangement).

For this series of measurements (and subsequent ones) the laser excitation beam was different from that used in earlier experiments. The high power Nd:YAG laser used to pump the MOPO was normally first passed through a harmonic generator which produced outputs at 355 nm, 532 nm and a residual beam at 1064 nm. The 355 nm beam is used to pump the MOPO and the other two beams are normally “dumped” in an optical trap. This combined 1064/532 nm beam provided an excellent source for acoustic wave generation which does not interfere with the operation of the MOPO

(removal of the harmonic generator to obtain a pure 1064 nm beam requires re-alignment of the MOPO). Hence this beam was used in subsequent work. The mixture of wavelengths does alter the relative reflectivity of targets such as brass and aluminium, compared to that which applies for 1064 nm, and hence alters their relative efficiency for acoustic wave generation but does not have any other significant effects. No attempt was made to measure the individual powers of the two components of the combined 1064/532 nm beam.

For the measurements reported in this section it was also convenient to use 100 mJ pulse and a shorter focal length lens to focus the radiation. In this case a 100 mm focal length lens was used (Newport KPX054). Results are presented in Figures 5.3.8 - 5.3.16 for the interferometer record of acoustic waveforms for various positions of the lens in front of the cured target. Clearly, in Figures 5.3.8 - 5.3.10, the acoustic generation is principally in the thermoelastic regime. In subsequent figures, ablation signatures are observed with strong signals occurring for lens positions in excess of 70 mm from the target surface. As in previous cases, when the laser is focused directly on the front surface (focal distance = 100 mm) the amplitude of the longitudinal wave generated is very small (Figure 5.3.16).

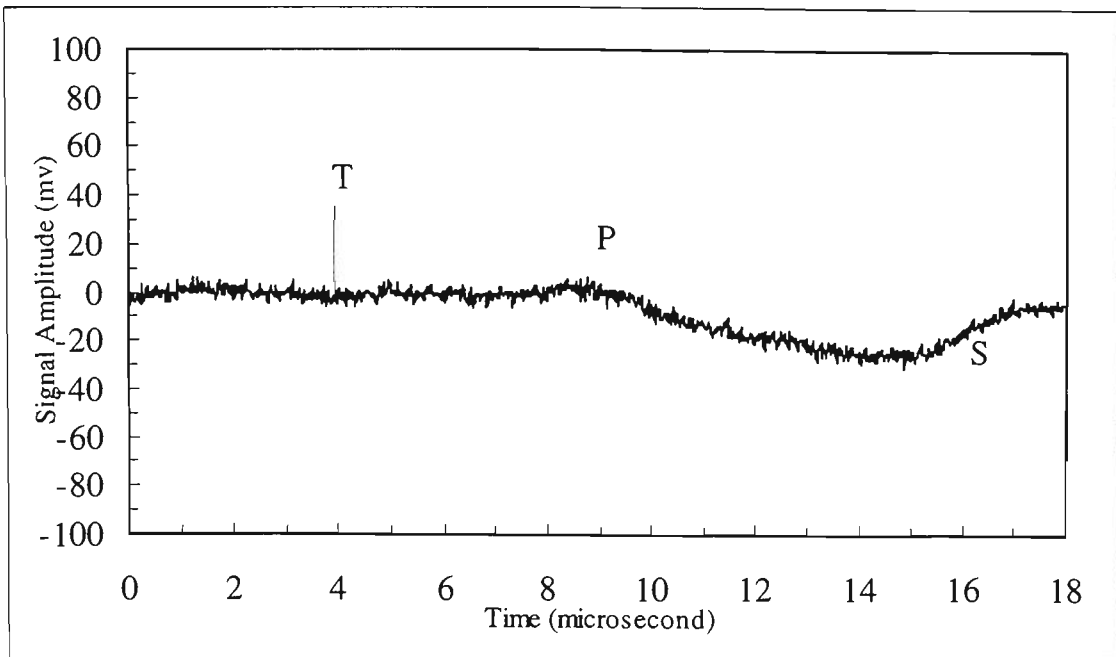


Figure 5.3.8 Acoustic waveforms measured at the epicentre of the cured epoxy/brass sample of thickness 1.3 cm, obtained by placing the lens ( $f = 100$  mm) at a distance of 50 mm from the target.

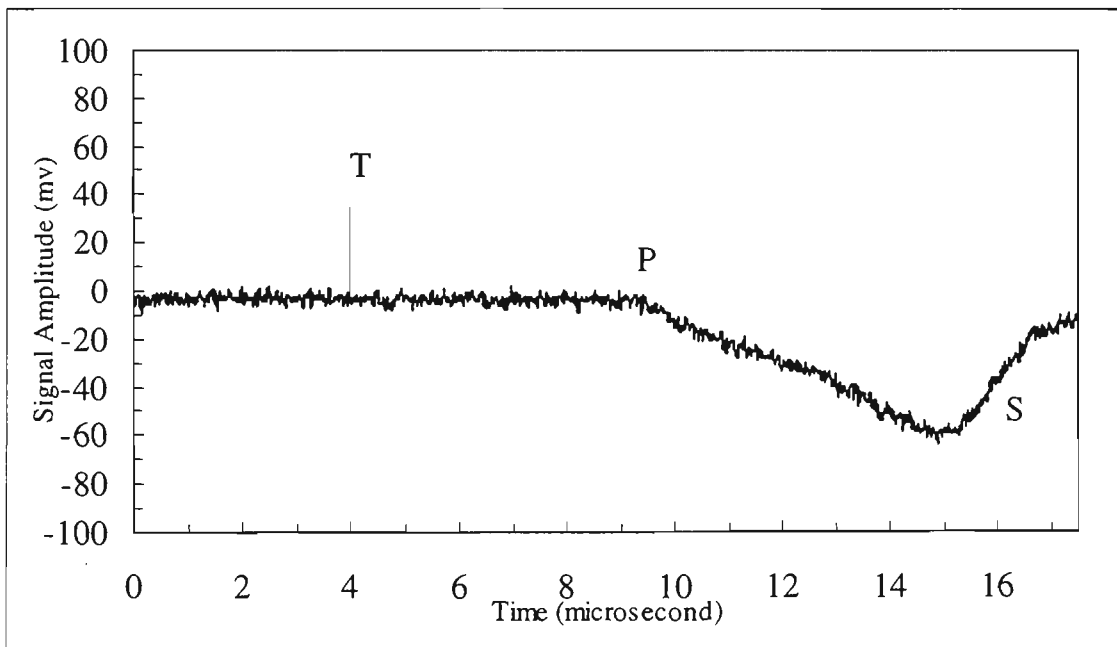


Figure 5.3.9 Acoustic waveforms measured at the epicentre of the cured epoxy/brass sample of thickness 1.3 cm, obtained by placing the lens ( $f = 100$  mm) at a distance of 55 mm from the target.

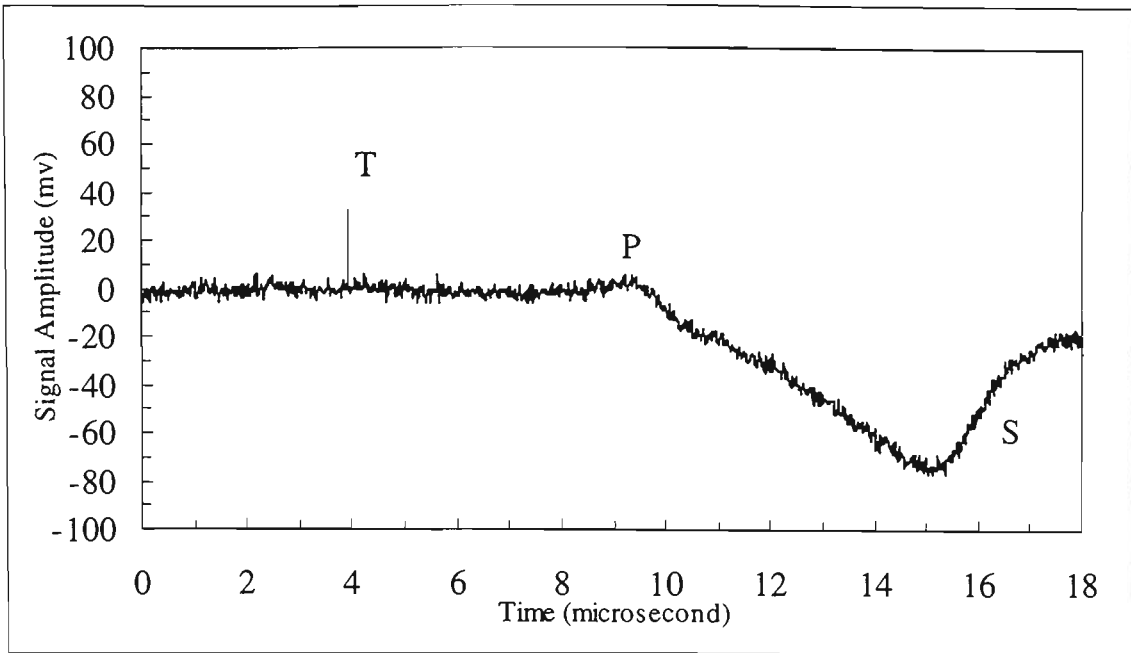


Figure 5.3.10 Acoustic waveforms measured at the epicentre of the cured epoxy/brass sample of thickness 1.3 cm, obtained by placing the lens ( $f = 100$  mm) at a distance of 60 mm from the target.

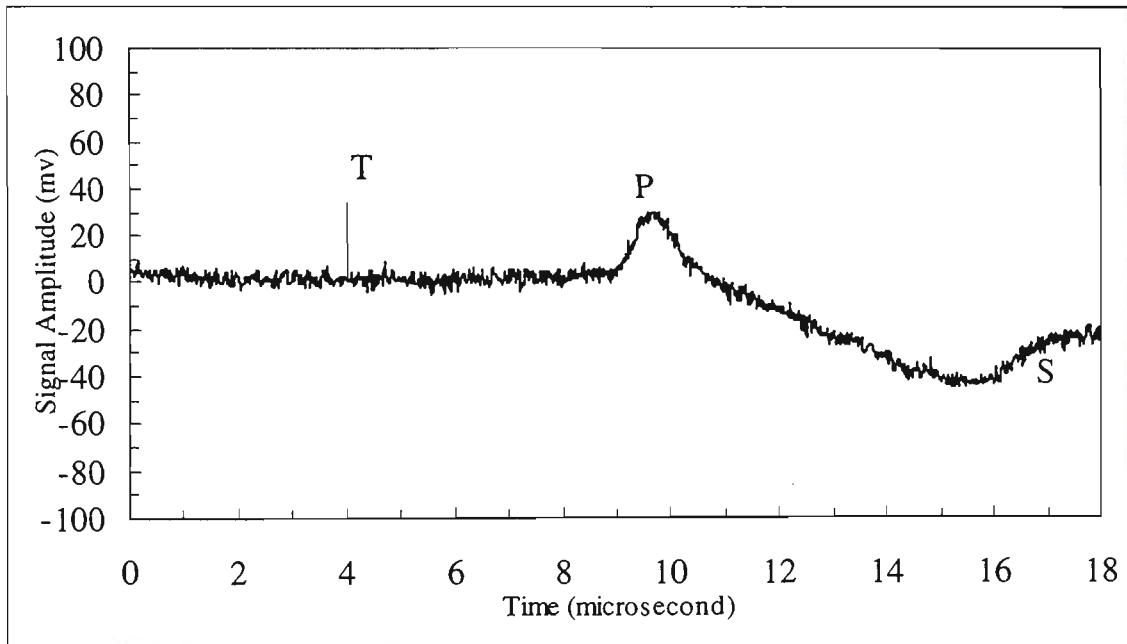


Figure 5.3.11 Acoustic waveforms measured at the epicentre of the cured epoxy/brass sample of thickness 1.3 cm, obtained by placing the lens ( $f = 100$  mm) at a distance of 70 mm from the target.

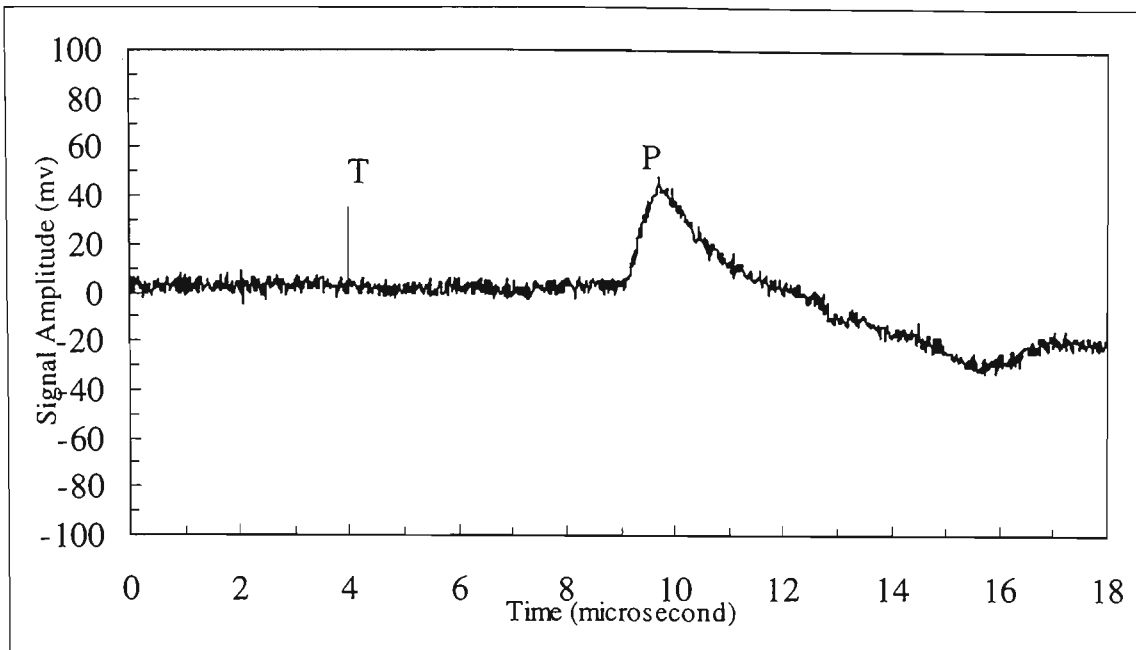


Figure 5.3.12 Acoustic waveforms measured at the epicentre of the cured epoxy/brass sample of thickness 1.3 cm, obtained by placing the lens ( $f = 100$  mm) at a distance of 80 mm from the target.

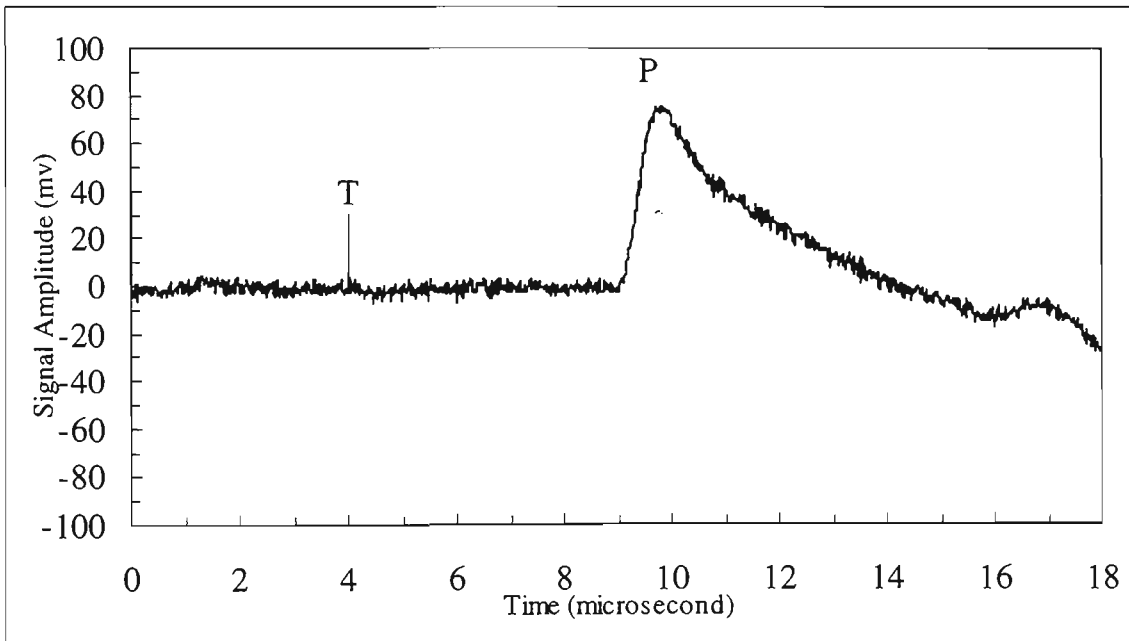


Figure 5.3.13 Acoustic waveforms measured at the epicentre of the cured epoxy/brass sample of thickness 1.3 cm, obtained by placing the lens ( $f = 100$  mm) at a distance of 85 mm from the target.

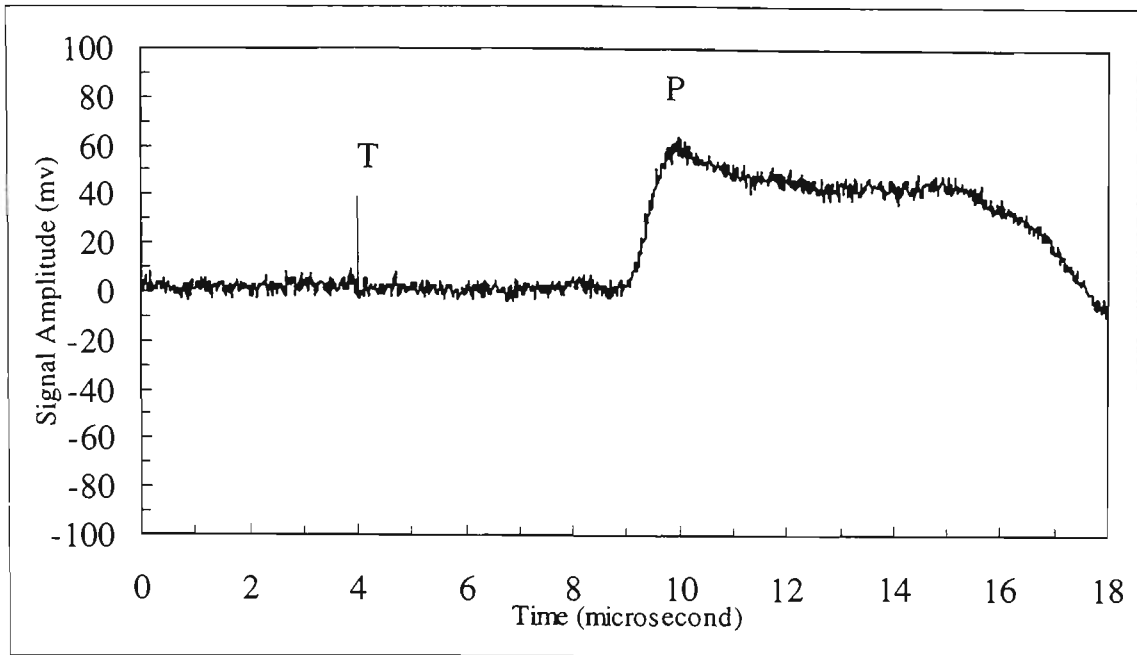


Figure 5.3.14 Acoustic waveforms measured at the epicentre of the cured epoxy/brass sample of thickness 1.3 cm, obtained by placing the lens ( $f = 100$  mm) at a distance of 90 mm from the target.

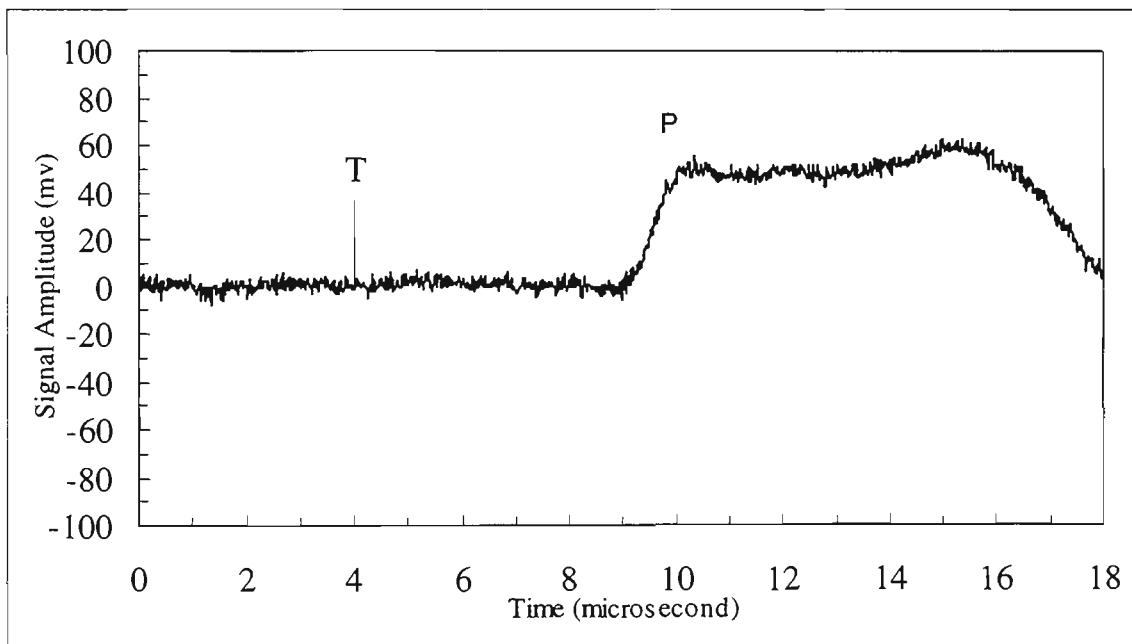


Figure 5.3.15 Acoustic waveforms measured at the epicentre of the cured epoxy/brass sample of thickness 1.3 cm, obtained by placing the lens ( $f = 100$  mm) at a distance of 95 mm from the target.

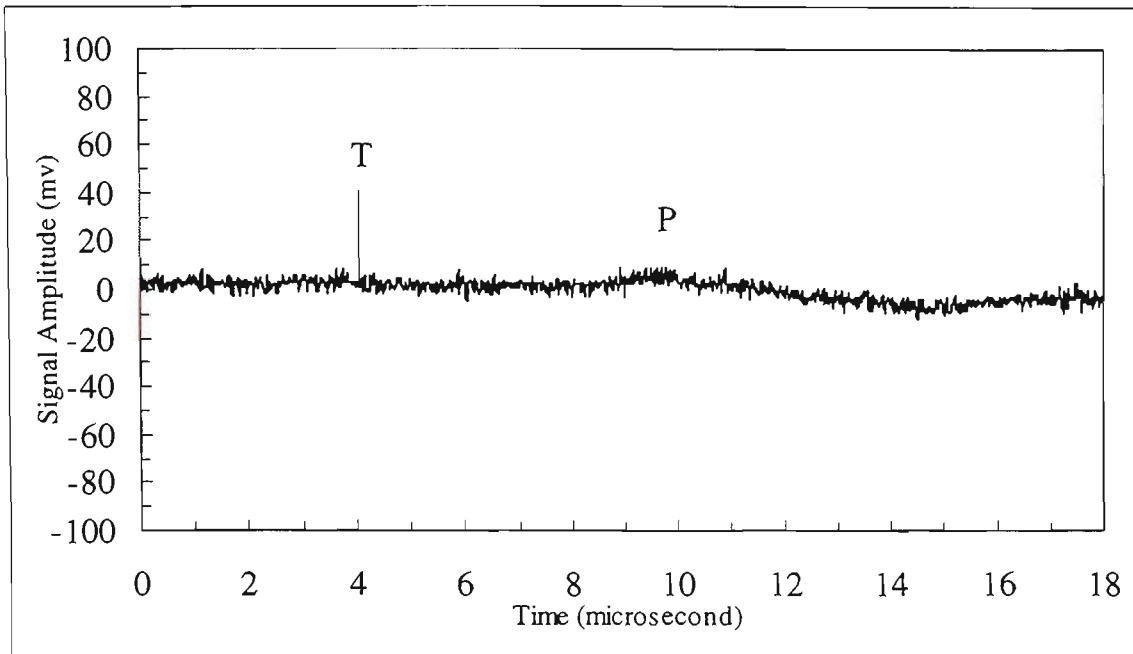


Figure 5.3.16 Acoustic waveforms measured at the epicentre of the cured epoxy/brass sample of thickness 1.3 cm, obtained by placing the lens ( $f = 100$  mm) at a distance of 100 mm from the target.

Figure 5.3.17 summarises the results for the amplitude of the first longitudinal wave as a function of lens position. The maximum signal amplitude is obtained at a focal distance of about 85 mm. The power density at this point is around  $3 \text{ GW/cm}^2$ . This is a little higher than was observed for aluminium targets at 1064 nm (chapter 4).

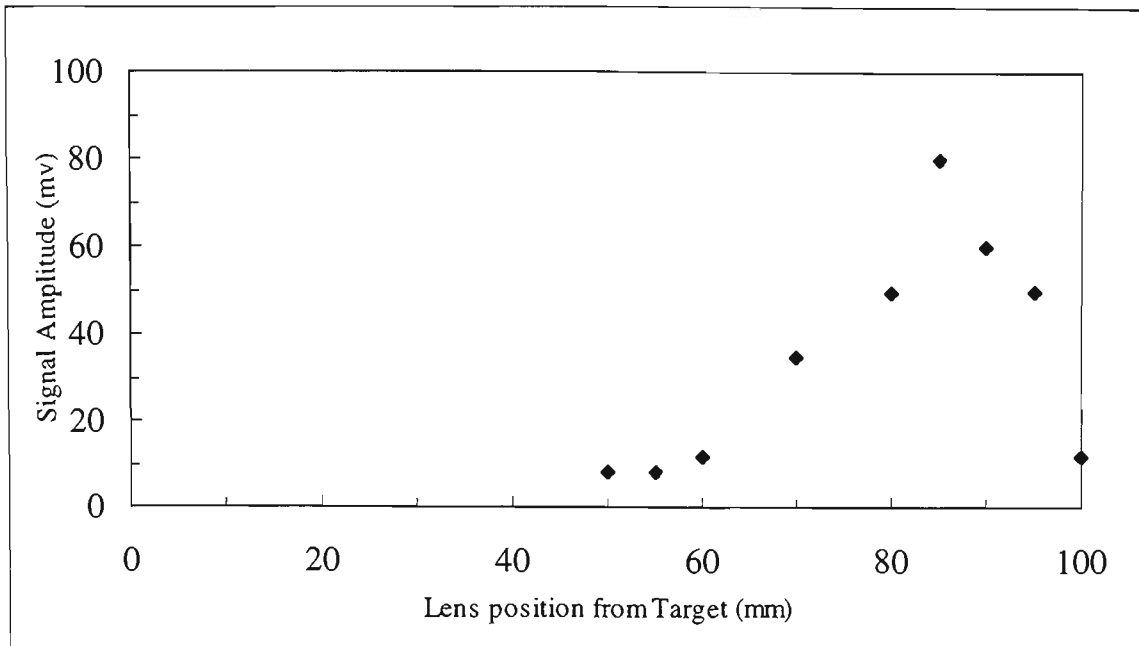


Figure 5.3.17 Variation of the amplitude of the P wave with the position of the plano-convex lens (focal length = 100 mm) in front of the cured epoxy sample at a constant pulse energy of 100 mJ.

### 5.3.3 Irradiation with lower pulse energies (47 mJ - 125 mJ)

This section contains results for measurements made during the whole of the curing process under ablation conditions which did not significantly damage the target and which are thus suitable for monitoring situations in which a large number of laser pulses are incident on a single point of the sample. Results are presented for 100 mJ and 47 mJ pulses incident on targets which have the brass shim in contact with the epoxy (similar to those described in section 5.3.1) and also for 125 mJ pulses with a slightly modified target which used the Scotch brand aluminium foil tape as the target.

Figures 5.3.18 and 5.3.19 give results for the interferometer acoustic signatures during cure for 100 mJ laser pulses focused by the 100 mm lens placed at a distance of 68 mm from the target. It can be seen that the signal to noise ratio is fairly poor in the early stages of cure but improves markedly in the latter stages. The overall change observed

in the propagation time for the arrival of the first longitudinal wave is similar to that shown in Figure 5.3.3 for 1300 mJ pulses. Propagation times in the latter stages of cure can be measured quite accurately under these conditions using 100 mJ pulses.

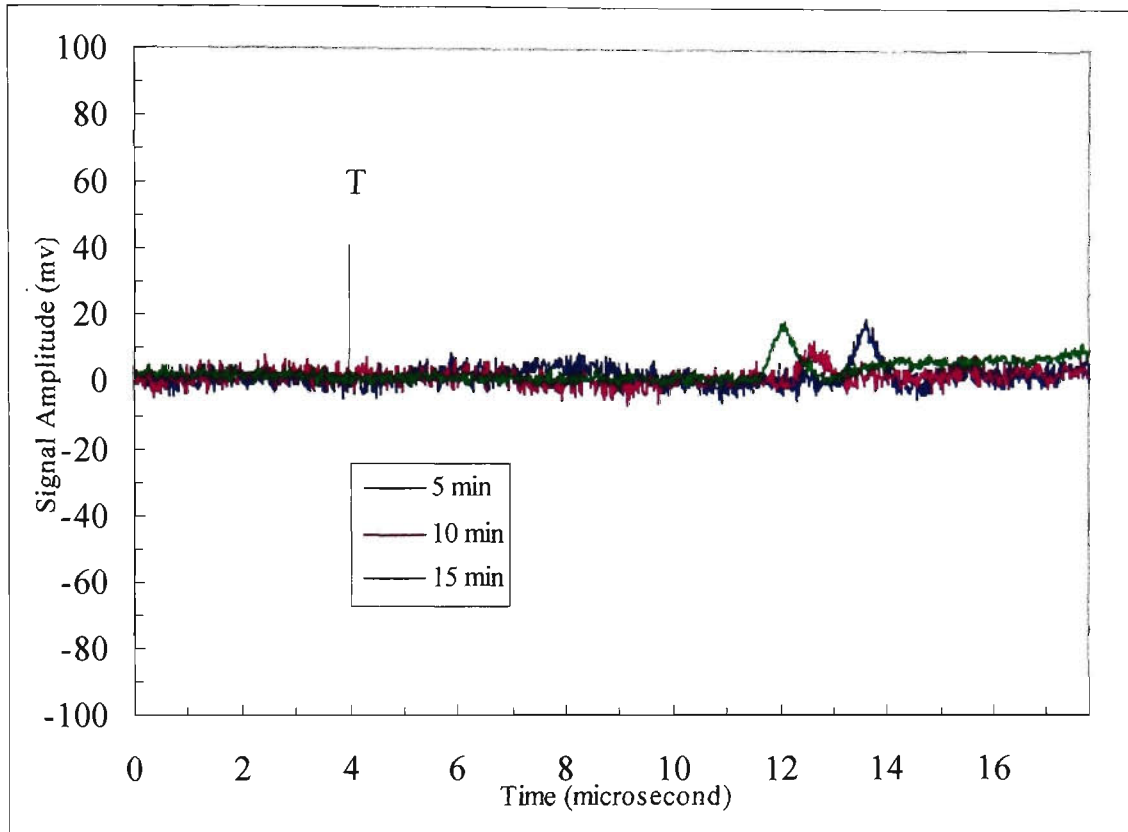


Figure 5.3.18 Interferometer waveforms for the arrival of acoustic waves during the early stages of curing of a rapid cure room temperature epoxy. The sample used a brass shim (thickness 0.05 mm) in contact with the front and rear surfaces of the epoxy. Records obtained by partially focusing (plano-convex lens with a focal length of 100 mm was placed at a distance of 68 mm from the target surface) a single laser pulse of energy 100 mJ.

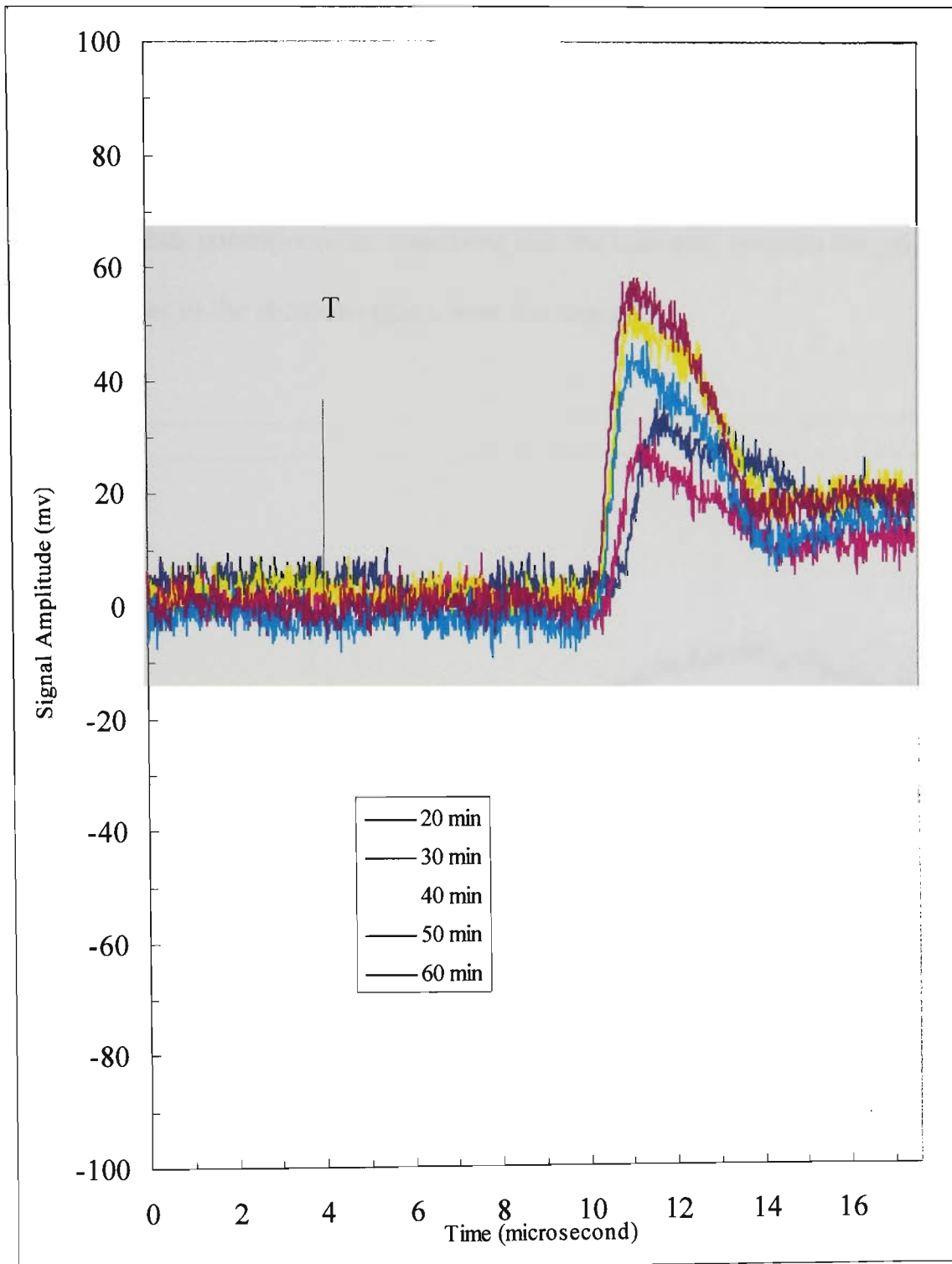


Figure 5.3.19 Interferometer waveforms for the arrival of acoustic waves after the early stages of curing of a rapid cure room temperature epoxy. The sample used a brass shim (thickness 0.05 mm) in contact with the front and rear surfaces of the epoxy. Records obtained by partially focusing (plano-convex lens with a focal length of 100 mm was placed at a distance of 68 mm from the target surface) a single laser pulse of energy 100 mJ.

Figures 5.3.20 and 5.3.21 show similar measurements to the previous ones for the same type of target using brass shim but with a reduced laser energy of 47 mJ. For these measurements the focusing lens is placed at a distance of 80 mm from the target surface and thus corresponds to something like the optimum position for generation of acoustic pulses in the ablation regime with this energy.

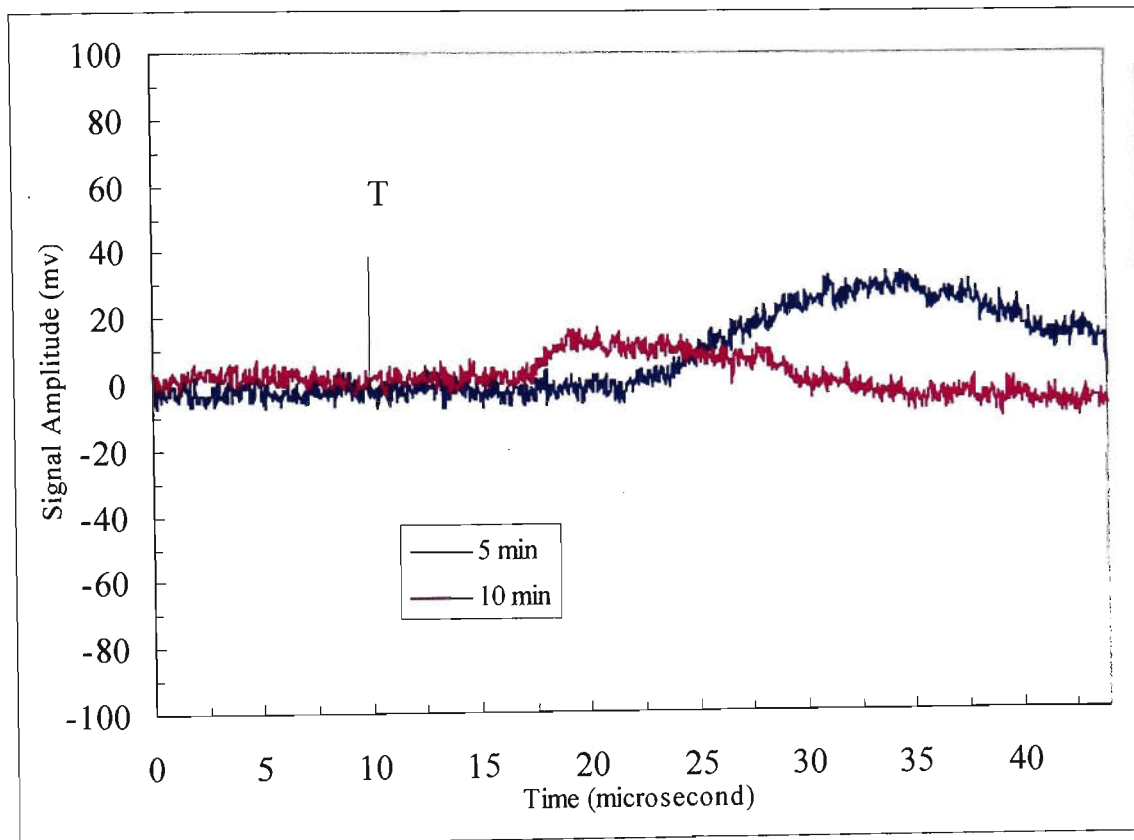


Figure 5.3.20 Interferometer waveforms for the arrival of acoustic waves during the early stages of curing of a rapid cure room temperature epoxy. The sample used a brass shim (thickness 0.05 mm) in contact with the front and rear surfaces of the epoxy. Records obtained by partially focusing (plano-convex lens with a focal length of 100 mm was placed at a distance of 80 mm from the target surface) a single laser pulse of energy 47 mJ.

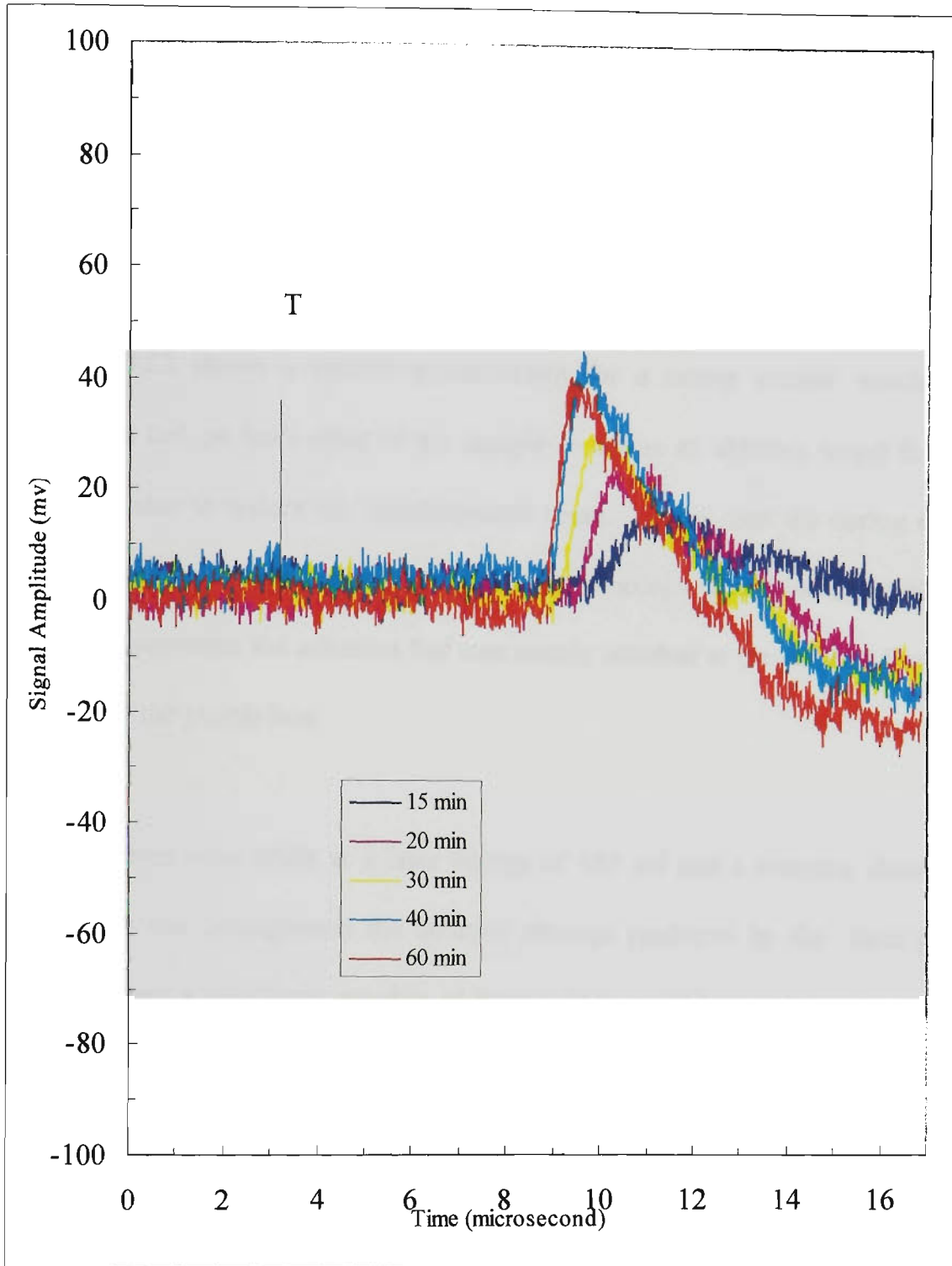


Figure 5.3.21 Interferometer waveforms for the arrival of acoustic waves after the early stages of curing of a rapid cure room temperature epoxy. The sample used a brass shim (thickness 0.05 mm) in contact with the front and rear surfaces of the epoxy. Records obtained by partially focusing (plano-convex lens with a focal length of 100 mm was placed at a distance of 80 mm from the target surface) a single laser pulse of energy 47 mJ.

As in the previous case, the signal to noise ratio was relatively poor in the early stages of cure but again improved markedly after about 15 minutes. Clearly the system performed very well even at these low energies and accurate measurements of propagation times were easily made.

Figure 5.3.22 shows a similar measurement for a curing sample which used the aluminium foil on both sides of the sample to act as an ablating target for the laser pulse and also to reflect the interferometer beam. In this case the curing epoxy was again placed in a plastic confectionery box but no holes were drilled in the plastic. For these measurements the adhesive foil was merely attached to the exterior front and rear surfaces of the plastic box.

Measurements were made at a laser energy of 125 mJ and a focusing distance of 80 mm. With this arrangement the ablation damage produced by the laser pulse was negligible and a very large number of laser pulses could be used on one point of the sample without any obvious effect on the quality of the measurements.

The aluminium target required slightly higher energy pulses and higher incident power densities than a similar brass target for good quality acoustic waveforms. This is due to the higher reflectivity of aluminium, as explained earlier, and this was the reason for the increase of the laser energy to 125 mJ. It was found that reduction of the laser energy to 100 mJ gave much poorer signal to noise ratios in the interferometer waveforms.

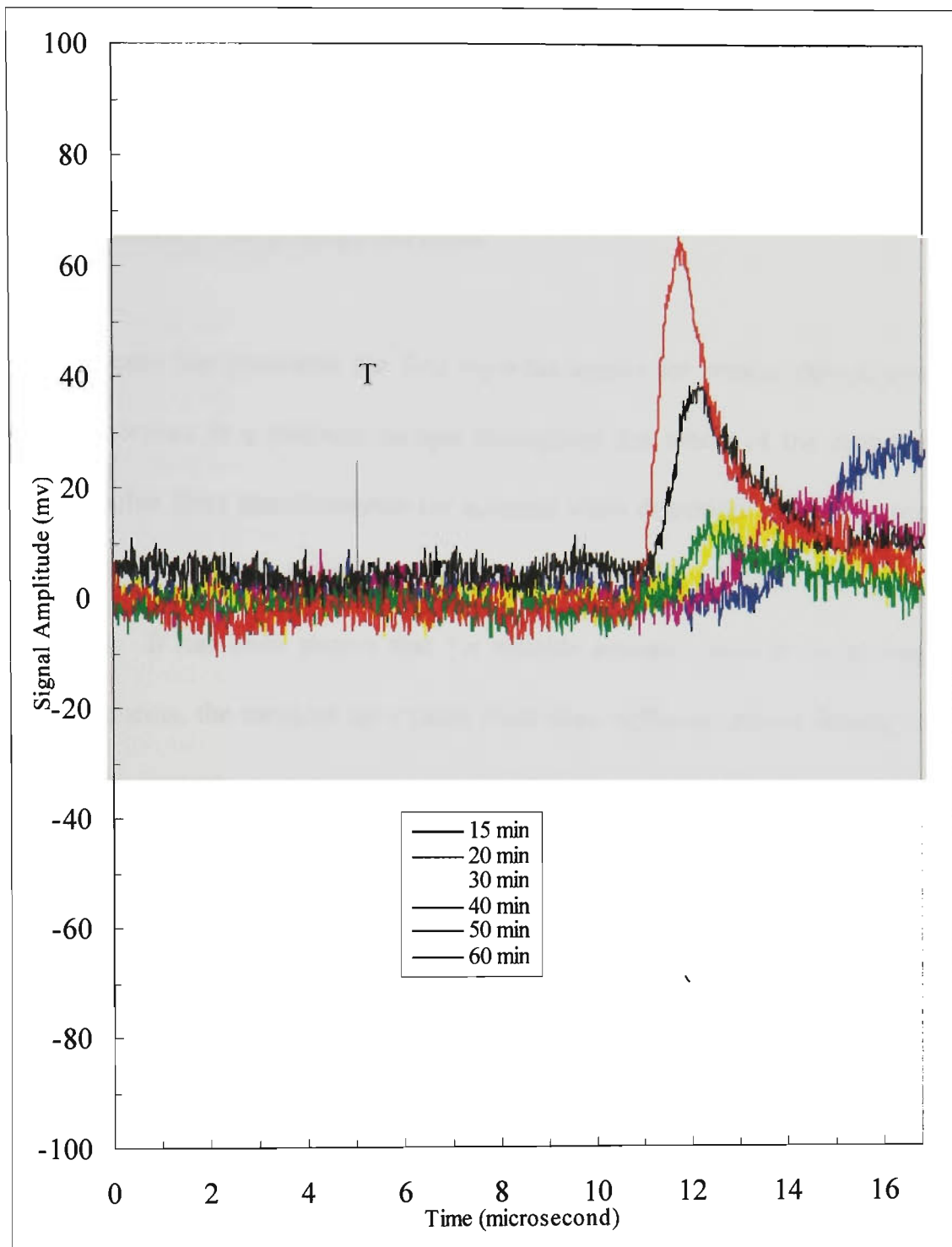


Figure 5.3.22 Interferometer waveforms for the arrival of acoustic waves after the early stages of curing of a rapid cure room temperature epoxy. The sample used aluminium foil tape attached to the front and rear surfaces of the plastic box containing the 1.3 cm thick epoxy. Records obtained by partially focusing (plano-convex lens with a focal length of 100 mm was placed at a distance of 80 mm from the target surface) a single laser pulse of energy 125 mJ.

As was the case with the brass targets, when using aluminium under the conditions outlined above, the signal to noise is not good during the earlier stages of cure. However again the signal to noise ratios increased after 15 minutes allowing excellent measurements of the propagation times.

This chapter has presented the first reported results for remote optical monitoring of acoustic waves in a polymer sample throughout the whole of the cure cycle using a very flexible fibre interferometer for acoustic wave detection. The technique has been shown to work very satisfactorily over a wide range of laser energies and power densities. It has been shown that for reliable acoustic velocity or propagation time measurements, the incident laser pulse must have sufficient power density on the target surface to generate acoustic waves in the ablation regime. Simple target arrangements using thin metallic shim or foil in the form of an adhesive tape were shown to be effective in acting as the interface between the curing sample and the optical beams responsible for generation and detection of the acoustic waves. It has also been demonstrated that although ablation is occurring on the target surface, the power density can be adjusted to give negligible target damage while still maintaining excellent acoustic waveforms which allow accurate measurement of propagation times. The lasers used for exciting the acoustic waves and in the interferometer detection system need not be large (about 50 mJ and 2 mW respectively) and would allow the system to be considered for practical monitoring situations.

## Chapter 6: Conclusion

The objectives of the work described in this thesis, as outlined in chapter 1, was to develop a system capable of remote generation and detection of ultrasonic waves in materials which is suitable for non-destructive evaluation and which is based on fibre optics rather than bulk optics. This system was to be used with metallic and non-metallic targets and an assessment made of its usefulness in both thermoelastic and ablation generation regimes. Finally, the system was to be used to try to measure acoustic waveforms in a suitably packaged epoxy-based material in order to see whether it is capable of monitoring the state of cure (via variation of longitudinal wave velocity) throughout the entire cure process. These objectives have all been achieved.

A Q-switched Nd:YAG laser with an output energy of about 60 mJ was constructed and this was used to generate acoustic waves in both thermoelastic and ablation regimes. Another commercial Nd:YAG laser with an output energy of up to 1300 mJ was also used for some of the measurements as this allowed greater variation of excitation conditions. However, all principal results can be obtained using the smaller laser together with appropriate focusing. The use of an optical fibre for delivery of the Q-switched pulse was not attempted as this has been done by several authors and is regarded as being straightforward (Davis *et al.*, 1991; Dewhurst *et al.*, 1988; Vogel and Bruinsma, 1987).

A sensitive wide-bandwidth optical fibre optic interferometer has been developed and used to demonstrate the remote detection of the bulk acoustic waveforms generated by

a pulsed laser in metallic and non-metallic materials. The fabrication and characterisation of 5 different versions of fibre interferometer which incorporate open air paths and use low power laser sources have been described. The optimised sensitivity obtained with this type of interferometer in a bandwidth of 200 kHz, under laboratory condition, is found to be 0.03 nm using a polished reflecting surface and an open air path of length 57 cm. This is comparable to the performance of the most sensitive fibre optic interferometer reported to date which does not incorporate an open air path (Jackson *et al.*, 1980). The final interferometer configuration, which was used for all measurements of laser generated acoustic waveforms, had a measured NED of 0.4 nm in a bandwidth of 15 MHz when using a natural transducer surface (similar to oxidised aluminium in reflectivity) to reflect the interferometer beam. An important aspect of this work is that the fibre interferometer, including the analogue circuitry used for feedback and signal processing, is inexpensive and is relatively simple to construct and operate. This, and its ease of use with only a single fibre needing to be near the material under test, is important for the practical application of the technique.

In order to assess the performance of the remote opto-ultrasonic technique, a series of experiments were conducted in thermoelastic and ablation regimes by varying the excitation energy and incident power density of the laser pulses. The system is found to be suitable for the detection of laser generated ultrasonic waveforms under thermoelastic and ablation regimes in metallic targets. The acoustic waveforms could be detected in these targets with an unfocused incident laser pulse energy as low as 25 mJ. The characteristics of the acoustic waveforms observed in metallic targets in thermoelastic and ablation regimes are similar to that observed by other researchers using bulk optic devices. Thus the fibre optic interferometer can be used as an

alternative to bulk optic devices. The detected waveforms are highly reproducible and sufficiently marked longitudinal and shear features are easily observed when investigation are carried out in slight ablation regime. Also, as no serious damage to the surface occurred in this condition, probing at the same location and signal averaging are possible. The technique has been applied to determine the longitudinal velocity of different metals.

With epoxy targets, it was found to be necessary to make measurements in the slight ablation regime in all cases except those with fully-cured samples. With optical excitation in the slight ablation regime, using partially-focused laser pulses of energy as low as 47 mJ, it has been demonstrated for the first time that ultrasonic measurements can be made with epoxy targets using only the remote reflection from an aluminium foil or similar material attached to the rear target surface. In the case of solid materials it is only necessary to apply some form of paint to the rear surface. It was further demonstrated that longitudinal wave propagation times can be monitored throughout the entire curing process from liquid to solid state. This has been done using an optical fibre interferometer; clearly it would be able to be done with even better signal to noise ratio with a bulk optic interferometer. It should also be noted that a fibre interferometer of the type used in this thesis can be used to measure target signals through an intervening window with a very small decrease in signal to noise ratio (Philp and Booth, 1994). Also, in chapter 5 it was shown that the material used to hold the curing epoxy does not interfere with measurements of changes in propagation time. Thus this all-optical remote excitation and detection system should be capable of monitoring in situations where pressure and elevated temperature are used. Such situations

commonly apply in manufacturing processes involving thermoset-resin based composite materials.

There are a number of areas in which the work described can be extended and which need to be investigated further:

- (a) The remote opto-ultrasonic sensor needs to be used to monitor the cure in a situation in which a number of cure monitoring techniques are used simultaneously. In this way, the comparative performance can be evaluated and further information may be obtained about the properties of the material during curing.
- (b) The remote opto-ultrasonic sensor should be applied to a real cure monitoring situation involving pressure and elevated temperature in an autoclave.
- (c) A number of non-destructive measurement systems rely on surface acoustic waves rather than waves propagated through the bulk material. It should be straightforward to demonstrate that the sensor is capable of making measurements of surface waves.

## **Publications resulting from the research described in this thesis**

1. Mitra B., Booth D. J. and Shelamoff A., "Laser generation and non-contact interferometric detection of ultrasonics in composite materials during curing", Proc. 12th Australian Institute of Physics Congress, Paper # 0705: Optics, Hobart, 1996.
2. Mitra B., Shelamoff A and Booth D. J., "An optical fibre interferometer for remote detection of laser generated ultrasonics". Submitted for publication in Measurement Science and Technology.
3. Mitra B and Booth D. J., "Remote cure monitoring of epoxy materials using optical techniques". Ultrasonics (in press).

## References

- Achenbach J. D., "Wave propagation in Elastic solids", North Holland, Amsterdam, 1973.
- Afromowitz M. A., "Fibre optic polymer cure sensor", J. Light. Tech, vol. 6, pp. 1591 - 1594, 1988.
- Aindow A., Dewhurst R. J., Hutchins D. A. and Palmer S. B., "Characteristics of laser generated ultrasonics in metals", Proc. SPIE, vol. 236, pp. 478 - 485, 1980.
- Alig I., Lellinger D., Nancke K., Rizos A. and Fytas G., "Dynamic light scattering and ultrasonic investigations during the cure reaction of an epoxy resin", J. Appl. Polym. Sci, vol. 44, pp. 829 - 835, 1992.
- Andersson P. O., Persson A., Thylen L. and Edwall G., "Fibre optic interferometer using integrated optics", Electron. Lett., vol. 21, pp. 245 - 246, 1985.
- Arrechi F. T., and Schultz Dubois E. O., Laser HandBook, vol. 1, North Holland Publishing, Amsterdam, 1972.
- Aussel J. D., Le Brun A. and Baboux J. C., "Generating acoustic waves by laser: theoretical and experimental study of the emission source", Ultrasonics, vol. 26, pp. 245 - 255, 1988.
- Aussel J. D. and Monchalain J. P., "Precision laser -ultrasonic velocity measurement and elastic constant determination", Ultrasonics, vol. 27, pp. 165 - 177, 1989.
- Bonderenko A. N., Drobot Y. B. and Kruglov S. V., "Optical excitation and detection of nanosecond acoustic pulses in non destructive testing", Sov. J. NDT, vol. 12, pp. 655 - 668, 1976.
- Bourkoff E. and Palmer C. H., "Low energy optical generation and detection of acoustic pulses in metals and non-metals", Appl. Phys. Lett., vol. 46, pp. 143 - 145, 1985.
- Bowers J. E., "Fiber-optical sensor for surface acoustic waves", Appl. Phys. Lett., vol. 41, pp. 231 - 233, 1982.
- Bowles S. J. and Scala C. M., "Laser based ultrasonics for improved non destructive evaluation", A O S News, vol. 7, pp. 7 - 11, 1993.
- Brown D. A., Cameron C. B., Keolian R. M., Gardner D. L., and Garrett S. L., "A symmetric 3x3 coupler based demodulator for fibre optic interferometric sensors" Proc. SPIE Fiber Optic and Laser Sensors IX, vol. 1584, pp. 328 - 335, 1991.

Bruisma A. J. A., "Non contact detection of pulse acoustic displacement for the evaluation of sub surface defect", SPIE vol. **789**, Fibre optic Sensors II, pp. 76 - 81, 1987.

Buchhave P., "Laser Doppler vibration measurements using variable frequency shift", DISA information Bulletin, vol. **18**, pp. 15 - 20, 1975.

Budenkov G. A. and Kaunov A. D., "The excitation of elastic waves in solids by means of a laser beam due to the thermoelastic effect", Ninth world conference on non-destructive testing, paper # 4A-14, Melbourne, 1979.

Bucholtz F., Koo K. P., Davis M. A., Marrone M. J. and Dandridge A., "Elimination of intensity-induced sideband noise in interferometric fibre sensors", Optical fiber sensors technical digest series, vol. **2**, pp. 52 - 55, 1988.

Bush I. J. and Sherman D. R., "High performance interferometric demodulation techniques", Proc. SPIE, vol. **1975**, pp. 412 - 420, 1992.

Carolan T. A., Hand D. P., Barton J. S., Jones J. D. C., Wilkonson P. and Rueben R. L., "Assessment of tool wear in milling using acoustic emission detected by a fiber-optic interferometer", J. Manuf. Sci. and Engg. Transaction of the ASME, vol. **118**, pp. 428-433, 1996.

Carslaw H. S. and Jaeger J. C., Conduction of heat in solids, Oxford University Press : London, 1971.

Chitnis V. T., Kumar S. and Sen D., "Optical fibre sensor for vibration amplitude measurement", J. Light. Tech, vol. **7**, pp. 687 - 691, 1989.

Claus R. O., Dhawan R., Gunther M. F. and Murphy K. A., "Quantitative measurement of in-plane acoustic field components using surface-mounted fiber sensors", Proc. SPIE, vol. **1798**, Fiber optic smart structures and skins V, pp. 144 - 152, 1992.

Cole J. H., Danver B. A. and Bucaro J. A., "Synthetic-Heterodyne interferometric demodulation", IEEE J. Quantum Electron., vol. **18**, pp. 694 - 697, 1982.

Dandliker R. and Willemin J. F., "Measuring microvibration by heterodyne speckle interferometry", Opt. Lett., vol. **6**, pp. 165 - 167, 1981.

Dandridge A., Tveten A. B., Miles R. O. and Giallorenzi T. G., "Laser noise in fiber optic interferometer systems", Appl. Phys. Lett., vol. **37**, pp. 526 - 528, 1980.

Dandridge A. and Tveten A. B., "Noise reduction in fiber optic interferometer systems", Appl. Opt., vol. **20**, pp. 2337 - 2339, 1981.

Dandridge A. and Tveten A. B., "Phase compensation in interferometric fibre optic sensor", Opt. Lett., vol. **7**, pp. 279 - 281, 1982.

- Dandridge A., Tveten A. B. and Giallorenzi T. G., "Homodyne demodulation scheme for fiber optic sensors using phase generated carrier", *IEEE J. Quantum Electron.*, vol. **18**, pp. 1647 - 1653, 1982.
- Dandridge A., Tveten A. B., Miles R. O. and Giallorenzi T. G., "Fiber optic interferometric sensor development at NRL", *Proc. OFS. 83*, pp. 48 - 52, 1983.
- Dandridge A. and Kersey A. D., "Overview of Mach-zehnder sensor technology and applications", *Proc. SPIE*, vol. **985**, pp. 34 - 52, 1987.
- Dandridge A., "Fibre optic sensors based on the Mach-Zehnder and Michelson interferometer", *Fiber optic sensors : An introduction for engineers and scientist*, Ed. Eric Udd, Willey : NewYork, pp. 271 - 323, 1991.
- Davis A., Ohn M. M., Liu K. and Measures R. M., "A study of an opto-ultrasonic technique for cure monitoring", *Proc. SPIE*, vol. **1588**, pp. 264 - 274, 1991.
- Deferrari H. A., Darby R. A. and Andrews F. A., "Vibrational displacement and mode shape measurement by a laser interferometer", *J. Acoust. Soc. Am.*, vol. **42**, pp. 982 - 985, 1967.
- Dewhurst R. J, Hutchins D. A., Palmer S. B. and Scruby C. B., "Quantitative measurement of laser generated acoustic waveforms", *J. Appl. Phys.*, vol. **53**, pp. 4064 - 4071, 1982.
- Dewhurst R. J., Edwards C. E., Mckie A. D. W. and Palmer S. B., "Comparative study of wide band ultrasonic transducer", *Ultrasonics* , vol. **25**, pp. 315 - 321, 1987.
- Dewhurst R. J, Nurse A. G. and Palmer S. B. "High power optical fibre delivery system for the laser generation of ultrasonics", *Ultrasonics*, vol. **26**, pp. 307 - 310, 1988.
- Dewhurst R. J. and Al'Rubai W. S. A. R., "Generation of short acoustic pulses from an energetic picosecond laser", *Ultrasonics*, vol. **27**, pp. 262 - 269, 1989.
- Digonnet M. J. F. and Kim B. Y., "Fibre optic components", *Fibre optic Sensors*, Ed. John Dakin and Brian Culshaw, Artech House : London, vol. **2**, , pp. 209 - 148, 1989.
- Dobbie L. G. and Builder G., "Calculation of Inductance", *Radio Designer's Hand Book*, Ed. F. Langford-Smith, ILLIFFE Books Ltd.: London, pp. 429-441, 1934.
- Doyle P. A., "On epicentral waveforms for laser-generated ultrasound", *J. Phys. D: Appl. Phys.*, vol. **19**, pp. 1613 - 1624, 1986.
- Doyle P. A. and Scala, "Toward laser-ultrasonic characterization of an orthotropic-isotropic interface", *J. Acoust. Soc. Am.*, vol. **93**, pp. 1385 - 1392, 1993.
- Drain L. E., Speake J. H. and Moss B. C., "Displacement and vibration measurement by laser interferometry", *Proc. SPIE*, vol. **136**, pp. 52 - 62, 1977.

- Dray M. A., Elandjian L. and Stevenson W. A., "Review of progress in Quantum Nondestructive Evaluation", vol. **9**, pp. 2039 - 2048, 1990.
- Edwards C., Taylor G. S. and Palmer S. B., "Ultrasonics generation with a TEA CO<sub>2</sub> laser", J. Phys. D: Appl. Phys., vol. **22**, pp. 1266 - 1270, 1989.
- George G. A., Cole-Clarke P., John N. ST. and Friend G., "Real-time monitoring of the cure reaction of a TGDDM/DDS epoxy resin using fiber optic FT-IR", J. Appl. Polymer Science, vol. **42**, pp. 643 - 657, 1991.
- Giallorenzi T. G., Bucaro J. A., Dandridge A., Sigel G. H., Cole J. H., Rashleigh S. C., and Priest R. G., "Optical fiber sensor technology", IEEE J. Quantum Electron., vol. **18**, pp. 626 - 665, 1982.
- Gower J., Optical Communication Systems, Prentice-Hall International : London, pp. 403 - 429, 1987.
- Graff K. F., Wave motion in elastic solid, Clarendon : Oxford, 1975
- Green R. E. G., "Ultrasonic non destructive materials characterization", Material Analysis by ultrasonics, metals, ceramics and composites, Ed. A. Vary, Naves data corporation : New Jersey, pp. 1 - 15, 1987.
- Hahn H. T., "Application of ultrasonic technique to cure characterisation of epoxies", Non destructive method for material property determination, Ed. C. O. Rudd and R. E. Green (Jr), Plenum Press, pp. 103 - 108, 1984.
- Handerek V., "Single mode optical fiber sensors", Optical fiber sensor technology, Ed. K. T. Grattan and B. T. Meggit, Chapman and Hall : London, pp. 197 - 222, 1995
- Hrovatin R. and Mozina J., "Comparison of microphone and interferometric detection", Proc. Conf. Ultrasonic International, pp. 165 - 169, 1993.
- Hull D., An introduction to composite materials, Cambridge University Press : Cambridge, 1981
- Hutchins D. A., Dewhurst R. J, Palmer S. B., and Scruby C. B., "Laser generation as a standard acoustic source in metals", Appl. Phys. Lett., vol. **39**, pp. 677 - 679, 1981a.
- Hutchins D. A., Dewhurst R. J. and Palmer S. B., "Laser generated ultrasound at modified metal surfaces", Ultrasonics , vol. **19**, pp. 103 - 108, 1981b.
- Hutchins D. A., Dewhurst R. J. and Palmer S. B., "Directivity pattern of laser generated ultrasonics ", J. Acoust. Soc. Am., vol. **70**, pp. 1362 - 1369, 1981c.
- Hutchins D. A., and Nadeau F., "Non contact ultrasonic wave forms in metals using laser generation and interferometric detection", Proc. Ultrasonic Symposium, pp 1175 - 1176, 1983.

Hutchins D. A. and Wilkins D. E., "Elastic waveforms using laser generation and electromagnetic acoustic transducer detection", J. Appl. Phys., vol. **58**, pp. 2469 - 2477, 1985.

Hutchins D. A. and Tam A.C., "Pulse photoacoustic material characterisation", IEEE Trans. Ultrason., Ferroelectrics, Freq. Contr., vol. **UFFC-38**, pp. 429 - 449, 1986.

Jackson D. A., Dandridge A. and Sheem S. K., "Measurement of small phase shift using a single mode optical fibre interferometer", Opt. Lett., vol. **5**, pp. 139 - 141, 1980a.

Jackson D. A., Priest R., Dandridge A. and Tveten A. B., "Elimination of drift in a single mode optical fibre interferometer using a piezoelectrically stretched coiled fibre", Appl. Opt., vol. **19**, pp. 2926 - 2929, 1980b.

Jackson D. A., "A prototype digital phase tracker for the fibre interferometer", J. Phys. E., vol. **E14**, pp. 1274 - 1278, 1981.

Jackson D. A., Kersey A. D., Corke M. and Jones J. D. C., "Pseudoheterodyne detection scheme for optical interferometers", Electron. Lett., vol. **18**, pp. 1081 - 1083, 1982.

Jackson D. A., Kersey A. D., and Lewin A. C., "Fibre Gyroscope with passive quadrature detection", Electron. Lett., vol. **20**, pp. 399 - 401, 1984.

Jackson D. A., "Monomode optical fibre interferometers for precision measurements", Current advances in sensors Ed. B. E. Jones, Adam Hilger : Bristol, pp. 75 - 95, 1987.

Jackson D. A. and Jones D. C., Interferometers Optical Fiber Sensors: Systems and Applications, vol 2, Ed. B. Culshaw and J. Dakin, Artech House : London, pp. 329 - 380, 1989.

Jackson P., "Carbon-fibre reinforced epoxy resin; non-invasive viscosity measurement by NMR imaging", J. Matl. Science, vol. **27**, pp.1302 - 1306, 1992.

Jones J. D. C., "Signal processing in monomode fibre optic sensor system", Fundamentals of fibre optics telecommunication and sensor systems, Ed. B. K. Pal, Wiley : New York, pp. 657 - 705, 1992.

Kersey A. D., Jackson D. A. and Corke M., "Passive compensation scheme suitable for use in the single mode fibre interferometer", Electron., Lett. vol. **18**, pp. 392 - 393, 1982.

Kersey A., Jackson D. A. and Corke M., "Demodulation scheme fibre interferometric sensors employing laser frequency switching", Electron. Lett., vol. **19**, pp. 102 - 103, 1983.

Kersey A., Lewin A. C. and Jackson D. A., "Pseudo heterodyne detection scheme for the fibre gyroscope", Electron. Lett., vol **20**, pp 368 - 370, 1984.

- Kingsley S. A., "Optical fibre phase modulator", *Electron. Lett.*, vol. **11**, pp 453 - 454, 1975.
- Kline R. A., Green R. E. and Palmer C. H., "A comparison of optically and piezoelectrically sensed acoustic emission signals", *J. Acoust. Soc. Am.*, vol. **64** (6), pp. 1633 - 1639, 1978.
- Knopoff L., "Surface motions of a thick plate", *J. Appl. Phys.*, vol. **29**, pp. 661 - 670, 1958.
- Koch A. and Ulrich R., "Fibre-optic displacement measurement of rough surface", Technische Universitat Hamburg-Harburg, 1990
- Koehler W., *Solid state laser engineering*, Springer Verlag : Berlin, 1992.
- Koo K. P., Tveten A. B., and Dandridge A., "Passive stabilisation scheme for fibre interferometer using (3x3) fibre directional couplers", *Appl. Phys. Lett.*, vol. **41**, pp. 616 - 618, 1982.
- Koo K. P., Dandridge A. and Tveten A. B., "Performance characteristics of a passively stabilised fiber interferometer using a (3x3) fiber directional coupler", *Proc. First international conference on optical fibre sensors*, London, pp. 200 - 204, 1983.
- Koo K. P., Bucholtz F. and Dandridge A., "Sideband noise of a large phase carrier in interferometric sensors", *Electron. Lett.*, vol. **23**, pp. 1062 - 1063, 1987.
- Krautkramer J., "Unconventional methods of generating, coupling and receiving ultrasound in non-destructive testing", *Ninth world conference on non-destructive testing*, Melbourne, 1979.
- Krautkramer J. and Krautkramer H., *Ultrasonic Testing of Materials*, Springer-Verlag : Berlin, pp. 141 - 159, 1990.
- Krehl P., Schwirzke F. and Cooper A. W., "Correlation of stress-wave profiles and the dynamics of the plasma produced by laser irradiation of plane solid targets", *J. Appl. Phys.*, vol. **46**, pp. 4400 - 4406, 1975.
- Le Brun A. and Pons F., "Noncontact ultrasonic testing: Application to metrology and non destructive testing", *Proc. 4th European Conference on NDT*, Ed. J. M. Farley and R. W. Nichlos, vol. **4**, pp. 1593 - 1602, 1987.
- Lewin A. C., Kersey A. D. and Jackson D. A., "Non contact surface vibration analysis using a monomode fibre optic interferometer incorporating an open air path", *J. Phys. E.*, vol. **18**, pp. 604 - 607, 1985.
- Lin J., Chang Y. S. and Hung M., "High precision fiber-optic Mach-Zehnder interferometer for displacement measurement", *Phys. Science and Engg.*, vol. **18**, pp. 508-513, 1994.

- Lindrose A. M., "Ultrasonic wave and moduli changes in a curing epoxy resin", *Experimental Mechanics*, vol. **18**, pp. 227 - 232, 1978.
- Liu K., Ferguson S. M. and Measures R. M., "Fibre optic interferometric sensor for the detection of acoustic emission within composite materials", *Opt. Lett.*, vol. **15**, pp 1255 - 1256, 1990.
- Magi E. C., "Passive homodyne demodulation technique for remote interferometric sensor using 2x2 couplers", *Proc. ACOFT-18*, pp. 133 - 136, 1993.
- Markiewicz J. P. and Emmet J. L., "Design of flash lamp driving circuits", *IEEE J. Quantum Electron.*, vol. **2**, PP. 707 - 711, 1966.
- Martini G., "Analysis of a single mode optical fibre piezoceramic phase modulator", *Optical and Quantum Electronics*, vol. **19**, pp. 179 - 190, 1987.
- May C. A., "Resins for aerospace", *Applied polymer science*, Ed. W. R. Tess and G. W. Poehlin., ACS symposium series, Washington DC, pp. 559 - 580, 1985.
- McMaster C., *Non destructive testing Handbook*, vol. **2**. The Roland press company : NewYork, 1959
- Measures R. M., "Fibre optics in composite materials ... Materials with nerves of glass", *Proc. SPIE*, vol. **1267**, Fibre optic sensors, pp. 241 - 255, 1990.
- Measures R. M., "Advances towards fibre optic based smart structures", *Opt. Engineering*, vol. **31**, pp. 34 - 47, 1992.
- Melles Griot Application notes, "Quantifying photodiode performances", pp. C.1 (2-10), 1993
- Monchalain J. P., "Heterodyne interferometric laser probe to measure continuous ultrasonic displacement", *Rev. Sci. Instrum.*, vol. **56**, pp. 543 - 546, 1985a.
- Monchalain J. P., "Optical detection of ultrasound at a distance using a confocal Fabry Perot interferometer", *Appl. Phys. Lett.*, vol. **47**, pp. 14 - 16, 1985b.
- Monchalain J. P., "Optical detection of ultrasound", *IEEE Trans. Ultrason., Ferroelectrics, Freq. Contr.*, **UFFC-33**, pp. 485 - 499, 1986.
- Monchalain J. P., Heon R. and Muzak N., "Evaluation of ultrasonic inspection procedures by field mapping with an optical probe", *Canadian Metallurgical Quarterly*, vol. **25**, pp. 247 - 252, 1986.
- Monchalain J. P., Heon R., Bouchard P. and Podileau C., "Broadband optical detection of ultrasound by optical side band stripping with a confocal Fabry Perot", *Appl. Phys. Lett.*, vol. **55**, pp. 1612 - 1614, 1989.

- Moreau A., Ketterson J. B. and Huang J., "Three methods for measuring the ultrasonic velocity in thin films", *Material science and engineering*, vol. **A 121**, pp. 149 - 154, 1990.
- Mortimore D. B., "Theory and fabrication of 4x4 single-mode fused optical fiber couplers", *Appl. Opt.*, vol. **29**, pp. 371 - 374, 1990.
- Moss B. C., "The Harwell laser interferometer", Report of UK Atomic energy Authority, AERE R- 10417, 1982.
- Moss B. C., Private communication, 1994.
- Motchenbacher C. D. and Connelly J. A., *Low noise electronics system design*, Willey : NewYork, pp. 38 - 75, 1993.
- Mozima J. and Hrovatin R., "Detection of excimer laser induced sub-picometre ultrasonic displacement amplitude", *Ultrasonics*, vol. **34**, pp. 131 - 133, 1996.
- Murphy K. A., Miller III W. V., Tran T. A., Vengsarkar M. A. and Claus R.O., "Miniaturized fiber-optic Michelson-type interferometric sensors", *Appl. Opt.*, vol. **30**, pp. 5063 - 5067, 1991.
- Niemeier T. and Ulrich R., "Quadrature outputs from fiber interferometer with 4x4 coupler", *Opt. Lett.*, vol. **11**, pp. 677 - 679, 1986.
- Nokes M. A., Hill B. C. and Barelli A. E., "Fiber optic heterodyne interferometer for vibration measurements in biological systems", *Rev. Sci. Instrum*, vol. **49**, pp. 722 - 728, 1978.
- Ohn M. M., Davis A., Liu K. and Measures R. M., "Embedded fibre optic detection of ultrasound and its applications to cure monitoring", *Proc. SPIE Fiber Optic Smart Structures and Skins V*, vol. **1798**, pp. 134 - 143, 1992.
- Palais J. C., *Fibre optic communications*, Prentice Hall: NewJersey, 1992.
- Palmer C. H., "Circumventing laser relaxation oscillations in interferometer", *Appl. Opt.*, vol. **23**, pp. 3510 - 3512, 1984.
- Philp W. R. and Booth D. J., "Remote excitation and sensing of mechanical resonance in structures using laser diodes and an optical fibre interferometer", *Meas. Sc. Techno.*, vol. **5**, pp. 731 - 735, 1994.
- Ready J. F., "Effects due to absorption of laser radiation", *J. Appl. Phys.*, vol. **36**, pp. 462 - 468, 1965
- Ready J. F., *Effects of high power laser radiation*, Academic Press : NewYork, pp. 67 - 211, 1971.

- Ready J. F., "Laser processing - The first twenty year", Laser institute of America: Professional advancement course, pp. 193 - 204, 1982.
- Risk W. P., Youngquist R. C., Kino G. S. and Shaw H. J., "Acousto-optic frequency shifting in birefringent fiber", Opt. Lett., vol. **9**, pp. 309 - 311, 1984.
- Risk W. P., Kino G. S. and Shaw H. J., "Fiber-optic frequency shifter using a surface acoustic wave incident at an oblique angle", Opt. Lett., vol. **11**, pp. 115 - 117, 1986.
- Rose L. R. F., "Point-source representation for laser generated ultrasound", J. Acoust. Soc. Am., vol. **75** (3), pp. 723 - 732, 1984.
- Royer D., Dievlesaint E. and Martin Y., "Improved version of polarised beam heterodyne interferometer", Proc. Ultrasonic symposium, pp. 432 - 435, 1985.
- Scala C. M. and Doyle P. A., "Characterization of composite overlays by laser ultrasonics", Proc. Australian Institute of Non-destructive Testing National conference, Melbourne, 1991
- Scala C. M. and Doyle P. A., "Time and frequency domain characteristics of laser generated ultrasonics", J. Acoust. Soc. Am., vol. **85**(4) , pp. 1569 - 1576, 1989.
- Scruby C. B., Dewhurst R. J, Hutchins D. A., and Palmer S. B., "Quantitative studies of thermally generated elastic waves in laser-irradiated metals", J. Appl. Phys., vol. **51** (12), pp. 6210 - 6216, 1980.
- Scruby C. B., Smith R. L. and Moss B. C., "Microstructural monitoring by laser-ultrasonic attenuation and forward scattering", NDT International, vol. **19**, pp. 307 - 313, 1986.
- Scruby C. B., "Review on some applications of laser ultrasound", Ultrasonics, vol. **27**, pp. 195 - 209, 1989.
- Scruby C. B. and Drain L. E., Laser Ultrasonics: Techniques and Applications, Adam Hilger : Bristol, 1990.
- Scruby C. B. and Moss B. C., "Non-contact ultrasonic measurements on steel at elevated temperature", NDT&E International, vol. **26** (4), pp. 177 - 188, 1993.
- Shan Q., Chen C. M. and Dewhurst R. J., "Detection of laser generated ultrasound with a conjugate interferometer scheme", Ultrasonics, vol. **34**, pp. 173 - 175, 1996.
- Sharp E. J., "Solid optically pumped Laser", Electronics Engineers' Handbook, Ed. D. G. Fink and D. Christiansen, McGraw Hill: New York, pp. 11.15 - 11.35, 1982.
- Sheem S. K., Giallorenzi T. G. and Koo K., "Optical technique to solve the signal fading in fiber interferometers", Appl. Opt., vol. **21**, pp. 689 - 693, 1982.

- Silk M. G., Ultrasonic transducers for Nondestructive Testing, Adams Hilger : Bristol, pp. 120 - 135, 1984
- Sinclair J.E., "Epicentre solutions for point multipole sources in an elastic half-space", J.Phys. D:Appl. Phys., Vol. **12**, pp. 1309-1314, 1979.
- Smith R.G. and Personick S.D., "Receiver design for optical fibre communication systems", Semiconductor devices for optical fibre communications, Ed. H. Kressel, Springer-Verlag: Berlin, pp. 89 - 160, 1980.
- Sponcer R., Private communication, 1992.
- Sontag H. and Tam A. C., "Optical detection of nanosecond acoustic pulses", IEEE Trans. Ultrason., Ferroelectrics, Freq. Contr., vol. **UFFC-33**, pp. 500 - 506, 1986.
- Tam A C, "Pulsed-laser generation of ultra acoustic pulses: Application for thin film ultrasonic measurement", Appl. Phys. Lett., vol. **45**, pp. 510 - 512, 1984.
- Tam A. C. and Leung W. P., "Measurement of small elastic anisotropy in solids using laser induced ultrasonics pulses", Appl. Phys. Lett., vol. **45**, pp. 1040 - 1042, 1984.
- Tam A C, "Application of photoacoustic sensing technique", Rev. of Modern Physics, vol. **58**, pp. 381 - 431, 1986.
- Tapanes E. E., Hill A. J. and Rossiter P. L., "Development of intrinsic fibre optic evanescent-wave sensor for in-situ cure monitoring of polymeric materials", Proc. 17<sup>th</sup> Australian conference on optical fibre technology, pp. 206 - 209, 1992
- Taylor G. S., Hutchins D. A., Edwards C. and Palmer S. B., "TEA-CO<sub>2</sub> laser generation of ultrasound in nonmetals", Ultrasonics, vol. **28**, pp. 343 - 349, 1990.
- Ungarish M., Joseph R., Vittoser J. and Kenig S., "Cure cycle optimisation by dielectric measurement", Composite, vol. **21 (6)**, pp. 481 - 486, 1990.
- Vogel J. A. and Bruinsma A. J. A., "Contactless ultrasonic inspection with fibre optics", Proc. 4th European conf. on NDT, vol. **4**, pp. 2267 - 2278, 1987.
- Vogel J. A., Bruinsma A. J. A. and Berkhout A. J., "Beamsteering of laser generated ultrasound", Proc. Conf. Ultrasonics International, pp. 141 - 152, 1987.
- Von Gutfeld R. J. and Melcher R. L., "20 MHz acoustic waves from pulsed thermoelastic expansion of constrained surfaces", Appl. Phys. Lett., vol. **30**, pp. 257 - 259, 1977a.
- Von Gutfeld R. J. and Melcher R. L., "MHz acoustic waves from pulsed thermoelastic expansion and their applications to flaw detection", Mater. Eval, vol. **35**, pp. 97 - 99, 1977b.

- Von Gutfeld R. J. and Budd H. F., "Laser generated MHz elastic waves from metallic liquid interfaces", *Appl. Phys. Lett.*, vol. **34**, pp. 617 - 619, 1979.
- Von Gutfeld R. J., "Thermoelastic generation of elastic waves for non-destructive testing and medical diagnostics", *Ultrasonics*, vol. **18**, pp. 175 - 181, 1980.
- Wagner J. W., Deaton J. B. and Spicer J. B., "Generation of ultrasound by repetitively Q-switching a pulsed Nd:YAG laser", *Appl. Opt.*, vol. **27**, pp. 4696 - 4700, 1988.
- Wagner J. W., Deaton J. B., Spicer J. B. and McKie A. D. W., "Laser generation of narrowband and directed ultrasound for non contact ultrasonics testing", *Proc. ultrasonics symposium*, pp. 661 - 668, 1990.
- Warfield R. W., "Characterisation of polymer by electrical resistance" *Testing of Polymer*, Ed. John V. Schmitz, Interscience Publisher, Vol. **1**, pp. 271 - 295, 1965.
- Waszak L., "Power supply design for pulse lasers", *Microwave*, vol. **8**, pp. 130 - 138, 1969.
- White R. M., "Generation of elastic waves by transient surface heating", *J. Appl. Phys.*, vol. **34**, pp. 3559 - 3567, 1963.
- White S. R. and Mather P.T., "Ultrasonic and Thermal cure monitor of an epoxy resin", *Proc. 36<sup>th</sup> International SAMPE symposium*, pp. 284 - 296, 1991.
- Winfrey W. P. and Parker F. R., "Measurement of degree of epoxy cure with ultrasonic velocity", *Proc. ultrasonic symposium*, pp. 447 - 449, 1984.
- Xiaopin Z., Liping S. and Peida Y., "New structure of optical homodyne receiver utilising a 4x4 fibre directional coupler", *Electron. Lett.*, vol. **24**, pp. 1212 - 1213, 1988.
- Yang K. H., Zhang S.Y., Lu Z.N. and Chen L., "Thickness measurement of thin film using an improved laser probe", *Proc. Ultrasonic Symposium*, pp. 1175 - 1178, 1987.
- Zimmermann B., DiFrancia C., Murphy K., Vengsarkar A. and Claus R., "Optical fibre methods for autoclave and epoxy cure monitoring", *Rev. Progress in QNDE*, vol. **9**, pp. 2047 - 2053, 1990.

## Symbols used in this Thesis

$\delta$	skin depth
$\lambda$	wavelength in vacuum
$\sigma$	conductivity
$c$	velocity of light
$\mu$	permeability of the metal
$\mu_0$	permeability of the free space
$R$	reflectivity of the metal
$\delta T$	rise in temperature
$\delta E$	absorption of energy
$\rho$	density
$V$	volume
$S$	specific thermal capacity
$H(t)$	Heaviside step function
$\delta V$	change in volume
$\alpha$	coefficient of linear expansion
$x$	amplitude of the displacement
$c_1$	compression velocity
$r$	distance
$\delta t$	pulse length
$b_i$	dislocation loop Berger vectors
$A_i$	area

$U_3$	normal surface displacement
$G_{3i,j}$	Green's Function
$D_{ij}$	strength of a force dipole
$C_{ijkl}$	elastic constants
$\delta_{ij}$	Kronecker delta
$\xi$ and $\psi$	Lame constant
$G_{3m,n}^H$	Green's function for a Heaviside function source
$x_{ab}$	displacement under ablation effect
$F$	ablative force
$F_3$	normal point excitation force
$G_{33}$	Green's function
$\sigma$	standard deviation
$t$	time
$f$	frequency
$\phi$	optical phase delay
$n$	refractive index
$\kappa$	optical wave number
$L$	length of the fibre
$E_S$	optical field in signal arm of the interferometer
$E_R$	optical field in the reference arm
$E_O$	optical source field
$\omega_O$	angular frequency of the source field
$k_1$ and $k_2$	power coupling coefficient of the two couplers
$\alpha_R$ and $\alpha_S$	optical loss factor associated with the reference and sensing arm

$\alpha$	optical loss factor when $\alpha_r = \alpha_s$
$\phi_r$ and $\phi_{sg}$	phase delay in the reference and sensing arms.
$\langle \rangle$	time average
$I_0$	optical source intensity
$I_a$ and $I_b$	intensity of the complementary outputs of the interferometer
$\Delta\phi$	differential phase shift
G,H and J	constant
$\phi_s$	amplitude of the signal
$\omega$	angular frequency of the signal
$\phi_d$	slowly varying phase shift in the interferometer
I	output of the photodetectors
$di$	change in output of the photodetectors
$\epsilon$	responsivity of the photo detectors
$J_i(\phi_s)$	the Bessel function of order i and argument $\phi_s$ .
$\nu$	optical frequency
$n\Delta L$	optical path difference
$d\nu_f$	frequency range over which the laser may be driven in a single longitudinal mode
$d\nu_n$	rms frequency instability of the laser source
$di$	change in drive current
$\phi_c$	amplitude of the phase carrier
$\omega_c$	angular frequency of the sinusoidal modulation (phase carrier)
$I_c$ and $I_d$	output signals of the passive homodyne techniques
$I_1, I_2$ and $I_3$	outputs of the 3x3 coupler

$A_1$ ,  $A_2$  and  $A_3$  constants determined by the coupling coefficient between the fibres within the coupling region in a 3x3 coupler

$\omega_B$	offset frequency
$\theta$	phase difference term
$\phi_m$	amplitude of the phase modulating signal
$\omega_m$	angular frequency of the modulating signal
$\Delta L$	optical path imbalance in the interferometer
$G(t)$	gated square wave
$f_r$	ramp repetition frequency
$T$	Time period
$m$	integer
$I_{RSH}$	thermal noise of the detector shunt resistance
$k$	Boltzmann's constant
$T$	absolute temperature
$R_{SH}$	shunt resistance of the photodiode junction
$I_{SH}$	shot noise current
$I$	photo-current
$I_{DK}$	dark current
$e$	electronic charge
$I_{1/f}$	1/f noise current
$I_i$	Inverse function of the active area of the semiconductor devices
$\beta$	empirically derived constant
$s$	Laplace operator = $j\omega$
$R$	resistance

$R_F$	feedback resistance
$R_B$	bias resistance
$R_S$	bulk semiconductor and contact resistance
$G_D$	shunt conductance
$C_D$	junction capacitance
$C_S$	stray capacitance
$C_A$	shunt capacitance
$I_{TH}$	thermal noise in the resistive element
$\Delta f$	bandwidth
$I_A$	equivalent current noise in the amplifier
$V_A$	equivalent voltage noise in the amplifier
$V_F$	voltage noise generated in the feedback resistor
$V_{ti}$	thermal noise voltage in different resistors
$I_{A2}$	noise current contribution reflected into non-inverting input of the operational amplifier
$V_{A2}$	noise voltage contribution reflected into non-inverting input of the operational amplifier
$V_{eq}$	equivalent noise of the differential amplifier
$V_N$	rms noise voltage
$V_0$	peak signal voltage
$\bar{V}$	DC bias voltage
$V$	signal voltage
$\langle V_N^2 \rangle$	mean square noise at the output of the detector
$\langle V_S^2 \rangle$	mean square interference signal

$x_N$	noise equivalent displacement
$E_0$	energy stored in capacitor
$C$	capacitance
$v_0$	initial voltage across capacitor
$\tau$	time constant of the circuit
$L$	inductance
$T$	pulse length at 1/3 peak height
$\eta$	damping parameter
$k_0$	impedance constant of the lamp
$L_S$	cylindrical current sheet inductance
$N$	total number of turns
$a$	radius of the coil
$l$	length of the solenoid
$K$	Nagaoka constant
$E_{in}$	input energy supplied to the flash tube
$E_{out}$	output energy of the pulse)
$A_L$	initial amplitude of the acoustic pulse
$A$	amplitude of the acoustic pulse during curing